DEVELOPMENT OF GREEN CORROSION INHIBITORS FROM NATURAL PRODUCTS OF NEPAL

A THESIS SUBMITTED TO THE

CENTRAL DEPARTMENT OF CHEMISTRY

SCIENCE AND TECHNOLOGY

TRIBHUVAN UNIVERSITY, NEPAL

FOR THE AWARD OF

DOCTOR OF PHILOSOPHY

IN CHEMISTRY

BY

NABIN KARKI

AUGUST, 2020

RECOMMENDATION

This is to recommend that **Mr. Nabin Karki** has carried out research entitled **"Development of Green Corrosion Inhibitor from Natural Products of Nepal"** for the award of Doctor of Philosophy (PhD.) in **Chemistry** under my supervision. To my knowledge, this work has not been submitted for any other degree.

He has fulfilled all the requirements laid down by the Institute of Science and Technology (IOST), Tribhuvan University, Kirtipur for the submission of the thesis for the award of PhD. degree.

Prof. Dr. Amar Prasad Yadav
Supervisor
Professor
Central Department of Chemistry
Tribhuvan University
Kirtipur, Kathmandu, Nepal

August, 2020

LETTER OF APPROVAL

On the recommendation of **Prof. Dr. Amar Prasad Yadav**, this PhD. thesis submitted by **Mr. Nabin Karki**, entitled **"Development of Green Corrosion Inhibitor from Natural Products of Nepal"** is forwarded by Central Department Research Committee (CDRC) to the Dean, IOST, T.U.

Prof. Dr. Ram Chandra Basnyat

Professor,

Head,

Central Department of Chemistry

Tribhuvan University

Kirtipur, Kathmandu

Nepal

EXTERNAL EXAMINERS

The Title of Ph.D. Thesis : "Development of Green Corrosion Inhibitors from Natural Products of Nepal"

Name of Candidate : Nabin Karki

External Examiners:

(1) Prof. Dr. Rajaram Pradhanang
    Central Department of Chemistry
    Tribhuvan University
    Kathmandu, NEPAL

(2) Prof. Dr. V.S. Raja
    Department Metallurgical Engineering and Materials Science
    Indian Institute of Technology (IIT) Bombay, Mumbai
    INDIA

(3) Prof. Dr. Eiji Akiyama
    Institute for Materials Research
    Tohoku University, JAPAN

October 1, 2021

Dr. Surendra Kumar Gautam
(Assistant Dean)

DECLARATION

Thesis entitled **"Development of Green Corrosion Inhibitor from Natural Products of Nepal"** which is being submitted to the Central Department of Chemistry, Institute of Science and Technology (IOST), Tribhuvan University, Nepal for the award of the degree of Doctor of Philosophy (PhD.), is a research work carried out by me under supervision of Prof. Dr. Amar Prasad Yadav, Central Department of Chemistry, Tribhuvan University. This research is original and has not been submitted earlier in part or full or any other form to any university or institute, here or elsewhere, for the award of any degree.

_____

Nabin Karki

ACKNOWLEDGEMENTS

academic staffs of the department for their unhindered support during my stay at the Central Department of Chemistry.

Finally, I would like to express my heartfelt thanks to my wife Amrita, son Niwesh, daughter Niharika for their understanding and moral support. I am thankful to my beloved father, mother, brothers, and all other members of the family for their endless love, encouragement and inspiration throughout my study and life.

<div align="right">

_____

Nabin Karki

August, 2020

</div>

ABSTRACT

Mild steels have widespread applications in a broad field of industries and machinery due to their mechanical properties, availability, and low cost. Steel materials such as pipelines, machinery are exposed to aggressive environments like acidic environments in the industrial processes for pickling, de-scaling, oil well acidizing etc. Base metal applied in these processes undergoes dissolution, which causes not only an economic loss but also a significant loss on the ecosystem and for living beings. The use of corrosion inhibitors is an efficient and cost-effective technique to reduce the metal dissolution among various means. Most of the traditionally used inorganic and organic inhibitors are expensive and hazardous to the environment and human health during their synthesis and application. According to registration, evaluation, authorization, and restriction of chemicals (REACH) legislation, in conjunction with Paris commission (PARCOM) recommendations (1991), the present research trend is growing to develop green and low-cost inhibitors. Plant extracts are good alternatives for the green corrosion inhibitors as they are economically feasible, eco-friendly, and rich in several organic compounds that have similar electronic and molecular structure to the conventional organic inhibitors.

Methanolic extract of four Nepali origin plants, *Artemisia vulgaris* (AVE), *Equisetum hyemale* (EHE), *Mahonia nepalensis* (MNE), and, *Berberis aristata* (BAE) were studied as green corrosion inhibitor for mild steel (MS) in acidic medium. Inhibition properties were investigated by weight loss, potentiodynamic polarization, and electrochemical impedance spectroscopy (EIS) measurements. Surface characterization was done by scanning electron microscope (SEM) in combination with energy-dispersive x-ray spectroscopy (EDX). ATR-FTIR spectroscopy of extract was carried out to confirm the different functionalities present in it. Kinetic and thermodynamic parameters were calculated to explain the mechanism of inhibition.

The effect of the plant extract concentration on inhibition efficiency (IE) of MS corrosion was studied in 200, 400, 600, 800, and 1000 ppm. Results revealed that the IE increased with the concentration of the extract. Maximum efficiency computed by potentiodynamic polarization of MS sample as immersed in 1000 ppm extract was 94.21 % for AVE, 92.74 % for EHE, 98.15 % for MNE, and 98.18 % for BAE.

Similarly, the effect of immersion time and temperature for IE was investigated by weight loss method. In AVE and EHE, IE, after reaching a maximum value, decreased with an increase in time, but the IE remains increasing in the case of MNE and BAE. IE in MNE and BAE was found above 90 % after immersion for 15 min and increased gradually and reached above 95 % after immersion for 24 h

The effect of temperature on IE was studied from 298 K to 338 K at a regular interval of 10 K. In the case of AVE, IE increased up to 308 K and decreased onwards whereas in EHE it decreased with increase in temperature from 298 K reaching a value of 56.27% at 338 K. In the case of MNE, IE increased from 298K (92.93 %) to 328K (96.60 %) and decreased significantly to 75.47 % at 338K. Similarly, the IE decreased from 308 K (95.92 %) onwards and became constant above 80 % at 338 K for BAE. Results reflect that MNE and BAE are thermally stable inhibitors.

 Plant extracts suppress the corrosion rate due to the adsorption of organic molecules on the MS surface. Adsorption follows Langmuir adsorption isotherm in all plants, which indicates that there was monolayer adsorption without interaction between adsorbed molecules. Calculated value of free energy of adsorption (ΔG^*) showed that adsorption of extract molecules takes place by both physical as well as chemical interactions with the metal surface. However, in AVE and EHE, the adsorption was dominated by physical interaction. In the case of MNE and BAE, chemisorption dominated mixed adsorption was observed. The value of the energy of activation, enthalpy, and entropy of adsorption showed that the adsorption was endothermic and spontaneous. High energy of activation obtained for BAE supported its thermal stability. Surface studies by SEM with EDX indicate the film formation on the MS surface due to the adsorption of the extract molecules. Electrochemical parameters from open-circuit potential (OCP) and polarization measurements suggested that all plant inhibitors are mixed types of inhibitors. Similarly, EIS results showed the occurrence of only one time constant in the corrosion of MS in plant extracts in acidic solutions.

TABLE OF CONTENTS

LIST OF TABLES

LIST OF FIGURES

LIST OF SYMBOLS

ϕ	Phase Shift
$\downarrow$	Sign for precipitate
$\|Z\|$	Impedance modulus
C_{dl}	Double layer capacitance
Ea	Energy of activation
E_{corr}	Corrosion potential
E_r	Antropov's rational corrosion potential
I_{corr}	Corrosion current
K	Kelvin
^{0}C	Degree celcius
R_{ct}	Charge transfer resistance
Z_{imag}	Imaginary Impedance
Z_{real}	Real Impedance
γ	Activity Coefficient
ΔG^{*}_{ads}	Free energy of adsorption
ΔH^{*}	Enthalpy of adsorption
ΔS^{*}	Entropy of adsorption
θ	Surface coverage

LIST OF ACRONYMS AND ABBREVIATIONS

AVE	*Arteisia vulgaris* extract
BAE	*Berberis aristata* extract
CIs	Corrosion Inhibitors
cm^{-1}	Per centimeter
CPE	Constant phase element
CR	Corrosion Rate
EDX	Energy Dispersive x-ray Spectroscopy
EHE	*Equisetum hyemale* extract
EIS	Electrochemical Impedance Spectroscopy
FTIR	Fourier Transform Infrared spectroscopy
g	gram
GDP	Gross Domestic Product
h	hours
H-AVE	n-hexane extract of *Artemisia vulgaris*
H-BAE	n-hexane extract of *Berberis aristata*
H-EHE	n-hexane extract of *Equisetum hyemale*
H-MNE	n-hexane extract of *Mahonia nepalensis*
IE	Inhibition Efficiency
IUPAC	International Union of Pure and Applied Chemistry
LPR	Linear polarization resistance
mL	millilitre
mm	millimetre
M-AVE	Methanolic extract of *Artemisia vulgaris*
M-BAE	Methanolic extract of *Berberis aristata*
M-EHE	Methanolic extract of *Equisetum hyemale*
M-MNE	Methanolic extract of *Mahonia nepalensis*
MNE	*Mahonia nepalensis* extract
mV	millivolt
NACE	National Association of Corrosion Engineers

OCP	Open Circuit Potential
OCV	Open circuit Voltage
ppm	Parts per million
PZC	Potential of zero charge
SCE	Saturated calomel electrode

CHAPTER 1

1. INTRODUCTION

1.1 Historical background

When human civilization started to use metals for their convenience, corrosion came together with it. It is difficult to sustain human civilization without the use of metals these days. However, corrosion makes the use of metals vulnerable (Sastri, 2011). In the past, the scientific community did not pay much attention to corrosion phenomenon, although it was well adapted to the existing condition. When Robert Boyle published his work in 1675 A.D. under the name of "Mechanical origin of corrosiveness and 'corrodibility'" regarding causes and mechanisms of corrosion, it became a turning point in spreading the understanding and curiosity about corrosion. Michael Faraday (1791-1876) elaborated it further, establishing a corelation between chemical reaction and electric current. Rate of corrosion of various metals are calculated on the basis of his first and second laws. (Ghali et al., 2007)

It was found in the early 18th century that iron remains unattacked in the concentrated nitric acid even if it has rapid interaction with dilute nitric acid. Schonbein illustrated in 1836 that iron could be rendered inactive. In the 19th century beginning, corrosion control ideas began to be generated due to progress in the study of corrosion. Several facts and theories proposed earlier were established, verified, and rediscovered by different scientists. For instance, in 1831, Wollaston proposed the electrochemical theory of corrosion, developed by de La Rive in 1830, verified by Ericson-Auren and Palmaer in 1901 and rediscovered by Whitney in 1903. (Lynes, 1951). Whitney proposed an electrochemically based scientific approach to corrosion control. In 1923, U.R. Evans used his classical electrochemical theory to establish a modern knowledge of the causes and control of corrosion. Well-known books of Evans, Uhling, and Fontana made a noteworthy contribution to considerable progress towards the understanding of corrosion. Corrosion laboratories established at leading universities and research institutes have contributed to the advancement and expansion of corrosion science and technology as an interdisciplinary discipline. Corrosion science and engineering have become an important element of material science and

engineering curriculum in leading universities throughout the world in recent years.(Ahmad, 2006)

1.2 General introduction of corrosion

The word corrosion derives from the Latin word "corrosus," meaning eaten away or consumed by degrees, an unpleasant word for an offensive process. (Evans, 1972). Corrosion is the destructive phenomenon resulting from the interaction of metals with a corrosive environment, which leads to the failure of the structure of surfaces of metallic materials. (Ghali et al., 2007; Sastri, 2011). Corrosion of iron and its alloy is also known as rust, and corrosion products called rust, consisting mainly of the hydrated ferric oxide.

Corrosion is the gradual destruction and unintentional attack of a material caused by its reaction with its environment. The International Union of Pure and Applied Chemistry (IUPAC) define corrosion as an irreversible interfacial reaction of materials (metallic, ceramic or polymer) with their environment resulting in the material consumption or decomposition of a constituent of the surroundings into a substance" (Heusler, et al., 1989)**.** The term corrosion now refers to a wide range of natural and artificial materials, including biomaterials and nanomaterials, and is no longer limited to metals and alloys alone. The scope of corrosion corresponds to the dynamic advances in material development that have occurred in recent years. However, the IUPAC definition of corrosion has not been widely accepted by the corrosion scientific community.

Uhling in the 1960s defined corrosion as a destructive attack on the surface of metallic materials by chemical or electrochemical reaction with its environments leading to their degradation. It is an electrochemical phenomenon involving two reactions: an anodic (site of oxidation) that releases electrons and a cathodic (site of reduction) that consume electrons. For instance, metal corrosion proceeds by the following general anodic and cathodic reactions. (Uhlig & Revie, 2008)

    The anodic reaction is

$$M \longrightarrow M^{n+} + ne^-$$
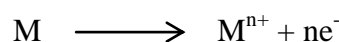
Where 'M' indicates the metal,

'n' indicates the number of electrons that can be easily released by an atom of the metal.

According to the environment where corrosion is taking place, the possible cathodic reaction can be of the following types.

a. oxygen reduction in acidic solution

$$O_2 + 4H^+ + 4e^- \longrightarrow 2H_2O$$
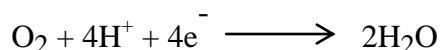
b. oxygen reduction in neutral or basic solution

$$\tfrac{1}{2} O_2 + H_2O + 2e^- \longrightarrow 2OH^-$$
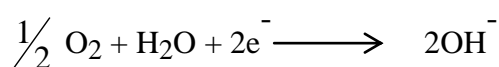
c. Hydrogen evolution from neutral water

$$2H_2O + 2e^- \longrightarrow H_2 + 2OH^-$$

d. Metal reduction

$$M^{x+} + ye^- \longrightarrow M^{(x-y)+}$$
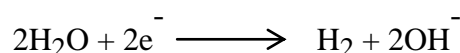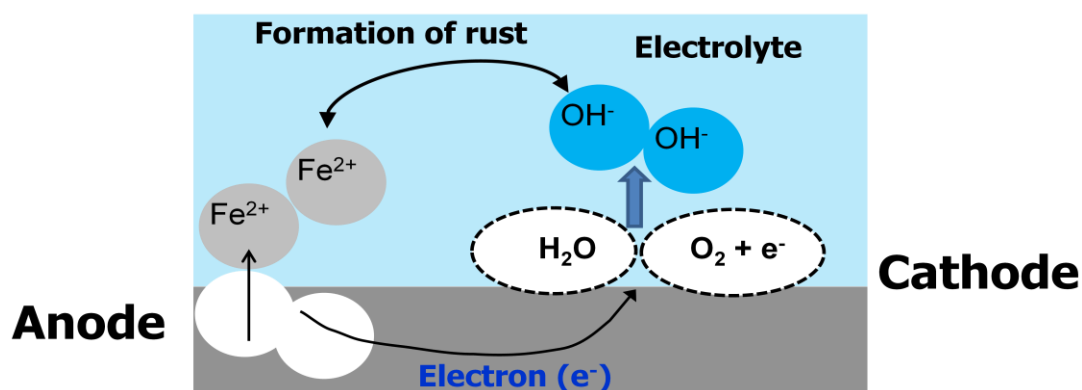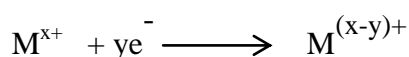
Figure 1.1: A schematic representation of the corrosion on a metal surface in an acidic solution showing both the anodic and cathodic site.

In corrosion process, metal ions migrates at the actives sites (anode) where as electrons are transported from the metal to an acceptor at less active sites (cathode) into the solution. Corrosion involves the flow of ionic current in the solution where as electric current flows in the metal, Fig. 1.1. An electron acceptor is required for cathodic process. Oxygen or oxidizing agents or hydrogen ions are the examples of the electron acceptor. Metals are stable in the ionic state than in the atomic state. According to the thermodynamic principle, metals are converted into their combined

3

state in chemical compounds as in minerals from which they are extracted. So, corrosion is a spontaneous process.

1.3 Economic impacts of corrosion

Corrosion not only causes material loss but causes untimely failure of plants, equipment, and components also, which leads to loss of life and property. The main reasons for the importance of corrosion are as follows:

a. Safety: Corrosion may cause the failure of equipment resulting in a decrease in efficiency and durability. It makes the equipment unsafe to use. Similarly, corrosion products may be poisonous, which may be mixed with machinery products or with water in the pipeline.

b. Conservation: Corrosion study is essential to conserve the precious metals and energy and human effort used to produce, fabricate, and rebuilding.

c. Economic: Economic factor is an important motivating factor for corrosion study. Corrosion causes economic loss to the individuals or the whole nation directly or indirectly.

Some examples of direct loss due to corrosion are as follows:

➢ cost for replacing corroded machinery, structures, and components, such as metal roofing, pipelines, condenser tubes, and mufflers, including necessary labor.

➢ cost for repainting structure.

➢ capital cost and maintenance cost of the cathodic protection system for underground pipelines.

➢ for the additional expense of corrosion-resistant metals and alloys instead of mild steel.

➢ for the cost of corrosion protection system like the addition of inhibitors, galvanizing, dehumidifying storage rooms of equipment.

Some examples of indirect loss due to corrosion are as follows:

➢ loss and severe problems were created due to the shutdown of plants such as nuclear plants, power plants, process plants, and refineries.

➢ loss of products such as water, oil due to leakage in containers, storage tanks, oil transportation lines, and fuel tanks. Gas leaking from a corroded pipe may cause an explosion if it enters the basement of the building.

➢ loss of efficiencies such as reducing heat transfer and piping capacity of heat exchanger tubings and pipelines due to accumulation of corrosion products.

➢ Chemicals, pharmaceuticals, dyes, packaged good, etc. may be contaminated with corrosion products which make them risky to use.

➢ Design of equipment such as reactions vessels, boilers, condenser tubes, oil-well sucker rods, pipelines transporting oil and gas at high pressure, water tanks, and marine structures can be simple, more reliable, and light with adequate knowledge of corrosion, which is generally overdesigned i.e. made heavy to withstand high operating pressure and stress.

Due to several direct and indirect factors mentioned above, the economic cost of corrosion is very high. The study released by NACE entitled "International Measures of Prevention, Application, and Economics of Corrosion Technology (IMPACT)" (*NACE International Institute IMPACT PLUS*, 2020) estimated the global cost of corrosion to be US$2.5 trillion annually, equivalent to approximately 3.4% of the global Gross Domestic Product (GDP) in 2016, Table 1.1.

Table 1.1 : Map of cost of corrosion studies to economic regions.

Economic Regions	CoC study used for Region CoC	Agriculture %CoC	Industry %CoC	Services %CoC
United States	United States, 1998	1.1	9.3	1.3
India	India, 2011	6.1	4.7	3.4
European Region	United Kingdon, 1970	1.1*	8.6	2.2
Arab World	Kuwait, 1987	9.5	2.2	8.3
China	India, 2011	6.1	4.7	3.4
Russia	India, 2011	6.1	4.7	3.4
Japan	Japan, 1997	1.1*	3.6	0.1
Four Asian Tigers + Macau	Average of India and Japan studies	1.1*	3.6	0.1
Rest of the world	Average of all studies	3.8	7.4	1.2

Note: * CoC was not reported in the primary study but value for the United States 1998 Study was used.

The GDP of a nation has been broken down into three sectors such as agriculture, industry, and services. The cost of corrosion was studied in different sectors of different economic regions. Map of cost of corrosion (CoC) studies to economic regions presented in table 1.1 can be used to estimate the corrosion loss in any countries (*NACE International Institute IMPACT PLUS*, 2020).

CORROSION 2016 conference in Vancouver, B.C. has analyzed the corrosion loss economy and proposed corrosion prevention strategies as best practices that can avoid 15-35 percent loss due to corrosion, which is about US$375-875 billion. The significant contributors to corrosion expenditure are petroleum, chemical, petrochemical, construction, manufacturing, pulp and paper, and transportation (rail, automotive, and aerospace) industries.

Many corrosion cost studies have been and still are being carried out in many countries. As a result of corrosion damage, the US and India reportedly lost more than US$ 276 billion and IRS 8,000 billion per year, respectively. (The US Federal Highway Administration, 2002, C.C. Technologies Laboratories, 2001). Corrosion costs are estimated at 5258 trillion yen per annum in Japan. Corrosion of reinforcement and subsequent concrete spills account for over 95% of actual damage in the Arab Gulf's coastal region. It is estimated that every new-born baby has a corrosion debt of $40 a year in the world (Ahmad, 2006).

In Nepal, basic research on the corrosion of materials used in infrastructures such as GI pipe, roofing, automobiles are limited. Additionally, data on the atmospheric environment and its effect on the corrosion of commonly used materials are not available. Data for economic loss due to corrosion damage in Nepal are by far not available. However, the cost of corrosion of Nepal can be roughly estimated based on the cost of corrosion studies of neighboring countries India and China by NACE work, as listed in Table 1.1. GDP of Nepal is USD 29.813 billion in 2019 A.D. in which agriculture, industry and service sector contribute 27%, 13.5%, and 59.5% respectively. Calculation of corrosion cost of on the above basis shows that the corrosion cost of Nepal comes around 1.28 billion USD which is equivalent to 154

billion NRS (NPR.1.54 kharab) and it is 4.3% of the GDP. The various contributions used in the calculation are shown in Table 1.2.

Table 1.2 : Corrosion cost of Nepal based on corrosion cost study of neighboring countries.

S.No.	Sector	% Contribution	Amount (billion $)	% CoC	Amount (billion $)
1	Agriculture	27	8.05	6.1	0.49
2	Industry	13.5	4.05	4.7	0.19
3	Service	59.5	17.74	3.4	0.6
				Total	1.28

The enormous amount of loss due to corrosion in Nepal can be judged from the budget allocated for education, environment, science and technology that comes around 11.64% of the annual budget of Nepal. The cost of corrosion comes about 10.44% of annual budget, of which 15% to 35% can be saved by using proper knowledge of corrosion, which comes around NPR 23.1 billion (23 arab 10 crore) to NPR 53.9 billion (53 arab 90 crore).

So, corrosion studies are important for several reasons. Some of which are listed as follows:

- ➢ for designing engineering structures and materials appropriately in the early of the design stages.
- ➢ for the protection or reduction of the various types of disasters caused by corrosion damages.
- ➢ for the protection from the contamination of air, water, and soil.
- ➢ for the preservation of valuable natural resources.
- ➢ for using the corrosion-resistant surgical implants in the human body (Ghali et al., 2007).

1.4 Mild steel (MS)

Mild steel (MS) is a type of low carbon steel that contains about 0.05-0.25% of carbon by the weight. It does not contain other elements in substantial amounts besides iron. Table 1.3 shows typical composition of MS. The presence of carbon and other alloying elements in fewer amounts make its properties different from higher carbon

or alloy steel. Affordability, availability, weldability, and machinability make it more popular since its development in middle age and led to an exponential increase in its usage. It has become in-demand materials for infrastructural construction, industrial, and engineering application for sustainable development. However, the lack of alloying elements makes it susceptible to corrosion. Its deterioration due to corrosion is a major issue as it is widely employed for human civilization and sustainable development. Hence, the study mild steel corrosion phenomenon has become important, particularly in acidic medium.

Table 1.3 : Typical elemental composition of a mild steel.

Element	wt%
Carbon	0.16-0.18%
Silicon	0.40% max
Manganese	0.70-0.90%
Sulphur	0.040% Max
Phosphorus	0.040% Max
Iron	balance

Mineral acids like HCl and H_2SO_4 are frequently used in various industrial processes such as acid pickling, de-scaling, cleaning boilers, oil wells, acidizing, and many other processes. These processes are adopted to clean the MS surface by removing powdery deposits or corrosion products or scales. However, the so-called cleaned mild steel surface is also attacked by aggressive acid solution resulting in a reduction in equipment efficiency and durability, making them vulnerable. The primary prevention strategy to protect materials from its corrosion is controlling the exposure of metallic structure to the acidic environments, but it is practically impossible. So, corrosion protection methods are such as barrier coating, alloying, galvanization, and cathodic protection methods are in practice to control corrosion. Among these, inhibitors are a reasonably cost-effective, simple-to-apply, and effective technique to protect materials.

1.5 Corrosion control

Although corrosion is inevitable, it can be controlled by employing different methods. It is the electrochemical reaction, including two or more half-cell reactions. So, it can

be controlled by slackening the rate of cathodic or anodic or both reactions. Several attempts are employed as the most practical methods of mitigating the effects of corrosion to decrease the vulnerability of the materials. The fundamental motive of the methods to control corrosion is to maintain the durability and credibility of the structures. It decreases the risk of harmful leakages and explosion. It is cost-effective ways to reduce the premature failure of materials and structures and to protect life, property, and environment.

The following methods are used to protect metals against corrosion:
1. Inspection and monitoring
2. Selection of the right material of construction
3. Surface coating
4. Proper equipment design
5. Electrical protection
6. Inhibitors

1.5.1 Inspection and monitoring

Inspection of structure and machinery should be done periodically to be prevented from their sudden failure. It helps to reduce significant damage to life, property, and the environment. It helps to provide relevant information and data necessary to assess the existing structure in an aggressive environment (Davis, 2000). It can be done using visual inspection, fiberscope, borescope, caliper tools, etc. In general, inspection involves a short-term once-off measurement, based on the schedule for maintenance and inspection.

Monitoring involves long term measurement of the corrosion damage to understand the fluctuation of corrosion over time as well as the cause of failure. It is carried out to ensure the proper working condition of equipment and structure since it provides an early signal about their failure (Davis, 2000; Roberge, 2012) Monitoring can be carried out by using either electrical or mechanical probes such as potentiodynamic polarization, AC impedance measurement, weight-loss method, etc.

1.5.2 Selection of the right material of construction

Some of the factors that should be considered for the selection of materials for a

specific purpose are corrosion behavior, Physical (electrical conductivity, thermal conductivity), mechanical (tensile strength, density, ductility, fracture toughness, etc.), and the cost.(Finšgar & Jackson, 2014; Roberge, 2012) Mild steel is used for various industrial and engineering materials due to its low cost. Since mild steel is easily attacked by corrosion, austenitic or duplex stainless steels are used in some applications due to their corrosion-resistant properties despite the high cost. However, the use of mild steel in combination with chemical treatment, such as corrosion inhibitors, is still cost-effective. (Finšgar & Jackson, 2014).

The material selection usually involves various steps considering environmental conditions and the overall cost of the structure. It involves the following steps :

- Initial selection: Based on Prior experience, accessibility and safety concerns.
- Laboratory inverstigation: Reevaluation of materials that appeared to be appropriate under process conditions.
- Analysis of laboratory findings and other information: Effect of probable impurities, excessive temperature, excessive pressure, agitation, and air presence in material.
- Cost comparison of ostensibly suitable equipment: Material and its repairment cost, possible life, cost of product deterioration, and liability to special risk.
- Final selection.

1.5.3 Surface coating

The coating is one of the standards and most used methods of corrosion control. It is a thin material deposited on the metal surface to improve surface properties. The coating forms a protective barrier, which decreases the contact of metal with the environment and controls the corrosion. Factors that should be considered for the selection of effective corrosion are low cost, low porosity, good adhesion to the substrate, fire, heat and abrasion resistance, sufficient thickness, and uniform appearance. Similarly, it should be chemically resistant to the environment for which it is exposed. The failure of coatings may be ascribed to the absorption of water, blistering due to gas or air inclusion, surface contamination, surface defects, and temperature differentials. In many cases, failure results from the inadequate surface

preparation and careless application of the coating by relatively unskilled human resources.

Coatings are of two types, namely metallic and non-metallic, which could be further subdivided into many categories.

A. The following methods are adopted for the metallic coating.

1) Electroplating
2) Immersing the sample in fused metal covered with a flux
3) Spraying of the fused metal on the sample

B. The non-metallic coating is of two types.

1) Inorganic coating

(a) Oxidation (Passivation)

(b) Phosphating

(c) Enamels

(d) Cement coating

2) Organic coating

(a) Paints

(b) Lacquers

(c) Coal tar

(d) Temporary coating (lubricating oil)

1.5.4 Proper equipment design

The corrosion rate of the material can be reduced by proper design of equipment also.

Some factors which should be considered during equipment design are discussed here.

1. The risk of corrosion is more when the difference in corrosion potential of two metals joined together is more in the galvanic series. So, contacts of such types of metals should be avoided in the presence of electrolytes. If the use of such types of metals having more corrosion potential difference is required, insulators such as plastic or rubber should separate them to decrease corrosion.

2. Welding is preferred than riveting while joining sections of the materials to reduce crevice corrosion. Heat affected zone (HAZ) ought to be post-weld heat treated (PWHT) to mitigate residual stresses, that could cause corrosion.

3. The risk of erosion-corrosion can be minimized by thickening sensitive areas subjected to strong turbulence (high shear stress) or running solutions containing suspended solids. Examples of such suspended solids are elbows, bends, tube inlets, impellers of agitated vessels and so on.

4. The vibration of the equipment should be avoided as far as possible to control oxygen transfer from the solution to the corroding surface.

5. Equipment should not be left wet for a long time to avoid severe corrosion. It should be dried by passing nitrogen gas.

6. Stresses in the structure should be avoided.

1.5.5 Electrochemical protection

It is one of the most important approaches of the corrosion prevention techniques, and it involves two methods:

1.5.5.1 Cathodic protection method:

Cathodic protection method is a method widely used for the protection of underground and undersea metallic structures from corrosion. Oil and gas pipelines, cables, utility lines, structural foundation, condenser tubes of heat exchangers, bridges, and so on are protected from corrosion by this method. According to the electrochemical concept of corrosion, electrons produced at the anode are consumed by cation of the electrolyte solution, and metal ion at anode combines with the anion of the solution resulting in the dissolution of metal. If additional electrons are supplied to the metal from an external source, cathodic hydrogen evolution is increased; an anodic metal dissolution is decreased. Thus, the supply of electrons from external sources decreases or eliminates the difference in potential between the cathodic and anodic site of metal to be protected, and it reduces or eliminates corrosion. When metal becomes cathode, cathodic protection of metal is attained. Cathodic protection can be done in two ways.

1. **By the application of direct current:** In this method, the additional electrons are supplied by direct electric current, which shifts the potential of the cathode to that of the anodic area. On the application of sufficient potential, the potential difference between cathode and anode is reduced to control metal corrosion.

2. **By using sacrificial anode:** It is an easy and cheap method for cathodic protection that can be used without an external power supply. In this method, electrons are supplied to the metallic structure by other more active metal, then the metal to be protected becomes the cathode, whereas more active metal becomes the sacrificial anode and corrodes. For example, iron can be protected by more active metals such as zinc, magnesium, aluminum, etc.

1.5.5.2 Anodic protection

Anodic protection is a method to control a metal surface's corrosion by connecting is as an anode concerning an inert cathode of an electrochemical cell and ensuring that the electrode potential is controlled to keep the metal in a passive state. In the process, barrier protective film is formed on the metal surface, which protects it from corrosion. This method is only applicable to the active-passive metallic substance. It is preferred in an extremely aggressive environment, such as mild steel vessels containing concentrated acid or alkali, such as concentrated sulphuric acid. It is done when cathodic protection is not cost-effective. For certain metals like steel alloy or stainless steel, anodic protection is preferred over cathodic protection. It requires careful design and control, because loss or instability in passivation accelerates the corrosion.

1.5.6 Corrosion inhibitors

The use of corrosion inhibitors is one of the effective procedures for corrosion control. It has been used for corrosion control since the nineteenth century. Baldwin awarded the first patent on inhibitor, using molasses and vegetable oils to prevent corrosion in acids from pickling sheet steel (El-Meligi, 2010). It is commonly practiced in industrial sectors due to the low cost and easy practice method. (Dariva & Galio, 2014; Obot et al., 2009; Yıldırım & Çetin, 2008). These are used in a wide range of applications such as cooling water systems, refinery units, chemical plants, power generation, oil and gas production units, etc.

Corrosion inhibitors are a chemical substance that, when added (continuously or intermittently) in small amounts to an aggressive environment, decelerates the exposed metals corrosion rate significantly. It may be in a liquid or vapor state. The concentration and quantity of corrosion inhibitor required for a system depend on the type and strength of the acid, type of metal, pH of the solution, temperature, and exposure time. The corrosion inhibitors that are effective under certain conditions need not be effective in another condition.

1.6 Classification of corrosion inhibitors:

Based on the mechanism of corrosion, corrosion inhibitors are classified into two types, as shown in Fig.1.2.
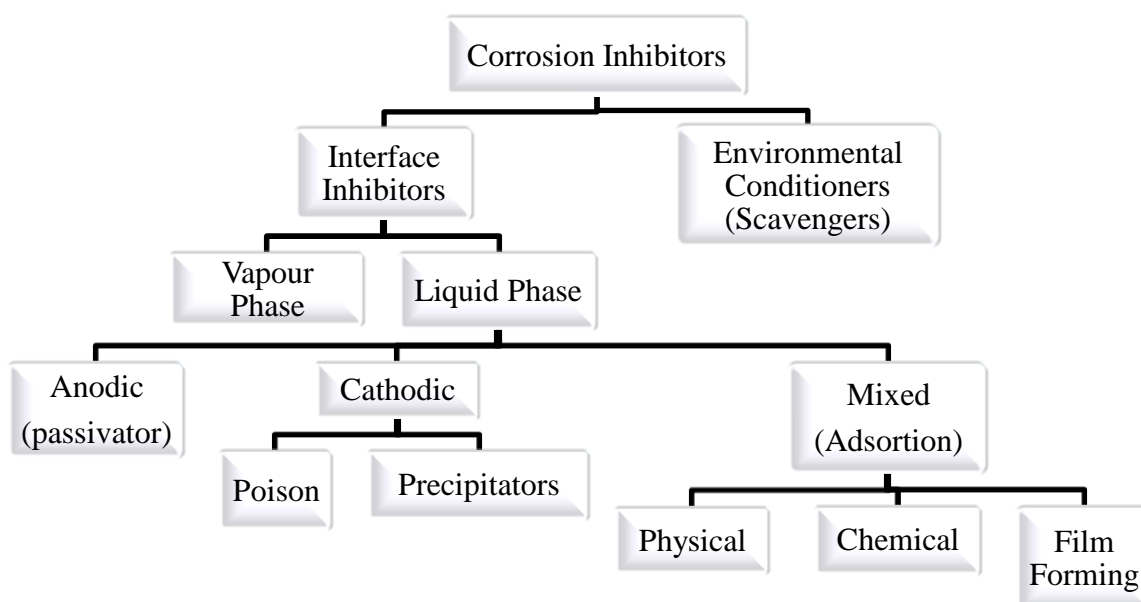
Figure 1.2 : Classification of corrosion inhibitor.

1.6.1 Environmental conditioners (Scavengers):

Corrosion inhibitors that inhibit the corrosion by removing the corrosive species in the medium are known as environmental conditioners or scavengers. For example, oxygen reduction cathodic reaction in the near-neutral or alkaline solution can be reduced by decreasing the amount of oxygen using hydrazine as scavengers.

$$5O_2 + 2(NH_2\text{-}NH_2) \rightleftharpoons H_2O + 4H^+ + 4NO_2^-$$
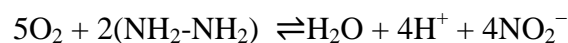
1.6.2 Interface inhibitors:

Corrosion inhibitors that inhibit corrosion by forming a protective film at the metal/solution interface are known as interface inhibitors. Interface inhibitors are classified into vapor-phase and liquid phase inhibitors.

a. Vapour phase inhibitors:

Vapour phase inhibitors (VPIs) are the volatile inhibitors transported in the vapor phase to the surface of a metal and get adsorbed on metal to form a protective layer on the metallic surface against atmospheric corrosion, especially in a closed system (Olajire, 2017; Roberge, 2012). The substance with low but significant vapour pressure and inhibitory properties are effective vapour phase inhibitors. Vapour phase inhibitors may either vaporize either in molecular form or dissociate first and then vaporize. Amines are VPIs that vaporize in a molecular form, whereas dicyclohexylamine nitrite dissociates first to form amine and nitrous acid, that deposit on the metal surface.

b. Liquid phase inhibitors:

Chemical compounds that inhibit the corrosion of a metallic material exposed to corrosive solution in the liquid phase are known as liquid phase inhibitors. They are classified into anodic, cathodic, or mixed inhibitor based on the electrochemical reaction inhibited.

i. Anodic inhibitors:

Anodic corrosion inhibitors are the compounds that decrease the corrosion rate by retarding anodic metal dissolution reaction. These inhibitors react with the corrosion product and form a cohesive and insoluble film on the metal surface, resulting in the reduction of effective anodic area and inhibiting the corrosion. Furthermore, anodic inhibitors shift the corrosion potential to a more positive direction and decrease the corrosion current density, as shown in Fig. 1.3. They are known as passivating inhibitors because they create an anodic shift in corrosion potential, driving the metallic surface into the passivation zone. (Ahmad, 2006) Anodic inhibitors are of two types, which are oxidizing anion and non-oxidizing anions. Oxidizing anions such as chromates, nitrites are useful in the absence of oxygen and non-oxidizing anions such as phosphate, molybdate, tungstate, are useful in oxygen presence. The

concentration of the anodic inhibitor must be sufficient in the solution. Otherwise, the metallic surface will not be covered completely; leaving the metal exposed sites leads to the localized corrosion of the metal. (Dariva & Galio, 2014).
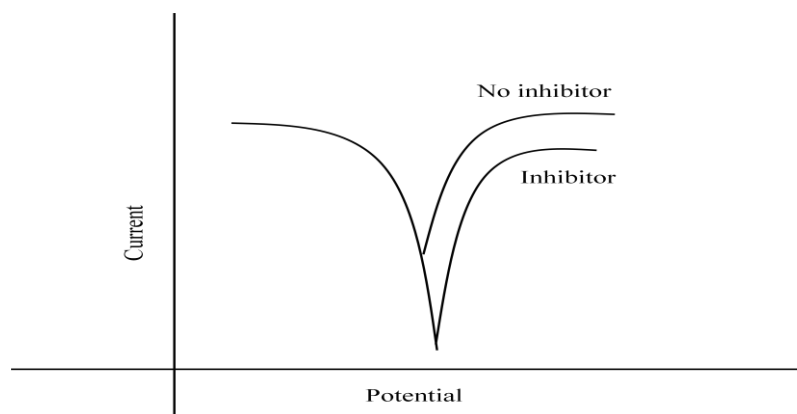
Figure 1.3 : Anodic inhibitor**.**

ii. Cathodic inhibitors:

Cathodic corrosion inhibitors are the compounds that decrease the corrosion rate by retarding a cathodic reaction. These inhibitors shift the corrosion potential to a more negative direction and decrease the corrosion current density. These are classified into two types, which are cathodic poisons and cathodic precipitators. Cathodic poisons retard the corrosion rate by decreasing the reduction rate through different mechanisms. For example, Cathodic poisons such as arsenic, antimony, and bismuth compounds are reduced at the cathode and inhibit corrosion by forming a metallic layer, whereas sulfides, and selenides inhibit due to adsorption on a metal surface. Additionally, in near-neutral and alkaline solutions, inorganic anions, such as phosphates, silicates, and borates form a protective film that limits oxygen diffusion to the metal surface. On the other hand, cathodic precipitators inhibit corrosion by increasing alkalinity at the cathodic sites, resulting in barrier film formation on the cathodic sites due to precipitating selectively. Some examples of cathodic precipitators are polyphosphate, salts of zinc, calcium, and magnesium. (Anbarasi et al., 2013)

iii. Mixed inhibitor (Adsorption inhibitor):

Inhibitors that retards corrosion rate due to adsorption to form thin barrier films are called adsorption or film former inhibitors. The barrier film blocks the contact of both

cathodic and anodic sites to control corrosion. So, it reduces both anodic metal dissolution and cathodic hydrogen evolution process. So, they are also known as mixed inhibitors. Adsorption of inhibitor could be physical or chemical or mixed type involving both. The effectiveness of inhibitor depends upon the extent of adsorption and surface coverage. Factors that affect adsorption are surface charge of the metal, the structure of inhibitor, and electrolyte type.

More than 80% of organic inhibitors are mixed inhibitors. They inhibit corrosion in three possible ways, which are physical adsorption, chemical adsorption, or film formation. Physical adsorption is due to electrostatic attraction force between oppositely charged metal and inhibitor molecule or ion. Chemical adsorption is due to charge transfer between π-electrons or lone pair in heteroatoms of inhibitor molecule to vacant d-subshell of metal to form a coordinate type of bond. Film formation is due to the surface reaction of adsorbed molecules.

1.7 Selection of inhibitors:

The use of inhibitors is a natural, cheap, and effective method for corrosion protection, which offers the advantage of the in-situ application without causing any significant disruption to the process. It is one of the best corrosion protection methods because even a small amount of inhibitor is sufficient to decrease the rate of corrosion of the metal significantly. These are several conditions that must be fulfilled while selecting a chemical as an inhibitor, which are as follows:

- It should be soluble in a corrosive environment to achieve an optimum result.
- Corrosion inhibitors should be cheap. It should not be required in a high amount.
- It should be environmentally friendly. It should not have any jeopardizing effect on human beings and environment during their preparation and application.
- It should have thermal stability. It should not be decomposed at a higher temperature.
- It should be easily available because less available material could be expensive. (Jones, 1996; Khan et al., 2015)

1.8 Adsorption of inhibitors

Corrosion inhibition of organic chemicals can be attributed to the adsorption of large-sized organic molecules, hence blocking the active site of corrosion due to the formation of barrier film. The extent of adsorption or the coverage of the metal surface by inhibitor molecules is the measure of the efficiency of such an inhibitor. It has been reported that organic compounds having heteroatoms such as nitrogen, sulphur, oxygen, phosphorus, or having multiple bonds are found effective for corrosion inhibition as they have high tendency to be adsorbed. Factors affecting the adsorption of organic compounds are some molecules' physicochemical properties, possible steric effect, the functional groups, electron density of donor atoms, and the probable interaction of p-orbitals of the donor atom to vacant d-orbital of metal atoms.
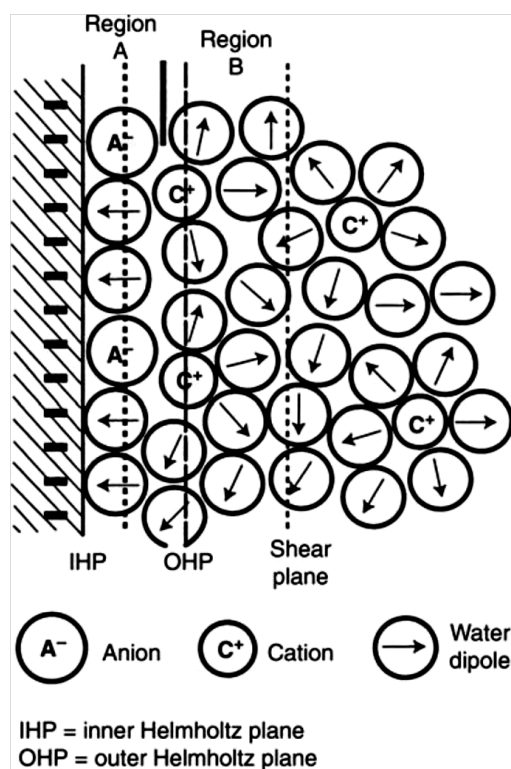
Figure 1.4 : The formation of a double or triple layer interphase.

The metal–solution interface is the site where adsorption of the inhibitor molecule takes place. This results in a change in potential difference across metal-solution interface. A typical metal–electrolyte interface consisting of a sheet of charge at the metal surface and an equivalent charge in the solution side forming a double or triple layer interphase is shown in Fig. 1.4.

An excess or deficiency of electron on the metal surface forms a negative or positive charge layer on the metal surface. The contact adsorbed ions by replacing water dipoles forms the second layer of charge (region A) on the solution side of the interface, forming an inner Helmholtz plane (IHP) at the metal-solution interface. These ions are mainly large size anion and are known as potential-determining ions. The unbalanced charge in the solution side is then partially balanced by hydrated ions of opposite charge forming an outer Helmholtz plane (OHP) in region B. Remaining charge in the solution side of the interface is balanced by a scattered Gouy–Chapman diffuse charge layer (region C).

Besides kinetic, thermal and electric field as the driving force for the distribution of ions at the metal-solution interface, specific chemical interactions between the ions and interface also plays important role so that region A is reached by the specific ions. These interactions depend upon distance and encompass hydrogen and covalent bonds and π bonds or hydrophobic interactions that do not occur in the outer regions.
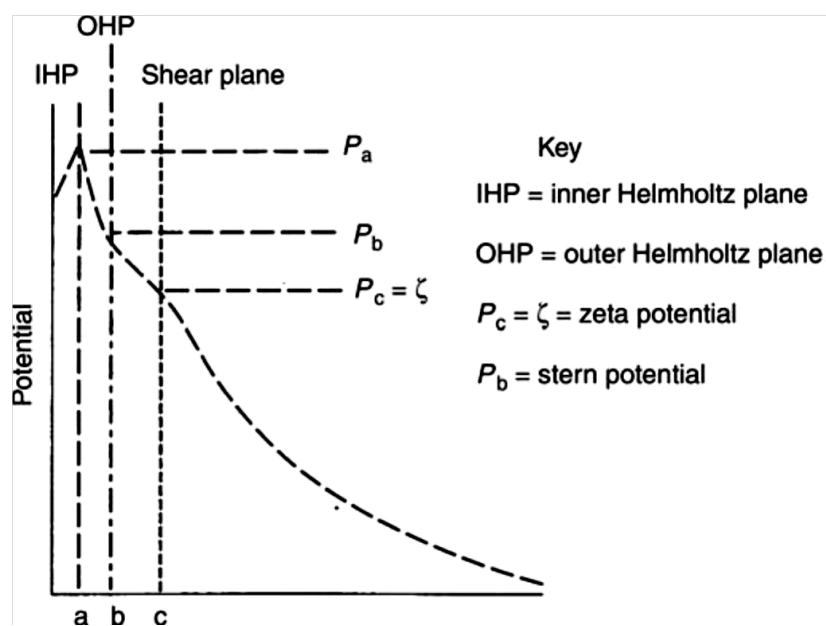
Figure 1.5 : The potential variation in the interphase region.

Fig. 1.5 describes the potential variation in the interphase region. The metal-solution interface can be represented as an electrical equivalent of a parallel plate condensor in the regions A and B. Therefore a linear drop of the potential from P_a to P_b, occurs which can only be measured with respect to a non-polarizable interface such as a

hydrogen electrode. Thus a standard relative electrochemical potential can be obtained. A corrosion inhibitor changes the composition and structure of the electric double layer. As a result, the adsorption of the inhibitor on the metal-solution interface may be monitored using double layer capacitance measurements of the metal-solution interface with and without the presence of corrosion inhibitor.

The zeta potential (ζ), which is the potential required to cause electrokinetic movement within the electrolyte and is considered to be just outside the OHP, can be used to understand the adsorption of inbihitors on the metal-solution interface. In the presence of supporting electrolyte the total potential drop across the metal-solution interface remains constant through a decrease in the thickness of the double layer occurs. This leads to lowering of the zeta potential. It is well known that the interaction of ions or neutral polar molecules with the electric double layer affects its structure as well as its properties. The displacement of water dipoles from the surface of metal facilitates the adsorption of inhibitor molecules, according to:

$$Org_{(sol)} + xH_2O_{(ads)} \rightleftharpoons Org_{(ads)} + H_2O_{(sol)}$$
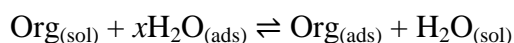
The adsorption of the inhibitor molecules is accompanied by displacing x water dipoles initially adsorbed on the metal surface due to strong interaction energy between inhibitor molecules and the metal surface compared to metal and the water molecules.

The presence of inhibitor molecuels also affects the dielectric properties of solvent due to the ordering effect of π-electrons of the inhibitor molecules on the water molecules at the interface, in addition to electronic and geometric factors.

The possible ways of adsorption of organic compounds on the metal surface, as discussed above, can be summarized as follows:

  a. Due to electrostatic force of attraction between the charged inhibitor molecules and charged metal surface.
  b. Due to interaction of lone pairs of electrons present in heteroatoms of the inhibitor molecules with the metal.

c. Due to interaction of the presence of multiple bonds (π electron) present in inhibitor molecule with metal.

d. Due to the combination of both (a) and (c). (Ostovari et al., 2009)

After adsorption organic molecules inhibit the corrosion rate by following ways :

➢ Reducing the rate of diffusion for reactants to the metal surface.

➢ Increasing or decreasing the anodic or cathodic reaction.

➢ Decreasing the electrical resistance of the metal surface.

Most of the organic inhibitors are mixed inhibitor (Rani & Basu, 2012). Mixed inhibitors inhibit corrosion in three possible ways: Physical adsorption, Chemical adsorption, and film formation.

a. Physical adsorption:

In physical adsorption, organic inhibitors are adsorbed on the metal surface by the electrostatic force of attraction. The mode of physical adsorption of an inhibitor molecule depends upon the surface charge of the metal at the open circuit potential, which can be calculated using the equation [1-1]:

$$E_r = E_{OCP} - E_{PZC} \hspace{4cm} [1\text{-}1]$$

Where E_r is Antropov's rational corrosion potential, E_{OCP} is open circuit potential, and E_{PZC} is the potential of zero charges of metal.

The net charge on the metal surface is positive when the value of E_r is positive, and it is negative when the value of E_r is negative.

When open circuit potential is less than the potential of zero charges, the value of E_r becomes negative, and the net charge on the metal surface is negative. Positively charged inhibitor molecules or cations are then adsorbed on a negative metal surface by physical adsorption, as shown in figure 1.6. For example, protonated carboxamide derivatives are adsorbed on the negatively charged metal surface and perform as a corrosion inhibitor. (Sadeghi Erami et al., 2019)
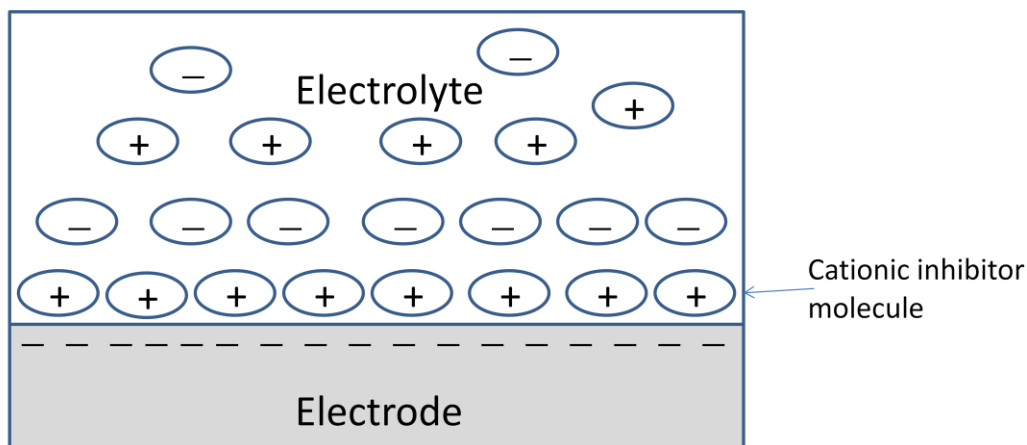
Figure 1.6 : Adsorption of positively charged inhibitor on a metal surface with a net negative charge.

When open circuit potential exceeds the potential of zero charges, the value of E_r becomes positive which results the positive on the metal surface. In such cases, adsorption of anionic inhibitor is facilitated as shown in Fig. 1.7. In acidic media, lone pair present on heteroatoms abstracts proton, which makes an inhibitor molecule positively charged or some site of the organic molecule itself could be positive due to the presence of quaternary nitrogen. In such a condition, there will be electrostatic repulsion between inhibitor molecules and metal surfaces, Fig. 1.8. However, inhibitor molecules are adsorbed on the metal surface via the anion bridge as demonstrated in Fig 1.9. In the process, anions, left by acid after donation of proton to inhibitor molecules, are first adsorbed on the surface of metal due to low hydration energy, resulting in an increased negative charge close to the interface and positively charged inhibitor molecules are adsorbed. In other words, there is a synergism between inhibitor molecules and anion derived from acid for physical adsorption. For example, Ginko leaf extract on X70 steel in HCl (Qiang et al., 2018) and 2-thiohydantion on mild steel in HCl (Yüce & Kardaş, 2012) are adsorbed due to their synergism with chloride ion derived from acid. This adsorption in inhibitor in competition with H^+ ion in the cathodic site of mild steel leads to inhibition of cathodic hydrogen evolution. Inhibitor molecules that are adsorbed physically interact quickly, but their desorptions is easy. The degree of desorption increases with an increase in temperature. This adsorption is characterized by lower activation energy and lower free energy of adsorption.
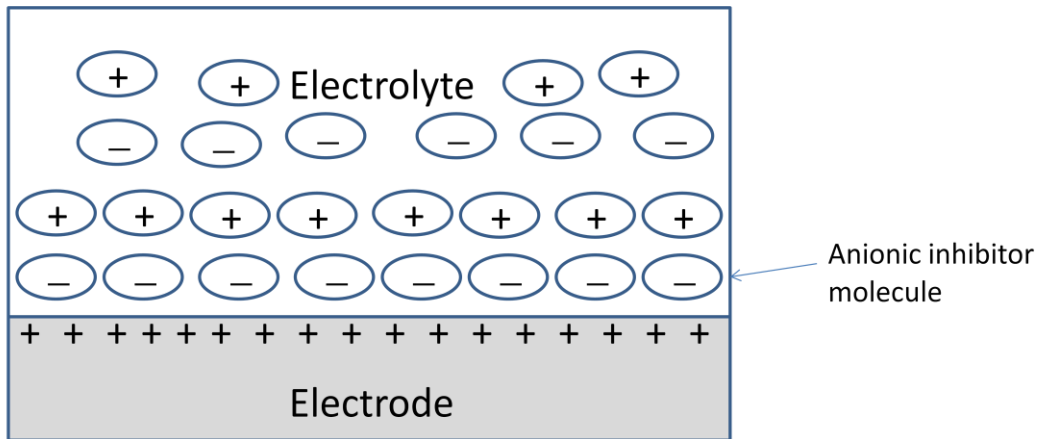
Figure 1.7 : Adsorption of negatively charged inhibitor on a metal surface with a net positive charge.
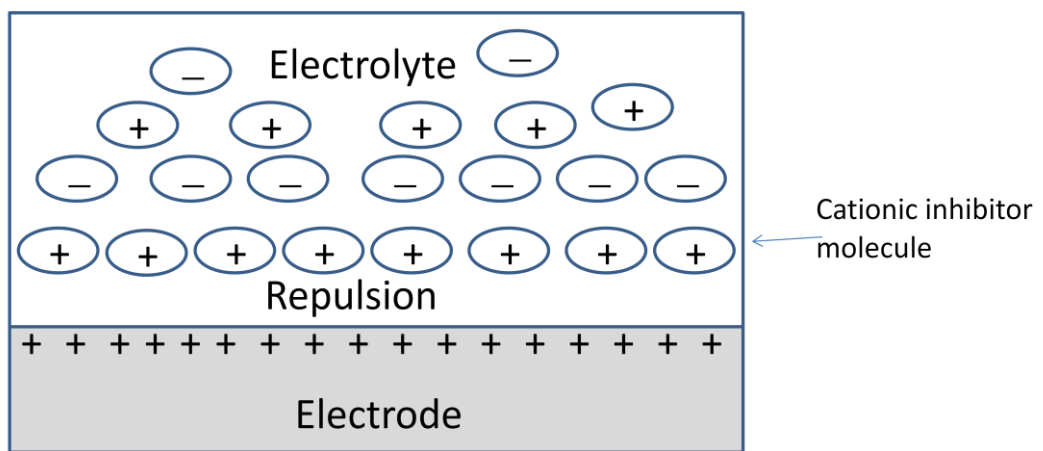
Figure 1.8 : Positively charged inhibitor does not have interaction on the metal surface with a net positive charge.
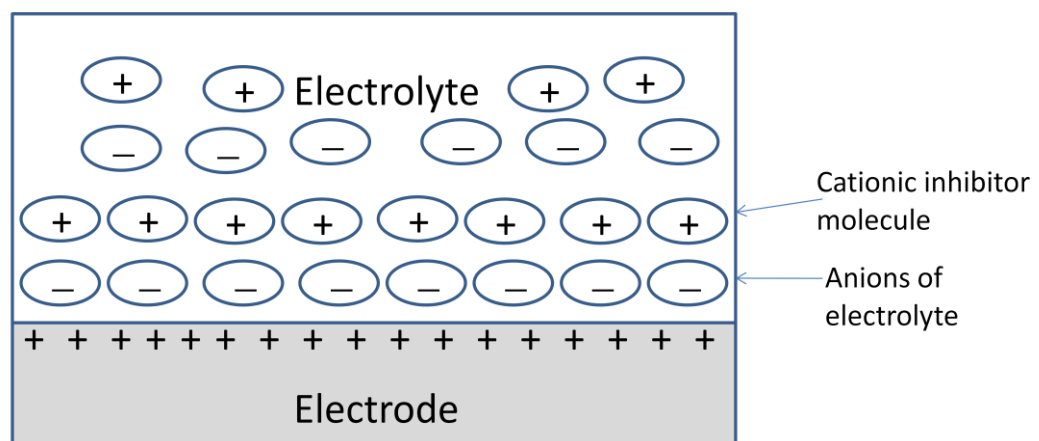
Figure 1.9 : Synergistic adsorption of positively charged inhibitor and anion on a metal surface with a net positive charge.

23

b. Chemical adsorption:

Chemical adsorption involves the adsorption of neutral of cationic inhibitor molecules on metal surface with replacement of water from the surface by inhibitor molecules. It is due to the formation of a coordinate bond with donor-acceptor interaction, which involves the interaction of highest occupied molecular orbital (HOMO) of organic molecules with vacant d-orbital of iron. The orbital with the higher electron density, like the bonding π orbital or the orbital containing unshared electron pair, is referred to as HOMO. Owing to the electron pair on heteroatoms, the big organic inhibitor molecules behave as a soft base with high polarizability and low ionization potential. The metal surface acts as a soft acid. As there is rapid interaction between soft acid and soft base to form strong bond according to HSAB theory, the donor-acceptor interaction between inhibitor molecules and metal is anticipated to be stronger (Sadeghi Erami et al., 2019). Extra negative charges accumulate on the metal surface as a result of this interaction. To alleviate the condition of increased negative charge on the surface of metal due to this interaction, retrodonation may occur between metal atom and LUMO of inhibitor molecules, which is the return of electrons from 4S or 3d orbital of the metal atom to LUMO of inhibitor molecules to form feedback bond. The orbital with higher orbital density such as vacant antibonding π* orbital is known as lowest unoccupied molecular orbital (LUMO). The formation of a feedback bond strengthens the coordinate bond. Inhibitors have loosely bound electrons transfer charges easily. So, a decrease in electronegativity of heteroatoms in the organic molecules increases inhibition efficiency in the sequence of P > S > N > O.

Besides this, inhibition is also due to chelation that forms a stable and insoluble metal-inhibitor complex on the metal surface in combination of organic molecules with Fe^{+2} ions. The solubility of the protective layer reduces as the number of such complex molecules increases, inhibiting anodic metal dissolution. It explains why the inhibition efficiency increases as the function of concentration and time.

Chemisorption is slower than physical adsorption, and the degree of chemisorption increases with an increase in temperature. So, inhibition efficiency due to chemisorption increases with an increase in temperature. It is characterized by a high

energy of activation and high free energy of adsorption. It is specific and not completely reversible(Sastri, 1998).

c. Film formation:

Protective films are formed on the metal surface due to the surface reaction of adsorbed molecules. This type of film serves as a barrier to contact aggressive media with metal and inhibits corrosion. Inhibition is significant if surface film grows up to several hundred angstroms thick polymeric films. When films are adherent, insoluble, it prevents the access of the aggressive solution to the metal and inhibits corrosion effectively. These types of films are of two types, conducting and non-conducting. Conducting films is also known as a self-healing film, and non-conducting sometimes terms as an ohmic inhibitor as they increase the circuit's resistance, hence inhibiting the corrosion.(Rani & Basu, 2012).

Factors affecting the efficiency of organic inhibitors are as follows:

➢ chemical structure, such as the size of the inhibitor molecule;

➢ aromaticity / conjugated bonding

➢ type and number of π or σ bonding atoms or groups in the molecule;

➢ nature and the charges of the metal surface of adsorption mode like bonding strength to the metal substrate;

➢ capability for a layer to form compact or cross-linked film,

➢ ability to form a complex with the atom as a solid within the metal lattice;

➢ nature of the electrolyte solution such as sufficient solubility in the environment. (Sanyal, 1981)

The existence of polar functional groups containing S, O, or N atoms in the molecule, heterocyclic compounds, and electrons, all of which have ionizable hydrophilic or hydrophobic sections, determines the effectiveness of these organic corrosion inhibitors. For the development of the adsorption process, the polar function is commonly regarded as the reaction center.(Yaro et al., 2013)

As the concentration of inhibitor is proportional to surface coverage, it is critical in the medium. (Roberge, 2012; Sherif & Park, 2006)

1.9 Adsorption isotherm

Adsorption of inhibitor occurs through various mechanisms such as physical adsorption due to electrostatic force of attraction, chemical adsorption resulting from the coordinate bond, and feedback back bond due to charge-transfer interactions between inhibitor molecule and metal atom, and due to formation organometallic complex formation. The adsorption isotherm is the relationship between adsorbate amount and its bulk concentration on the adsorbent as a function of its concentration or pressure at a constant temperature. Adsorption isotherm of inhibitor on the metal surface is more informative to understand the mechanism of corrosion inhibition. Necessary information on mode and interaction degree between an inhibitor and metal surface can be investigated with adsorption isotherm. Chemical composition, inhibitor molecule structure, temperature, and the electrochemical potential at the metal/solution interface are the factors which influence the adsorption.

In this study, several adsorption isotherms, such as Langmuir, Tempkin, Flory-Huggins, and Freundlich, were tested to describe the adsorption behavior of inhibitors. The best isotherm that fits the data collected was determined by plotting the degree of surface coverage (θ) obtained from the weight loss method against the inhibitor concentration. The magnitude of the linear correlation coefficient (R^2) has been used to determine the fitness of adsorption data into an isotherm. Surface coverage (θ) of inhibitor is calculated by using the formula shown in equation [1-2].

$$\theta = \frac{IE}{100} \qquad\qquad [1\text{-}2]$$

Where IE is the inhibition efficiency of the inhibitor.

Adsorption models are tested as follows:

Langmuir adsorption isotherm:

Langmuir adsorption isotherm is represented by the equation [1-3]:

$$\frac{C_{inh}}{\theta} = \frac{1}{K_{ads}} + C_{inh} \qquad\qquad [1\text{-}3]$$

Where C_{inh} is the concentration of inhibitor, θ is the degree of surface coverage by inhibitor, and K_{ads} is adsorption equilibrium constant.

Here, a plot of $\frac{C_{inh}}{\theta}$ vs. C_{inh} gives a straight line. The equilibrium constant can be computed from the intercept of the straight line. A significant value of equilibrium constant implies the strong adsorption of inhibitor molecules on the metal surface. The slope of the straight line is unity in Langmuir isotherm because each inhibitor molecule is adsorbed on an individual active site on the metal surface. Langmuir adsorption isotherm is valid in both physical and chemical adsorption, and it implies the monolayer adsorption of inhibitor molecules on the metal surface without interaction. (Yaro et al., 2013).

El-Awady adsorption isotherm

El-Awady adsorption isotherm is a modified form of Langmuir adsorption isotherm. It is given by the equation [1-4]:

$$\log \frac{\theta}{1-\theta} = \log K_{ads} +\ y\ \log C_{inh} \qquad\qquad [1\text{-}4]$$

Where, C_{inh} is the concentration of inhibitor, θ is the degree of surface coverage by inhibitor, and K_{ads} is adsorption equilibrium constant. Here plot of $log \frac{\theta}{1-\theta}$ vs. log C_{inh} gives a straight line, where the slope is y, which gives the number of inhibitor molecules occupying one active site. If the value of y is greater than one, it indicates the multilayer adsorption of inhibitor on metal. The equilibrium constant can be calculated from the intercept of the straight line. (Karthikaiselvi & Subhashini, 2014)

Temkin adsorption isotherm:

Temkin adsorption isotherm is given by the equation [1-5]:

$$\theta = -\ \frac{2.303\ log K_{ads}}{2a} - \frac{2.303\ log C_{inh}}{2a} \qquad\qquad [1\text{-}5]$$

Where C_{inh} is the concentration of inhibitor, θ is a degree of surface coverage by inhibitor, K_{ads} is adsorption equilibrium constant, and a is an attractive parameter.

Here, a plot of C_{inh} vs. θ gives a straight line, where the slope is $-\frac{2.303}{2a}$. The equilibrium constant can be computed from intercept, which is $-\frac{2.303\ log K_{ads}}{2a}$. (Nwabanne & Okafor, 2012). Temkin isotherm is chemisorption and monolayer's feature with the interaction of uncharged molecules on a heterogeneous surface. The negative value of a is the indication of the existence of repulsive interaction among the molecules in the metal surface.

Freundlich adsorption isotherm:

Freundlich adsorption isotherm is given by the equation [1-6]:

$$\log\theta = \log k_{ads} + n\ \log C_{inh} \hspace{2cm} [1\text{-}6]$$

Where, $\theta < n < 1$, C_{inh} is the concentration of inhibitor, θ is the degree of surface coverage by inhibitor, K_{ads} is adsorption equilibrium constant, and n is related to adsorption intensity.

Here, a plot of $\log\theta$ vs. $\log C_{inh}$ gives a straight line. The equilibrium constant can be computed from the intercept of the plot, and slope gives the adsorption intensity, n. The value of n depends upon the heterogeneity of the metal. The typical value of n is 0.6 at 301K.

Flory-Huggins adsorption isotherm

Flory-Huggins adsorption isotherm is given by the equation [1-7]:

$$\log\frac{\theta}{C_{inh}} = \log K_{ads} + x\ \log\ (1\text{-}\theta) \hspace{2cm} [1\text{-}7]$$

Where, Where, C_{inh} is the concentration of inhibitor, θ is the degree of surface coverage by inhibitor, K_{ads} is adsorption equilibrium constant, and x is size parameter.

Here, a plot of $\log\frac{\theta}{C}$ vs. log (1-θ) gives a straight line where slope, x gives size parameter, and equilibrium constant can be computed from an intercept. The parameter x indicates the number of active sites occupied by one inhibitor molecule or the number of water molecules replaced by one molecule of the inhibitor. If one inhibitor molecule replaces more than one water molecules or occupies more than one active site in the adsorption process, the value of x will be greater than 1 whereas value could be less than one if more than one inhibitor molecules occupy one active site replacing one water molecule in the process. (Adejo et al., 2014)

1.10 Determination of Gibb's free energy of activation:

The value of equilibrium constant (K_{ads}) can be calculated from the slope of the adsorption isotherm plot. The value of free energy of adsorption ($\Delta G°$) can be calculated by using the value of K_{ads} according to equation [1-8].

$$\Delta G° = -\ RT\ \ln(55.5K_{ads}) \hspace{2cm} [1\text{-}8]$$

Where R refers to the universal gas constant (8.314J/mol K), and 55.5 refers to the concentration of water in solution in mol/L. The value of Gibb's free energy of activation (ΔG^o) reveals the mode of adsorption of inhibitor on the metal surface. If the value of ΔG^o is less than -20 kJ/mol, adsorption is physical adsorption, and if the value is more than -40 kJ/mol, adsorption is chemical adsorption. Value of ΔG^o between -20 kJ/mol and -40 kJ/mol, adsorption is mixed adsorption, which involves both physical and chemical adsorption.

1.11 Determination of energy of activation (Ea)

Temperature dependency on corrosion rate (C.R.) is given by Arrhenius equation [1-9] :

$$\log(\text{C.R.}) = \log A - \frac{E_a}{2.303\,RT} \qquad [1\text{-}9]$$

where Ea is the activation energy, A is the Arrhenius pre-exponential constant, T is the absolute temperature.

When log (C.R.) is plotted against $\frac{1}{2.303\,RT}$, a straight line is obtained. The slope of this line is the activation energy, and Arrhenius pre-exponential constant can be computed from the intercept of the line.

1.12 Determination of enthalpy of adsorption and entropy of adsorption:

Entropy and enthalpy of adsorption can be calculated from an alternative form of Arrhenius equation, which is also known as the transition state equation [1-10].

$$log\left[\frac{C.R.}{T}\right] = \left[log\left[\frac{R}{hN}\right] + \frac{\Delta S^*}{2.303\,R} - \frac{\Delta H^*}{2.303\,RT}\right] \qquad [1\text{-}10]$$

Where, ΔH^* represents the enthalpy of adsorption, ΔS^* represents the entropy of adsorption, h refers to plank's constant, 6.6261×10^{-34} Js and, N refers to the Avogadro's number, 6.0225×10^{23} mol^{-1}

When $log\left[\frac{C.R.}{T}\right]$ is plotted against $\frac{1}{2.303\,RT}$, a straight line is obtained. The slope of this line is the enthalpy of activation. The intercept of the line, $\left[log\left[\frac{R}{hN}\right] + \frac{\Delta S^*}{2.303\,R}\right]$ can be used to compute the entropy of activation. The value of enthalpy of activation also suggests the mode of adsorption. The value of ΔH^* less than -40 kJ/mol implies the

physical adsorption whereas value more than 80 kJ/mol is chemical adsorption. If the value of ΔH^* is between 40 kJ/mol and 80 kJ/mol, adsorption is mixed adsorption, which involves both physical and chemical adsorption.

1.13 Factors in applying inhibitors

Factors needed to be considered while applying inhibitors are as follows:

Application techniques:

An inhibitor must be appropriately applied because an efficient inhibitor may not give good results due to improper application. An inhibitor must contain the surface of the entire metal and forms a continuous persistent film. Otherwise, it may be failed to show inhibition property. Failure of the inhibitory property can also be caused by the loss of the inhibitor before it reaches the metal surface. Another reason for the inhibitor's failure is its loss before it changes the environment to the required extent. The efficiency of a volatile inhibitor decreases if it is lost to the outside environment.

Temperature effects:

Temperature is another factor that affects the inhibition efficiency of the inhibitor. An increase in temperature causes desorption of barrier film formed by physical adsorption and decreases efficiency. In such cases, a higher amount of inhibitor is required. On the other hand, chemisorption increases with increases in temperature as it strengthening the coordinate bond. An increase in temperature increases the efficiency of inhibitors that are absorbed by chemisorption. However, at a higher temperature, organic molecules are decomposed, resulting in a decrease in inhibition efficiency. It can be concluded that inhibition due to chemisorption increases until the decomposition of the inhibitor molecule.

Poisoning:

Corrosion inhibitors used for hydrogen damage should inhibit the rate of absorption and permeation of hydrogen into the steel. If inhibitors decrease the hydrogen recombination reaction, hydrogen formed at the surface of steel enters into it, which causes hydrogen damage. For example, thiourea inhibits the steel corrosion in sulphuric acid but decreases the hydrogen recombination reaction with other hydrogen

atoms. So, bubbles of hydrogen do not escape from the system but enter the steel, causing hydrogen damage.

Secondary inhibition:

In acidic solution, the nature of the inhibitors may change over time due to chemical and electrochemical reactions. The inhibition showed by initially added inhibitor is call in primary inhibition, while inhibition due to reaction product is called secondary inhibition. Secondary inhibition may be more or less than primary inhibition, which depends upon the efficiency of the reaction product. For instance, diphenyl sulfoxide produces diphenyl sulfide as a result of the electrochemical reaction, which is more effective than the primary compound (Trabanelli et al., 1967). On the contrary, the reduction product of thiourea and its alkyl derivatives (e.g. methyl, ethyl) produces HS^- that accelerates corrosion.

Synergism and antagonism:

Lateral interaction between two or more adsorbed molecules on metal surface alters the inhibition performance of corrosion inhibitor. If the degree of inhibition due to interaction is higher than the sum of the individual effect of inhibitors, the phenomenon is known as synergism. For example, the Inhibition efficiency of a mixture of furfurlimine and formaldehyde is more than the sum of their effect. On the other hand, the degree of inhibition due to interaction is less than the individual effect of inhibitors, it is called antagonism. For example, inhibition performance of a mixture of narcotine and thiourea is less than their individual performance.

Green inhibition:

Some chemicals are effective inhibitors, but they are toxic and readily absorbed through the skin. The use of such type of inhibitor is hazardous to human beings and the environment. The effective inhibitor should be nontoxic and biodegradable. Such types of inhibitors, which are nontoxic, biodegradable, and no or very less adverse effect to the living beings and environment, are called green inhibitors. Nontoxic inhibitors have at least 60% biodegradation or biological oxygen demand (BOD). The BOD is a measure of the persistence of inhibitors in the environment.

1.14 Natural products as green inhibitors

As the successful inorganic inhibitors have jeopardizing effect on life and environemt, organic compounds are studies as an alternative. Several natural compounds having heteroatoms or multiple bonds in conjugation with the aromatic ring are found effective as well. Some effective inhibitors are synthesized and are being synthesized. Unfortunately, these compounds are also not devoid of limitations. These compounds are expensive as well as they are hazardous during their synthesis and use. A recent development in green chemistry does not allow using such types of chemicals as an inhibitor. This motivates investigators to develop nontoxic, environment-friendly, biodegradable, renewable, and cheap inhibitors. For this regard, natural products such as plant extract, essential oil, etc. obtained from plants could be a good candidate. The molecular and electronic structure of phytochemicals found in plant extracts resembles to that of conventional organic inhibitors. So, researchers are fascinated to investigate natural products as a green corrosion inhibitor. Several investigations proved that plant extract could be an effective corrosion inhibitor. (Alkhathlan et al., 2014)

Plants have been shown as chemical factories able to produce a large number of highly complicated and strange chemical substances with structures that are beyond the imagination of synthetic chemists. Alkaloids, flavonoids, polyphenols, proteins, tannins, glycosides, and carbohydrates are some of the phytochemicals that plants can provide. These hetero phytomolecules have polar functionalities such as nitrogen, sulfur, oxygen atoms, conjugated double bonds, and aromatic rings in their molecular structures, which may adsorb firmly on the surface of metal and prevent metal corrosion efficiently. (Aiad & Negm, 2009). In most cases, conjugated aromatic systems and long aliphatic chains with free electron pairs act synergistically to exhibit good efficiency (Hackerman et al., 1962) .

Plant extract inhibits corrosion efficiently without purifying into pure compounds. They can be obtained easily from readily available, a cheap solvent with low toxicity. Conventional ethanol, methanol, n-hexane extracts are also used. This is why plant extract is a cheap inhibitor (Hackerman et al., 1962).

Several Scientists have propounded many theories regarding the mode of action of the green inhibitors. Mann had suggested that onium ions are formed due to protonation in organic molecules in acidic solutions which are adsorbed on the cathodic sites of the metal interfering with cathodic reaction. With the increasing number of ongoing research for discovering various novel natural products as green inhibitors, several theories regarding the corrosion inhibition property of such inhibitors have been postulated (Rani & Basu, 2012).

1.15 Stability of inhibitors

In general, inhibitors must be stable in the environment, such as aggressive solutions, working temperatures, to be more productive. The adsorbed inhibitor molecule should not decompose at an aggressive solution or at a higher temperature. Decomposition of adsorbed compound or chelate formed at a higher temperature may lead to an inhibitor's desorption, and it fails to show excellent efficiency at a higher temperature. However, in some cases, the new product formed due to decomposition shows good efficiency. In these cases, the inhibitor is valid even after their decomposition due to their secondary inhibition.

1.16 Industrial application of inhibitors

Corrosion inhibitors are applied widely in industries to protect material. According to a recent analysis by Grand View Research, Inc., the global corrosion inhibitors market was valued at US$7.4 billion in 2019 and is predicted to increase at a compound annual growth rate (CAGE) of 3.8 percent to reach US$9.9 billion by 2027.(Grand View Research, 2020) This is evidence to show that the use of inhibitors is increasing every day. Some applications of corrosion inhibitors in industries are discussed here.

Petroleum productions:

Corrosion in petroleum industries is classified into two types; wet and dry corrosion. Wet corrosion is due to the presence of an aqueous phase, which occurs at low temperatures, generally below the boiling point of water. Temperature, pressure, and compositions of aqueous, gaseous, and oil phases are the factors affecting the wet corrosion. In refineries and petrochemical plants, corrosivity is high even at a small amount of water because it is localized at the region of metal in contact with the aqueous phase. Water may contain dissolved carbon dioxide, hydrogen sulfide,

chloride, and even 0.1% of such water content may cause corrosion. On the other hand, dry corrosion generally occurs at higher temperatures above the boiling point of water in the lack of an aqueous phase. Film-forming organic inhibitors are used as an inhibitor in most of the refinery and petroleum plants. Mostly, they use long-chain nitrogenous organic compounds such as amines and amides. They form film due to their attraction with the metal surface through the polar end, whereas nonpolar end jutted upright. On this nonpolar end, hydrocarbons of petroleum are adsorbed physically to increase the film's thickness and enhance the efficiency of the inhibitor.

Similarly, the internal corrosion of pipelines during fluid flow is also a problem in petroleum industries. Erosion-corrosion and pitting corrosion are common inside pipelines at high and low flow rates, respectively. This type of corrosion can be controlled by pigging (Cleaning) or by adding inhibitors such as sulphonated oils, sodium nitrite etc.

Water:

For many industries, water is used in a cooling system where the primary cause of cooling is evaporation. When evaporation occurs, several dissimilar metals and non-metals are deposited in the cooling system, which leads to galvanic corrosion. Such type of corrosion can be controlled by cathodic inhibitors such as zinc salt or anodic inhibitors such as nitrate and chromate or organic inhibitors such as benzotriazole, which inhibits by secondary inhibition.

Similarly, drinking water is also corrosive due to dissolved oxygen. The corrosive nature of drinking water can be controlled by using cathodic inhibitors like calcium carbonate, silicates, polyphospates, and zinc salts.

Automobile:

Automobiles are suffered by two types of corrosion, internal and external corrosion. Internal corrosion is due to the corrosivity of the fluid system. Anodic inhibitors such as nitrites, nitrate, phosphates, silicates, arsenates, chromates, or mixed inhibitors such as amines, benzoates, mercaptans, organic phosphates or film formers such as polar or emulsifiable oils can be dissolved in antifreeze to control this corrosion. External corrosion is due to the exposure of the metal surface to the atmosphere containing

34

moist air, SO_2 gas, and deicing salt such as NaCl, $CaCl_2$. This type of external corrosion can be controlled by the rustproofing formulations containing grease, wax-resin, and resin-emulsion, along with metalorganic and asphaltic compounds. Fatty acids, phosphonates, sulphonates, carboxylated, etc. are commonly used inhibitors in rustproofing applications.

Acid:

Acid is used widely in many industrial processes such as acid pickling, descaling, cleaning of the boiler, in the cleaning of oil refinery equipment and heat exchangers, and an oil well acidizing. The dissolution of base metal in aggressive acid media is the problem in these processes. Mixed inhibitors are used to control this type of corrosion. For example: thiourea and amino and its derivatives, propargyl alcohol are used to control corrosion during acid pickling(Gentil, 2003). Ammonia, Cyclohexylamine, alkanol and Morpholine are used as inhibitors in boilers in various processes.

Paints (Organic coatings):

Finely divided inhibiting pigments such as red lead, lead azelate, calcium plumbate, lead suboxide are added in the printer in organic coatings. They inhibit corrosion as well as preserve the physical properties of paints.

Concrete: Corrosion inhibitors such as phosphate ion are mixed with cement or concrete paste to improve the durability of reinforced concrete structures.

Miscellaneous:

Corrosion is protected by the use of inhibitors in fuel oil tanks, hot chloride dye baths, refrigeration brines, artifacts, etc.

1.17 Corrosion monitoring

The corrosion monitoring process is carried out to evaluate and monitor the equipment components, structure, process unit, and facilities for signs of corrosion. Aim of monitoring is to identify specific conditions to extend asset life, reliability, and durability, which increases safety and reduces corrosion cost. Monitoring determines the trends and processing parameters that may induce a corrosive environment and detects the early corrosion warning signs. It also determines the efficiency of

corrosion prevention methods. The process includes monitoring of all forms of materials and corrosion. A strong corrosion monitoring program should be done at specific intervals to reduce maintenance costs, improve safety, and efficiency.

There are several methods of corrosion monitoring. Some of them are listed as follows:

a. Direct corrosion monitoring methods:
  i)   Weight loss method
  ii)   Faraday's equation for monitoring corrosion rate
  iii)   Tafel extrapolation method
  iv)   Linear polarization resistance method
  v)   Electric resistance method
  vi)   Electrochemical impedance spectroscopy

b. Indirect corrosion monitoring methods:
  i)   Corrosion (open circuit) potential method.
  ii)   Hydrogen monitoring method.

Some of these techniques are widely used monitoring techniques which are discussed below:

1.17.1 Weight loss method:

The weight-loss method is widely used and easiest and low-cost corrosion monitoring techniques. It is used to determine the corrosion rate as well as surface coverage and corrosion inhibition efficiency of organic coatings. In this technique, a small coupon of known weight and surface area is exposed to a corrosive environment. After elapsing a specific time, it is removed from the environment, followed by the removal of corrosion products from the surface of the coupon. The difference in initial and final weights is the mass loss due to corrosion from which corrosion rate, surface coverage, and inhibition efficiency can be calculated by using equations [1-11, 1-12, 1-13].

$$CR = \frac{87.6W}{AtD} \qquad\qquad [1\text{-}11]$$

36

Where W is weight loss (mg) of MS coupon, A is surface area (cm^2) of the coupon, t is time (h) of immersion, and D is density (g/cm^3) of MS. The relation given below can be used to estimate surface coverage (θ):

$$\theta = \frac{W_1 - W_2}{W_1} \qquad\qquad [1\text{-}12]$$

Where, W1 and W2 represent the weight loss of metal with and without inhibitor, respectively. The inhibition efficiency can then be estimated as:

$$IE\% = \left(\frac{W_1 - W_2}{W_1}\right) \times 100 \qquad\qquad [1\text{-}13]$$

1.17.2 Open circuit potential (OCP):

Open circuit potential is known as the potential developed on a working electrode relative to the reference electrode when there is no current or potential existing in the cell. It is also known as open-circuit voltage (OCV), rest potential, equilibrium potential, or corrosion potential. Measurement of OCP vs. time provides a significant idea to evaluate the corrosion performance of the organic coatings. OCP provides information on whether the electrochemical system is stable or not. A constant OCP or fluctuation by ± 5 mV or less for a minute or more implies that the system is stable enough for a perturbation-based experiment. OCP is measured as a voltage between the working electrode and the reference electrode. Measurement of OCP requires voltmeter with high input impedance such as electrometer to measure the voltage with no current or voltage applied to the cell.

The measurement of OCP can give the information about;
- Data for corrosion monitoring in a plant.
- Information on the free corrosion potential as the starting point of the electrochemical methods.
- Data for control potential before electrochemical measurements.
- A method for determining whether the corrosion system is in the active or the passive state (Khamis & Al-Andis, 2002).

1.17.3 Potentiodynamic polarization (Tafel extrapolation) method:

Potentiodynamic polarization measurement is one of the commonly used DC electrochemical methods used for laboratory corrosion testing. It is an easy and quick determining process for the evaluation of corrosion current, corrosion potential, corrosion rate, and efficiency of corrosion protection. This technique can provide valuable information about the mechanism of corrosion and the vulnerability of different corrosion materials in specified environments. The potentiodynamic polarization technique involves varying the potential of the working electrode in a wide range at a selected rate and monitoring the current produced as a function of time or potential (Pierre, 2008). The variation in potential brings about oxidation or reduction reaction on the electrode surface, depending upon the direction of polarization to produce current. In other words, Potentiodynamic polarization involves the characterization of the sample by its current- potential relationship. The current response is measured as the potential is shifted away from the corrosion potential. A three-electrode corrosion system is used to polarize the electrode of interest.

When the potential is changed into a more positive direction than corrosion potential in the polarization, the working electrode becomes the anode, and the polarization is known as anodic polarization. In anodic polarization, the working electrode loses electrons. Similarly, the potential is changed into a more negative direction than corrosion potential in cathodic polarization. The working electrode becomes cathode in cathodic polarization and gains electrons and sometimes accompanied by electrodeposition. If both cathodic and anodic polarization is performed in a cyclic manner, it is called cyclic polarization

The most frequently used law in the field of electrochemistry is due to Tafel. Tafel's law states that the logarithm of the current density in an electrochemical reaction varies linearly with the electrode potential (at potentials removed from the open-circuit rest potential). (McCafferty, 2005)

Electrochemistry of corrosion of metals or alloy involves two or more half-cell equations. For example, half-cell equations in corrosion of metal in acidic media involve oxidation of metal and reduction of H^+ ion, represented as follows:

$$M \longrightarrow M^{n+} + ne^-$$

$$nH^+ + ne^- \longrightarrow \frac{n}{2}H_2$$
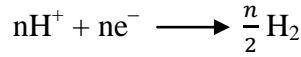
For a single electrode reaction, relation of the net current density,I, to the electrode potential, E is expressed by Butler-Volmer equation [1-14]

$$I = I_0[e^{\alpha nF(E-E_0)/RT} - e^{-(1-\alpha)nF(E-E_{0r})/RT}] \qquad [1-14]$$

Where, I_0 = exchange current density (rate of half-cell reaction) at the equilibrium potential E_0, a = transfer coefficient (usually 0.5), n = number of electrons transferred

Wagner and Traud have given a detailed analysis of uniform corrosion based on the principles of superposition of partial current-voltage curves of partial half-cell reactions in 1938 in their paper on mixed potential theory. (Paper Wagner and Traud) The net measured current (i_m) for a corrosion system at equilibrium is zero because of equal cathodic and anodic rate.

$$i_m = i_{red} - i_{oxd} = 0 \qquad [1-15]$$

When a metal is in contact with a solution, it will assume a potential independent of the metal and the nature of the solution. This potential is known as open circuit potential or corrosion potential, E_{corr}. Electrochemically, the corrosion rate is based on the determination of I_{corr}, which is the net rate of either metal dissolution or hydrogen evolution at E_{corr} at the freely corroding condition. For such condition, Butler-Volmer equation can be modified as,

$$I = I_{corr}[e^{\alpha nF(E-E_{corr})/RT} - e^{-(1-\alpha)nF(E-E_{corr})/RT}] \qquad [1-16]$$

When the rate of back reaction is negligible, Eq. [1-16] gives:

$$E = a + b \log I \qquad [1-17]$$

where a and b are constants. Eq. [1.17] is Tafel's law. Moreover, in Eq. [1-16], when E = E_{corr} then

I = I_{corr}. This is the basis for the Tafel extrapolation.

On polarizing the specimen with the application of current in both the anodic and cathodic directions, the experimental polarization curve originates at E_{corr} and high current densities become linear on a semi-logarithmic plot. The presentation of the potential in current density (I) or (logI) functions for each measured point results in obtaining the polarization curve, which usually consists of two diverging logarithmic

plot lines representing anodic and cathodic currents. Extrapolation is performed by extending the linear portions of the anodic and cathodic plots back to their intersection. These two lines eventually intersect the Ecorr horizontal at the point that corresponds to I_{corr}, which is shown in figure 1.10. After finding the value of I_{corr}, it can be used to evaluate the corrosion inhibition efficiency of inhibitors. (Bouyanzer et al., 2006)

$$IE\% = \frac{I_{corr}^0 - I_{corr}}{I_{corr}^0} \times 100\% \qquad\qquad [1\text{-}18]$$

Where I_{Corr} and I_{corr}^0 are corrosion current densities in the presence and absence of inhibitor.

Additionally, Tafel extrapolation helps to find E_{corr}, cathodic, and anodic slope. Value of Ecorr, implies the type of inhibitor, whether it is a cathodic, anodic, or mixed inhibitor. Change in cathodic anodic slope indicates the effect of the inhibitor on the mechanism of corrosion.

The Tafel extrapolation can be used to determine the corrosion rate when metal is immersed in the de-aerated acid solution, and metal dissolution is activation controlled. In de-aerated solution, the cathodic reaction is limited to the reduction of hydrogen ion only without involving the reduction of oxygen. In such conditions, oxide films initially present on the metal surface are dissolved by the acid solution while attaining the steady-state, open-circuit potential. Thus, the sole anodic reaction is the dissolution of the bare metal surface.

The Tafel extrapolation method is valid in the following conditions, when:
a. Both the anodic and cathodic branches of the polarization curves are under activation control.
b. Well-define anodic and cathodic Tafel regions exist.
c. The anodic and cathodic reactions that occur at the corrosion potential are also the only reactions during the determination of the polarization curves.
d. Corrosion is uniform in nature, and localized corrosion does not occur (Chetouani et al., 2004).

The corrosion rate can also be determined by Tafel extrapolation of either the cathodic or the anodic polarization curve alone as shown in Fig. 1.10. If only one polarization

curve is used, it is generally the cathodic curve, which usually produces a longer and better define Tafel region.
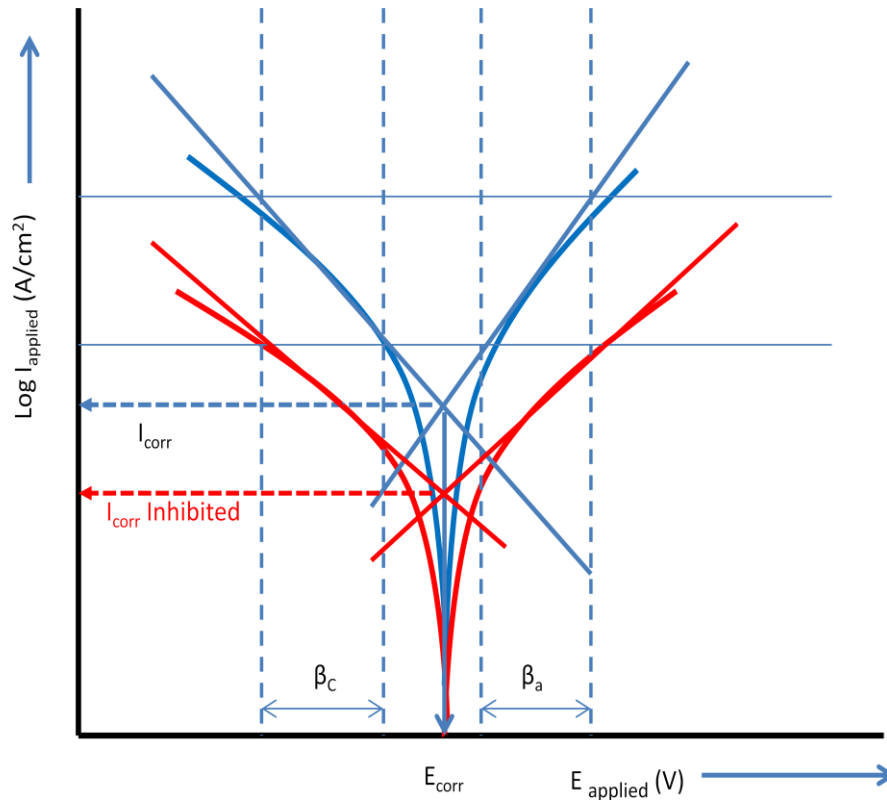
Figure 1.10 : Tafel extrapolation method for determination of Tafel parameter.

1.17.4 Linear polarization resistance:

Corrosion monitoring by measuring linear polarization resistance is quick and reliable technique and has been used in industry for more than half a century. In this technique, a potential of $\pm$ 25 mV of corrosion potential is applied between the electrodes, and the resulting current is measured. Anodic and cathodic reactions are exponentially dependent upon the applied potential as both reactions occur near to the corrosion potential. As potential is applied in small range, the exponentials are linearized and current-potential relationship is approximately linear as shown in Fig. 1.11. Applying Ohm's law, polarization resistance (R_p) is defined as the slope of a potential (E) vs current density plot. As the polarization resistance is calculated from approximately linear curve, it is called liner polarization resistance (LPR).

$$R_p = LPR = \frac{\Delta E}{\Delta I}$$
[1-19]

After obtained linear polarization resistance, it is used to calculate inhibition efficiency as shown in equation [1-20].

$$IE = \frac{LPR - LPR^o}{LPR} \times 100 \qquad\qquad \text{[1-20]}$$

Where, LPR and LPR° are linear polarization resistance in presence and absence of inhibitor.

As the application of potential perturbation is in small range, this method can be applied to measure corrosion rate non-destructively.
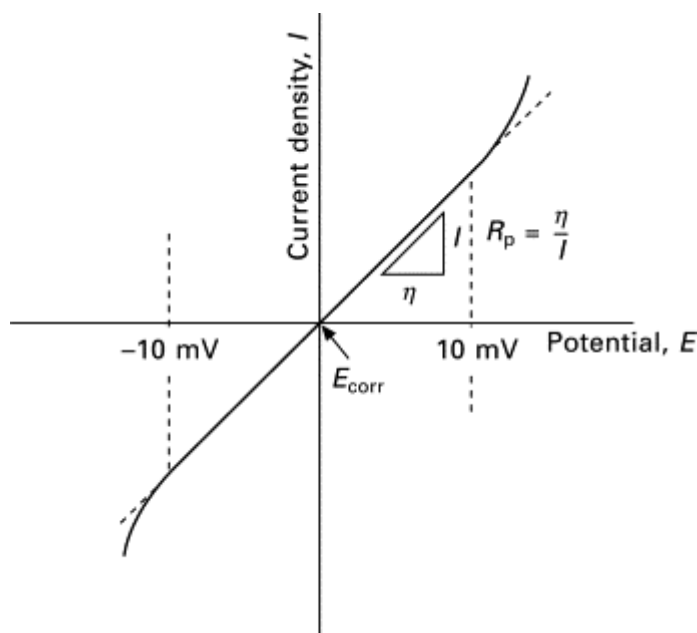
Figure 1.11 : Linear polarization method for determination of corrosion rate.

1.17.5 Electrochemical impedance spectroscopy (EIS) technique

Electrochemical impedance spectroscopy (EIS) is the most promising AC electrochemical technique for the investigation of the corrosion system, which involves AC impedance measurement. It is a multifrequency AC electrochemical measurement technique that measures the electrical resistive and capacitive characteristics of the metal/solution interface over a wide range of frequencies. Results obtained from EIS can be used to determine the solution resistance (Rs), Charge transfer resistance (Rct), and double-layer capacitance (Cdl) using curve fitting software.

EIS provides kinetic and mechanistic information of corrosion when AC impedance is applied to the electrochemical system. It can be applied in the field of corrosion for rate determination, inhibitor performance, coating performance, and passive layer characteristics. The power of EIS lies in the fact that it is essentially a steady-state

technique that is capable of accessing the relaxation phenomenon whose relaxation times vary over many orders of magnitude. Epelboin et al. (Zhang & Lyon, 1994), was the first to apply the impedance method to the measurement of corrosion rate, and Haruyama (Muto et al., 1994) developed the mathematical analysis of the impedance of mixed potential electrodes.

EIS technique has advantages over potentiodynamic polarization technique due to the following reasons:

   a. Minimal excitation amplitude (in the rage of 5-10 mV) used in EIS perturb the electrochemical test system to a minimum extent. So, errors caused due to the technique itself are less in EIS.
   b. EIS provides valuable mechanistic information because it provides data on both electrode capacitance and charges transfer kinetics.
   c. A potential scan is not done in EIS so that it can be applied to a low conductivity solution. (Sastri, 2011)

Electrochemical impedance is usually measured by applying an AC potential to an electrochemical cell and measuring the current through the cell. A small excitation signal is applied so that the cell's response is pseudo-linear. The response to this potential is an AC current signal, containing the excitation frequency and its harmonics.

In a linear (or pseudo-linear) system, the current response to a sinusoidal potential will be a sinusoid at the same frequency but shifted in phase. The excitation signal, expressed as a function of time, has the form

$$E(t) = E_0 \cos(\omega t) \qquad\qquad [1\text{-}21]$$

$E(t)$ is the potential at time t, E_0 is the amplitude of the signal, and ω is the radial frequency ($\omega = 2\pi f$). In a linear system, the response signal, I_t, is shifted in phase (θ) and has a different amplitude, I_0:

$$I(t) = I_0 \cos(\omega t - \theta) \qquad\qquad [1\text{-}22]$$

An expression analogous to Ohm's Law allows one to calculate the impedance of the system as:

$$Z = \frac{E(t)}{I(t)} = \frac{E_0 \cos(\omega t)}{I_0 \cos(\omega t - \theta)} = Z_0 \frac{\cos(\omega t)}{\cos(\omega t - \theta)} \qquad \text{[1-23]}$$

Therefore, the impedance is expressed in terms of magnitude, Z_0, and a phase shift, θ.

The impedance of an electrochemical interface is a complex number, which can be represented either in polar coordinates or in Cartesian coordinates:

$$Z(\omega) = \mathrm{IZI}\, e^{j\theta} \qquad \text{[1-24]}$$

$$Z(\omega) = Z' + j\, Z'' \qquad \text{[1-25]}$$

where IZI is the impedance modulus, $j = \sqrt{-1}$, Z' and Z" are the real and imaginary part of the impedance related to the magnitude of the impedance and phase by

$$|Z(\omega)| = \sqrt{(Z')^2 + (Z'')^2} \qquad \text{[1-26]}$$

$$\tan\theta = \frac{Z''}{Z'} \qquad \text{[1-27]}$$

$$|Z|\cos\theta = Z' \qquad \text{[1-28]}$$

$$|Z|\sin\theta = Z'' \qquad \text{[1-29]}$$

The equivalent mathematical forms of the complex impedance given by equations [1-23] and [1-24] lead directly to the two common methods for displaying impedance data, as Z" versus Z' (Nyquist or complex plane) and as log IZI and θ versus log ω (Bode plane).

The corrosion of metals is an electrochemical process. However, there are no electrochemical methods to measure the corrosion rate directly. They depend on a certain number of hypotheses. In usual practice, polarization resistance is obtained from the impedance method, which is related to the corrosion rate by an inverse proportionality relationship according to Stern & Geary (1957),

$$i_{\mathrm{corr}} = k\, R_{\mathrm{p}}^{-1} \qquad \text{[1-30]}$$

Here k is a proportional constant whose value depends on the Tafel slopes.

An equivalent circuit that represents the electrochemical system under study is elucidated form the EIS results for the metal in the given environment. Fig. 1.12 represents a simple equivalent circuit representing an electrode-solution interface. This equivalent circuit model is used to fit the impedance spectra using curve fitting software. The Constant phase element (CPE) is used in the circuit model to take into account the electrode surface non-homogeneity caused by surface roughness, inhibitors adsorption, dislocations, grain boundaries, and the creation of a porous layer in corrosion of metal in aggressive acidic media.
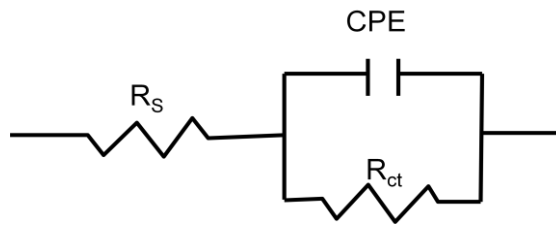
Figure 1.12 : The equivalent circuit model used to fit the EIS data**.**

The impedance of CPE is described by equation [1-31]

$$Z_{CPE} = Y_0^{-1}(j\omega)^{-n} \qquad [1\text{-}31]$$

Where Y_0 is the magnitude of the CPE, j is the imaginary number ($j^2 = -1$), ω is angular frequency ($\omega = 2\pi f$), and n is the CPE exponent ($-1 \leq n \leq +1$), whose value is used to evaluate the surface's non-homogeneity or roughness. The CPE depicts a pure resistor when n=0, an inductor when n=-1, and a pure capacitor when n=+1.

Analysis of change in electrochemical parameters such as solution resistance (R_s), Charge transfer resistance (R_{ct}), and double-layer capacitance (C_{dl}) obtained from software reveal the properties of the electrode interface, mechanisms involved in the corrosion, effect and inhibition efficiency of inhibitor. For example, increment in phase angle in the Bode-phase plot, the value of impedance at low frequencies in the Bode-modulus plot, and the capacitive loop diameter in the Nyquist plot by using inhibitor reveal the adsorption of inhibitor molecules on the metal surface and extent of increment implies its effectiveness. Once the value of Charge transfer resistance is obtained from curve fitting software, the inhibition efficiency of corrosion inhibitor can be calculated by the equation [1-32].

$$IE\% = \frac{R_{ct} - R_{ct}^0}{R_{ct}} \times 100\% \qquad [1\text{-}32]$$

Where R_{ct}^0 and R_{ct} indicate charge transfer resistances of acid solution with and without inhibitor.
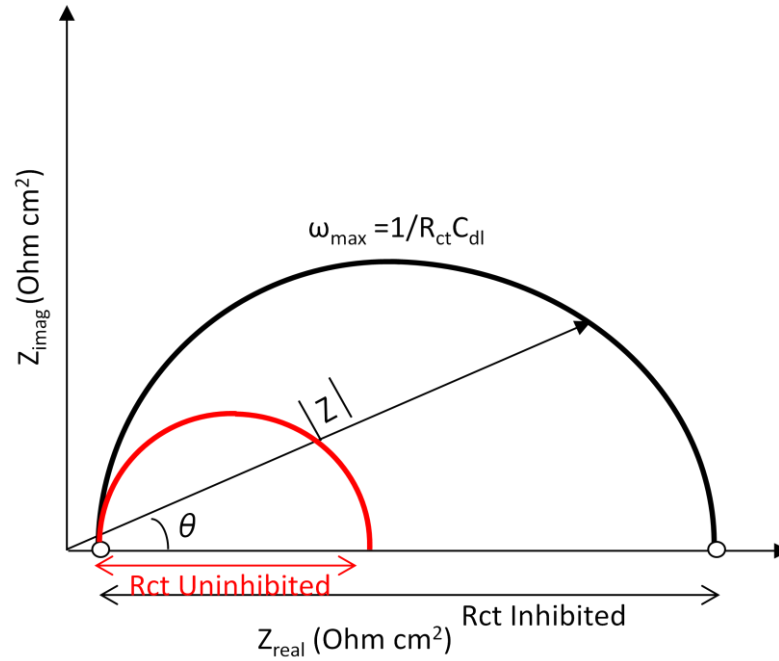
Figure 1.13 : Nyquist plot.

Similarly, double layer capacitance can be computed by the equation [1-33].

$$C_{dl} = \frac{1}{2\pi R_{ct} f_{max}}$$ [1-33]

Where the frequency at which the maximal imaginary component of the impedance is achieved is denoted by fmax. A decrease of C_{dl} value can be ascribed to the increase in the thickness of the electric double layer or the decrease in the local dielectric constant due to the adsorption of inhibitor molecules to the metal surface. The relation of thickness, dielectric constant with C_{dl} is expressed in equation [1-34].

$$\delta_{org} = \frac{\varepsilon_0 \varepsilon_r A}{C_{dl}}$$ [1-34]

Where δ_{org} represents the thickness of the protective layer, ε_0 represents the dielectric constant, ε_r represents the relative dielectric constant, and A is surface area.

Relaxation time (τ) is the time taken for the charge distribution to restore to equilibrium following an electrical disruption. Mathematically, relaxation time is the product of double-layer capacitance and charge transfer resistance if there is no disturbance introduced to replace the C_{dl}.

46

$$\tau = C_{dl}R_{ct} = \frac{1}{2\pi f_{max}}$$ [1-35]

Finally the effect of inhibitor concentration is evaluated from the the relationships between the concentration of an inhibitor and the corrosion rate as shown in Fig. 1.14. Similarly, the degree of inhibition resulting from the concentration effect of inhibitor molecules is shown in Fig. 1.15. These relationships resemble adsorption isotherms and tell that small concentrations of the inhibitor are effectively bringing the corrosion rate to an acceptable level. A corrosion inhibitor should not only mitigate corrosion but also be compatible with the environment.
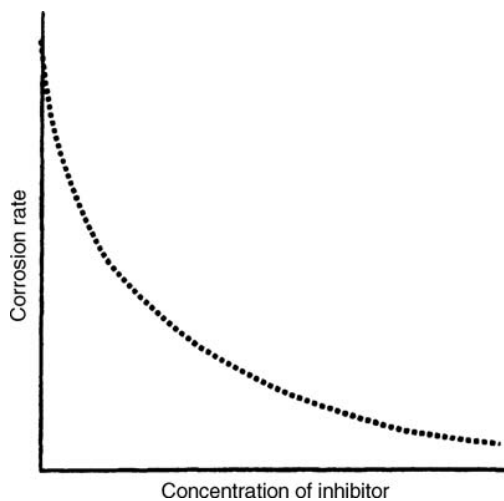
Figure 1.14 : Relationship between corrosion rate and concentration of inhibitor.
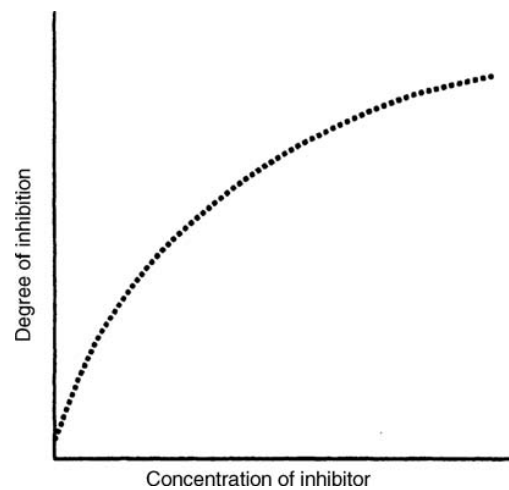
Figure 1.15 : Relationship showing the effect of concentration of inhibitor on the degree of inhibition.

1.18 Rationale

The use of corrosion inhibitors is an efficient and cost effective practice to inhibit corrosion for many alloy systems, including aluminum, zinc, and steel, in a wide range of aqueous environments. However, due to increased environmental concerns and legislation limiting (Trabelsi et al., 2005), the use of traditional inhibitors due to their jeopardizing effect to humans and nature during their preparation and use. Therefore, there is a need to develop alternative coatings corrosion susceptible materials, which are more environmentally friendly and are less toxic. Thus, in recent years, much research has been carried out in trying to fulfill this demand. One strategy is to search for green corrosion inhibitors from natural product extracts. Nepal is

blessed with high altitude plants that have yet to be investigated for corrosion inhibiting properties of their extracts. High altitude plants of Nepal have potent to be corrosion inhibitors. This work is dedicated to developing eco-friends inhibitor from natural products obtained from Nepal's plants as a green corrosion inhibitor.

1.19 Objective of the study

General objective

The general objective of this thesis is to develop green corrosion inhibitors from natural products of Nepal.

Specific Objectives

The specific objectives are highlighted as:

* ❖ To extract the plant and to analyze the extracts by FTIR.
* ❖ To study inhibition efficiency of extracts by electrochemical methods such as potentiodynamic polarization, electrochemical impedance spectroscopy (EIS) and differential pulse voltammetry (DPV).
* ❖ To study the effect of inhibitor concentration, temperature, and time of exposure on the inhibition efficiency by weight-loss method.
* ❖ To discuss the adsorption isotherm, thermodynamic and kinetic parameters of inhibition process.
* ❖ To characterize the surface of metal sample immersed in an acid solution in the presence and absence of inhibitor by SEM, EDS
* ❖ To discuss the inhibition mechanism involved in the protection of mild steel from acid corrosion attack.

CHAPTER 2

2. LITERATURE REVIEW

The use of corrosion inhibitor is one of the best methods among other methods for corrosion control such as barrier protection, galvanization, and cathodic protection (Li et al., 2014) because inhibitors are cheaper as well as they have more inhibition efficiency. There are several industrial and commercial applications of inhibitors such as refinery units, pipelines, cooling systems, boiler, concrete structures, paints, lubricants, chemical and petroleum production units, pipelines, etc.(Sanyal, 1981). There is a remarkable history behind corrosion prevention or control by the use of corrosion inhibitors. The first patent in corrosion inhibition was given to Baldwin, British patent 2327 (El-Meligi, 2010). Since the early nineteenth century, there has been evidence of the use of inhibitors. In fact, inhibitors were already used to protect metal against aggressive water, acidified oil wells, and cooling systems and in-process such as acid pickling. As an example of the application of electrochemistry to evaluate corrosion inhibitors, substantial improvements in the development of technology for corrosion inhibitors have occurred since the 1950s and 1960s. Inhibitors have long been used in industry due to their outstanding anticorrosive properties. The most widely used inhibitors were chromate, nitrite, molybdate, phosphate, and silicates. Owing to toxic effects, some popular industrial inhibitors such as chromate, phosphate and arsenate are restricted for its use by international laws as inhibitors these days. Hence substitute for these needs to be discovered with similar anticorrosive properties. (Znini et al., 2012).

Several research works were carried out to study organic compounds as corrosion inhibitors as an alternative to toxic inorganic inhibitors. Organic compounds having heteroatoms such as nitrogen, sulphur, oxygen in conjugation with aromatic rings, or multiple bonds are found effective as well. At present, several organic inhibitors belonging to different chemical families such as Schiff base, Mannich base, triazoles, mercaptobenzothiazole, carboxamide, fatty amides, pyridines, imidazolines, azodyes, 1,3-azoles, and polymers have shown excellent performance as corrosion inhibitors.

Several research works have been carried out to study the inhibition efficiency of organic compounds. Polymeric compounds are also investigated and found as

effective corrosion inhibitors. Synthesis of some compounds and polymers is done for the study. It is reported by several researchers that synthesized Shiff bases have significant inhibition efficiency. Shahabi et al., (2015) synthesized two Schiff bases as effective inhibitors for carbon steel in acidic media. Asegbeloyin et al. (2015) and Al-Amiery et al. (2014) separately prepared two Schiff bases and found effective for mild steel in acidic medium. Murmu et al. (2019) studied the inhibitive behavior of double azomethine based Schiff base on mild steel in acid medium experimentally with density functional theory and molecular dynamics simulation study. Yurt et al. (2004) examined four Schiff bases as acid corrosion inhibitors for carbon steel. Bedair et al. (2017) synthesized some surfactants based on azodye and Schiff base and investigated corrosion inhibition properties for steel in the acid medium by electrochemical and quantum chemical studies.

Investigations show that few synthetic drugs and dyes also show the inhibition efficiency. Biotin (Xu et al., 2017), streptomycin (Shukla & Ebenso, 2011), cefixime (Naqvi et al., 2011), ampicilin (Eddy et al., 2010), sparfloxacin (Eddy et al., 2008) and ceftazidime (Singh et al., 2011) were studied as corrosion inhibitor for mild steel in acidic media. (Sivakumar et al., 2018) studied the inhibition efficiency of colocid dye for mild steel corrosion in acid media. Verma et al. (2016) investigated the inhibition efficiency of three Bis (indolyl) methanes (BIMs) on the mild steel corrosion in acid media. Ahamad et al. (2010) found four Mannich bases of isatin derivatives are effective corrosion inhibitors for mild steel in acidic media. Yüce & Kardaş, (2012) investigated the inhibition properties of 2-thiohydantoin on mild steel in acid media. . The inhibition properties of 2-mercaptobenzothiazole on copper surface in acidic media were studied by Wu et al in 2020 (Wu et al., 2020). Sadeghi Erami et al. (2019) investigated the inhibition efficiency of carboxamide derivatives as corrosion inhibitor for mild steel in acid media.

John et al. (2017) tested two N(4)-substituted thiosemicarbazones and found them as corrosion inhibitors for mild steel in acidic media. Karthikaiselvi & Subhashini (2014) studied inhibition efficiency of poly (vinyl alcohol-o-methoxy aniline) PVAMOA in acidic media for corrosion inhibition of mild steel. Rahiman & Sethumanickam (2017) carried out a synthesis of water soluble conducting polymer composite poly(vinyl

alcoholcysteine) [PVAC] and found it a corrosion inhibitor for mild steel acidic medium.

Ma et al. (2017) found 1,2,3 triazole derivatives as corrosion inhibitor for mild steel in acidic medium. Li et al. (2008) investigated the inhibition behavior of three S-triazole-triazole derivatives for mild steel in acidic medium. Similarly, Desai & Indorwala (2015) found benzotriazole and benzyl benzotriazole as a corrosion inhibitor for mild steel in acidic media. Tebbji et al studied the inhibitive effect of bipyrazolic derivatives for the protection of mild steel corrosion in acid solution (Tebbji et al., 2005). Morad & El-Dean (2006) studied 2,2'-dithiobis (3-cyano-4,6-dimethylpyridine) as a new candidate of acid corrosion inhibitors for mild steel.

Few organic compounds were studied as eco-friendly green corrosion inhibitors. Verma et al. (2015) synthesized three 2-Aminobenzene-1,3-dicarbonitriles compounds and studied them as effective green corrosion inhibitors for mild steel in acidic media. Fernandes et al. (2019) carried out the green synthesis of 1-benzyl-4-phenyl-1 H-1,2,3-traizole and found it applicable for corrosion inhibition of mild steel in acidic medium. Awad (2006) studies quinine as an eco-friendly inhibitor for carbon steel in acid media. Verma & Quraishi (2007) studied three Schiff bases of glutamic acid and aldehydes as a green corrosion inhibitor for mild steel in acid media.

Several other studies establish the fact that organic compounds are effective inhibitors, they also have limitations. They are hazardous to human beings and the environment during their synthesis and use. Few organic compounds are found eco-friendly green inhibitors but their usage is limited for not being cost-effective (Arab & Noor, 1993; Bentiss et al., 2000; Znini et al., 2012). So, researchers are provoked to develop an alternative inhibitor that should be eco-friendly and cheap. Many research works have proved that natural products such as plant extract or essential oils could be promising candidates as alternatives. Natural products with large organic molecules such as alkaloids, flavonoids, polyphenol, terpenoids, and carbohydrate proteins are similar in molecular and electronic structures to conventional organic compounds (Oguzie et al., 2010). These phytochemicals contain heteroatoms with aromatic rings and multiple bonds and can function as a corrosion inhibitor. Plant extracts could be nontoxic, environmentally acceptable, biodegradable, renewable, readily available,

and cheap inhibitor that can be used to replace toxic and expensive inhibitors. (Hamdy & El-Gendy, 2013; Mourya et al., 2014; Oguzie et al., 2010; Ostovari et al., 2009)

The first evidence of natural products used as corrosion inhibitors was in 1930 when extracts of *Chelidonium majus* (Celandine) and other plants were used for the first time in H_2SO_4 pickling baths (Sanyal, 1981). However, environmentally acceptable green inhibitors were investigated mostly after1970s. Since then, the investigation quality has improved, with the focus shifting from finding a new, effective inhibitor for metallic corrosion to elucidating inhibition mechanism through discussions of electrochemical experiment and surface analysis data, as well as the use of inhibitor physical and chemical properties. For discussing the mechanism of corrosion inhibition, the linear free energy relationship, the hard and soft acids and bases concept, and quantum chemical calculations were introduced. (Aramaki, 2004).

Significant numbers of workd have been done to develop eco-friendly corrosion inhibitors, and still, lots of ongoing researches are aiming to develop green inhibitors. There are research works on natural products, like plant extracts, essential oils, and isolated compounds in order to obtain eco-friendly corrosion inhibitors (El Bribri et al., 2013).

In recent years, plant extract for the best alternative of corrosion inhibitor has been sought out by almost all researchers and scientists. Numerous studies regarding this potentiality of plant extracts have already been carried out. Many have successfully devised that certain plant extracts are effective only for particular metal or alloys. However, incessant researches are still being followed day by day for the universal plant extract.

Srivastava & Srivastava (1981) reported that tobacco, black pepper, castor oil seeds, acacia gum, and lignin could be good steel inhibitors in acid medium. Saleh et al. (1982) found that *Opuntia* extract, *Aloe vera* leaves, orange, and mango peels give adequate protection to steel in 5% and 10% HCl at 25 and 40ºC.

Gunasekaran & Chauhan (2004) reported the inhibitory action of the extract of *Zenthosylum alatum* for mild steel in aqueous orthophosphoric acid. Sethuramn and

Raja tested datura metel extract in the year 2005 for corrosion inhibition of mild steel in acidic medium. Their findings concluded that acid extract of the studied plant showed significant corrosion inhibitive effect, and they attempted to probe the mechanism of inhibition by fitting the isotherm where both Tempkin and Langmuir adsorption isotherm was followed by phytoconstituents (Sethuraman & Raja, 2005). Leaf extract of *Occimum viridis* was studied for the inhibition of corrosion in acidic medium by Oguzie (2006). Abdel-Gaber et al. (2006) reported inhibitive action of the extract *of Chamaemelum mixtum* , *Cymbopogon proximus*, *Nigella sativa*, and *Phaseolus vulgaris* plants and showed their efficient capacity to inhibit acid corrosion for mild steel.

El-Etre & El-Tantawy (2006) studied the extract *of Ficus nitida* leaves for their inhibitive action on general and pitting corrosion of various metals viz. carbon steel, nickel, and zinc in the aqueous medium. Okafor et al. (2007) and his coworkers had also investigated ethanol extracts of *Garcinia kola* for similar purposes, where they found increased inhibition efficiency on the addition of potassium iodide indicating synergism suggested physical adsorption of molecules based on values obtained for the activation energy of inhibition. Noor (2007) had studied the inhibition capability of extracts of *Fenugreek* leaves. Inhibitive behavior of mangrove tannins and their flavonoid monomers on mild steel in acidic medium was studied by Rahim et al. (2007). Acid inhibition of carbon steel in low chloride media by an aqueous *Hibiscus rosa-sinensis Linn* extract was successfully demonstrated by Anuradha et al. (2007). Aqueous extract of Olive (*Olea europaea*) was studied by El-Etre (2007) as green corrosion inhibitor carbon steel in 2.0 M HCl by gravimetric method and obtained 91% inhibition efficiency for 900 ppm extract concentration at 30°C. Efficiency decreases with an increase in temperature. Efficiency was 24% for 60°C and 7% for 70°C.

Besides, El-Etre (2008) studied corrosion inhibition efficiency of zallouh (*Ferula harmonis*) root extract for mild steel in 2.0 M HCl by gravimetric and polarization method and obtained inhibition efficiency was 91% and 93%. The inhibition mechanism was explained based on adsorption of ferutinol beznoate compound found in the extract. The inhibitive action of leaves, seeds, and combination of leaves and seeds extracts of   *Phyllanthus amarus* was studied by Okafor et al. (2008) where the

mechanism of chemical adsorption of the plant components on the surface of the metal is proposed for the inhibition behavior, and adsorption characteristics were approximated by Temkin isotherm. Oguzie (2008) reported on the efficacy of *Telfaria occidentalis, Occimum viridis, Azadirachta indica, Hibiscus sabdariffa* leaf extracts as well as the seeds of *Garicina kola* as a green inhibitor in acidic medium Umoren (2008). Similarly, Umoren et al. (2009) reviewed that gum Arabic and *Raphia hoookeri* exudates inhibit acid corrosion of mild steel.

Raja and Sethuraman discussed a new type of green chemical (natural substance) that can be utilized to prevent rust. They discussed the function of inhibitors on metal surfaces, as well as the implementation and shortcomings of natural corrosion inhibitors, concluding that natural substances will emerge as powerful rust inhibitors in the long run due to their advantages of ease of access, eco-friendliness, environmental biodegradability, and non-toxicity; with the remark that the era of green corrosion inhibitors has arrived. (Raja & Sethuraman, 2008).

Likewise, Raja & Sethuraman (2009) have analyzed the extract of *Calotropis procera* for their inhibition action in an acidic medium for the mild steel and found out studied plant extract was indeed significantly effective (Raja & Sethuraman, 2009). Raja & Sethuraman (2009) investigated the extract *of Solanum Tuberosum* as an inhibitor of acid corrosion of mild steel. The study revealed that plant extract acted as a good inhibitor. This evidence was supported by double-layer capacitance and charge transfer resistance values derived from Nyquist plots obtained from AC impedance. Abdel-Gaber et al. (2009) had also inquired lupine extract for their inhibitive property. Eddy et al. (2009) looked into the joint effect of halides and ethanol extract of *Lasianthera Africana* on inhibition of acid corrosion of mild steel. They revealed that, of the investigated halides, only KCl might enhance the adsorption of the inhibitor, whereas KBr and KI antagonized its adsorption. Inhibiton efficiency of *Justicia gendarussa* plant extract in acidic solution was expressed in terms of adsorption and protective film formulation by Satapathy et al. (2009). Eddy & Mamza (2009) obtained 94.24% and 92.34% inhibition efficiency of *Azadirachta indica* leaves extract by gravimetric and gasometric method respectively by 500 ppm of extract in acid for mild steel corrosion inhibition.

Several researchers found Henna plant extract as an effective corrosion inhibitor for different metals in different acid solutions. Ostovari et al. (2009), studied inhibitory action of aqueous extract of leaves of Henna (*Lawsonia inermis*) for corrosion inhibition of mild steel in 1.0 M HCl by different methods such as gravimetric, potentiodynamic polarization and EIS and found its efficiency up to 92.59% for 1.2 g/l concentration of extract by gravimetric method and inhibition efficiency decreases with increase in temperature. Inhibitory action was ascribed to adsorption as well as chelation of compounds like lawsone with mild steel. Aqueous extract Henna was tested by Hamdy & El-Gendy (2013) for carbon steel in 1.0 M HCl. The maximum efficiency obtained was 92.72% by potentiodynamic polarization for 3000 ppm extract solution. Chaudhari & Vashi (2016) carried out a similar investigation to study the inhibition effect of leaves extract of Henna for mild steel in 0.5M acetic acid, and maximum inhibition found by EIS and the gravimetric method was 86.27% for 1000 ppm solution. Nair-IJTIMES (2018) studied ethanolic extract of Lawsonia alba Lam. leaves for corrosion inhibition of aluminum alloy AA6063 in 0.5M HCl and efficiency obtained was 76.47% for 0.14 g/l concentration.

Quraishi et al. (2010) studied green approach to corrosion inhibition of mild steel in acidic medium by the extracts of *Murraya koenigii* leaves and proved both HCl and H_2SO_4 media are successfully inhibited. Ekanem et al. (2010) employed two methods: weight loss and hydrogen evolution to identify the corrosion inhibition action of leaves extracts of pineapple (*Ananas camosus L*) for mild acid in acidic medium and found them to be an efficient green inhibitor. In the article published by Singh et al. (2010), aqueous extract of Kalmegh (*Andrographis paniculata*) leaves was used as a green inhibitor for acidic corrosion control of mild steel in 1.0 M HCl which proved to be an effective inhibitor. They studied inhibition efficiency by EIS, gravimetric and potentiodynamic polarization methods, and 98.2%, 98.1%, and 97.4% inhibition efficiency for 1200 ppm concentration. Avci & Keleş (2011) found that leaves extract of *Acacia cyanophylla* inhibits mild steel corrosion in 1.0 M H_2SO_4. The maximum inhibition efficiency calculated was 95% for 20 g/l concentration of inhibitor.

Lahhit *et al.* in 2011 published their paper in which they studied corrosion inhibition for carbon steel from essential oil extracted from fennel (*Foeniculum vulgare*) in 1.0M HCl using electrochemical impedance spectroscopy (EIS), Tafel polarization method

and weight loss measurements. The study showed the oil adsorption of oil molecules on the metallic surface, thereby increasing charge transfer resistance with oil concentration. Fennel oil acted as a mixed type inhibitor in which maximum efficiency of 76% was reported at 3.0 ML/L. Chemical compounds limonene and β-pinene were accounted for such results (Lahhit et al., 2011).

Furthermore, Ji et al. (2011) established the corrosion inhibition action of leaves extracts of *Argemone Mexicana* for mild steel acid corrosion. The plant being rich in organic inhibiting molecules such as proteins, amino acids, tannins,phenolic compounds, saponins, and flavonoids and nonalkaloids organic compounds such as fused benzene rings, hetero N atom rings, -OCH$_3$ and –OH groups, showed excellent inhibition property with the efficiency of 92.5% for 500 mg/L extract concentration in 1.0 M HCl. A similar satisfactory result was also obtained by Hussin & Kassim (2011) in their previous research, where they explored the inhibitory action of extracts of *Uncaria gambir* for similar material under similar acidic conditions. The influence *of Xylopia ferruginea* leaves extract and partitions in hexane and chloroform on the corrosion behavior of mild steel in acidic solution was studied by Amira et al. (2011) by gravimetric, polarization and EIS methods. It was found that chloroform partition was an effective inhibitor with the inhibition efficiency of 93%. Vimala et al. (2011) reported 86% inhibition efficiency for mild steel in 1.0 M HCl with 0.15% (v/v) concentration of *Cassia auriculata* flower extract.

Hmamou et al. (2012) investigated prickly pear seed oil extracts (*Opuntia ficus-indica L*) as potential green inhibitor for mild steel in the acidic medium after encouraging results were obtained in the past by natural oils as an inhibitor. In an attempt of finding new sources of natural inhibitors various natural substances were already identified as effective inhibitors such as: Menthols , Rosemary oil, *Thymus* oil, *Eugenol* and *Acetyleugenol* , Lavender oil, *Limonene, Pulegone* and *Pulegone* oxide, Jojoba oil and B*ifurcaria bifurcata* extract, Pennyroyal Mint oil, Argan oil, *Argania* plant extract and *Argania spinosa* kennels extract and cosmetic oil. In the study carried out by Gerengi & Sahin (2012), green corrosion inhibition was demonstrated by extract of *Schinopsis lorentzii* in acidic medium for low carbon steel where the adsorption of the molecules of the extract on the surface of the metal was in accordance with the Temkin adsorption isotherm. *Punica granatum* peel was tested

for inhibitive action of acid corrosion of mild steel by Behpour et al. (2012). Inhibition action of *Argan hulls* extract as an inexpensive, eco-friendly, naturally occurring substance, on the corrosion of mild steel in 1.0M HCl was studied by Afia et al. (2012). Likewise, essential oil of leaves *of Asteriscus graveolens*, obtained by hydrodistillation was studied by Znini et al. (2012) for their anticorrosive action in acidic medium for mild steel. *Piper longum* extract was used by Singh et al. (2012) for corrosion inhibition of aluminum in 1.0 M NaOH Inhibition efficiency was studied by using the gravimetric and polarization method. 94% inhibition efficiency was reported in the gravimetric experiments by using 400 ppm inhibitor concentration.

Likewise, Kairi & Kassim (2013) studied rhizomes extract of *curcuma longa* for corrosion inhibition of mild steel in 1.0 M HCl and found inhibition efficiency of 79.81% only in 80ppm concentration. Similarly, Leelavathi & Rajalakshmi (2013) reported 89.1% inhibition efficiency for Dodonaea viscosa leaves extract for corrosion inhibition of mild steel in 1.0 M HCl with 0.6% v/v concentration of inhibitor. Inhibition was ascribed to the adsorption of organic compounds present in extract such as Hautriwaic lactone, Kaempferol, Santin, Vanillic acid etc. Cang et al. (2013) reported corrosion inhibition properties of aloes to extract for mild steel in acid medium. Investigations were carried out using gravimetric, EIS and polarization methods and found 77% inhibition by EIS method for 1.0 M HCl with 800 ppm extract. *Chlorophytum borivilianum* root extract was studied for corrosion inhibition by Ji et al. (2013) for mild steel in acidic medium by electrochemical methods. 91% and 90% inhibition efficiency was obtained in the experiments by polarization and EIS methods, respectively in 1.0 M HCl.

Moreover, Yaro et al. (2013) investigated apricot (*Prunus*) juice as green corrosion inhibitor of mild steel in phosphoric acid. Patel et al. (2013) investigated various extracts of plants leave for their inhibition action in an acidic medium for mild steel, and all the studied plants were found to be effective, which consisted of extracts of *Wrightiantinctoria, Clerodendrumphlomidis, Ipomoeatriloba*. Umoren et al. (2013) also conducted similar work where inhibition effect of date palm (*Phoenix dactylifera*) seed extracts for mild steel in 1.0M HCl and 0.5 M H_2SO_4 solutions was investigated where extract worked better for HCl solution. The inhibition efficiency trend with extract concentration for mild steel in 1.0M HCl revealed an increase in

inhibition efficiency with an increase in extract concentration reaching a maximum value of 90.95% and 61.95% at 25 and 60ºC, respectively. However, in 0.5 M H_2SO_4, maximum inhibition efficiency of 86. 25% was obtained at the concentration of 1.0 g L^{-1} at 25°C and 42.14% at 1.5 g L^{-1} at 60ºC.

In another study carried out by Umoren et al. (2014), they checked coconut coir dust extract for their potential inhibition action for mild steel in acidic mediums, with 0.5 M H_2SO_4. They reported maximum inhibition efficiency to be 87% and 45% for methanol and water extract, respectively, at 30°C with the highest concentration (0.5g/L). The adsorption of some extract components on the mild steel surface is attributed to the retardation of metal. In the next study carried out by Umoren et al. (2015), fruit extract of red apple (Malus domestica) behaved as mixed type organic inhibitor for mild steel in HCl solution, which showed increased inhibition efficiency with an increase in concentration and temperature in the range 30-60 ^{o}C. A chemisorption process has retarded the acid-induced corrosion process with an efficiency up to 87% at 60°C. Antioxidant phyto-nutrients flavonoids and polyphenolics are significant constituents of apple extract, including quercetin, epicatechin, and procyanidin B2 as tartaric acid. These compounds are known to contain a heteroatom such as oxygen atom that regarded as centers of adsorption.

Pentaclethra macrophylla Bentham extract was studied by Nnanna et al. (2014) for mild steel corrosion in HCl solution. For the exploration of green alternatives for combating the mild steel corrosion in acidic medium, Roy et al. (2014) used polyacrylamide grafted guar gum (GG-g-PAM) with various grafting levels. The study revealed inhibition efficiency higher than 90% for about 50h of exposure where inhibitor acted as mixed type following Langmuir isotherm. Results also suggested a synergistic effect between GG and PAM moieties to influence each other for the adsorption and subsequent corrosion inhibition. Similarly, Patel et al. (2014) studied various parts of *Rotula Auatica* plant extract in H_2SO_4 acid medium and found them to be effective. Soltani et al. (2014) obtained 96.4% inhibition efficiency for leaf extract of *Silybum marianum* for 304 stainless steel in 1.0 M HCl by polarization method when 1 g/l concentration of the extract was used. Comparable results were obtained by gravimetric (95.7%) and EIS (96%) methods.

In a study conducted by Krishnaveni & Ravichandran (2014), an aqueous extract of leaves of *Morinda tinctoria* was found to be an efficient green inhibitor with an efficiency of 96.72% in 2h of immersion for aluminum in acidic medium. Similarly, *Tagetes erecta* (Marigold flower) extract as a green inhibitor for acid corrosion of mild steel in 0.5M H_2SO_4 was studied by Mourya et al. (2014) using polarization, EIS and gravimetric methods. 98.07% inhibition efficiency was calculated by the EIS method in the presence of 1 g/l of extract. Lutein was considered as a significant component in extract responsible for inhibition, and inhibition mechanism was explained with quantum chemical calculation. Nwankwo et al. (2014) investigated the extracts of *Amaranthus cordatus* as green inhibitor for mild steel in H_2SO_4 and NaCl and came up with the conclusion that the plant extract under study inhibits corrosion inappreciable extent and can cause passivation since its pH value of 8.1 falls within the region in which passivation occurs in pourbaix diagram. Fouda et al. (2014) established *Punica* plant extract as a green corrosion inhibitor in an acidic medium for carbon steel at the same time, *Anacardium occidentale* Gum was studied by Arthur et al. (2014).

The essential oil extracted from garlic was tested as corrosion inhibitor for carbon steel in 1.0 M H_2SO_4 by Afia et al. (2014) by conventional methods such as gravimetric, polarization and EIS methods and inhibition efficiency was computed up to 95.8% in 2.5 g/l concentration of inhibitor. Essential oil Showed stability up to 55ºC. Bammou et al. (2014) investigated the extract of aerial part of *Chenopodium ambrosioides* for corrosion inhibition of carbon steel in 0.5M H_2SO_4 by EIS, polarization, and gravimetric methods. The maximum inhibition efficiency was calculated by the polarization method, which was 94% for 4 g/l concentration of inhibitor. 93.35% inhibition efficiency was calculated by Karthik et al. (2014) for corrosion inhibition of mild steel in 1.0 M HCl in the presence of 500 ppm of *Cassia sena* leaves extract. Muthukrishnan et al. (2014) studied the inhibition properties of aqueous extract of *Hyptis suaveolens* leaves for corrosion of mild steel in acidic medium using polarization and EIS technique. Results indicated that the inhibition efficiency of the extract was 95% in 1.0 M H_2SO_4 with 250 ppm of extract. Inhibition efficiencies obtained by Saedah (2014) for juniperus extract for corrosion inhibition of

mild steel in 2.0 M H_2SO_4 were 85.05%, 84.9%, 82.83% and 81.34% by EIS, polarization, gravimetric and gasometric methods respectively.

The study of *Artemisia Mesatlantica* essential oil as green inhibitor for carbon steel in 1.0M HCl solution was carried out by Boumhara et al. (2015) where efficiency value up to 92% at 3 g/L was achieved. Bhawsar et al. (2015) examined leaves extracted of *Nicotiana tabacum* for their acid corrosion inhibition of mild steel and postulated that protective barrier layer formation occurs according to the modified Langmuir adsorption isotherm. Alike, Mohd & Ishak (2015) analyzed *Piper nigrum* extract as an attractive alternative to prevent corrosion, for they had found excellent inhibition efficiency of the studied plant for mild steel in the corrosive medium. Al-Senani et al. (2015) examined the effects of some green leafy vegetable extracts, namely *Lactuca sativa, Eruca sativa, Petroselinum crispum*, and *Anethum graveolens* for their anti-corrosion action for carbon steel in acidic medium using gravimetric method. Similar conclusions were drawn where the physical adsorption mechanism facilitated inhibition that followed the Langmuir, Freundlich, and Temkin adsorption isotherm models. Popular major crop barley (*Hordeum vulgare)* is a rich source of chemical constituents like alnine, glycine,serine, aspartic, leucine, valine, tyrosine, and isoleucine with a various number of the functional group which is able to chelate metal cations (Saadawy, 2015). For the same reason in a paper published in 2015, Saadawy presented evidence for inhibiting acid corrosion of steel up to 94% by extract of barley.

Sharma et al. (2015) explored a new aspect of the use of the most prominent and most fruitful source of secondary metabolites, *Azadirachta indica* commonly known as "Neem". This plant, which is a vibrant source of natural products, proved to be potential green inhibitors for mild steel protection. The various phytoconstituents with different functional groups, conjugated double bonds with aromatic rings, got adsorbed on the metal surface to block the destruction reaction with aggressive media. Equivalently Tuaweri et al. (2015) performed the experiment showing the inhibitory action of leaves of *Azadirachta indica* in a chloride medium and found it an effective inhibitor for mild steel. However, microbiologically influenced corrosion of carbon steel in a hypersaline environment was studied by Parthipan et al. (2017) with the

Neem extract as a green inhibitor.

The rind, seed, and peel extract of watermelon (*Citrullus lanatus*) were inspected for its efficiency as green corrosion inhibitor for mild steel in 1.0 M HCl by Odewunmi *et al.* where the investigation was carried out by EIS, LPR and polarization method. The seed extract was found more effective. IE calculated by the EIS method for 2 g/l concentration inhibitor was 85.96% (Odewunmi et al., 2015). The inhibition efficiency of ankako (Calotropis gigantea) leaves extract for corrosion inhibition of mild steel in 1.0 M HCl was 96.14%, which was calculated by Desai (2015). Similarly, gravimetric results showed 88.07% inhibition efficiency by Bidens biternanta weed extract for corrosion inhibition of Al-alloy AA6063 in 0.5M HCl (Choudhary et al., 2015). *Musa paradisica* peel extract as a green corrosion inhibitor for mild steel in acidic solution was studied by Ji et al. (2015). Again, Soltani & Khayatkashani (2015) had also established *Gundelia tournefortii* as a green inhibitor for mild steel in acidic solution.

Similarly, Singh et al. (2016) showed effects of *Aloe vera* gel on mild steel corrosion in 1.0M HCl medium with efficiency greater than 90% with lowest corrosion rate and optimum concentration of extract solution being 200 ppm. Soltani et al. (2016) published a paper in which they discussed the corrosion inhibition of low carbon steel by *Strychnos nux-vomica* extract as a green corrosion inhibitor in acidic solution. Hussin et al. (2016) revealed that ultra-filtrated alkaline and organosolv oil palm (*Elaeis guineesis)* fronds lignin acts as a green corrosion inhibitor for mild steel in acidic solution. The maximum inhibition efficiency was obtained at a concentration of 500 ppm for both the compound with the conclusion that the inhibition process was spontaneous, and the adsorption process was primarily physical. Prabakaran et al. (2016) reported 92% efficiency by methanol extract of *Ligularia fischeri*, indicating the decreased dissolution of mild steel in acidic medium. Anabarasi and Vasudha (2016) established the extract of *Cucurbita maxima* as a potential inhibitor for mild steel acid corrosion. Anupama et al. (2016) inquired *Phyllanthus amarus* leaf extract for corrosion inhibition of mild steel in the acidic medium as well as electrochemical and computational aspects of surface interaction. Additionally, Chigondo & Chigondo (2016) had published a review article that provides recent work done on the application of natural plant extracts as a corrosion inhibitor for mild steel.

Similarly, Mohammadi et al. (2016) investigated apricot gum as a corrosion inhibitor for mild steel in 0.5M H_3PO_4 by EIS and polarization technique. The inhibition efficiency of the inhibitor obtained by the polarization technique was 86% in 100 ppm concentration of inhibitor. *Sida acuta* leaves extract was reported as a corrosion inhibitor for mild steel by Umoren et al. (2016). 85% inhibition efficiency was obtained by 500 ppm of extract in 1.0 M H_2SO_4 by the gravimetric method. It has been reported by Odusote et al. (2016) that methanolic extract of *Moringa olifera* is a good corrosion inhibitor for the inhibition of reinforced steel bar in acid media. 95.45% inhibition efficiency was obtained at 1000 ppm of extract in 2.0 M HCl. Zheng et al. (2018) studied *Eriobotrya japonica* as a green corrosion inhibitor for corrosion inhibition for mild steel in acidic medium. In the experiment, the plant's leaf extract was prepared in 0.5M H_2SO_4, and it was tested for corrosion inhibition by polarization, EIS, and gravimetric methods. Maximum inhibition was obtained in 100% (v/v) solution. Inhibition efficiencies calculated by polarization, gravimetric, and EIS were 96.3%, 96.2%, and 94.3%, respectively.

The paper published in 2017 by Oukhrib et al. (2017) had shown effective inhibition action of *Ziziphus lotus* extract for metal like copper in seawater. The corrosion process's kinetics was found to be significantly decreased, with an efficiency of 93% at an extract concentration of 5 g/L. The formation of chemisorbed film onto the surface of the metal is what resulted in decreased corrosion rate in this study. Murthy & Karungamye (2017) investigated the extract of fruit, seed and pulp of baobab (*Adansonia digitata*) for corrosion inhibition of mild steel in 0.5M HCl by gravimetric, polarization, and EIS methods. Maximum efficiency (91.92%) was obtained for pulp extract by gravimetric methods, whereas for fruit seed extract maximum efficiency (88.87%), the polarization method was obtained.

Qiang et al. reported 90% inhibition efficiency for Ginko leaves extract for corrosion inhibition of X70 steel in 1.0 M HCl with 200 ppm concentration of inhibitor. Results obtained by both EIS and polarization methods were comparable. Inhibition was ascribed to adsorption of organic compounds such as Isorhamnetin, Sciadopitysin, 6-hydroxykynurenic acid, 4-O-methylpyridoxine. In paper, results were explained on the basis of quantum chemical study (Qiang et al., 2018). Boudalia et al. (2019)

studied essential oil extracted from the aerial part of *Artemisia herba* as a green corrosion inhibitor for stainless steel in 1.0 M H_3PO_4 by EIS and polarization method. Inhibition efficiency calculated by the polarization method was 88.03% for 1 g/l concentration of inhibitor.

Several investigations on extracts from naturally occurring materials as corrosion inhibitors have been done, for example, plant extracts *of Rauvolfia serpentina* (Raja & Sethuraman, 2010), *Isertia coccinea* (Lebrini et al., 2011) and *Palicourea guianesis* (Lebrini et al., 2011), *Areca catechu* (Kumar et al., 2011), have been tested as corrosion inhibitors for steel in HCl medium. Similarly, plant extract of *Spirulina platensis* (C. Kamal & Sethuraman, 2012), *Litchi Chinensis* peel (Singh et al., 2015), *Carica* seed (papaya) (Pushpanjali et al., 2014), *Hunteria umbellata* (Alaneme et al., 2016), *Tilia cordata* (Fouda et al., 2017) etc. are also found corrosion inhibitor.

The work on plant extract as a corrosion inhibitor has significant limitations due to a lack of phytochemical investigation. Several research works have been carried out on isolated compounds from plant extracts to investigate the compound's corrosion inhibition properties. In the research carried out by Li et al. (2005), berberine's inhibition behavior for mild steel in 1.0 M H_2SO_4 media was successfully studied. The optimized geometry of the alkaloid berberine facilitates the interaction of iron atoms with its cyclic molecular π orbital. Berberine extracted from *Coptis chinensis* formed a uniform layer on the mild steel surface and results show that only $5\times10^{-3.0}$ mole/litre is sufficient to show inhibition efficiency by 98.3%. Gravimetric and polarization methods also show a similar result of 97.7% and 97.9% efficiency, respectively. The inhibition effect was ascribed to chemical adsorption, which follows Flory-Huggins isotherm. A similar result was obtained by Na et al. (2019) for P110SS steel in 3.5% NaCl solution, where inhibition efficiency obtained by the EIS technique was 99%, when 1.5 g/l is the concentration of berberine extracted from *Coptis chinensis*. These results are compared with the results obtained from commercial berberine. Ju et al. (2012) investigated to study the inhibition efficiency of berberine purchased from the market and the Gravimetric method for hot-dip coated steel in 37% HCl. Results showed that 99% efficiency was obtained only by 10^{-2} mole/liter of berberine.

Dahmani et al. (2010) compare the inhibition effect of seed extract of black pepper

and piperine compound isolated from the extract for corrosion of C38 steel in 1.0 M HCl by gravimetric method. Results showed the improvement in efficiency when the isolated compound was used. Inhibition Efficiency (IE) of 1 mole/ltr (285 ppm) solution of piperine was 98.9%, whereas IE of 2000 ppm and 400 ppm solution extract were reported 95.8% and 92.4% respectively. Results reveal that the major component in black pepper extract responsible for its inhibition effect is piperine.

In the study carried out by Garai et al. (2012), this limitation was avoided by investigating the phytochemicals of methanolic extract of *Artemisia pallens* that lead to arbutin isolation as a major component. Arbutin undergoes hydrolysis in acidic medium (HCl) to yield D-glucose and hydroquinone (HQ). Inhibition efficiency up to 98% with the crude methanolic extract, 93% with arbutin, 33% with HQ, and 43% with HQ and D-glucose mixture were achieved at $300^{\circ}C$ in the investigation. Equivalently, Kamal & Sethuraman (2012) established caulerpin, a bis-indole alkaloid extracted from marine green algae *Caulerpa racemosa* to be the reason behind anticorrosive nature for mild steel in acidic medium and adsorption of the extract occurs at steel/acid interface. Moreover, Znini et al. (2012) scrutinized the inhibition capability of essential oil of *Salvia aucheri mesatlantica* which predominantly contained camphor. The inhibitory effect on the corrosion of steel in the acidic medium had strong dominance of anodic character; however, the inhibitor acted as a mixed type with an efficiency of 86.12% at 2 g/L oil content.

Raja *et al.* studied corrosion inhibition property of alkaloid extracts of Ochrosia *oppositifolia* leaves (OOL) and isoreserpiline as the major alkaloid isolated from OOL against mild steel in acidic medium where the corrosion current densities are lowered by the inhibitors by mixed-mode mechanism thereby reducing the corrosion rate (Raja et al., 2013). In another paper published in the same year 2013 by Raja *et al.*, they established *Neolamarckia cadamba* alkaloids as ecofriendly corrosion inhibitor for mild steel in acidic medium. They accounted for the shielding effect of alkaloid for a reduction in corrosion rate by mixed-type inhibition, and crude extract from bark and leaves of the studied plant contained 3β-isodihydrocadambine as major alkaloid (Raja et al., 2013). Chevalier et al. (2014) made an inquiry on alkaloids extracts from *Aniba rosaeodora* plant for their enhanced corrosion resistance of mild steel in 1.0 M HCl solution.

Fiori-Bimbi et al. (2015) examined naturally occurring polymer i.e. pectin, for its potential control of the corrosive attack on mild steel during the acid cleaning operation. The geometric blocking effect of adsorbed inhibitive species at the metal surface attributed to corrosion resistance. Pectin, a mixed type inhibitor, was extracted from *Citrus* peel (lemon), which showed its potential to form a complex with Fe^{2+} ions released during the corrosion reaction. Michael and Olubunmi (2014) investigated flavonoid (catechin) separated from *Nypa fruticans Wurmb* leaves extract for their inhibitive action for mild steel acid corrosion. Interesting work was done by Adewuyi et al. (2014) in which the seed oil *of Adenopus breviflorus* was used for the synthesis of succinyl amide Gemini surfactant by simple chemical process and it was used as corrosion inhibition of mild steel in 0.5 M HCl.

Correspondingly, in research carried out by Saidi et al. (2015) on pectin extract of *Opuntia cladodes* significant efficiency of 96% was obtained in the presence of 1 g/L at 308K. The increase in inhibitor concentration decreased the double-layer capacitance and increased charge transfer resistance, which increased the inhibition efficiency. The potentiodynamic polarization study showed that inhibitor acted as a cathodic type inhibitor. Odewunmi et al. (2015) compared the inhibition efficiency of rind extract of watermelon with L-citruline isolated from the extract for corrosion inhibition of mild steel in 1.0 M HCl. The investigation was done by electrochemical methods viz EIS and polarization techniques. Results revealed that extract is more effective than the isolated compound. Inhibition Efficiency computed by polarization method for extract was 88.1%, whereas it is 51.4% for L-citruline for 1000 ppm concentration of inhibitor. It shows that there is a role of other compounds and synergism of different compounds for the inhibition of extract.

Similarly, in 2019 Muthukrishnan *et al.* investigated stigmasterol extracted from *Ficus hipsida* leaves as an inhibitor for 1.0M HCl and revealed an efficiency of 90% with 250ppm of extract solution at308 K (Muthukrishnan et al., 2019).

Nepal is rich in high altitude endemic plants. Research history for Nepali plants as green corrosion inhibitors is not long. In recent days, the extract of a few plants has

been tested for corrosion inhibition. Few of them are listed in table 2.1.

Table 2.1 : Plants of Nepalese origin studied as corrosion inhibitors.

S. No.	Plants	Corrosion Medium	IE %	Method
1	Lantana camara (P. R. Shrestha et al., 2019)	1 .0 M HCl	97.33	polarization
2	*Euphorbia royleana* (Thapa et al., 2019)	1.0 M HCl	99.60	Gravimetric
3	Pogostemon benghalesis (Chaudhary et al., 2016; P. C. Lama et al., 2016)	1.0 M H_2SO_4	99.4 90.6	polarization Gravimetric
4	*Gaultheria fragrantisima* (R. Lama et al., 2018)	1.0 M H_2SO_4	94.56	polarization
5	*Jatropha curcas* (Gupta et al., 2020)	1.0 M H_2SO_4	91.34	polarization
6	*Eucalyptus Globulus* (Awasthi, 2018)	0.1.0 M HCl	97.87	Gravimetric
7	*Magnifera indica* (T. P. Joshi, 2018)	1.0 M H_2SO_4	75.21	Gravimetric
8	*Rhynchostylis retusa* (Chapagain, 2019)	1.0 M H_2SO_4	84.91 88.94	Gravimetric polarization
9	*Crotalaria spectabilis* (Bohara, 2019)	1.0 M H_2SO_4	90.43 92.86	Gravimetric polarization
10	*Cassia tora* (Bist, 2019)	1.0 M H_2SO_4	88.64 90.11	Gravimetric polarization

Although several other kinds of research carried out for the studies of inhibition effect of plant extracts, several types of research are still ongoing to search newer and better green inhibitors in different parts of the world. Still, several plants are not explored in the field of corrosion inhibition. As green chemistry's consciousness is growing day by day, more green inhibitors must be developed to fulfill the demand of the market of corrosion inhibitors and replace the toxic and expensive inhibitors. As green inhibitors' market is growing day by day, the development of new corrosion inhibitor helps to generate revenue for the country. Keeping these points on view, this research work entitled "Development of green corrosion inhibitors from natural products of Nepal" has been carried out for which no reference could be found in the literature reviewed so far. This work is an effort to add some endemic plants of Nepal in the growing green inhibitor list.

CHAPTER 3

3. MATERIALS AND METHODS

3.1 Selection of plants as corrosion inhibitors:

Based on the reference of published papers on plant extracts, four non-toxic plants *Artemisia vulgaris, Equisetum hyemale, Mahonia nepalensis,* and *Berberis aristata* were selected to study as green corrosion inhibitors.

3.1.1 Non-toxic nature of plant extracts selected for study

In an acute toxicity study carried out by Gilani et al. (2005) to a group of ten mice at a dose of 3g/kg intraperitoneally, extract of *Artemisia vulgaris* did not produce any mortality and no change in the behavior. It showed the non-toxic nature of the extract. Similarly, Queiroz et al. (2014) in their acute oral toxicity test in vivo found that extract of *Equisetum hyemale* is safe to use for different applications. When the experiment was carried out following the guidelines of the OECD (Organization for Economic Co-operation and Development, Guideline, 423) by administering extract to a group of ten mice at a concentration of 100mg/kg by gavage, it showed changes in the piloerection pattern during initial minutes and any other behavior changes, and, the mortality of mice was not observed during the subsequent 14 days.

The acute oral toxicity of methanol extract of Mahonia nepalensis was investigated by Das & Chhetry (2016) in mice according to the OECD guidelines for testing chemicals-425. Mortality and behavior changes were not observed in any mice during the subsequent 14 days study period when 2000 mg/kg of methanolic extract was administered orally to them. This result showed that the extract of *Mahonia nepalensis* is safe to use for different applications. Toxicity of *Berberis aristata* extract was studied by Joshi et al. (2011) on swiss albino mice by an acute oral toxicity test. The results of the toxicological studies showed that oral administration of Berberis aristata extract at levels up to 5000 mg/kg body weight did not cause toxicity or mortality in experimental animals. In a similar study carried out by Sood et al. (2019), Up to two weeks of observation, Berberis aristata diterpenes revealed no fatality and no deleterious effect on the responses of the tested mice at a level of 5000 mg/kg. Behavior and mobility patterns, respiration, skin, fur, eyes, salivation, and sleep did

not show any alterations. There were no tremors, diarrhea, or lethargy reported. So the crude extract of *Berberis aristata* does not show a toxic effect.

A brief description of the selected plants for the corrosion studies of mild steel in acidic media are as follows:

3.1.2 Artemisia vulgaris

Kingdom : Plantae
Division : Magnoliophyta
Class : Magnoliopsida
Order : *Asterales*
Family : *Asteraceae*
Genus : *Artemisia*
Species : *vulgaris*

Artemisia vulgaris, commonly known as mugwort, grows in slightly alkaline, nitrogen-rich loamy soils. It is called 'Titepati' in Nepali. It can be found along roadsides and waste areas, preferably in sunny places.   It is found in Europe, Asia, northern Africa, Alaska, and North America. It is a perennial tall herbaceous plant that is about 1-2 m tall, Fig. 3.1. It has 5-20 cm green and leaves with a smooth texture and dense white tomentose hairs on the underside. It has a woody root and erect stems that are grooved with red-purplish tinge. It bears reddish-brown or yellow flowers from mid-summer to early autumn.

Artemisia vulgaris is a plant with medicinal value. It has been used as medicine traditionally and in homeopathic also. The essential oil and plant extract have been used as anti-epileptic, anti-hysteric, diuretic, digestive, and stimulant. Additionally, it shows antispasmodic, antiseptic, antibacterial, antimalarial, antitumor, antirheumatic a nd hepatoprotective behavior (Pandey et al., 2017). Traditionally, the plant and its extract have been used for the treatment of diabetes, epilepsy, psychoneurosis, depression, irritability, insomnia, anxiety, and stress. The paste of the leaf of the plant can be used for the treatment of skin disease. Its extract can give women relief for

several gynecological problems such as the treatment of irregular menstruation and relief of menopausal ailments. (Abu-Shandi & Al-Marahleh, 2017).

Figure 3.1 : *Artemisia vulgaris* plant.

Although essential oils and extract of the Artemisia genus were tested for corrosion inhibition properties, the methanolic extract of *Artemisia vulgaris* is not tested yet for corrosion inhibition properties. In phytochemical screening done by a natural chemist, it was observed that *Artemisia vulgaris* contains alkaloids and flavonoids in more amount, tannin, saponin, quinone, sterols, and terpenoid in moderate amount, and cardiac glycoside, reducing sugar and protein in less amount (Pandey et al., 2017). Flavonoids isolated from methanolic extract of *Artemisia vulgaris* are luteolin and morin (Pandey et al., 2017) , and other major compounds isolated from the extract and essential oil are camphor, Sabinene, β-thujone, chrysanthenone, borneol, germacrene D, artemisia ketone, 1,8 cineol, octadecanamide, , D-fructose, Artinniun b. (Abu-Shandi & Al-Marahleh, 2017; Pandey et al., 2017). Similarly, it contains alkaloids and nitrogenous compounds such as 3-methyl butanamide, 1-napthyl amine, 2-napthyl amine, 3 amino biphenyl, 4-amino biphenyl, serotonin, Prunacin (Ur Rashid et al., 2019). Structural formulae of some compounds which can show inhibition behavior are given in Fig. 3.2.

serotonin

Prunacin

N,N-dimethyl-4-nitroso-3-trimethylsilylaniline

Luteolin

Morin

Camphor
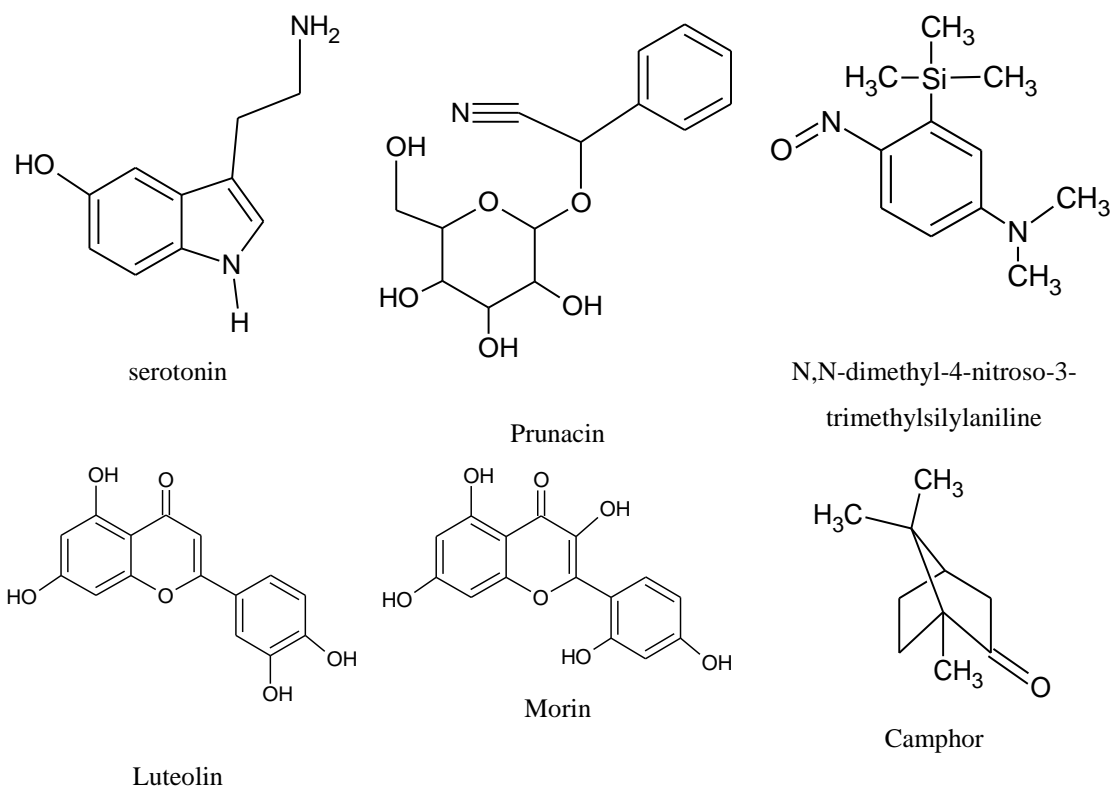
Figure 3.2 : Structural formula of some compounds present in *Artemisia vulgaris* Plant.

(Abu-Shandi & Al-Marahleh, 2017; Pandey et al., 2017, Ur Rashid et al., 2019)

3.1.3 *Equisetum hyemale*:

Kingdom : Plantae

Division : Equisetophyta

Class : Equisetopsida

Order : Equisetales

Family : Equisetaceae

Genus : *Equisetum*

Species : *hyemale*

Equisetum hyemale is a perennial herb commonly found in a tropical and temperate climate. The plant typically grows in wet places, ponds, marshes, wet woodland, and the banks of lakes and rivers. It has small leaves that are connected together around the hollow, unbranched stem, forming a narrow black-green band or sheath at each joint, generating dense spreading colony in full to partial sun, and resembles a ponytail. For this reason, it is commonly known as horsetail. It is called 'Aankhe jhar' or 'Talcha marne jhar' in Nepali. Its stems are up to 3 feet in height and medium to dark green, Fig. 3.3. Its stems have conspicuous ridges that feel rough and harsh due to the presence of silica. Its stems are usually deciduous in winter season but retain green in summer. It is a non-flowering plant that reproduces by spores.

Traditionally, the plant is used by people Nepal for removing a mole from skin. It is used to cure kidney disorders, edema, urinary tract infection, alopecia, tuberculosis, brittle fingernails, rheumatic diseases, gout, frostbite, and profuse menstruation, and nasal, pulmonary, wounds, burns and gastric hemorrhage. The liquid prepared by boiling stalk of Equisetum is used as a diuretic drink, for the treatment of venereal disease, and to wash sores on children's skin. Due to high silica content, it can be used to strengthen the connective tissue. So, it relieves symptoms of rheumatoid arthritis and osteoporosis (G. Pandey & Khatoon, 2017). It is used as a homeopathic remedy.

Figure 3.3 : *Equisetum hyemale* plant.

This plant has been reported to contain several phenolic compounds, flavonoids, alkaloids, glucosides etc (Jin et al., 2014). The chemical constituents isolated from the alcoholic extract of this plants are rutin, quercetin, L-uridine, ellagic acid, 2-(sophorosyl)-1-(4-hydroxyphenyl) ethanone, α-D-fructofuranose,ferulic acid, 5-hydroxymethyl furfural, feruloyl, caffeoyl, flavonol, Phenyl glycosides, nicotine, and dimethyl sulfone etc (Jin et al., 2014; Manske, 1955; G. Pandey & Khatoon, 2017; Park & Tomohiko, 2011) which are the compounds with heteroatoms with conjugation with multiple bonds. So, the methanolic extract of *Equisetum hyemale* can show the inhibition properties. The plant extract has not been tested yet for corrosion inhibition properties. This work attempts to explore methanoic extract in the plant as a new member of the green corrosion inhibitor. Figure 3.4 shows the molecular structure of a few compounds isolated from a plant extract of *Equisetum hyemale*.
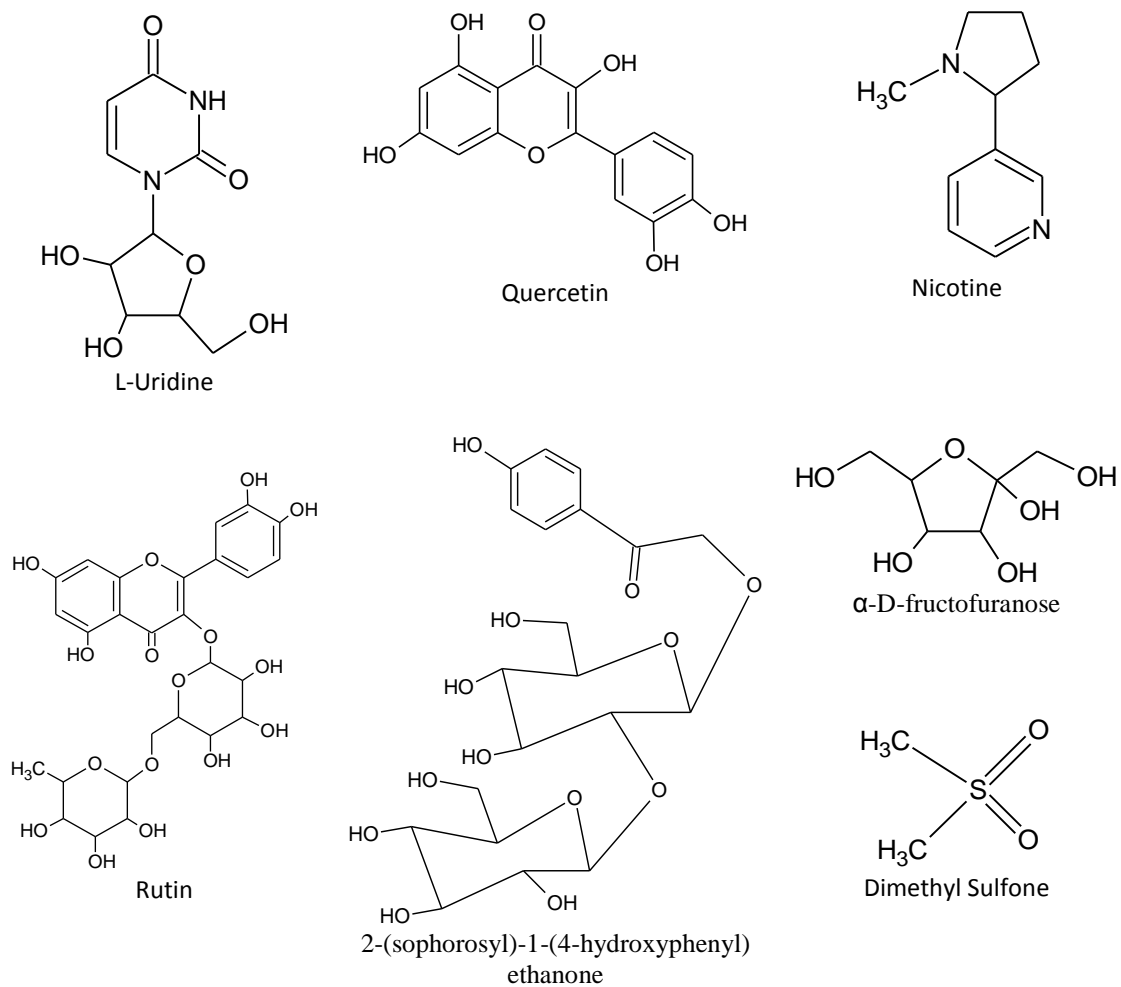
Figure 3.4 : Structural formula of some compounds present in *Equisetum hyemale* plant.

(Jin et al., 2014; Manske, 1955; G. Pandey & Khatoon, 2017; Park & Tomohiko, 2011)

3.1.4 *Berberis aristata*

Kingdom: Plantae

Division: Magnoliophyta

Class: Magnoliopsida

Order: *Ranunculales*

Family: *Berberidaceae*

Genus: *Berberis*

Species*: aristata*

Berberis aristata belongs to the Berberidaceae family which is named as 'Chutro' in Nepali and Indian berberry in English. It is a spiny shrub that grows in the northern Himalayas. The plant is widely distributed from the Himalayas to Srilanka, Bhutan, and hilly areas of Nepal. It is an erect spiny shrub ranging between 2 and 3 meters in height. Its wood is hard and yellow. Outer part of the bark of the plant is yellow to brown and inner part is deep yellow. Its bark can be removed by hand in longitudinal strips. It features three-branched, 1.5-cm-long spines that are modified leaves. The leaves are in a small culster of five to eight, phyllotaxy veticillate simple spiny, petiolate, toothed, fleshy, sessile acuminate, with reticulate pinnate venation, 4.9 cm long 1.8cm broad, deep green on the dorsal surface and light green on the ventral surface, Fig. 3.5. These plants bear yellow flowers which are stalked, complete, cyclic, bisexual, actinomorphic, and perigynous. The average radius of a fully opened cluster is 6.25 mm. Fruits are spherical to ovoid in shape and are generally covered in blossom, similar to plums. The fruit is aconite violet in color. Colour of Seeds varies from yellow to pink which are 2 to 5 in number.

Figure 3.5 : *Berberis aristata* plant.

74

People are using *Berberis aristata* plants for several purposes. Fruits of this plant are juicy and contain plenty of sugars and other nutrients. People eat fruits of this plant. The roots can also be used for making an alcoholic drink. Dye and tannin obtained from this plant are used for dyeing clothes and tanning leather. The plant has medicinal value as well. It is used in ayurvedic medicine for a very long time. Traditionally, it is used in diarrhea, wound healing, inflammation, skin disease, jaundice, menorrhagia, and affection of eyes. A very valuable ayurvedic "Rashut" is prepared from this plant. It is useful in the treatment of jaundice, diabetes, cancer, malaria, etc. and has good anti-oxidant property, anti-pyretic, anti-analgesic, anti-fungal, anti-microbial, anti-inflammatory property, and anti-platelet activating factor.

Phytochemical screening of methanolic extract of the plant shows that it contains alkaloids, flavonoids, quinones, terpenoids, and steroids in more amount and glycosides and cardiac glycosides in fewer amounts (Thusa & Mulmi, 2017). The main constituent of the plant is berberine alkaloid. Besides this other organic compounds such as berberubine, jattrorhizine, oxyberberine, palmatine, dihydropalmatine, 7,8 dihydro-8-hydroxyberberine, berbamine, pakistanamine,oxycanthine, epiberberine, dehydrocaroline, karachine, taximaline, aromaline, pseudo palmatine chloride, pseudo berberine chloride, lanost-5-en-β-ol etc. (Bajpai et al., 2015; Chander et al., 2017; Thusa & Mulmi, 2017) were isolated from the stem of the plants. Among the isolated compounds, berberine is identified as an effective corrosion inhibitor. Since the extract contains several alkaloids along with berberine, it could be a suitable corrosion inhibitor, and inhibition may be enhanced due to synergistic effect. So, *Berberis aristata* is the next plant selected for the study to explore its methanolic extract as an eco-friendly inhibitor on mild steel in acid medium. Fig. 3.6 shows the molecular structure of a few compounds isolated from a plant extract of *Berberis aristata*.

Berberine

Jatrorrhizine

7,8-dihydro-8-hydroxy berberine

Berbamine

Oxyberberine

Pakistanamine
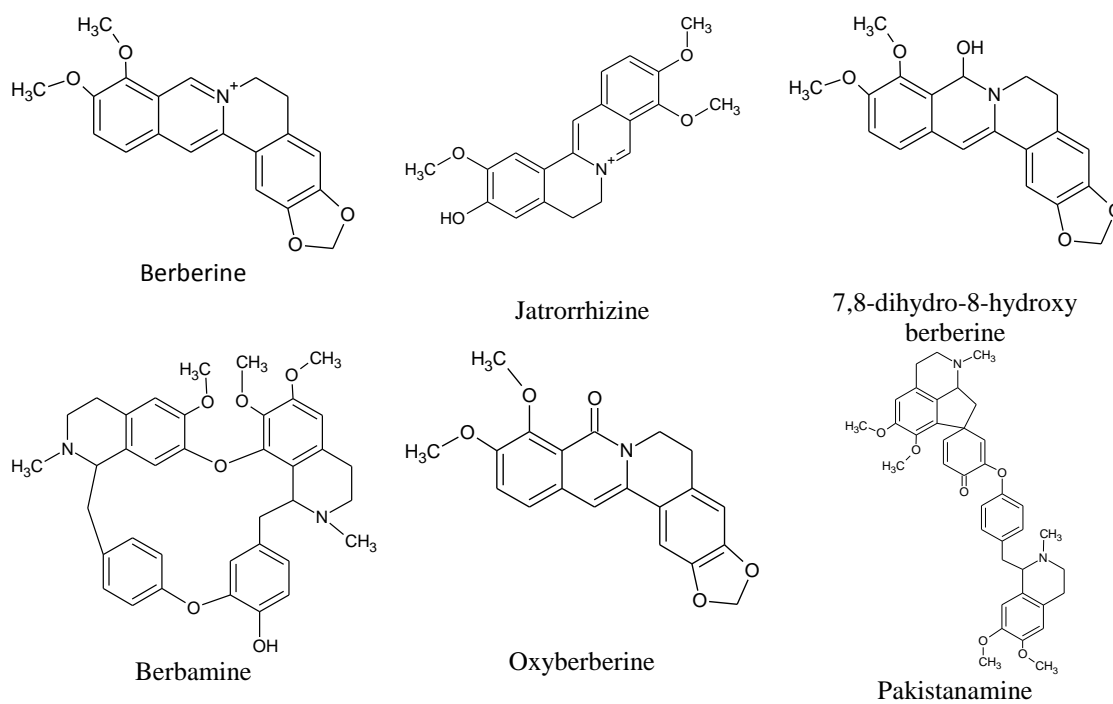
Figure 3.6 : Structural formula of some compounds present in *Berberis aristata* plant.

(Bajpai et al., 2015; Chander et al., 2017; Thusa & Mulmi, 2017)

3.1.5 *Mahonia nepalensis*:

Kingdom: Plantae

Division: Magnoliophyta

Class: Magnoliopsida

Order: *Ranunculales*

Family: *Berberidaceae*

Genus: *Mahonia*

Species: *nepalensis*

Mahonia nepalensis belongs to Berberidaceae's family, and it is known vernacularly as 'Jamanimandro' in Nepali. M.nepalensis is a medium-sized, totally hardy perennial evergreen shrub that blooms with yellow flowers in winter season. The flowers are arranged in spike inflorescence. This shrub has an all-year-round interest. It withstands -15°C/5F and grows in soil ranging from pH 6 to 8. Clay loam, loam, loamy sand, sandy clay loam, and sandy loam soils are all suitable for it. This shrub reaches a maximum height of 6 meters (19.7 feet). Their green leaves have spiny margin. Fig. 3.7. They are aristate in shape. Beginning in the spring and finishing in the spring, there is a large amount of fruit and seeds. Colour of fruit is blue. Its origins can be traced back to Nepal. It can be found in abundance in high mountainous places at an altitude of 1000 and 2000 meters of Nepal, Sikkim, Bhutan, China, Vietnam, and so on.

This plant is highly useful in architectural and security barriers in the garden. This plant is vital from a traditional standpoint, as it is considered a necessary flower for the Newar community in 'Bel Bibaha' and 'Bratabanda' rituals. Its flower is used for worshiping goddess 'Swosthani' in Nepali, so it is also known as 'Swosthani flower' in Nepal. This plant has medicinal value as well. The stem and wood of this plant have long been believed to have anti-inflammatory, anti-bacterial, anti-fungal effects and have been applied to treat the skin diseases like eczema, psoriasis, etc. as diuretic cemulent and as anti-dysentery medicine.

Figure 3.7 *: Mahonia nepalenis* plant and its flower.

Phytochemical screening of methanolic extract of the plant shows that it contains alkaloids, flavonoids, quinones, terpenoids, and steroids in more amount and steroids, glycosides and cardiac glycosides in fewer amounts (Thusa & Mulmi, 2017). The main constituent of the plant is alkaloids, which belongs to class protoberberine, and bisbenzylisoquinolines. Berberine is the primary alkaloid present in the methanolic extract of the stem of the plant. Besides this, other organic compounds such as homoaromaline, isotetradine, O-methyl pulijabine, 7,8-dihydro-8- methoxy berberine, umbellatin, neprotine, jatrorrhizine, were isolated from the stem of the plants (Mai et al., 2009; Thusa & Mulmi, 2017). As discussed earlier, berberine is identified as an effective corrosion inhibitor. Since the extract contains several alkaloids and berberine, it could be a good corrosion inhibitor, and inhibition may be enhanced due to the synergistic effect. So, *Mahonia nepalensis* is the next plant selected for the study to explore its methanolic extract as an eco-friendly inhibitor on mild steel in acid medium. Fig. 3.8 shows the molecular structure of a few compounds isolated from a plant extract of *Mahonia nepalensis*.
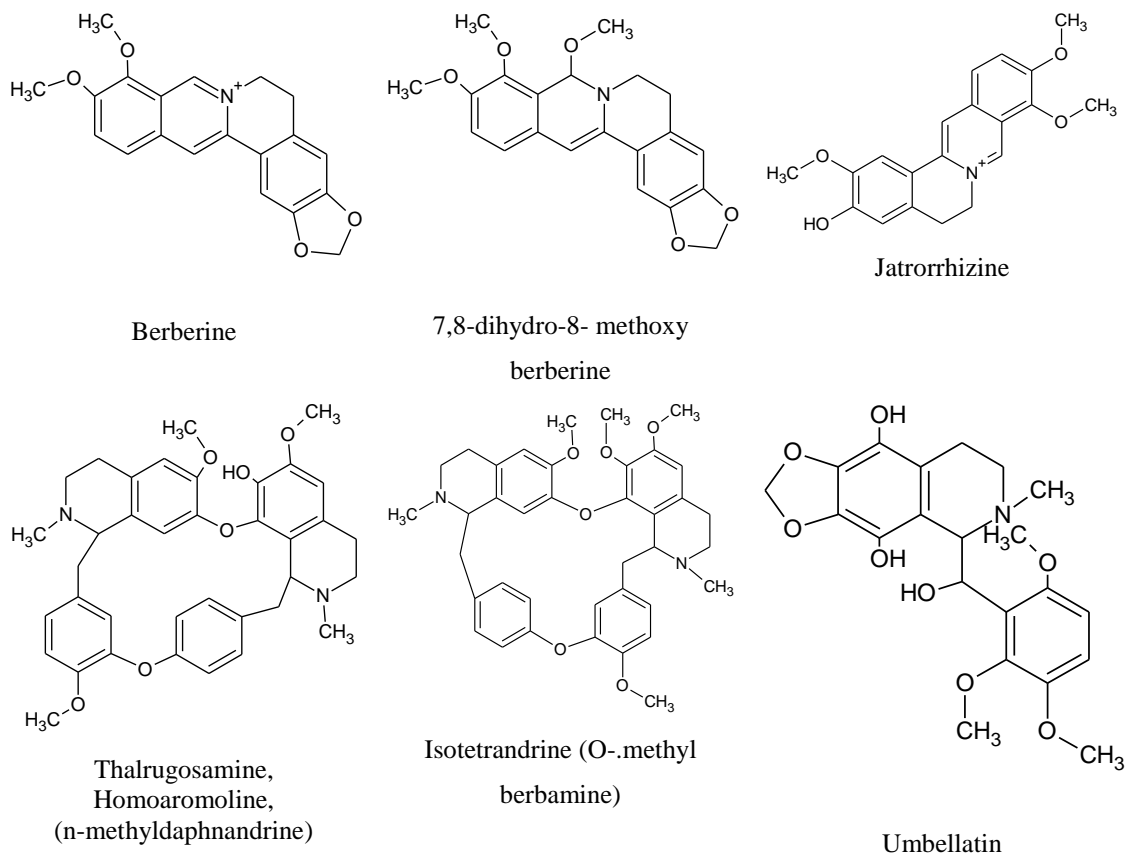
Figure 3.8 : Structural formula of some compounds present in *Mahoina nepalensis* plant.

(Mai et al., 2009; Thusa & Mulmi, 2017)

3.2 Acid used in the process

As discussed earlier, acid is used widely in many industrial processes such as acid pickling, descaling, cleaning of the boiler, cleaning oil refinery equipment and heat exchangers, and in oil, well acidizing to remove corrosion products, scales, chalky deposits, etc. However, limitation in these processes is the dissolution of clean base metal. Hydrochloric acid and sulphuric acid are commonly used acid for these processes. As sulphuric is widely used acid for these processes due to its low cost, it is selected as an acidic medium in this study. It is a diprotic mineral acid having formula H_2SO_4. It is highly corrosive acid with molecular weight 98.079 g/mol. It is colorless or slightly yellow viscous liquid and also known as oil of vitriol. Density and concentration of 98% sulphuric acid are 1.83 kg/L and 18 mol/L, respectively. Anhydrous H_2SO_4 is a very polar liquid having a dielectric constant around 100 and shows high electrical conductivity due to autoprotolysis. It is soluble in water. It is used for several purposes, such as domestic acidic drain cleaner, as an electrolyte in

lead-acid batteries, fertilizer production, oil refining, mineral processing, wastewater processing, dehydrating agent, and production of dyes, detergents, insecticides, antifreeze, in pharmaceutical industries, etc.

3.3 Collection of plants
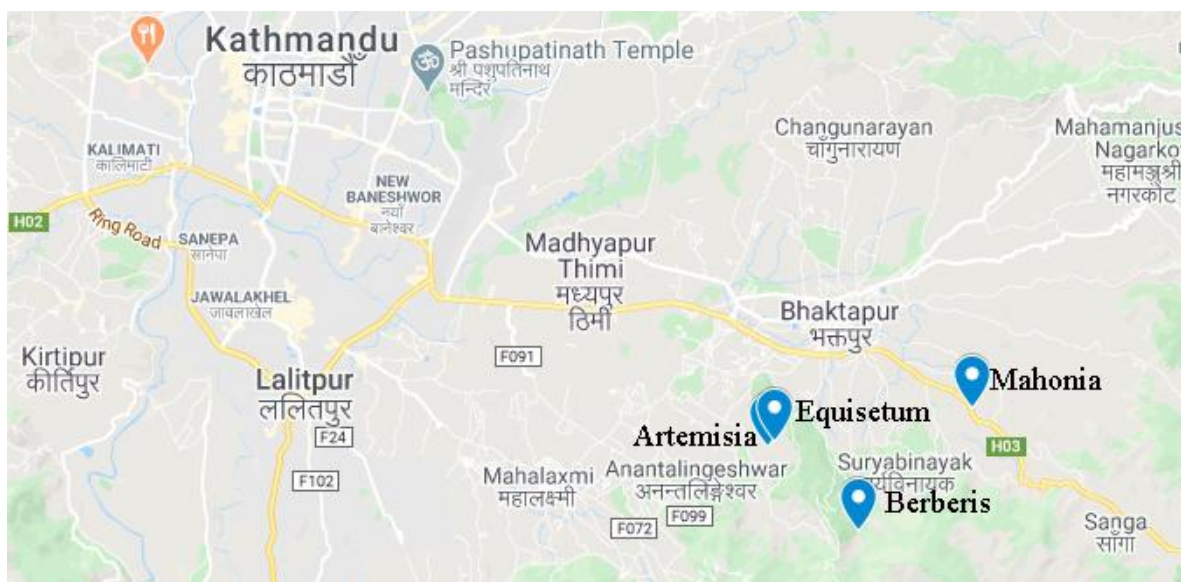
Figure 3.9 : Map showing site of a collection of specimens used in the study.

Different parts of different plants were selected for this study. Aerial parts of *Artemisia vulgaris* and *Equisetum hyemale* and stem of *Mahonia nepalensis* and *Berberis aristata* were used to prepare the extract, which is applied as the inhibitor. Plants used for this study were collected from different places of Bhaktapur, Nepal. *Artemisia vulgaris* was collected from Gundu (latitude: 27º38'59.3" N, longitude: 85º24'55.1" E and altitude: 1402 m), Bhaktapur, Nepal. *Equisetum hyemale,* was collected from Gundu (latitude: 27º39'2.5"N, longitude: 85º24'59.6"E and altitude: 1402 m), Bhaktapur, Nepal. *Berberis aristata* was collected from Sipadol (latitude: 27º38'6.2" N, longitude: 85º25'58.7" E and altitude: 1511 m), Bhaktapur, Nepal, and Mahonia nepalensis was collected at Nangkhel, Bhaktapur, Nepal (latitude: 27° 39' 23.3" N, longitude: 85° 27' 19.0" E, altitude: 1347 m). Map showing Collection places of different plants are presented in Fig. 3.9.

3.4 Preparation of powder of plant specimen

The aerial part of Artemisia and Equisetum, and the stem of Berberis and Mahonia were used for the study. Parts of plants were washed with distilled water and cut into smaller pieces and dried in the shade for one month Then the dried sample was ground into a fine powder with the help of an electric grinder machine, Fig. 3.10.

Figure 3.10 : Powder of plants.

3.5 Preparation of methanol and n-hexane extract of plants

Figure 3.11 : Maceration of plant powder in solvent.

The extraction of phytoconstituents was done through a cold percolation method.1000 mL of methanol of LR grade was added to 200 g. of the powdered sample, and the

mixture was well stirred and macerated for 3,4 days so that constituents from the plant powder get dissolved in it. The mixture was shaken occasionally. Then the mixture was filtered with the help of ordinary filter paper. The filtrate was collected, and again, methanol was added to the residue. Maceration, shaking, and filtration were continued until the clear supernatant liquid was obtained, Fig. 3.11. The filtrate was concentrated using IKA RV-10 digital rotary evaporator, Fig. 3.12. The concentrated solution was dried at 40ºC using the Clifton water bath model no. NE2-4D dried to get extract powder.

n-hexane extract was also prepared in a similar method as mentioned above, using n-hexane as a solvent instead of methanol.

Figure 3.12 : Concentration of plant extract in a rotary evaporator.

3.6 Preparation of solution

1.0M H$_2$SO$_4$: 55.6 mL of concentrated (17.98 M) H$_2$SO$_4$ was taken in a 1000 mL volumetric flask, and it was diluted up to the mark using distilled water.

Inhibitor solution: 1 liter of inhibitor solution was prepared by dissolving 1 g of plant extract in 1.0M warm H$_2$SO$_4$ at 40-50ºC. The undissolved extract was discarded by filtration. Thus prepared 1000 ppm inhibitor solution was considered as a stock

82

solution. This stock solution was further diluted with 1.0 M H_2SO_4 to prepare an inhibitor solution of 200 ppm, 400 ppm, 600 ppm, and 800 ppm.

3.7 Preparation of mild steel coupon

A flat sheet of mild steel procured from the local market of Kathmandu was used for this study. The sheet was mechanically cut into coupons having dimensions about 3.25cm×3.25cm×0.15cm for gravimetric experiments, coupons having 2cm×2cm×0.15cm for electrochemical experiments and about 1cm×1cm×0.15cm for surface investigation such as SEM and EDX. Samples were abraded and polished by silicon carbide paper of different grades with coarse one of 100, proceeding in steps with 400, 600, 800, 1000 grades to the finest 1200 grade. The polished coupons were ultrasonicated in ethanol for 15 minutes to remove residual particles, dried with air blower, and stored in desiccators. A reproducible surface was then obtained for each coupon after removing air-formed oxide film and other dirt and used for the weight loss, surface investigation, and electrochemical process as a working electrode.

3.8 Electrochemical experiments

3.8.1 Open circuit potential (OCP) measurement

Measurement of corrosion potential (E_{corr}, ϕ_{corr}) to monitor the corrosion damage is an intrusive indirect method. This approach can be valuable in some cases, particularly where alloys could show active and passive corrosion behavior. Corrosion potential measurements would indicate the development of active corrosion. When viewed in Pourbaix diagrams, the corrosion potential can give a fundamental indication of the thermodynamic corrosion risk. Measurement of OCP is necessary to describe the mode of inhibition.

OCP was measured before each electrochemical experiment, carried out in a three-electrode cylindrical glass cell connected to Gamry Potentiostat (Reference 600) supported with Gamry framework software. In the three-electrode cell, polished MS specimen (surface area 0.608 cm^2) was used as a working electrode, a saturated calomel electrode (SCE) as a reference electrode and a platinum wire as an auxiliary electrode as shown in Fig. 3.13. Then OCP was measured using a 300 mL electrolyte solution until it attains the stable state. OCP measurements were carried out for 1.0 M H_2SO_4 without and with an inhibitor of different concentrations.
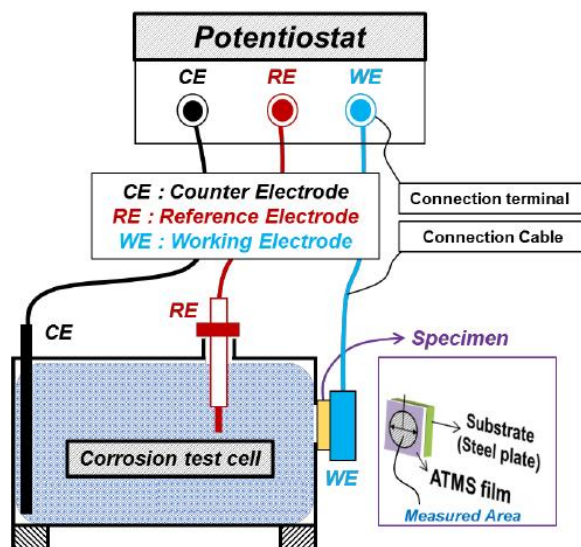
Figure 3.13 : A schematic representation of a three-electrode cell electrochemical set-up.

3.8.2 Electrochemical impedance spectroscopy:
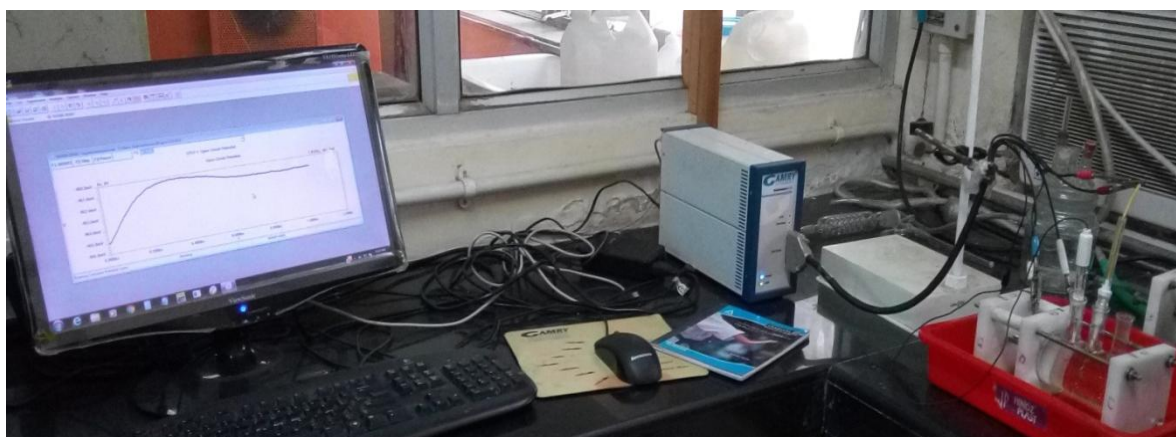
Figure 3.14 : Apparatus set up for electrochemical impedance spectroscopy and potentiodynamic polarization using Gamry potentiostat.

After the measurement of OCP, Electrochemical impedance spectroscopy (EIS) was carried out in the same electrochemical set up used for OCP, Fig. 3.14. EIS was used to measure the ac response of the mild steel coupons in 1.0M H_2SO_4 without and with plant extract of different concentrations. For the ac response measurement, a superimposing sine wave signal of 10 mV peak to peak at frequencies between 100 kHz to 0.01 Hz was applied at OCP. The response of the AC signal in terms of charge transfer resistance (Rct) and double layer capacitance was analyzed by fitting the

response with an equivalent circuit. These parameters were derived from the equivalent circuit using Z-view 2 software. Inhibition efficiency is calculated by the equation [3-1].

$$IE\% = \frac{R_{ct} - R_{ct}^0}{R_{ct}} \times 100\%$$ [3-1]

Where, R_{ct} and R_{ct}^0 are the charge transfer resistances in the presence and absence of inhibitor.

3.8.3 Potentiodynamic polarization

The potentiodynamic polarization curve was obtained with a scan rate of 0.5 mV s^{-1} in the potential range from -300 to +300 mV relative to the OCP in the same experimental setup using Gamry potentiostat.

Potentiodynamic polarization was carried out in a three-electrode system using Hokuto Denko potentiostat (HA-151) as shown in Fig. 3.15. In this polarization experiment, cathodic and anodic polarization is done with different metal coupon. Potential was swept from OCP + 0.025 mV to OCP – 0.3 mV in cathodic polarization and OCP – 0.5mV/s to OCP + 0.3 mV in anodic polarization. The exposed surface area for the experiments was 0.785 cm^2.

Cathodic and anodic slopes were calculated from the corresponding polarization method. The values of corrosion potential and corrosion current density were obtained by the Tafel extrapolation method. The values of corrosion current density in the absence and presence of inhibitor were used to calculate inhibition efficiency using the equation [3-2].

$$IE\% = \frac{I_{corr}^0 - I_{corr}}{I_{corr}^0} \times 100\%$$ [3-2]

Where, I_{corr} and I_{corr}^0 are corrosion current densities in the presence and absence of inhibitor.

MS coupons were used in two ways for the polarization experiments. Coupons were used as immersed in the electrolyte solution and after 24 h of immersion in electrolyte solution using acid without and with the inhibitor of different concentrations. In the

beginning, inhibition efficiency of 1000 ppm solution of n-hexane extract and methanol extract of plants was calculated for both types of metal coupons as immersed and immersed for 24 h. Experiments were carried out using Hokuto Denko potentiostat. Since the performance and amount of methanol extract were good, it was selected for a detailed investigation. Then, polarization experiments of metal coupons immersed for 24 h were carried out using Hokuto Denko potentiostat and that of MS coupons as immersed were carried out using Gamry potentiostat.
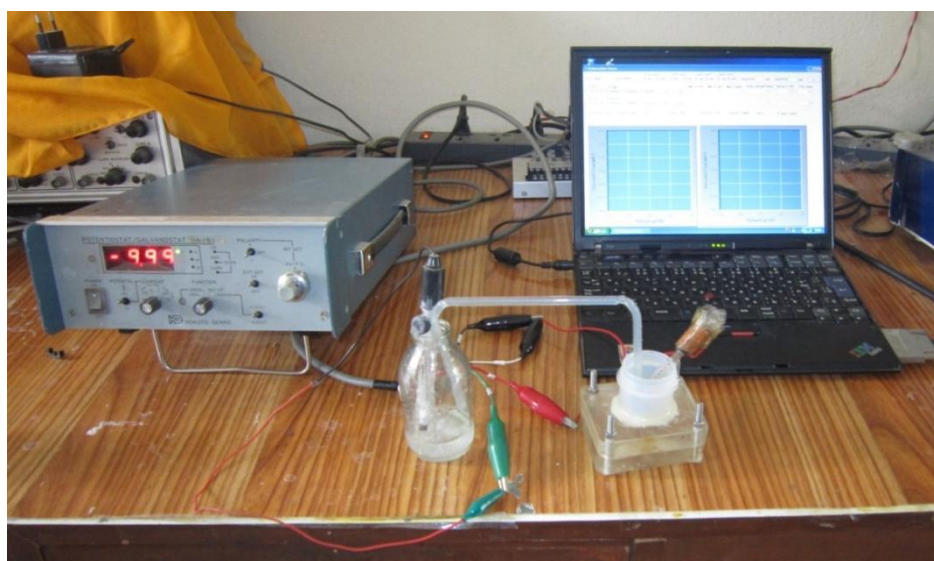
Figure 3.15 : Experimental set up for potentiodynamic polarization of mild steel using Hokuto Denko potentiostat.

3.8.4 Differential pulse voltammetry (DPV) and cyclic voltammetry (CV)

Autolab potentiostat/ galvanostat with GPES 4.9 software (Eco-Chemie, Utrecht, The Netherlands) was employed to carry out differential pulse voltammetric (DPV) and cyclic voltammetric (CV) measurements in this study. Differential pulse voltammetry (DPV) is a voltammetry technique that uses a series of constant amplitude pulse on a linear scan potential as shown in Fig. 3.16a. The final current signal measured is the difference between current just before the pulse is applied and current just before the pulse end.

$$\Delta i = i_{S2} - i_{S1} \qquad\qquad\qquad [3\text{-}3]$$

Thus DPV produces a peak rather than a wave (sigmoid) with the height of the current signal located at roughly at $E_{1/2}$ of direct current voltammetry (DCV) as shown in Fig. 3.16b.

The height of the current is proportional to the concentration of the analyte, which can be calibrated for quantitation. However, in this study reduction in peak current was used to find out the effect of the addition of plant extracts on the corrosion of MS. The effect of time corrosion and concentrations of plant extracts on the peak current was therefore used to estimate the corrosion inhibition efficiency. This is a novel approach in the study of corrosion inhibitor with much better resolution so that very small amount of iron dissolution can be detected at very short time of corrosion and at very high concentration of extract where in both these conditions the amount of iron dissolution is extremely low. In addition, any shift of the peak potential can be used to understand the chelation effect of dissolved iron species with molecules of the plant extracts.

A potential pulse ΔE_p of 50 mV was applied for the pulse time of 50 ms which was superimposed on a DC potential ramp of 20 mV/s. Current was measured twice; once just before pulse was applied and once just before pulse ends so that charging current is kept at very low value. The current was measured for 0.2 ms on a glassy carbon electrode (GCE) as working electrode with reference to a silver-silver chloride (SSE) reference and platinum wire counter electrode in a 10 mL voltammetric cell. The DC potential ramp was started from -0.6 V to 0.8 V in a 0.1 M KCl as a supporting electrolyte at a pH 1.1 so that oxidation of Fe^{2+} to Fe^{3+} was recorded.
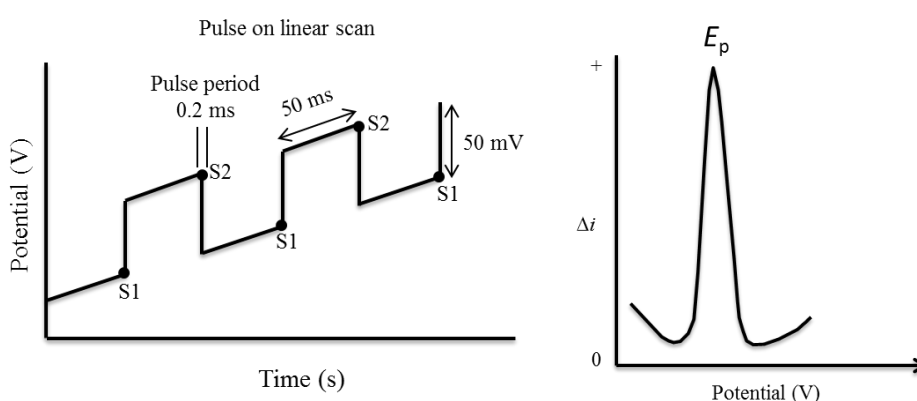
Figure 3.16 : a. Pulse sequence on a linear scan used in differential pulse voltammetry and b. The differential current response against applied potential.

The corrosion test was performed in 50 mL of 1.0M H_2SO_4 solution with various concentrations of plant extracts using 2 x 2 x 0.15 cm^3 mild steel (MS) sample. After fixed time intervals 1 mL solution was withdrawn and transferred to voltammetric cell containing 9 mL of 0.1 M KCl buffered at 1.1 pH. Both DPV and CV analyses were performed in the same set up and before voltammetric measurements, GCE was

maintained at -0.6 V for 30 as a pre-treatment process so that surface of working electrode is contamination free.

The peak potential E_p is related to half wave potential $E_{1/2}$ as:

$$E_p = E_{1/2} \pm (\Delta E_p)/2 \qquad\qquad [3\text{-}4]$$

Therefore, it is easy to identify the species detected in the voltammogram. E_p is a function of amplitude of the pulse ΔEp. As ΔEp decreases the E_p approaches $E_{1/2}$ as seen from the above relation.

Cyclic voltammetry (CV), which is one of the most versatile electroanalytical techniques for the study of electroactive species, was used to study the redox behaviors of iron species dissolved in the absence and presence of plant extracts in 1.0M H_2SO_4 solution. The main aim was to get information about chelation behavior of the iron species with the molecules of the plant extracts. CV measurements were carried out using the electrochemical set up as described above for DPV using a scan rate of 100 mV/s.

CV consists of applying a periodic, triangular potential excitation signal, which cycles the potential of an electrode in between two limits and measured the resulting current. The electrode potential is ramped linearly to a more negative/positive potential, and then ramped in reverse back to the starting voltage, Fig. 3.17.
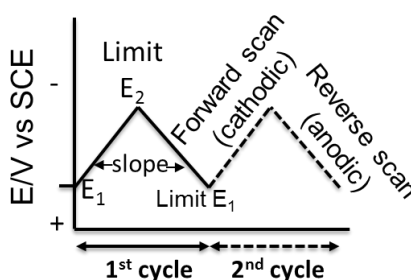
Figure 3.17 : Potential sequence used in a cyclic voltammetry measurement.

The forward scan produces a current peak for any analytes that can be reduced through the range of the potential scan. The current will increase as the potential reaches the reduction potential of the analyte, but then falls off as the concentration of the analyte is depleted close to the electrode surface. As the applied potential is reversed, it will reach a potential that will reoxidize the product formed in the first reduction reaction, and produce a current of reverse polarity from the forward scan.

This oxidation peak will usually have a similar shape to the reduction peak. The peak current, i_p, is described by the Randles-Sevcik equation:

$$i_p = (2.69 \times 10^5) \, n^{3/2} \, A \, C \, D^{1/2} \, \upsilon^{1/2} \qquad\qquad [3\text{-}5]$$

where n is the number of moles of electrons transferred in the reaction, A is the area of the electrode, C is the analyte concentration (in moles/cm^3), D is diffusion coefficient (cm^2/s) and υ is the scan rate. It can be seen that peak current, which results due to presence of redox species, varies linearly with square root of scan rate for a mass transfer controlled process. Important parameters in cyclic voltammograms are peak potentials and peak currents. For a reversible redox system anodic peak current i_{pa} should be equal to cathodic peak current i_{pc}. However, the peak ratio is often strongly affected by chemical reactions coupled to the redox process.

Peak positions are related to formal potential of redox process, which results in half wave potential $E_{1/2}$.

$$E_0{}' = (E_{pa} + E_{pc})/2 = E_{1/2} \qquad\qquad [3\text{-}6]$$

The separation of peaks for a reversible couple is close to 0.059/n V but depends on limiting potential.

$$\Delta E_p = E_{pa} - E_{pc} = 2.302RT/nF = (0.0591/n) \text{ V} \qquad\qquad [3\text{-}7]$$

So, for one electron reversible redox system a separation by 59 mV should occur. However, for a steady state curve, $\Delta E_p = 58/n$ mV is obtained. Higher values than this means system tends to be irreversible or quasi-reversible.

Both DPV and CV measurements were standardized with respect a Fe^{2+}/Fe^{3+} redox system using 0.1 M KCl as supporting electrolyte under the same experimental set up as discussed above. In the CV measurements, effect of scan rate was studied and a diffusion controlled electron transfer process was verified from Randles Sevcik equation relating peak current with square root of scan rate. The separation of peak potentials for cathodic and anodic reaction showed that kinetic of electron transfer was rather slower than expected for a reversible one electron redox reaction. The voltammetric signal was calibrated in 1 mM to 50 mM Fe^{2+}/Fe^{3+} redox couple at pH

1.1 and containing 0.1 M KCl as supporting electrolyte. A linear relationship between peak current and concentration of redox couple confirmed that CV analysis could be used for the quantitation of corrosion rate and inhibition efficiency in the corrosion media containing plant extracts under same experimental conditions.

Similary, standardization of DPV peak current was done using similar experimental condition as for CV and a linear relation was obtanied for peak current and concentration of redox couple Fe^{2+}/Fe^{3+}.

3.9 Gravimetric (weight loss) experiments

Weight loss measurements were used to evaluate the performance of the inhibitor and the nature of adsorption isotherms. Prior to each weight loss measurement, the abraded MS coupons were retrieved from desiccator, washed thoroughly with distilled water, dried, and preserved in a desiccator overnight. Next day, the dimensions of the abraded coupons were measured using a digital vernier caliper, and initial weights were taken using Ohaus E1RR80 four-digit electronic analytical balance

In pursuance of studying the effect of time on inhibition efficiency, after the measurements of initial weights, coupons were immediately immersed in 100 mL of 1.0M H_2SO_4 without and with 1000 ppm inhibitor solutions separately maintaining the temperature of 298 K for 3, 6, 9, 12, and 24 h. For every different time periods, different samples were used for both acid and inhibitor solution.

For the study of the concentration effect of the inhibitor on its efficiency, pre-weighed mild steel coupons were immersed in 100 mL of 1.0M H_2SO_4 without and with inhibitor solutions of different concentration viz. 200, 400, 600, 800, and 1000 ppm for 6 h at 298 K in a water bath.

The effect of temperature on inhibitor efficiency was studied by immersing mild steel coupons in 100 mL of 1.0 M H_2SO_4 without and with 1000 ppm inhibitor solutions for 6 h at different temperature viz. 298 K, 308 K, 318 K, 328 K, 338 K.

Clifton Unstirred water bath model no.NE2-4D was used to adjust the temperature in all gravimetric experiments, Fig. 3.18. After the elapsed time, coupons were retrieved

from solution, cleaned with running water with the help of a brush to remove corrosion products, degreased with acetone, dried with air blower, and preserved in desiccators for 24 h. Then coupons were weighed again. The weight loss was then calculated for each sample from the weight difference before and after the immersion in the electrolyte solutions. Three samples were used in all the measurements to assure the results' reproducibility and illustrated data were mean values of three measurements.

The corrosion rate (CR) of MS coupons in each experiment was calculated by equation [3-8]:

$$CR = \frac{87.6W}{AtD} \qquad\qquad [3\text{-}8]$$

Where, W is weight loss of coupon (mg.), A is the surface area of the coupon (cm^2), t = time of immersion (h) and D is the density of coupon (g/cm^2).

Inhibition efficiency and surface coverage (θ) were calculated by equations [3-9 and 3-10]:

$$IE\% = \left(\frac{CR_1 - CR_2}{CR_1}\right) \times 100 \qquad\qquad [3\text{-}9]$$

Where, CR_1 and CR_2 are the corrosion rates in the absence and presence of inhibitor respectively.

$$\theta = \left(\frac{W_1 - W_2}{W_1}\right) \qquad\qquad [3\text{-}10]$$

Where, W_1 and W_2 are the weight loss in the absence and presence of inhibitor respectively.

Figure 3.18 : Apparatus set up for weight loss method.

3.10 Material characterization:

3.10.1 Attenuated total reflectance- Fourier transform infra-red (ATR-FTIR) spectroscopy

Infrared (IR) beam is passed onto an optically dense ATR crystal in ATR-FTIR spectroscopy. ATR crystal is made up of substance with a high refractive index (usually a diamond or germanium), which can offer a high total internal reflection at a specific incidence angle. The internal reflection of the IR beam at the ATR crystal surface creates an evanescent wave that extends into the sample at a certain depth of penetration (Dp), usually between 0.5-5 μm. The magnitude of Dp depends on the wavelength of IR light, the angle of incidence and the refractive index of the ATR crystal. The internally reflected beam exits the crystal and then collected by a detector, where it is analyzed and displayed as an ATR-FTIR spectrum. Further sample preparation is not required in ATR-FTIR spectroscopy. So, it is considered as a good technique for analyzing samples. The basic principle of ATR-FTIR is schematically represented in Fig. 3.19 (a and b).
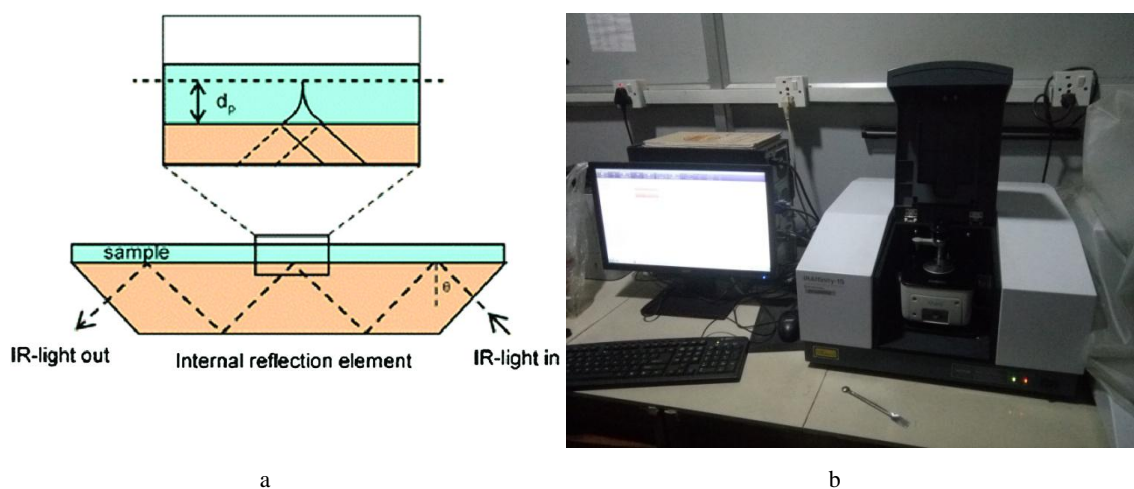
Figure 3.19 : a. A schematic illustration of ATR-FTIR principle and b. Shimadzu FTIR spectrophotometer.

Different functional groups in plant extract were confirmed by making Fourier transform infrared (FTIR) analysis in attenuated total reflectance (ATR) mode using a Shimadzu FTIR spectrophotometer. Crude samples of plant extracts were placed on a diamond crystal, and all spectra were recorded in the wavenumber range of 4000-400 cm^{-1}.

3.10.2 Scanning electron microscopy and energy-dispersive X-ray spectroscopy

The interaction of a focused, energetic beam of electrons with sample results in producing several signals such as secondary electrons (SE), backscattered electrons (BSE), characteristic X-rays, and continuous X-rays, and fluorescence X-rays as shown in Fig. 3.20. BSE is produced when incident electrons interact with the atomic nucleus of a sample, and these electrons deflect elastically through an angle of about 180°. In this type of interaction, the kinetic energy loss is negligible. The higher atomic number of a sample leads to a higher amount of an elastically scattered BSE, resulting in a brighter image. In other words, the heavier the elements present, the brighter the region of the BSE image. BSE gives information about the elemental composition of a sample. Secondary electrons (SEs) are produced when an incident beam of electrons elastically collides with an atom, resulting in the ejection of a loosely bound valence electron of the K-orbital of the atom. The ejected electrons are known as SEs having a kinetic energy of less than 50 eV. Secondary and backscattered electrons are the two signals that are commonly used to produce images.

Primary incident beam

Depth of penetration

Auger electrons (~1 nm)
Secondary electrons (~100 nm)

Inelastically backscattered electrons(~1μm)

Characteristic X-rays (~10 μm)

Continuum X-rays (~10 μm)
Fluorescent X-rays (~10 μm)

a

b
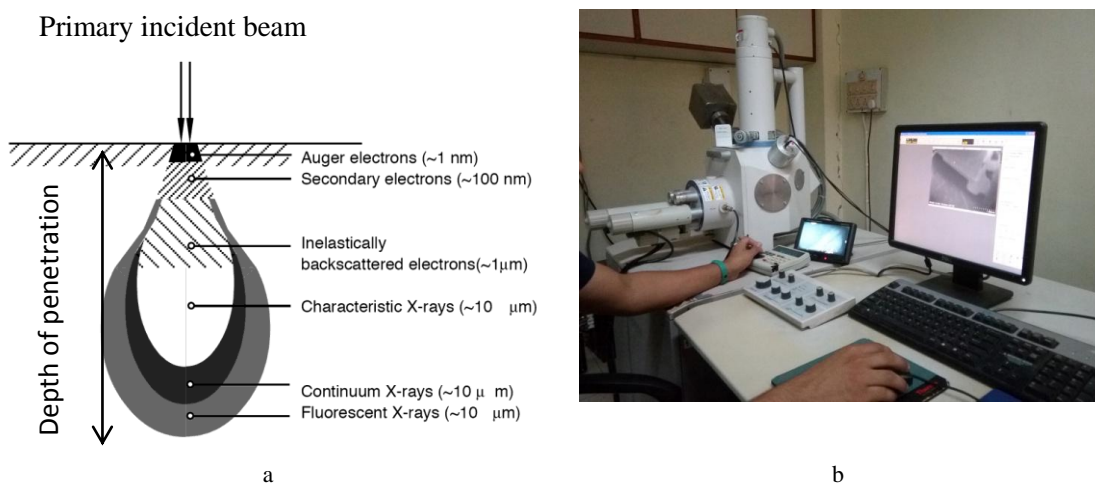
Figure 3.20 : a. Interaction volume of the incident beam of electrons with a sample and b. Bio-Logic M470 Ac-SECM, Scanning electron microscope in conjugation with an energy dispersive spectrometer.

Scanning electron microscope (SEM, Bio-Logic M470 Ac-SECM) in conjugation with an energy dispersive spectrometer (EDS, accelerating voltage 15 kV) was used for the surface study of MS surface under different experimental conditions. For surface observation, 1.0 M H_2SO_4 without and with inhibitor solutions of 400 ppm and 1000 ppm of all plant extracts were used for immersion of MS coupons for 24 h The surface analysis of the coupons was performed after taking out from the test solution at three different locations to ensure reproducibility. Similarly, EDS analysis was carried out for elemental information employing a beam of 15 kV accelerating voltage.

CHAPTER 4

4. RESULTS AND DISCUSSION

The results of the corrosion tests such as potentiodynamic polarization, electrochemical impedance spectroscopy (EIS), differential pulse voltammetry (DPV), and, gravimetric test for each of the plant extract as corrosion inhibitor are presented separately in different sub-headings. These results are used to find inhibition efficiency of inhibitor in different parameters. Different types of adsorprtion isotherms are fitted from the results obtained to find best-fit adsorption isotherm, and the free energy of adsorption is calculated. The activation energy is obtained from the Arrhenius plot. Enthalpy and entropy are calculated from the trasitional state plot. Furthermore, material characterization is done using FTIR, SEM and EDX results.

4.1 Artemisia vulgaris:

Results of corrosion tests of extract of aerial part of *Artemisia vulgaris* plant are presented as follows:

4.1.1 Potentiodynamic polarization of Mild Steel in 1.0 M H_2SO_4 with and without n-hexane and methanol extract of *Artemisia vulgaris*

Artemisia vulgaris extracts prepared in n-hexane and methanol solvents were subjected for potentiodynamic polarization for the selection of proper extract for detail study. Potentiodynamic polarization curves for mild steel coupon as immersed in 1.0 M H_2SO_4 in presence and absence of AVE 1000 ppm, and that for mild steel coupon immersed for 24 h in 1.0 M H_2SO_4 + AVE 1000 ppm are shown in Fig. 4.1.1 a and b for n-hexane and methanol solvents respectively. Potentiodynamic polarization parameters such as corrosion current (Icorr), corrosion potential (Ecorr), Cathodic slope (βa), and anodic slope (βa) obtained from the Tafel extrapolation method of the polarization curve along with inhibition efficiency are presented in table 4.1and table 4.2 for n-hexane and methanol solvents respectively.

Polarization curve and observed data obtained for AVE in both solvents imply that both cathodic hydrogen evolution and anodic metal dissolution are suppressed with the addition of AVE. However, the cathodic hydrogen evolution is more suppressed. The addition of AVE does not affect cathodic and anodic slope, which reveals that

inhibition is due to the adsorption of inhibitor molecules, forming barrier film to block the active site of corrosion. Parallel cathodic curves are observed in the polarization, which indicates that the hydrogen evolution is activation-controlled without changing the reduction mechanism (Benabdellah et al., 2006). There is marginal shift of Ecorr value with the addition of AVE which is less than 85 mV, it reveals that AVE works as a mixed type of inhibitor. (Riggs Jr., 1973)

Table 4.1 : Potentiodynamic polarization parameters for the corrosion of mild steel with n-hexane extract of *Artemisia vulgaris*.

Electrolyte	Sample	$-E_{corr}$ (V/SCE)	I_{corr} (A/cm^2)	βa (V/dec)	$-\beta c$ (V/dec)	I.E.%
Acid	Mild steel	0.454	8.02×10^{-4}	0.09	0.1	
Acid + H-AVE 1000 ppm	Mild Steel	0.448	2.16×10^{-4}	0.052	0.128	73.10
Acid + H-AVE 1000 ppm	Mild steel immersed in electrolyte for 24 h	0.408	9.64×10^{-6}	0.134	0.18	98.79

a   b
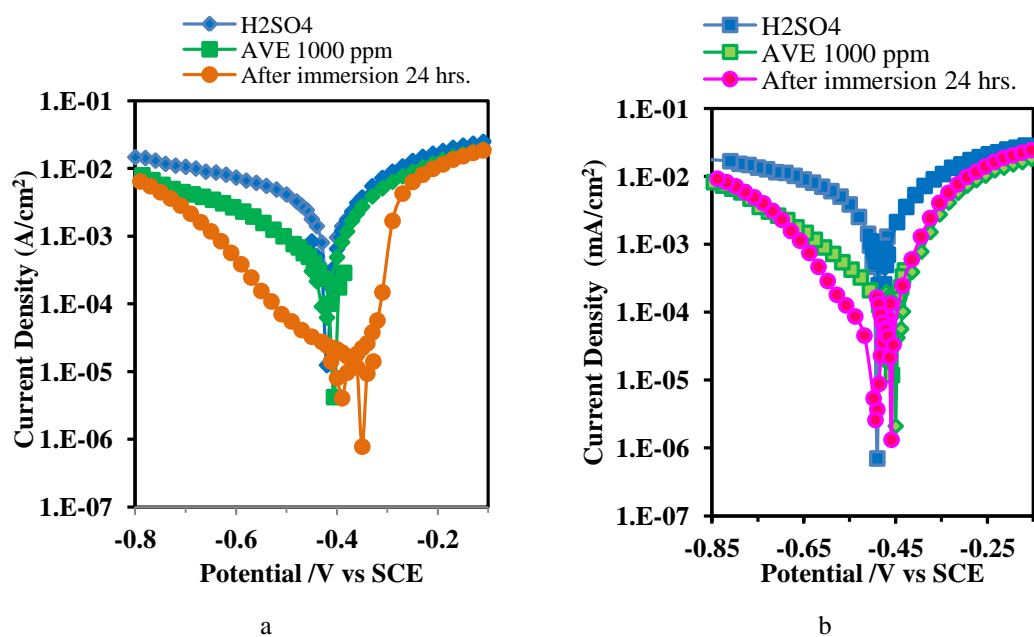
Figure 4.1. 1 : a. Polarization of Mild Steel in n-hexane extract of *Artemisia vulgaris* in 1.0 M H$_2$SO$_4$ and b. Polarization of Mild Steel in methanolic extract of *Artemisia vulgaris* in 1.0 M H$_2$SO$_4$.

Corrosion current decreases with the addition of AVE which implies the inhibition of corrosion of mild steel with AVE. The inhibition efficiency (IE) calculated for n-hexane extract is 73.10% and 98.79% for the mild steel sample as immersed in the electrolyte solution and immersed for 24 h in the electrolyte solution, whereas for

methanol extract, it is 93.29% and 96.73% for sample as immersed and immersed for 24 h. These data show that the inhibition phenomenon of methanol extract is quicker than n-hexane extract, and the obtained amount of n-hexane extract was less. So, *Artemisia vulgaris* extract in methanol solvent was selected for a detailed study.

Table 4.2 : Potentiodynamic polarization parameters for the corrosion of mild steel with methanol extract of *Artemisia vulgaris*.

Electrolyte	Sample	$-E_{corr}$ (V/SCE)	I_{corr} (A/cm^2)	βa (V/dec)	$-\beta c$ (V/dec)	I.E.%
Acid	Mild steel	0.474	9.57×10^{-4}	0.08	0.11	
Acid + M-AVE 1000 ppm	Mild Steel	0.443	6.42×10^{-5}	0.05	0.11	93.29
Acid + M-AVE 1000 ppm	Mild steel immersed in electrolyte for 24 h	0.476	3.13×10^{-5}	0.056	0.104	96.73

4.1.2 ATR-FTIR analysis of methanol extract of *Artemisia vulgaris*:

ATR-FTIR characterization of the extract was carried out to identify the functional groups present in it. The ATR-FTIR spectra of the extract are shown in Fig. 4.1.2. A list of absorption peaks and assigned functional groups are presented in table 4.3. Absorption peaks at 3687 cm^{-1}, 3653 cm^{-1} are attributed to N-H stretch of amide and O-H Stretching of alcohol. A Broad band in the range of 3359 cm^{-1} to 3213 cm^{-1} is ascribed to O-H stretching of alcohol, phenol, carbohydrate, and N-H stretching of amine. A strong absorption band at 2962 cm^{-1} and other bands at 2931 cm^{-1}, 2916 cm^{-1}, 2858 cm^{-1} are due to C-H stretching of alkane. A band at 1701 cm^{-1} is due to C=O carbonyl stretch and band at 1662 cm^{-1} is attributed to C=C stretching alkene, cyclic alkene, C=N stretching, imine, oxime, C=O stretching amide. A sharp band at 1585 is due to N-H bending of amine. The absorption band at 1504 cm^{-1} is associated with N-O stretching. Similarly, the absorption band 1454 cm^{-1} is due to C-H bending of alkane. O-H bending of alcohol, phenol and S=O stretching of sulfonate are characterized by the absorption band at 1373 cm^{-1}. The presence of alkyl, aryl ether, or aromatic ester is indicated by the C-O stretching band at 1250 cm^{-1}. Additionally, a band at 1176 cm^{-1} is ascribed to the C-O stretching of ester, and 3° alcohol and band at 1049 is attributed to S=O stretching of sulfoxide, C-N stretching of amine or S=O stretching of sulfoxide. These absorptions bands divulge that extract contains functionalities like alcohol, phenol, amine, amide, ether, ester, etc with aromatic rings.

Results show that extract contains aromatic rings with heteroatoms like N, O, which makes it easy to be adsorbed on MS Surface and makes it a good corrosion inhibitor.
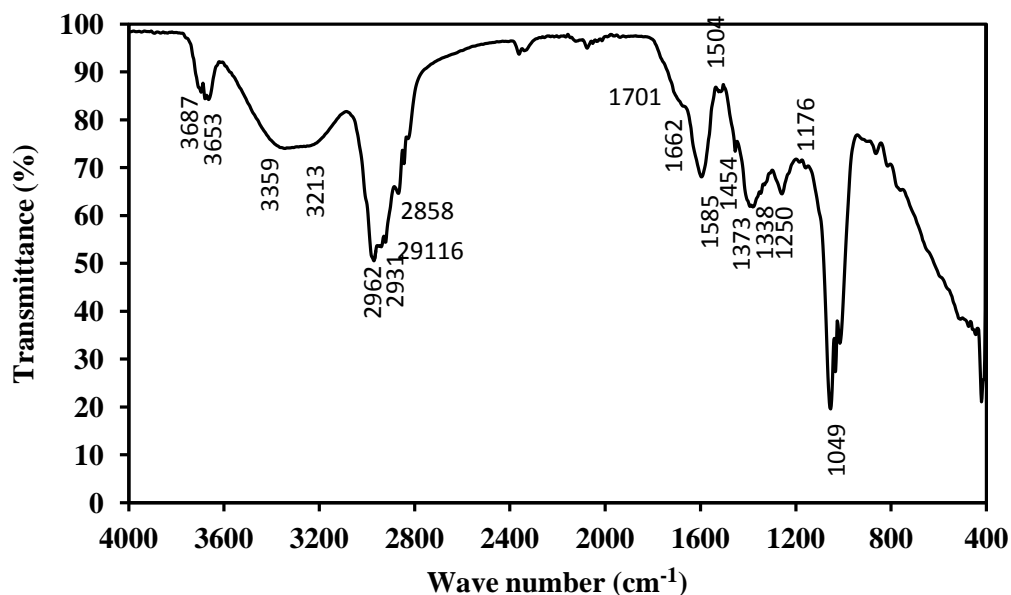
Figure 4.1. 2 : FTIR spectra of mthanolic extract of *Artemisia vulgaris.*

Table 4.3 : Some important absorption bands/ peaks from FTIR measurements of M-AVE.

Adsorption peak (cm^{-1})	Functional groups
3687, 3653	N-H stretch of amide, O-H Stretching of alcohol
3359	N-H stretching of amine
3213-3359 broad	O-H stretching of intermolecular bonded alcohol
2962, 2931,2916, 2858	C-H Stretch of alkane
1701	C=O carbonyl stretch
1662	C=C stretching of alkene, cyclic alkene, C=N stretching of imine, oxime, C=O stretching of amide
1585	N-H bending of amine
1504	N-O stretching,
1454	C-H bending of alkane,
1373	O-H bending of alcohol, Phenol, S=O stretching of sulfonate,
1338	C-N stretching of aromatic amine, S=O stretching of sulfone,
1250	C-O stretching of alkyl, aryl ether, aromatic ester,
1176	C-O stretching of ester, 3° alcohol,
1049	S=O stretching of Sulfoxide, C-N stretching amine,

4.1.3 Variation of open circuit potential with time

The OCP-time curves for MS specimen in 1.0 M H_2SO_4 solution without and with AVE of different concentrations against a SCE reference are represented in Fig. 4.1.3. It is observed that the OCP is shifted towards positive value with the addition of AVE

which can be ascribed to the formation of barrier film formed on the MS surface due to the adsorption of molecules present in AVE (Verma et al., 2015). However potential shift is not enough to classify it as a cathodic inhibitor since it is less than 85 mV. So, it can be said as a mixed inhibitor (Riggs Jr., 1973) .
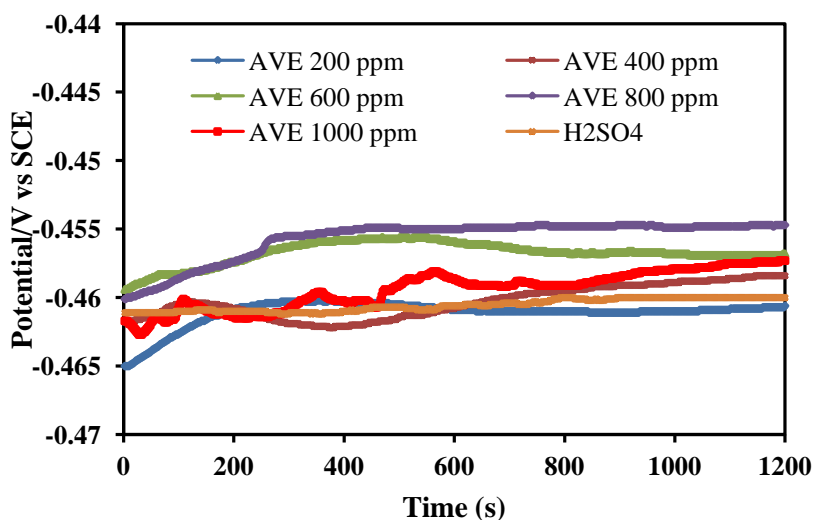
Figure 4.1. 3 : The OCP-time curves for MS specimen in 1.0 M H_2SO_4 solution without and with M-AVE of different concentrations against a SCE reference.

4.1.4 Polarization of mild steel in methanol extract of *Artemisia vulgaris* in 1.0 M H_2SO_4

Potentiodynamic polarization was carried out for mild steel coupon as immersed and after immersion of coupon in the electrolyte solution for 24 h and results are illustrated separately as follows:

Table 4.4 : Potentiodynamic polarization parameters for the corrosion of mild steel with various concentrations of M-AVE.

Concentration (ppm)	$-E_{corr}$ (V/SCE)	I_{corr} (A/cm^2)	βa (V/dec)	$-\beta c$ (V/dec)	I.E.%
Blank	0.4281	1.93×10^{-3}	0.0603	0.1122	
200	0.4377	5.94×10^{-4}	0.0329	0.1785	69.23
400	0.4347	4.31×10^{-4}	0.0404	0.171	77.72
600	0.4348	3.14×10^{-4}	0.0387	0.1638	83.76
800	0.431	2.53×10^{-4}	0.0326	0.1657	86.94
1000	0.4305	1.12×10^{-4}	0.0242	0.1616	94.21

Potentiodynamic curves for mild steel as immersed in 1.0 M H_2SO_4 were recorded in the presence and absence of AVE which is represented in Fig. 4.1.4(a). Electrochemical parameters viz corrosion current (I_{corr}), corrosion potential (E_{corr}), Cathodic slope (βc), and anodic slope (βa) obtained from the Tafel extrapolation method of the polarization curve are presented in Table 4.4 and variation in corrosion current and inhibition efficiency in the experiments is represented in figure 4.1.4(b).

a   b
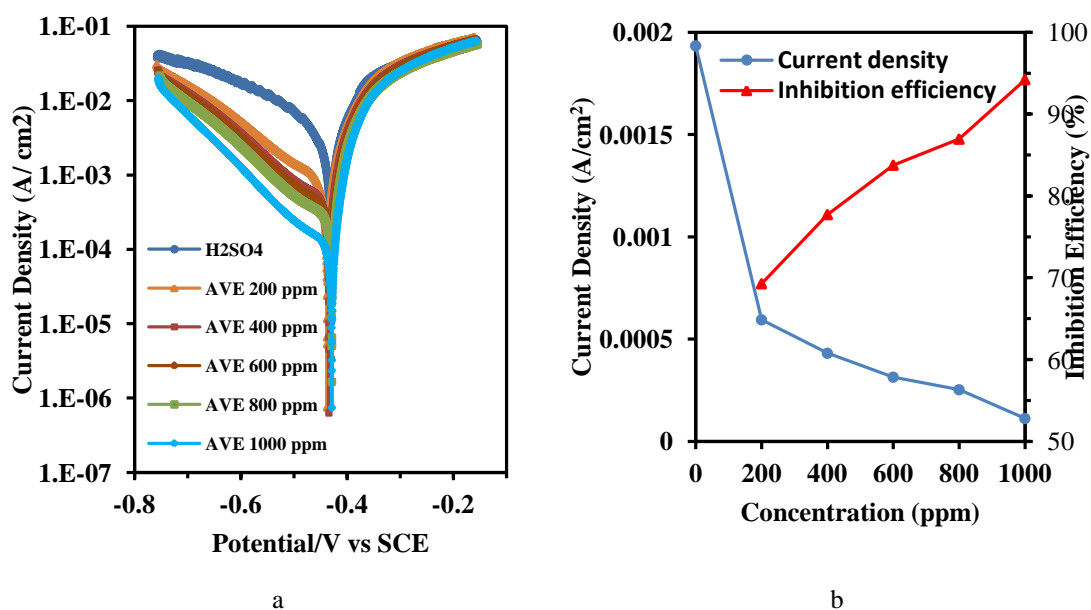
Figure 4.1. 4 : a. Polarization curve of mild steel in 1.0 M H_2SO_4 without and with M-AVE of different concentrations and b. Variation of current density and inhibition efficiency for mild steel coupon with the variation of concentration of inhibitor in 1.0 M H_2SO_4.

Table 4.5 : Potentiodynamic polarization parameters for the corrosion of mild steel immersed in electrolyte for 24 h with 1.0 M H_2SO_4 without and with various concentrations of M-AVE.

Concentration (ppm)	-E_{corr} (V/SCE)	I_{corr} (A/cm^2)	βa (V/dec)	-βc (V/dec)	I.E.%
Blank	0.474	9.57×10^{-4}	0.08	0.11	
200	0.472	1.34×10^{-4}	0.081	0.103	86.01
400	0.465	1.07×10^{-4}	0.06	0.156	88.87
600	0.454	8.02×10^{-5}	0.057	0.166	91.63
800	0.462	5.62×10^{-5}	0.054	0.1219	94.13
1000	0.476	3.13×10^{-5}	0.056	0.104	96.73

Potentiodynamic curves for mild steel in 1.0 M H_2SO_4 in the presence and absence of AVE after immersion of coupon in electrolyte for 24 h were recorded and it is

represented in Fig. 4.1.5(a). Electrochemical parameters viz corrosion current (I_{corr}), corrosion potential (E_{corr}), Cathodic slope (βa), and anodic slope (βa) obtained from the Tafel extrapolation method of the polarization curve are presented in Table 4.5 and variation in corrosion current and inhibition efficiency in the experiments is represented in figure 4.1.5(b).
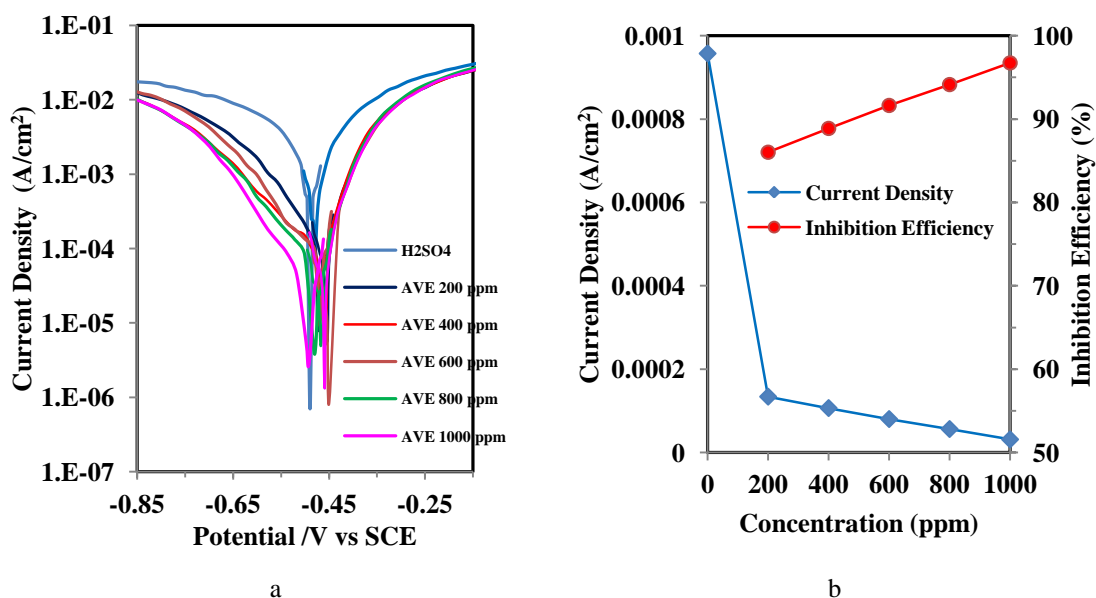
Figure 4.1. 5 : a. Polarization curve of mild steel in 1.0 M H_2SO_4 without and with M-AVE of different concentrations when mild steel coupon is immersed in electrolyte for 24 h and b. Variation of current density and inhibition efficiency for mild steel coupon immersed in electrolyte with the variation of concentration of inhibitor in 1.0 M H_2SO_4.

It is clear from the polarization curve that both cathodic and anodic curves show less current in the presence of AVE in aggressive acidic medium, but the cathode is more polarized. It reveals that both cathodic hydrogen evolution and anodic metal dissolution process are suppressed with the addition of AVE. However, the cathodic reduction of hydrogen is more suppressed. Parallel cathodic curves indicate that the hydrogen evolution is activation-controlled, which does not change the reduction mechanism (Benabdellah et al., 2006). Both cathodic and anodic slope is not more affected with the addition of AVE, which indicates that the inhibition observed in the presence of AVE is due to adsorption of inhibitor molecules on MS surface with the formation of barrier film to block the active site of corrosion. Adsorption might be enhanced due to the synergistic effect of different organic compounds present in the inhibitor (E.E. Oguzie et al., 2007). There is marginal shift of Ecorr value (less than

85 mV) with the addition of AVE which suggests that AVE works as a mixed type of inhibitor. (Riggs Jr., 1973)

Corrosion current decreases with an increase in the concentration of inhibitor and Suppression is maximum (about 17 times) in 1000 ppm solution where inhibition efficiency is 94.21%.. When mild steel coupon was polarized after immersion in electrolyte for 24 h. in the electrolyte, the current is suppressed about 30 times, and inhibition efficiency is 96.73%. Results divulge that inhibition efficiency increases with an increase in concentration, and inhibition efficiency is more when mild steel coupon is immersed in electrolyte for 24 h, and polarization is carried out. Inhibition efficiency of polarization of mild steel coupon when it is not immersed and immersed in the electrolyte is compared in Fig. 4.1.6.
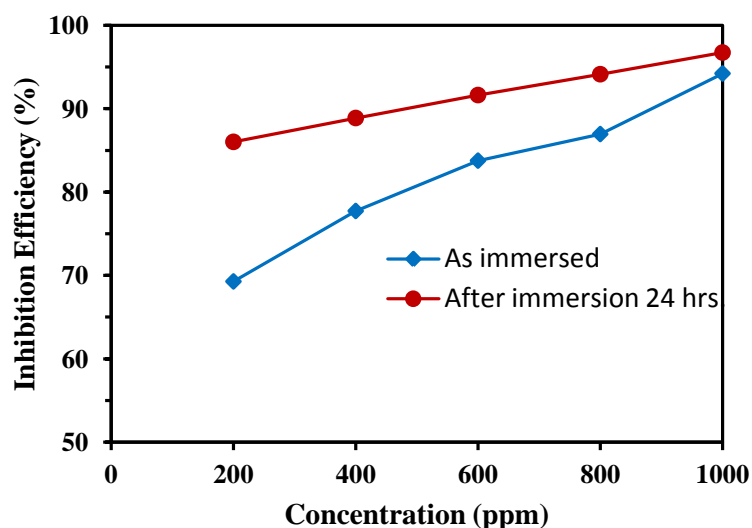
Figure 4.1. 6 : Comparison of Inhibition efficiency of M-AVE for polarization of metal as immersed and immersed for 24 h in 1.0 M H_2SO_4 without and with inhibitor of various concentrations.

4.1.5 Electrochemical impedance spectroscopy

The corrosion behavior of MS in the presence and absence of AVE was investigated by EIS measurement at OCP in a wide range of frequency. Impedance method was implemented to get information about the surface properties of the investigated system and kinetics of the electrode process. Nyquist, Bode modulus, and Bode phase plots for MS electrodes immersed in 1.0 M H_2SO_4 solution in the absence and presence of various concentrations of AVE are shown in Fig. 4.1.7(a), (b) and, (c) respectively. In the plots, curves with symbols represent the measured data, and solid lines represent the fitting data using Z-view software.
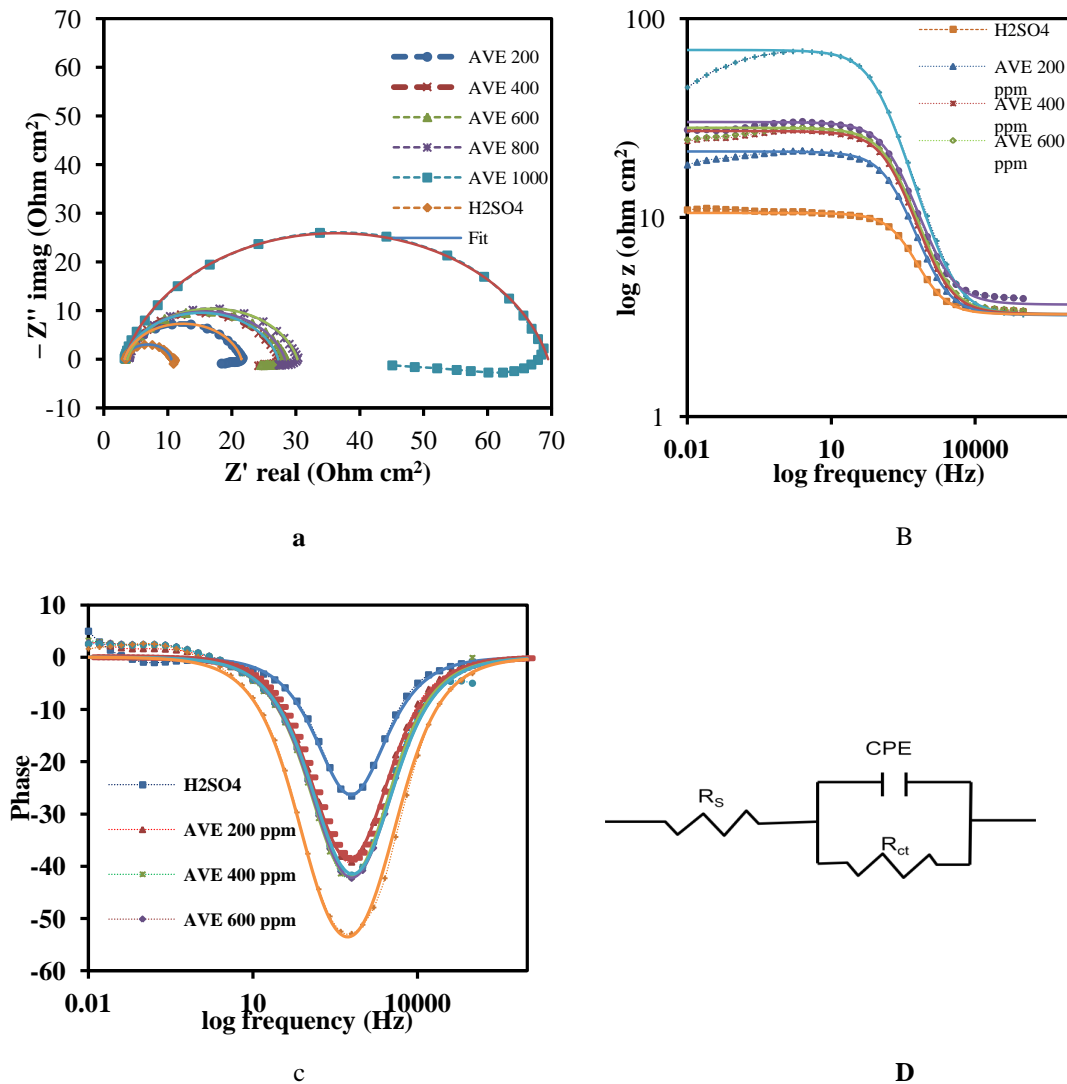
Figure 4.1. 7 : a. Nyquist plots for mild steel in 1.0M H_2SO_4 without and with M-AVE of different concentrations, b. Bode modulus plots of log Z vs. frequency for mild steel in 1.0M H_2SO_4 without and with M-AVE of different concentrations, c. Bode phase plots of phase angle vs. frequency for mild steel in 1.0M H_2SO_4 without and with M-AVE of different concentrations and d. The equivalent circuit model used to fit the impedance spectra.

The shapes of EIS plot without and with different concentration of the inhibitor are similar which reveals that the corrosion mechanism is similar for both acid and inhibited acid and the it is single relaxation process. A single depressed capacitive loop is observed at high frequency in the Nyquist plot, which can be ascribed to the time constant of the electric double layer and charge transfer resistance. Such behavior is characteristic of solid electrodes, which often shows frequency dispersion and ascribed to the roughness and other non-homogeneity of surface as in adsorption

processes (Verma & Quraishi, 2014). An inductive loop appears in the Nyquist plot at a low frequency region with AVE, and the diameter of the loop increases with an increase in concentration of AVE. The inductive behavior at lower frequency can be ascribed to the relaxation process achieved by adsorption of inhibitor molecules on the surface of the electrode or to desorption of adsorbed molecules at low frequencies. (Bentiss et al., 2000b; Veloz & González, 2002) It could be the result of the stabilization of adosrbed layer by the interaction of inhibitor molecules with corrosion products like $[FeSO4^{-2}_{(ads)}]$, $[FeOH]^-$, $[FeH]^+$ on the surface of electrode.

The diameter of capacitive loops in the Nyquist plot, which indicates charge transfer resistance, is increased with the addition of inhibitor, and it increases with an increase in concentration. It indicates that corrosion is inhibited with the addition of AVE and inhibition efficiency increases with an increase in concentration of AVE. An increment in phase angle in the Bode-phase plot and an increment in the value of impedance at low frequencies in the Bode-modulus plot with the concentration of AVE also confirm the inhibitive behavior of AVE increases with an increase in concentration of AVE. An increase in inhibition efficiency with an increase in the concentration of inhibitor is presumably due to more coverage of the MS surface by inhibitor molecules.

Single-phase peak observed in the Bode-phase plot indicates that the system under study has only one time constant, which is related to the electrical double layer. So, the equivalent circuit consisting of a one-time constant depicted in figure 4.1.7(d) was employed to analyze the impedance spectra. The circuit consists of solution resistance (R_s), charge transfer resistance (R_{ct}), and constant phase element (CPE). The CPE is used instead of a pure capacitor Which represents the interfacial capacitance. It is used in the circuit model to take into account the electrode surface non-homogeneity caused by surface roughness, adsorption of inhibitors, dislocations, grain boundaries, and the development of a porous layer. (Ahamad et al., 2010; Bammou et al., 2014; Bedair et al., 2017; Bentiss et al., 2000b; Fernandes et al., 2019a; Hosseini et al., 2003a; Jüttner, 1990; Ma et al., 2017; Murmu et al., 2019; Qiang et al., 2018; Shahabi et al., 2015; Yüce & Kardaş, 2012).

The impedance of CPE is described by equation [4-1]:

$$Z_{CPE} = Y_0^{-1}(j\omega)^{-n} \qquad\qquad [4\text{-}1]$$

Where Y_0 represents the magnitude of the CPE, j, the imaginary number ($j^2 = -1$), ω, being angular frequency ($\omega = 2\pi f$), and n, the CPE exponent ($-1 \leq n \leq +1$), whose value is used to evaluate the surface's non-homogeneity or roughness. (Jüttner, 1990) The CPE depicts a pure resistor when n=0, an inductor when n=-1, and a pure capacitor when n=+1. (Hosseini et al., 2003).

Electrochemical parameters obtained by fitting impedance data along with calculated IE is presented in table 4.6, and variation of inhibition efficiency and constant phase element with the variation of concentration of AVE is shown in Fig. 4.18.

Table 4.6 : Impedance parameters for corrosion of mild steel in 1.0 M H_2SO_4 without and with different concentration of M-AVE.

Concentration (ppm)	Rs (Ωcm^2)	CPE ($\mu\Omega^{-1}S^n cm^{-2}$)	n	R_{ct} (Ωcm^2)	I.E.%
Blank (0)	3.26	180.81	0.874	7.29	
200	3.238	126.49	0.857	18.28	60.12
400	3.265	109.65	0.852	24.00	69.63
600	3.27	106.30	0.846	25.03	70.87
800	3.65	95.53	0.845	26.60	72.59
1000	3.23	73.60	0.845	66.20	88.99

It can be observed from table 4.6 that value CPE decreases with the addition of AVE which is due to a decrease in local dielectric constant. The result can be ascribed to the increase in the thickness of the electric double layer which is due to adsorption of large size inhibitor molecule on the metal surface with the gradual displacement of water molecule leading to the formation of protective film or complex from an acidic solution (Bentiss et al., 1999). The value of CPE decreases with the concentration of AVE which implies that the adsorption increases with the concentration of AVE increasing the thickness of the electric double layer. Hence increase in inhibitor concentration increases the corrosion inhibition efficiency. (Quraishi & Ansari, 2003).
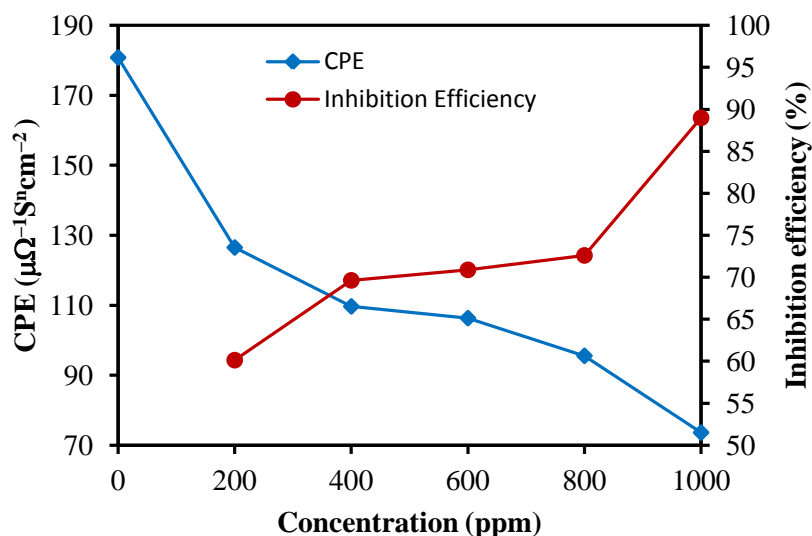
Figure 4.1. 8 : Variation of inhibition efficiency and constant phase element with the variation of concentration of M-AVE.

4.1.6 Determination of inhibition efficiency by weight loss (Gravimetric) method

Gravimetry is one of the simplest and probably most widely used methods for corrosion study. Inhibition efficiency for the long time up to 24 h can be studied by this method where as efficiency for short time is studied in electrochemical methods. Gravimetric measurements studied inhibitive behavior of AVE by varying time, concentration, and temperature which are discussed as follows:

4.1.6.1 Effect of immersion time

Inhibition behavior of AVE was studied by immersing mild steel coupon of known dimension and mass in 100 mL of 1.0 M H_2SO_4 without and with AVE of 1000 ppm concentration at 298 K for different time periods viz 3 h, 6 h, 9 h, 12 h, and 24 h. Inhibition efficiency is calculated from the results of the experiments. The obtained result, along with computed inhibition efficiency is shown in table 4.7. Variation in inhibition efficiency and corrosion rate of the metal sample in acid and inhibitor solutions is shown in Fig. 4.1.9(a) and loss of metal with and without inhibitor is shown in Fig. 4.1.9(b).

This data clearly shows that the loss of mild steel is less in acid with inhibitor. So, AVE can be used as a corrosion inhibitor. Inhibition efficiency increases up to 6 h. However, efficiency at 3 h and 6 h are almost the same. Inhibition efficiency

decreases after 6 h onwards slightly and gradually. IE is less in the beginning, means more metal ions are leached from the beginning. These leached Fe^{2+} forms chelate complex with inhibitors and after elapsing the time, amount of inhibitor molecules are less available and IE decreases with increase in time.

Table 4.7 : Corrosion rate of mild steel in the presence and absence of M-AVE and inhibition efficiency of M-AVE at various time of immersion.

Solution	Time (h)	Surface area (cm^2)	Weight Loss (mg.)	Rate (mg/cm^2hr)	Inhibition efficiency (%)
Acid		30.12	641.13	79.12	85.84
Inhibitor	3	30.14	90.90	11.21	
Acid		30.83	1287.33	77.57	87.84
Inhibitor	6	28.43	144.33	9.43	
Acid		29.56	1819.33	76.22	79.69
Inhibitor	9	29.50	368.83	15.48	
Acid		29.96	2439.17	75.61	78.62
Inhibitor	12	29.90	520.43	16.16	
Acid		28.50	4636.03	75.55	77.75
Inhibitor	24	29.51	1068.40	16.81	

a   B
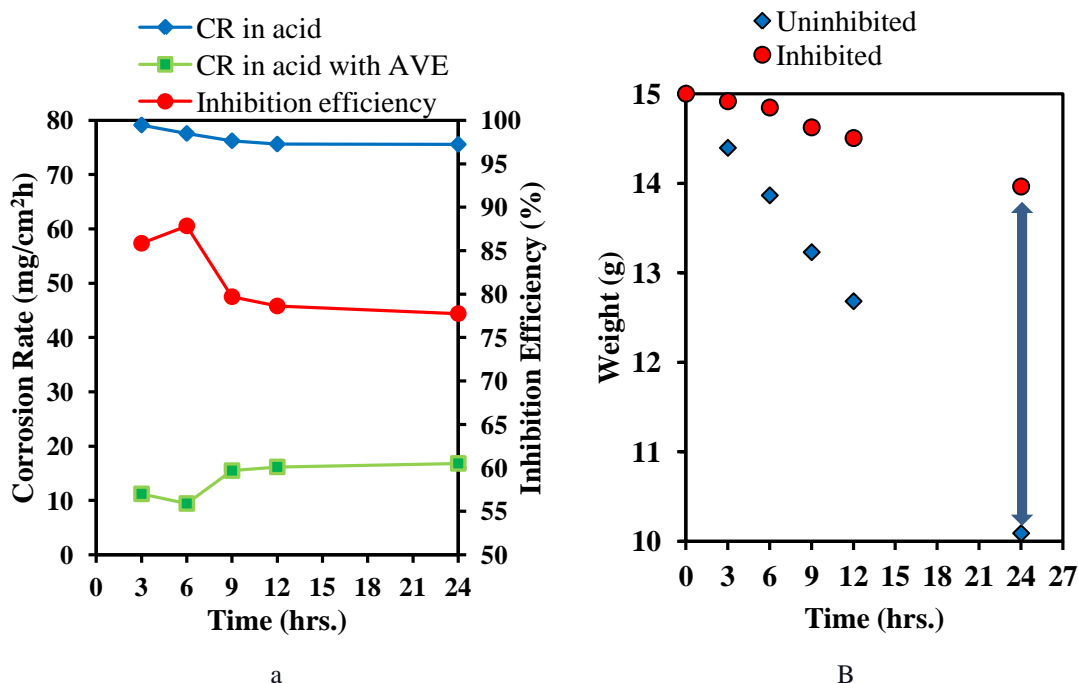
Figure 4.1. 9 : a. Variation in corrosion rate in presence and absence of inhibitor and variation in inhibition efficiency with different immersion time and b. Variation in weight of mild steel with and without inhibitor.

4.1.6.2 Effect of temperature:

Table 4.8 : Corrosion rate of mild steel in the presence and absence of AVE and inhibition efficiency of M-AVE at various temperatures.

Solution	Temperature (K)	Surface area (Cm^2)	Weight Loss (mg.)	Corrosion Rate (mg/cm^2hr)	Inhibition efficiency (%)
Acid	298	31.69	1323.97	77.60	86.50
Inhibitor		29.54	166.57	10.47	
Acid	308	29.59	1875.40	117.72	88.05
Inhibitor		31.02	234.83	14.06	
Acid	318	28.67	2750.07	178.26	80.14
Inhibitor		28.93	551.37	35.40	
Acid	328	30.29	3716.37	227.89	70.18
Inhibitor		29.67	1085.80	67.97	
Acid	338	29.97	4660.87	288.89	58.85
Inhibitor		30.17	1931.03	118.88	
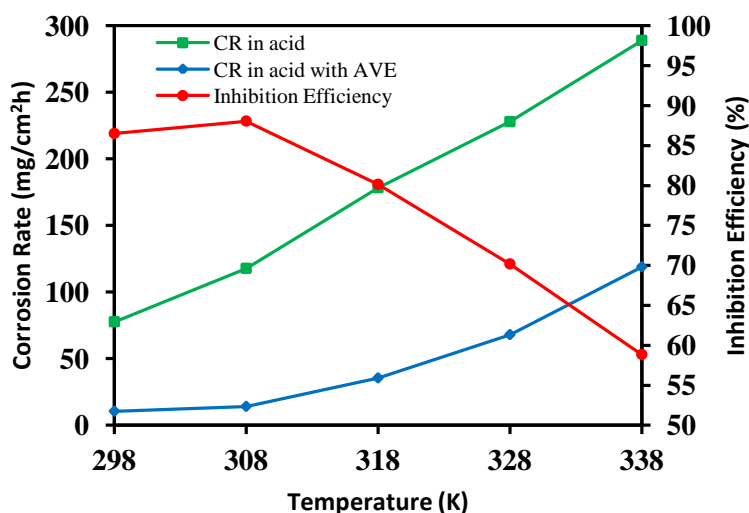
Figure 4.1. 10 : Variation of corrosion rate and inhibition efficiency with variation of temperature.

Gravimetric experiments were carried out at various temperatures (298 K, 308 K, 318 K, 328 K and, 338 K) to calculate corrosion rate and inhibition efficiency, and the results are shown in table 4.8. Results were used to investigate the stability of barrier film formed on metal surface due to adsorption of inhibitor molecules as well as activation parameters of the corrosion process of metal in acidic media. Variation in the corrosion rate of mild steel in acid with and without inhibitor, and inhibition efficiency at various temperatures is shown in Fig. 4.1.10. Up to 308 K, IE increases

with increasing temperature and decreases beyond that. A drop in IE as temperature rises could be attributed to desorption or breakdown inhibitors being released at a higher temperature. (Bentiss et al., 2009). This result shows that AVE is not stable at higher temperatures.

4.1.6.3 Effect of concentration:

Table 4.9 : Corrosion rate of mild steel in the presence and absence of M-AVE and inhibition efficiency of M-AVE at various concentrations.

Concentration	Surface area (cm^2)	Weight Loss (mg.)	Corrosion Rate (mg/cm^2hr)	Inhibition efficiency (%)	Surface coverage (θ)
0 ppm. (acid solution only)	30.83	1287.33	77.57		
200 ppm.	28.87	492.30	31.67	59.17	0.5917
400 ppm.	30.75	432.43	26.12	66.32	0.6632
600 ppm.	30.21	325.47	20.01	74.20	0.7420
800 ppm.	29.88	246.33	15.32	80.26	0.8026
1000 ppm.	28.43	144.37	9.43	87.84	0.8784
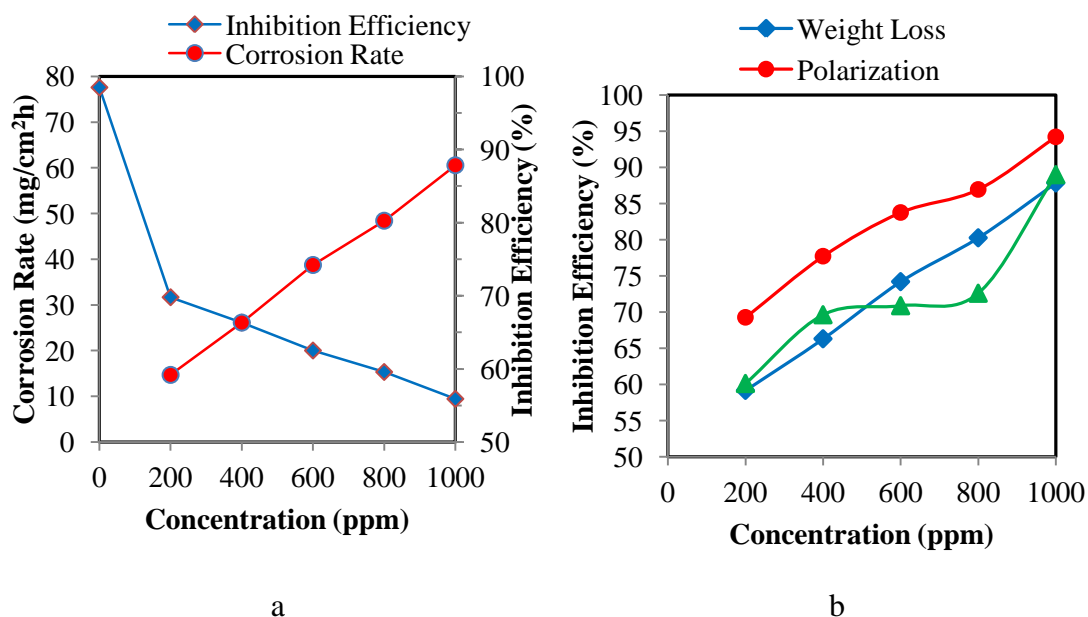
Figure 4.1. 11 : a. Variation in corrosion rate and inhibition efficiency with the variation of concentration of M-AVE and b. Inhibition efficiency of M-AVE from different methods for MS in 1.0 M H_2SO_4.

Gravimetric experiments were carried out in various concentrations (200 ppm, 400 ppm, 600 ppm, 800 ppm and, 1000 ppm) at 298 K for 6 h to calculate corrosion rate and inhibition efficiency by M-AVE and results are shown in table 4.9. Variation in

109

corrosion rate and inhibition efficiency with variation in concentration is represented in Fig. 4.1.11(a).

Results show that inhibition efficiency increases with the concentration of inhibitor in acid, which can be ascribed to more surface coverage of MS with more adsorption of inhibitor molecules on it. Electrochemical experiments such as potentiodynamic polarization and electrochemical impedance spectroscopy support the findings. Figure 4.1.11(b) shows a comparison of inhibition efficiency produced by various methods.

4.1.7 Adsorption isotherm:

Corrosion inhibition due to organic molecules can be attributed to their adsorption on the mild steel surface through their polar functions to from barrier film for the transfer of charge and mass between metal and the solution. So, adsorption isotherm is important to get information about the interaction between the inhibitor molecules and mild steel surface. Inhibitor molecules are adsorbed on metal surface displacing water molecules which were adsorbed in aqueous solution. So, the adsorption of organic molecules is a quasi substitution process (Cang et al., 2013; Verma & Quraishi, 2007). The best isotherm that fits the data collected was determined by plotting the degree of surface coverage (θ) obtained from the gravimetric method against the inhibitor concentration. In this study, the inhibitor used is a crude plant extract, which is the mixture of several organic compounds. All the compounds might affect the inhibitive action of inhibitor positively or negatively. However, the concentration used to fit suitable adsorption models is the average molar concentration of few essential compounds which plays a major role in inhibition. Several adsorption isotherms, like Langmuir, Tempkin, Freundlich, El-Awady, were evaluated to describe adsorption behavior of inhibitor molecules. Among them, the best fit adsorption isotherm obtained was Langmuir adsorption isotherm because when C_{inh} is plotted against C_{inh}/θ, a straight line was obtained where values of both linear correlation coefficient (R^2) and slope are almost equal to 1, Fig. 4.1.12. Little deviation of values from unity may be due to some interactions between adsorbed inhibitor molecules on the mild steel surface. Interactions may be either mutual attraction or repulsion force between different functional groups of different molecules or preferential adsorption of molecules at the cathodic and anodic site (Verma & Quraishi, 2007). As adsorption

follows Langmuir adsorption isotherm, adsorption of inhibitor on MS surface is a monolayer where adsorbate molecules do not interact with each other.
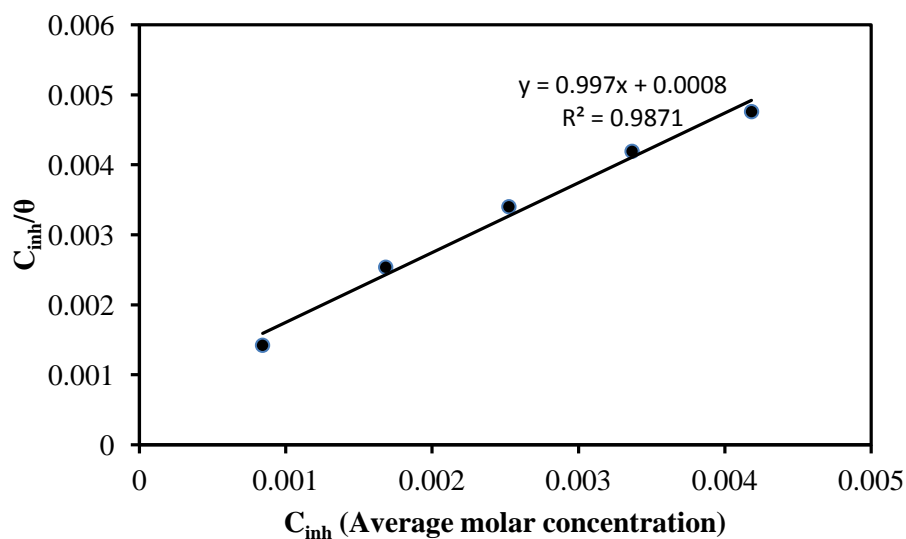
Figure 4.1. 12 : Langmuir adsorption isotherm plot for mild steel in 1.0 M H_2SO_4 with different concentration of M-AVE as the average molar concentration of some major compounds in M-AVE.

Relation of Langmuir adsorption isotherm is shown in equation [4-2],

$$\frac{C_{inh}}{\theta} = \frac{1}{K_{ads}} + C_{inh}$$ [4-2]

When C_{inh} is plotted against $\frac{C_{inh}}{\theta}$, a straight line is obtained. The value of adsorption constant K_{ads} can be calculated from the intercept of the line. This value can be used in the equation [4-3] to calculate the value of free energy of adsorption ($\Delta G°$).

$$\Delta G° = - RT \ln(55.5 K_{ads})$$ [4-3]

Where 55.5 is the concentration of water in solution in mol/L and R is the universal gas constant (8.314J/mol K). Calculated value of $\Delta G_{ads}°$ according to relation is -27.62 kJ/mol. Large negative value of $\Delta G_{ads}°$ implies that the AVE is adsorbed on mild steel surface spontaneously to form highly stable barrier film (Cang et al., 2013). Generally, physisorption is related with a value of $\Delta G°$ less than or around -20 kJ/mol, while chemisorption is associated with a value of $\Delta G°$ greater than or around -40 kJ/mol. Here, the computed value is intermediate, which implies that the adsorption is not merely physical or chemical but involves both. Adsorption involves physical adsorption with displacement of water molecules from the mild steel surface followed by chemisorption. (Cang et al., 2013).

111

4.1.8 Calculation of activation energy and thermodynamic parameters :

Arrhenius plots for corrosion rate at various temperatures can be used to compute activation energy (E_a) according to the relation [4-4]:

$$\log(C.R.) = \log A - \frac{E_a}{2.303\,RT}$$

[4-4]

where, A refers to the Arrhenius pre-exponential constant and, T refers to the absolute temperature.

From the Arrhenius plot shown in Fig. 4.1.13(a), calculated values of E_a and A are shown in table 4.10. The intense adsorption of inhibitor molecules on the metal surface is indicated by an increase in Ea with the presence of inhibitor. (Ostovari et al., 2009).

Enthalpy and entropy of adsorption can be computed using transition state equation [4-5] :

$$\log\left(\frac{C.R.}{T}\right) = \left[\log\left(\frac{R}{hN}\right) + \left(\frac{\Delta S^*}{2.303R}\right) - \frac{\Delta H^*}{2.303\,RT}\right]$$

[4-5]

Where, h refers to plank's constant (6.6261×10^{-34} Js) and, N refers to Avogadro's number (6.0225×10^{23} mol^{-1}).
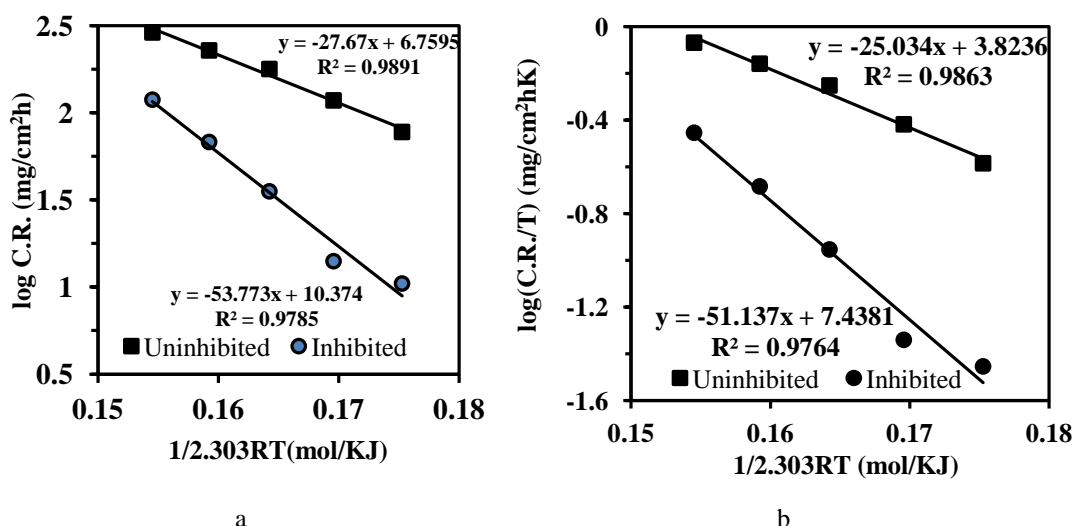
Figure 4.1. 13 : a. Arrhenius plot for mild steel in 1.0 M H_2SO_4 with and without M-AVE and b. Transition state plot for mild steel in 1.0 M H_2SO_4 with and without M-AVE.

When $log\left[\frac{C.R.}{T}\right]$ is plotted against $\frac{1}{2.303\,RT}$, a straight line shown in Fig. 4.1.13(b) is obtained. The slope of this line is the enthalpy of activation. The intercept of the line, $\left[log\left[\frac{R}{hN}\right]+\frac{\Delta S^*}{2.303\,R}\right]$ can be used to compute the entropy of activation. Calculated values of ΔH^* and ΔS^* for acid in absence and presence of inhibitor are Shown in table 4.10. Value of ΔH^* is intermediate between common physical adsorption heat and chemical adsorption heat, which again supports that adsorption is a mixed type involving both physical and chemical adsorption (Khadom, Abd, & Ahmed, 2018). The positive value of ΔH^* indicates the endothermic nature of the metal dissolution process. An increase in the value of ΔH^* with the addition of AVE indicates the reduction in corrosion rate is governed by kinetic parameters of activation (Hamdy & El-Gendy, 2013). The preceding calculations reveal that Ea is greater than ΔH^*, indicating that a gaseous reaction, namely hydrogen evolution processes, is involved, resulting in a reduction in overall reaction volume. (Ostovari et al., 2009) . The corrosion process is unimolecular in the condition, Ea $-\Delta H^* =$ RT. Here the difference in value of Ea $-\Delta H^*$ is about 2.64 kJ/mol which is nearly equal to RT.

The increase in ΔS^* shows that the activated complex in the rate-determining phase is an association rather than a dissociation step, implying that there is a decrease in disordering as the reaction progresses from reactants to the activated complex. With the addition of the inhibitor, the value of ΔS^* increases, indicating an increase in disorder as the reaction progresses from reactant to the activated complex. The replacement of water molecules during the adsorption of the inhibitor on the mild steel surface causes this behavior. (Hamdy & El-Gendy, 2013).

Table 4.10 : Activation parameters of the dissolution of mild steel in 1.0 M H_2SO_4 without and with M-AVE of 1000 ppm concentration.

Electrolyte	Ea(kJ/mol)	A (mg/cm^2)	ΔH(kJ/mol)	Ea-ΔH	ΔS(J/molK)
1.0 M H_2SO_4	27.67	5.7×10^6	25.034	2.636	-124.36
Acid with inhibitor	53.77	2.3×10^{10}	51.137	2.633	-55.16

4.1.9 Surface analysis

Energy dispersive X-ray (EDX) was carried out to estimate the percentage of heteroelements present on the surface of the MS coupon in the absence and presence of inhibitor when the coupons were retrieved after 24 h immersion in the test solution. EDX spectra and SEM micrograph of the surface of MS coupons immersed in acid

without and with inhibitor of 400 ppm and 1000 ppm are shown in Fig. 4.1.14 and the percentage of different elements present on the surface are presented in supplementary table 4.11. Figure and data show the increases in the amount of nitrogen, oxygen, phosphorus on the surface which supports the formation of protective film on the surface due to the adsorption of organic compounds on the surface. It can be seen from SEM image that severe damage with deep furrows and large cracks are seen on the surface of MS coupons immersed in acid in the absence of inhibitor. These cracks and furrows are relatively less in the surface immersed in inhibited acid, and a relatively smooth surface with protective film can be seen. This observation can be attributed to the adsorption of inhibitor molecules on the MS surface.

a   **b**   **C**
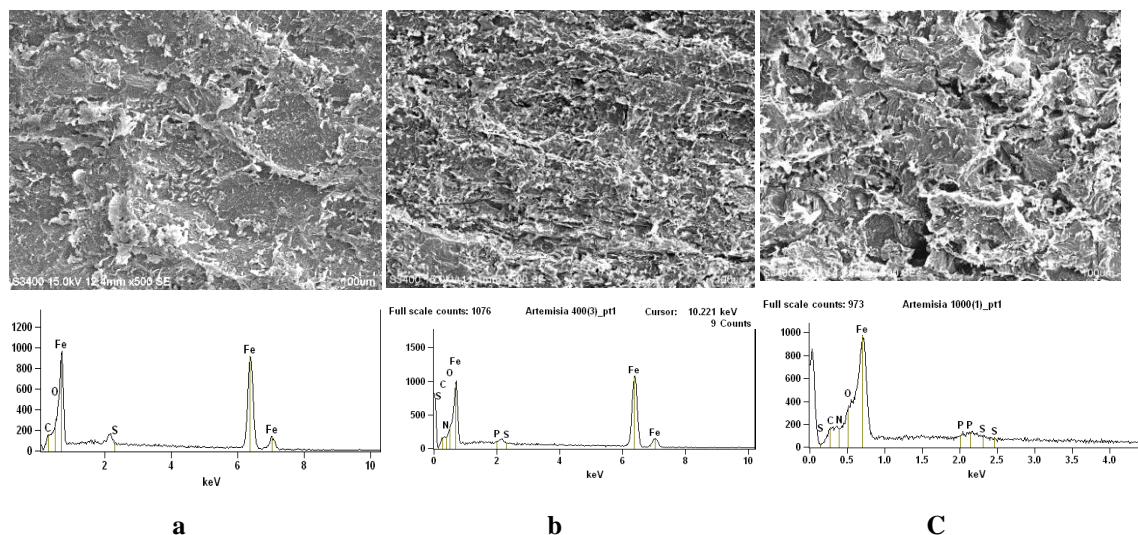
Figure 4.1. 14 : SEM images and corresponding EDX spectra of mild steel coupons after 24 h immersion in (a) 1.0 M H$_2$SO$_4$, (b) 400 ppm extract solution in 1.0 M H$_2$SO$_4$ and (c) 1000 ppm extract solution in 1.0 M H$_2$SO$_4$.

Table 4.11 : Weight difference of different elements on the MS surface after immersion in the sample in different solutions.

Surface dipped in	Iron	Carbon	Nitrogen	Oxygen	Phosphorus
Acid without inhibitor	89.94%	7.39%		2.76%	
Acid with inhibitor of 400 ppm	94.80%	1.78%	1.31%	2.11%	
Acid with inhibitor of 1000 ppm	92.91%	2.27%	1.58%	3.16%	0.07%

4.1.10 Mechanism of inhibition:

Corrosion inhibition by organic compounds is due to barrier film on the metal surface formed as a result of adsorption of large size molecule on metals surface. Computed

114

value of free energy activation (-27.62 kJ/mole) suggests that adsorption of molecules present in AVE is comprehensive adsorption involving both chemisorption and physisorption but observed predominantly physical adsorption. AVE contains organic molecules such as serotonin, prunacin, N,N-dimethyl-4-nitroso-3-trimethylsilylaniline, luteolin, morin, camphor etc. Mechanism of corrosion inhibition by adsorption of these molecules can be explained as follows:

The OCP value of MS in AVE is measured around -0.45 V, which is more than the potential of zero charge (PZC) of MS in sulfate solution. (Sivakumar et al., 2018). Therefore the value of Antropov's rational corrosion potential is positive, and the net charge of MS is positive. In acidic solution, the abstraction of a proton by lone pair of electron on heteroatoms makes organic molecules positively charge, and the possibility of their adsorption on the positive metal surface is denied due to electrostatic repulsion. However, adsorption is made feasible due to synergism with sulfate ion. Due to a modest degree of hydration, sulfate ions formed from H_2SO_4 are adsorbed on the mild steel surface, resulting in an increased negative charge near to the interface, which facilitates the adsorption of positively charged protonated inhibitor molecules. Thus, the positively charged organic molecules of AVE are adsorbed via electrostatic force of attraction with Sulfate. This adsorption in inhibitor in competition with H^+ ion in the cathodic site of mild steel leads to inhibition of cathodic hydrogen evolution, but positively charged organic molecules returns to neutral form.

Then, the highest occupied molecular orbitals (HOMO) of neutral organic molecules interact with vacant d-orbital of iron with the replacement of water from the surface to form a coordinate bond with donor-acceptor interaction. The orbital with the higher electron density, like the bonding π orbital or the orbital containing unshared electron pair, is referred to as HOMO. HSAB (hard and soft acid and base) theory also supports strong interaction between the organic molecule and mild steel surface. Owing to the electron pair on heteroatoms, the big organic inhibitor molecules behave as a soft base with high polarizability and low ionization potential and metal at zero oxidation state acts as a soft acid. According to HSAB theory, a soft acid reacts faster with a soft base with strong bond resulting in stronger donor-acceptor interaction (Sadeghi Erami et al., 2019). To relieve metal from accumulation of extra negative

charge on surface due to donor acceptor interaction, retrodonation may occur between metal atom and LUMO of inhibitor molecules, which is the return of electrons from 4S or 3d orbital of the metal atom to LUMO of inhibitor molecules to form feedback bond. Retro-donation strengthens the chemisorption of a molecule on the metal surface. Schematic representations of adsorption of two compounds serotonin and N,N-dimethyl-4-nitroso-3-trimethylsilylaniline are shown in Fig. 4.1.15.
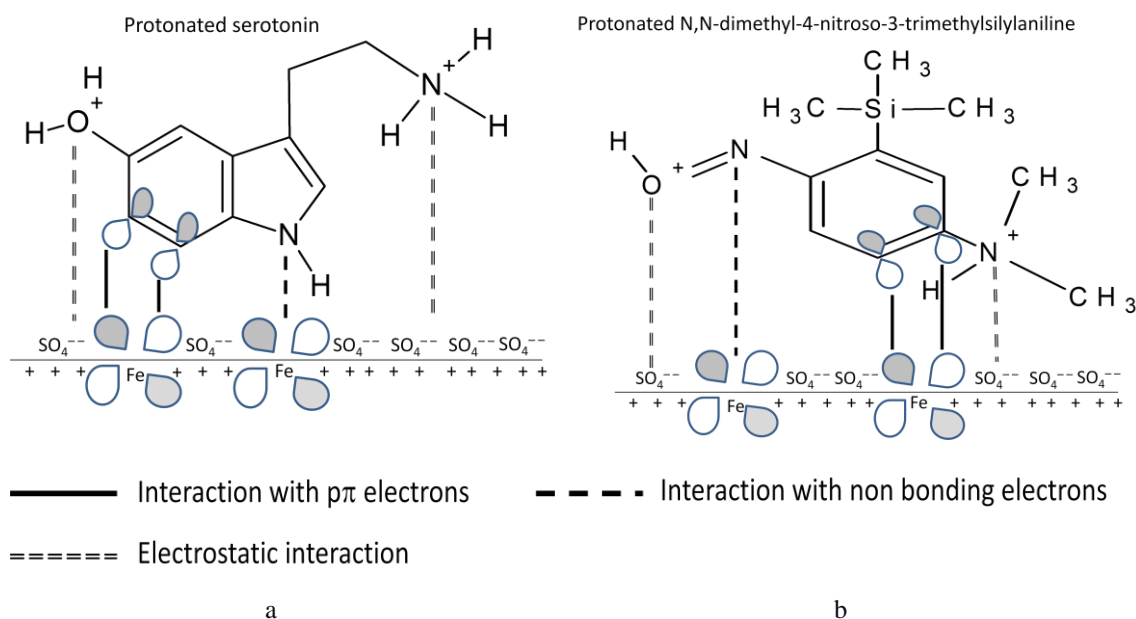
Figure 4.1. 15 : Schematic representations of adsorption of a. serotonin and b. N,N-dimethyl-4-nitroso-3-trimethylsilylaniline on mild steel/ 1.0 M H_2SO_4 interface.

Chelation due to the formation of the stable and insoluble metal-inhibitor complex on the metal surface as a result of the combination of organic molecules with Fe^{+2} ions is also the cause of corrosion inhibition. In low concentration of inhibitor, numbers of such types of complex molecules are less and cannot prevent corrosion significantly. However, increase in concentration increases the number of complex molecules which decreases the solubility of the protective layer formed and inhibits corrosion. It explains the high inhibition efficiency due to AVE at higher concentrations.

Chelation suppresses anodic reaction as follows :

$$Fe_{(s)} \longrightarrow Fe^{2+}{}_{(aq)} + 2e^-$$

$$Fe^{2+}{}_{(aq)} + AVE_{(ads)} \longrightarrow [Fe\text{-}AVE]^{2+}$$

116
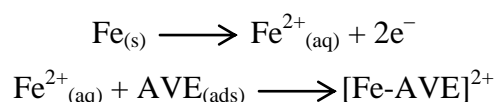
The possible chelate complexes of luteolin and morin are shown in Fig. 4.1.16.

a   b
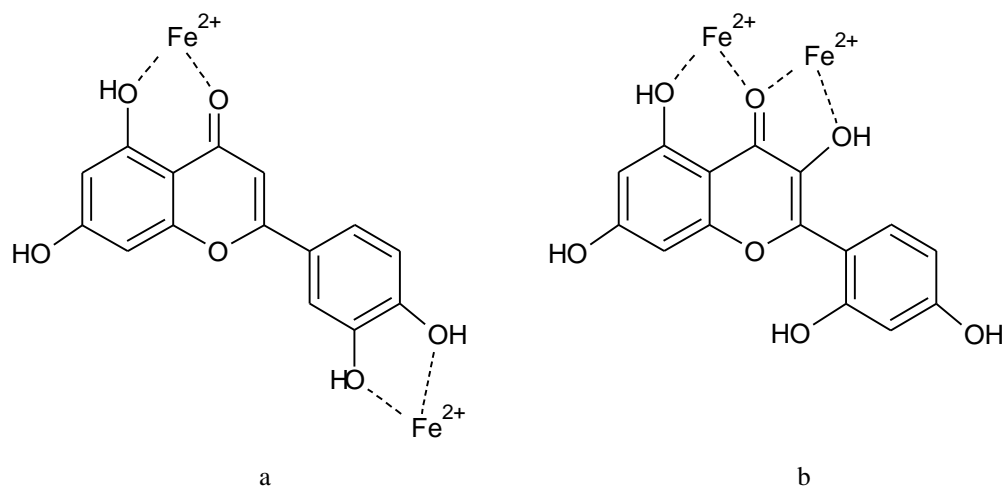
Figure 4.1. 16 : Possible complex formation between a. luteolin and b. morin with iron.

Both anodic and cathodic processes are suppressed by the adsorption of inhibitor molecules. The adsorption of sulphate inhibits the anodic dissolution as follows: (Karthik et al., 2014)

$$H_2SO_4 \longrightarrow H^+ + SO_4^{--}$$

$$AVE + H^+ \longrightarrow (AVE)H^+$$

$$Fe + SO_4^{--} \longrightarrow (FeSO_4^{--})_{ads}$$

$$(FeSO_4^{--})_{ads} \longrightarrow (FeSO_4^-)_{ads} + e^-$$

$$(FeSO_4^-)_{ads} \longrightarrow (FeSO_4)_{ads} + e^-$$

$$(FeSO_4)_{ads} \longrightarrow Fe^{++} + SO_4^{--}$$
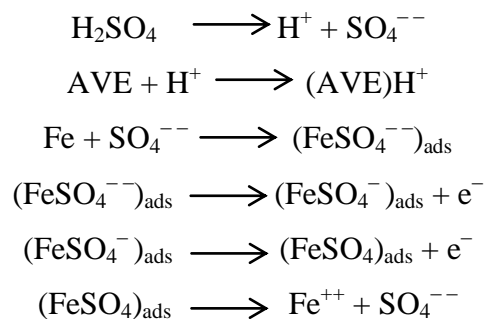
Adsorption inhibits cathodic hydrogen evolution as follows:

$$Fe + (AVE)H^+ \longrightarrow [Fe\text{-}(AVE)H^+]_{ads} \text{ (adsorption of protonated AVE molecules)}$$

$$[Fe\text{-}(AVE)H^+]_{ads} + e^- \longrightarrow [Fe\text{-}(AVE)H]_{ads} \quad \text{(Reduction of protonated H}^+)$$

$$[Fe\text{-}(AVE)H]_{ads} + H^+ + e^- \longrightarrow Fe + H_2 + AVE \quad \text{(Release of hydrogen)}$$
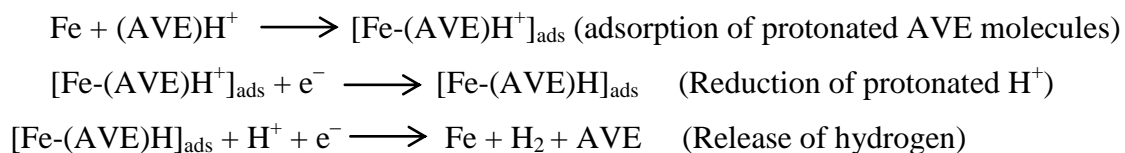
Part of this work is published in Journal of Nepal Chemical Society, volume 39, 76-85 (2018) (Karki et al., 2018). This was preliminary weight loss data. So, the error in estimated inhibition efficiency (73.76%) was relatively higher which was later rectified by electrochemical measurements (88.99 by EIS, 94.21 by potentiodynamic polarization) and verified again by weight loss method (87.84%).

4.2 *Equisetum hyemale*:

Results of corrosion tests of extract of aerial part of *Equisetum hyemale* plant are presented as follows:

4.2.1 Potentiodynamic polarization of mild steel in 1.0 M H₂SO₄ *Equisetum hyemale* extract in methanol and n-hexane solvents

Potentiodynamic polarization of mild steel was carried out in 1.0 M H_2SO_4 without and with n-hexane and methanol extract of *Equisetum hyemale*. Polarization curves obtained for mild steel as immersed and immersed for 24 h for n-hexane and methanol extracts are shown in Fig. 4.2.1 (a) and (b) respectively. Electrochemical parameters such as corrosion current (Icorr), corrosion potential (Ecorr), Cathodic slope (βa), and anodic slope (βa) obtained from the Tafel extrapolation method of the polarization curve along with inhibition efficiency are presented in table 4.12 and table 4.13 for n-hexane and methanol solvents respectively.

Table 4.12 : Potentiodynamic polarization parameters for the corrosion of mild steel with n-hexane extract of *Equisetum hyemale.*

Electrolyte	Sample	$-E_{corr}$ (V/SCE)	I_{corr} (A/cm^2)	βa (V/dec)	-βc (V/dec)	I.E.%
Acid	Mild steel	-0.434	8.02×10^{-4}	0.084	0.134	
Acid + H-EHE 1000 ppm	Mild Steel	-0.430	3.55×10^{-4}	0.057	0.095	55.77
Acid + H-EHE 1000 ppm	Mild steel immersed in electrolyte for 24 h	-0.409	3.58×10^{-5}	0.040	0.098	95.54

The polarization curve shows that both cathodic hydrogen evolution and anodic metal dissolution are suppressed with the addition of EHE. Cathodic and anodic slopes are not affected with the addition of EHE which reveals that inhibition is due to the adsorption of inhibitor molecules, forming barrier film to block the active site of corrosion. Parallel cathodic curves are observed in the polarization, which indicates that the hydrogen evolution if activation-controlled without changing the reduction mechanism (Benabdellah et al., 2006). Shift in corrosion potential is less than 85 mV, which suggests that EHE works as a mixed type of inhibitor. (Riggs Jr., 1973)
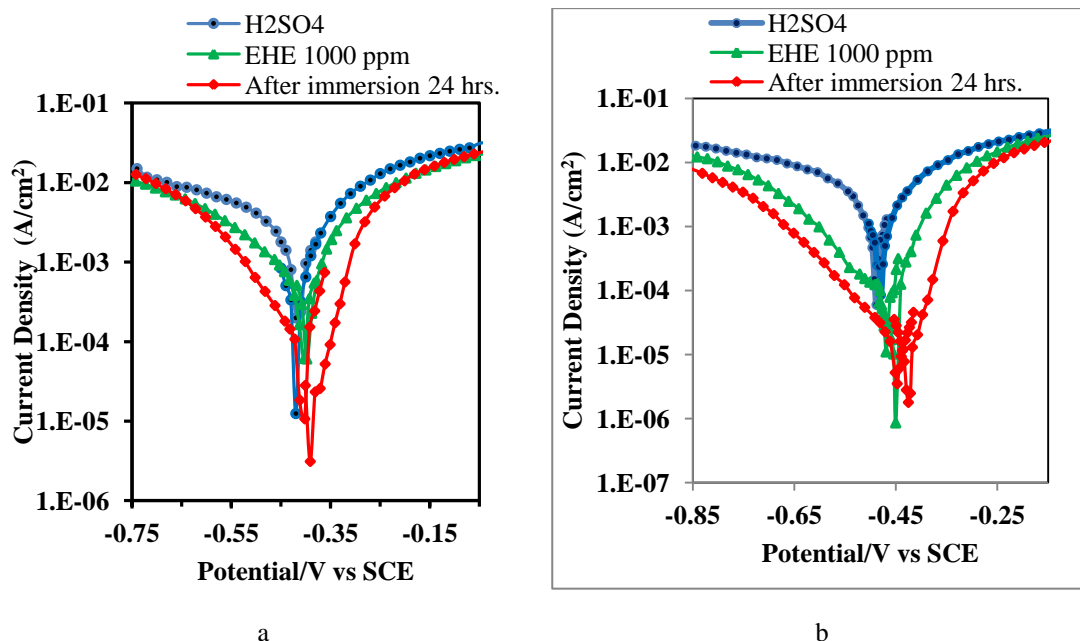
Figure 4.2. 1 : a. Polarization of Mild Steel in n-hexane extract of *Equisetum hyemale* in 1.0 M H_2SO_4 and b. Polarization of Mild Steel in methanolic extract of *Equisetum hyemale* in 1.0 M H_2SO_4.

Table 4.13 : Potentiodynamic polarization parameters for the corrosion of mild steel with methanolic extract of *Equisetum hyemale*.

Electrolyte	Sample	$-E_{corr}$ (V/SCE)	I_{corr} (A/cm²)	βa (V/dec)	-βc (V/dec)	I.E.%
Acid	Mild steel	0.474	9.57×10^{-4}	0.08	0.11	
Acid + M-EHE 1000 ppm	Mild Steel	0.454	8.02×10^{-5}	0.057	0.166	91.63
Acid + M-EHE 1000 ppm	Mild steel immersed in electrolyte for 24 h	0.423	1.31×10^{-5}	0.044	0.122	98.64

Inhibition efficiency calculated for n-hexane extract is 55.77% and 95.54% for the mild steel as immersed in the electrolyte solution, where as it was 93.29% and 96.73% when it was immersed for 24 h in the electrolyte solution for methanol extract. These data show that the inhibition phenomenon of methanol extract is quicker than n-hexane extract, and the obtained amount of n-hexane extract was less. So, *Equisetum hyemale* extract in methanol solvent was selected for a detailed study.

4.2.2 ATR-FTIR analysis of methanol extract of *Equisetum hyemale*:

Fig. 4.2.2 shows an ATR mode FTIR spectrum of crude EHE. The various adsorption peaks are indicative of the presence of different bonds and functional groups in the EHE. Broad peaks at 3367 to 3232 cm^{-1} are representative of the O-H group. A peak at 2935 is due to C-H stretching of alkane. The peak confirms the presence of C=O of amine and carboxylic acid at1635 cm^{-1}. Similarly, peaks at 1570 and 1400 cm^{-1} are due to the presence of the C=C bond. The peaks at 1570 and 1400 cm^{-1} attributed to N-H and C-O-H bending, respectively. Another peak at 1292 cm^{-1} indicates the C-O stretching of ether, alcohol, or carboxylic acid. The C-O of polysaccharide and C-N stretching are confirmed by the presence of a peak at 1026 cm^{-1}. FTIR result shows that the main constituents of plant extract contained an aromatic ring, oxygen, and nitrogen atoms as main constituents. Phytochemical studies of *Equisetum hyemale* have reported the presence of similar FTIR bands (Jin et al., 2014; Manske, 1955; G. Pandey & Khatoon, 2017; Park & Tomohiko, 2011). The presence of such functionality is a prerequisite for typical corrosion inhibitors (Khan et al., 2015). Therefore, its effect on corrosion inhibition of MS in acidic medium has to be clarified (Umoren et al., 2014).
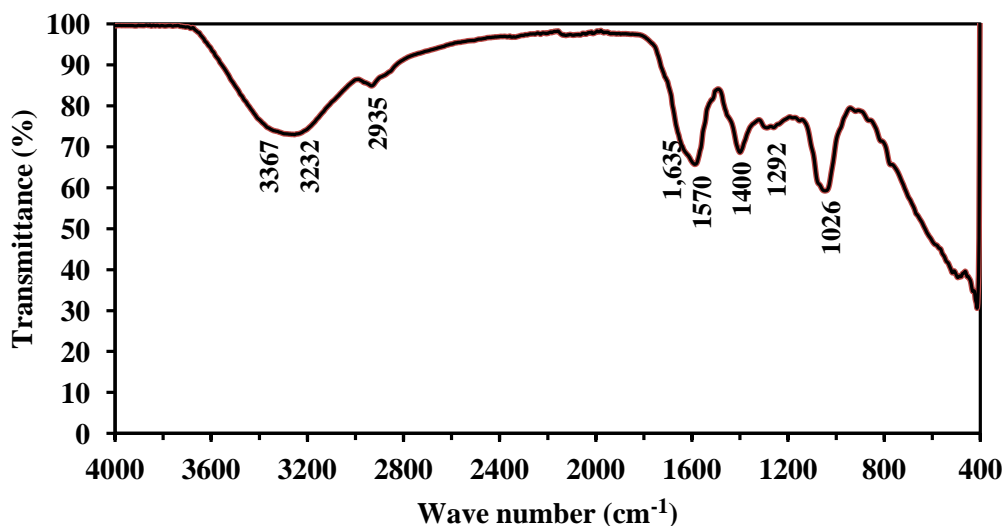
Figure 4.2. 2 : FTIR spectra of methanolic extract of *Equisetum hyemale*.

Table 4.14 : Some important absorption bands/ peaks from FTIR measurements of M-EHE

Absorption Peaks	Functional groups
3232 to 3367	O-H stretching of alcohol, phenol, carbohydrate N-H stretching of amines
2935	C-H stretching of alkane
1635	C=O stretch of amide or carboxylic acid
1570	C=C stretching or N-H bending
1400	C=C stretching aromatic, C-O-H bending
1292	C-O stretching of ether, alcohol, carboxylic acid,
1026	C-O of polysaccharide, C-N stretching

4.2.3 Variation of open circuit potential with time

OCP variation of MS samples recorded in the presence of EHE extract of different concentrations in 1.0 M H_2SO_4 solution with its bare counterpart is shown in Fig. 4.2.3(a). The result shows an increment of OCP in the beginning and attaining a steady potential after 15 minutes. The addition of EHE shifted the OCP towards positive value compared to 1.0 M H_2SO_4 solution without EHE. However, the shift in OCP is less than 10 mV, which proves that the EHE acts as a mixed type of inhibitor (Riggs Jr., 1973). The positive shift of OCP indicated the formation of a adsorb layer of EHE on the MS surface (Verma et al., 2015a).
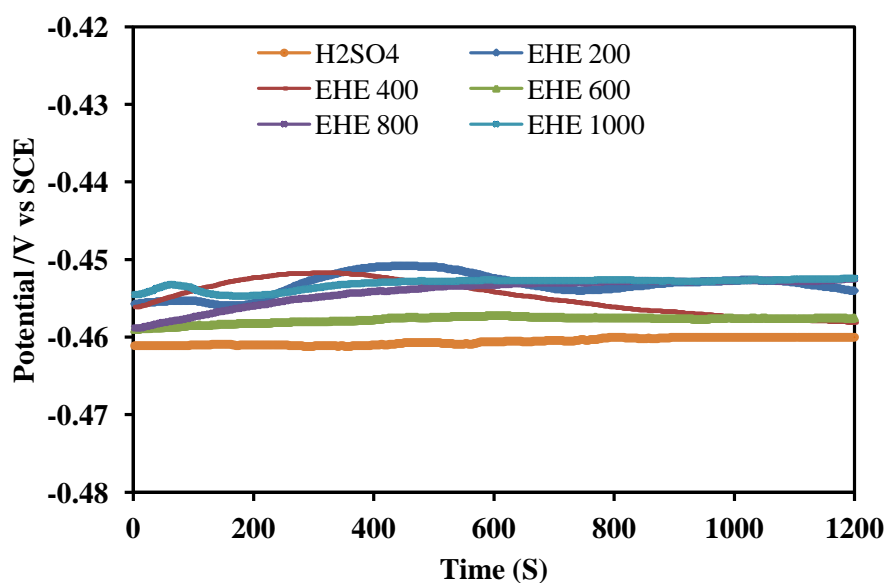
Figure 4.2. 3 : The OCP-time curves for MS specimen in 1.0 M H_2SO_4 solution without and with M-EHE of different concentrations against a SCE reference.

4.2.4 Polarization of mild steel in methanol extract of *Equisetum hyemale* in 1.0 M H_2SO_4

Potentiodynamic polarization was carried out for mild steel coupon without and with the immersion of coupon in the electrolyte solution for 24 h and results are illustrated separately as follows:

Potentiodynamic curves for mild steel as immersed in 1.0 M H_2SO_4 were recorded in the presence and absence of EHE which is represented in Fig. 4.2.4(a). The values of corrosion current (I_{corr}), corrosion potential (E_{corr}), and Tafel slopes used to interpret the effect of EHE on inhibition of the MS corrosion in acidic solution. Table 4.15 summarizes the I_{corr}, E_{corr}, βa, $-\beta c$, and *IE* values estimated form the polarization curves for various concentrations of EHE. Variation in corrosion current and inhibition efficiency in the experiments is represented in Fig. 4.2.4(b).

a   b
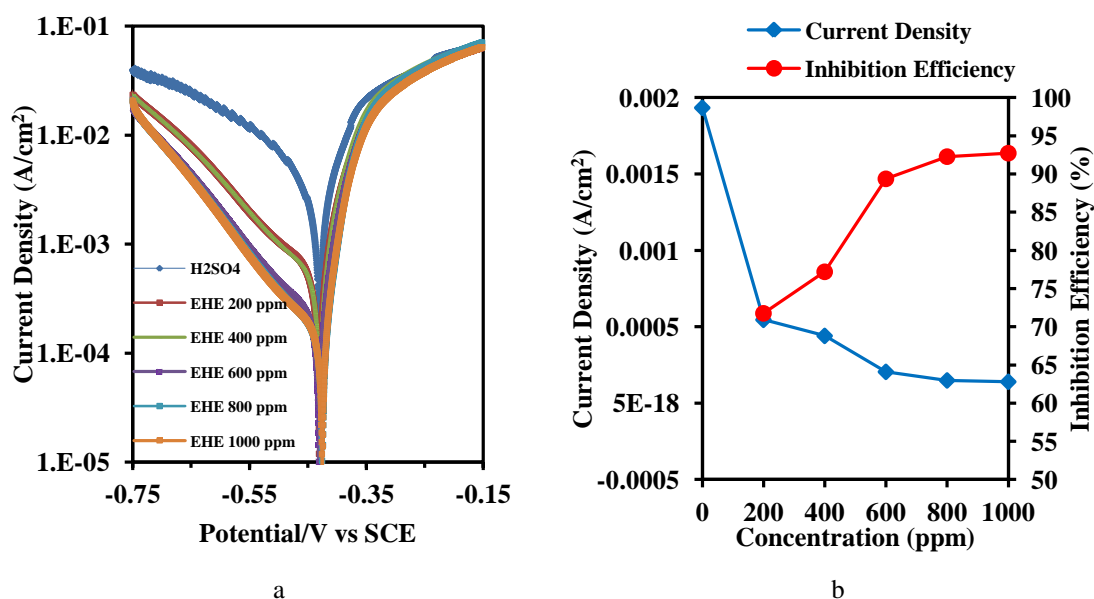
Figure 4.2. 4 : a. Polarization curve of mild steel in 1.0 M H_2SO_4 without and with M-EHE of different concentrations and b. Variation of current density and inhibition efficiency for mild steel coupon with the variation of concentration of inhibitor in 1.0 M H_2SO_4.

Table 4.15 : Potentiodynamic polarization parameters for the corrosion of mild steel with various concentrations of M-EHE.

Concentration (ppm)	$-E_{corr}$ (V/SCE)	I_{corr} (A/cm^2)	βa (V/dec)	$-\beta$c (V/dec)	*IE%*
Blank	0.428	1.93×10^{-3}	0.060	0.112	
200	0.432	5.47×10^{-4}	0.044	0.175	71.77
400	0.432	4.41×10^{-4}	0.035	0.168	77.21
600	0.432	2.05×10^{-4}	0.030	0.164	89.38
800	0.426	1.49×10^{-4}	0.027	0.155	92.29
1000	0.428	1.40×10^{-4}	0.022	0.156	92.74

Potentiodynamic curves for mild steel in 1.0 M H_2SO_4 in the presence and absence of EHE after immersion of coupon in electrolyte for 24 h were recorded, and it is represented in Fig. 4.2.5(a). Electrochemical parameters viz corrosion current (I_{corr}), corrosion potential (E_{corr}), Cathodic slope (βa), and anodic slope (βa) obtained from the Tafel extrapolation method of the polarization curve are presented in Table 4.16 and variation in corrosion current and inhibition efficiency in the experiments is represented in Fig. 4.2.5(b).

a   b
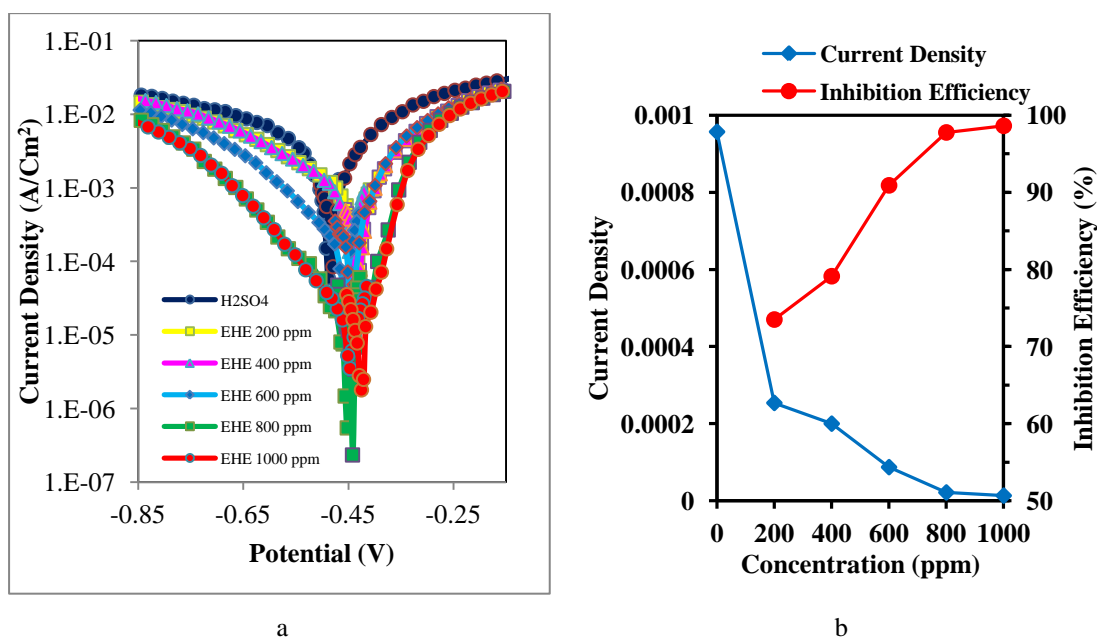
Figure 4.2. 5 : a. Polarization curve of mild steel in 1.0 M H_2SO_4 without and with M-EHE of different concentrations when mild steel coupon is immersed in electrolyte for 24 h. and b. Variation of current density and inhibition efficiency for mild steel coupon immersed in electrolyte with the variation of concentration of inhibitor in 1.0 M H_2SO_4.

Table 4.16 : Potentiodynamic polarization parameters for the corrosion of mild steel immersed in electrolyte for 24 h with 1.0 M H_2SO_4 without and with various concentrations of M-EHE.

Concentration (ppm)	$-E_{corr}$ (V/SCE)	I_{corr} (A/cm^2)	βa (V/dec)	$-\beta c$ (V/dec)	I.E.%
Blank	0.474	9.57×10^{-4}	0.080	0.110	
200	0.435	2.54×10^{-4}	0.052	0.071	73.50
400	0.419	2.00×10^{-4}	0.055	0.053	79.12
600	0.443	8.70×10^{-5}	0.060	0.104	90.91
800	0.444	2.13×10^{-5}	0.060	0.122	97.77
1000	0.423	1.31×10^{-5}	0.044	0.122	98.64

The addition of 1000 ppm of EHE inhibitor has resulted in significantly suppressing the corrosion current. This confirms the fact that EHE worked as a good inhibitor for the MS coupon. The inhibition efficiency increases with an increase in the concentration of EHE. Up to 600 ppm concentration of inhibitor, there is no significant difference in inhibition efficiency for mild steel coupons when polarization is done as immersed and after immersion for 24 h, but the increment in IE is visible beyond 600 ppm. Inhibition efficiency of polarization of mild steel coupon when it is as immersed and immersed for 24 h in the electrolyte is compared in Fig. 4.2.6.
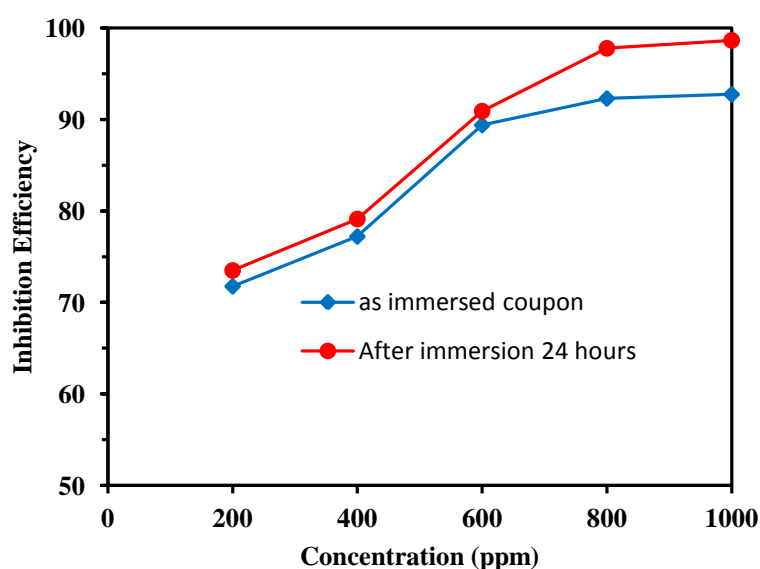
Figure 4.2. 6 : Comparison of Inhibition efficiency of M-EHE for polarization of metal as immersed and immersed for 24 h in 1.0 M H_2SO_4 without and with inhibitor of various concentrations.

The addition of EHE has mainly suppressed the cathodic current, and a marginal variation in slope with the concentration of inhibitor is found in the polarization of

mild steel coupons as immersed. Therefore, the cathodic reduction of hydrogen is suppressed by merely blocking the MS surface by organic molecules present in the EHE (Benabdellah et al., 2006). When polarization is done for coupon after immersion for 24 h, suppression in both cathodic hydrogen evolution and anodic metal dissolution reaction is observed. A shift in value of E_{corr} is less than 85 mV, which reveals that EHE worked as a mixed type of inhibitor(Riggs Jr., 1973). Adsorption phenomenon ascribed to the synergistic effect of different organic molecules with different functionalities facilitating the formation of an inhibiting film (Oguzie et al., 2007).

4.2.5 Electrochemical impedance spectroscopy

The effect of EHE was further studied at steady-state conditions by impedance measurements of the MS in 1.0 M H_2SO_4 + 1.0 M H_2SO_4 + EHE of different concentrations at OCP. Figure 4.2.7(a), (b), and (c) represent the Nyquist, Bode modulus, and phase plots, respectively. Here, the measured data is represented by symbols and the fitting data obtained by using Z-view software (V3.2b) is represented by solid lines. A simple Randles circuit consisting of a one-time constant is used to fit the impedance spectra, as shown in Figure 4.2.7(d). Solution resistance, charge transfer resistance, and constant phase element are represented as Rs, Rct, and CPE, respectively. The fitted parameters, along with *IE*, are tabulated in table 4.17. The use of *CPE* for depressed semicircle has been explained by several publications by taking into account the surface inhomogeneity and related relaxation process(Ahamad et al., 2010; Bammou et al., 2014; Bedair et al., 2017; Bentiss et al., 2000; Fernandes et al., 2019; Hosseini et al., 2003; Jüttner, 1990; Ma et al., 2017; Murmu et al., 2019; Qiang et al., 2018; Shahabi et al., 2015; Yüce & Kardaş, 2012).

The impedance function of *CPE* is represented by the expression [4-6](Cang et al., 2013):

$$Z_{CPE} = \frac{1}{Q(j\omega)^n} \tag{4-6}$$

Where Q represents the magnitude of the CPE, *j,* the imaginary number ($j^2 = -1$), ω, being angular frequency ($\omega = 2\pi f$), and *n,* the CPE exponent ($-1 \leq n \leq +1$), whose value is used to evaluate the surface's non-homogeneity or roughness. (Jüttner, 1990) The

CPE depicts a pure resistor when n=0, an inductor when n=-1, and a pure capacitor when n=+1. (Hosseini et al., 2003).
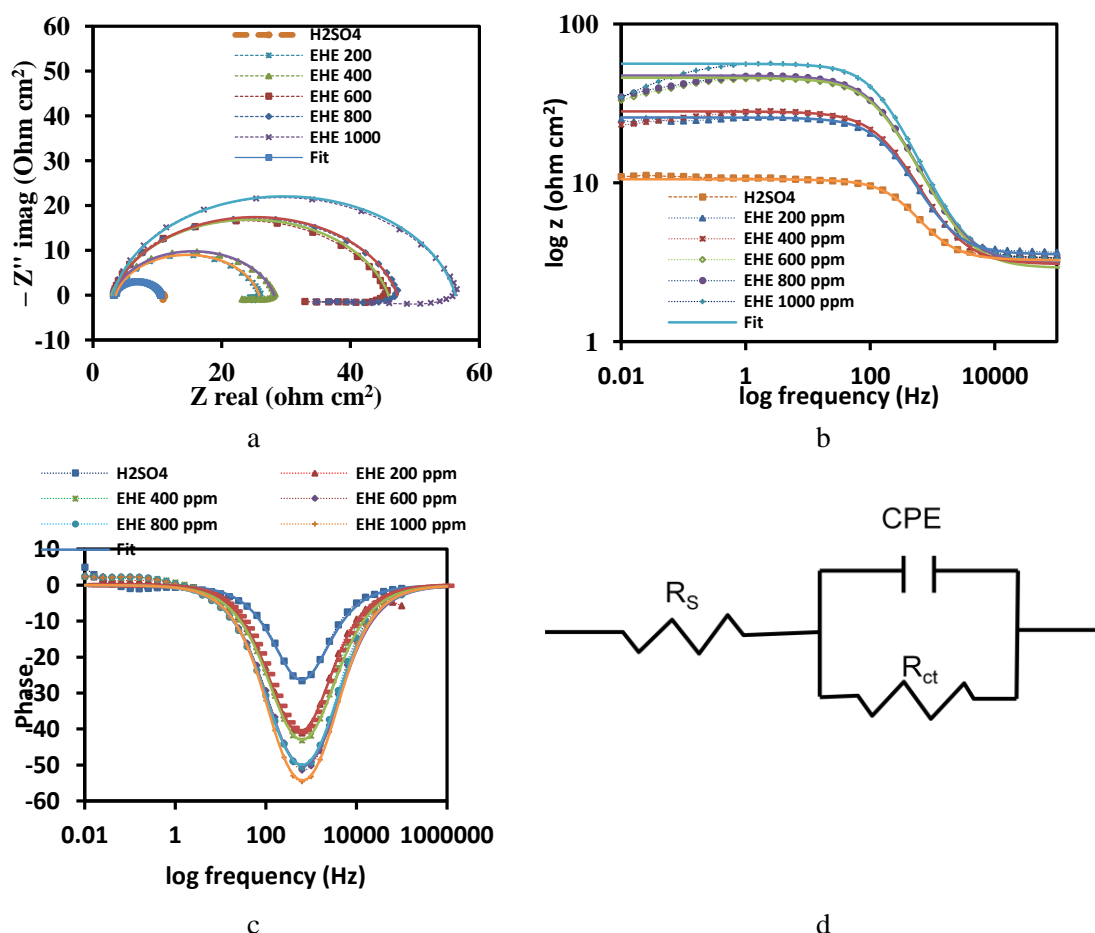
Figure 4.2. 7 : a. Nyquist plots, b. Bode modulus plots of log Z vs. frequency, c. Bode phase plots of phase angle vs. frequency for mild steel in 1.0 M H_2SO_4 with M-EHE of different concentrations and d. Equivalent circuit model used to fit the impedance spectra.

Nyquist plot showing a single depressed capacitive loop at high frequency is indicative of a single charge transfer process of Fe-dissolution. The Nyquist curve shape remains the same with the addition of EHE, which implies that the addition of EHE does not change the MS corrosion mechanism in 1.0 H_2SO_4. Nevertheless, the diameter of the capacitive loops i.e. charge transfer resistance increases with the concentration of EHE. Therefore, inhibition efficiency increases with the concentration of the EHE. The increment of the inductive loop observed in the lower frequency with the concentration of EHE might be attributed to the relaxation phenomenon of adsorbed intermediates such as sulfate ions $Fe(SO_4{}^{2-}{}_{ads})$ and inhibitors molecules(Bentiss et al., 2000; Veloz & González, 2002).

The increment of phase angle in a Bode-phase plot(Hegazy et al., 2014; B. Xu et al., 2014) and the value of impedance at low frequencies in the Bode-modulus plot(Fernandes et al., 2019) with the concentration of EHE also confirm the inhibitive behavior of EHE with its concentration. The increase of phase angle with the concentration of inhibitor is presumably due to more coverage of the MS surface by inhibitor molecules. A similar behavior is reported elsewhere(Yan Li et al., 2005; Mourya et al., 2014; Sadeghi Erami et al., 2019).

Table 4.17 : Impedance parameters for corrosion of mild steel in 1.0 M H_2SO_4 with different concentrations of M-EHE.

Concentration (ppm)	R_s) (Ωcm^2)	CPE $(\mu\Omega^{-1}S^n cm^{-2}$	n	R_{ct} (Ωcm^2)	IE%
Blank (0)	3.26	180.81	0.878	7.29	
200	3.527	104.36	0.865	22.31	67.32
400	3.06	112.50	0.843	25.11	70.97
600	2.89	81.10	0.845	42.9	83.01
800	3.099	78.49	0.849	44.22	83.51
1000	3.161	52.54	0.882	53.15	86.28

Figure 4.2. 8 : Variation of inhibition efficiency and constant phase element with the variation of concentration of M-EHE.

The fitting results show a decrease in *CPE* with the concentration of EHE, indicating that the adsorption of inhibitor molecules results in decreasing the dielectric constant of the double layer, Fig. 4.2.8. It may also be attributed to an increment in the thickness of the electric double layer which is due to adsorption of the large size of

inhibitor molecules compared to water dipole, which is substituted in the adsorption process. It is noteworthy that inhibitor molecules have a larger size compared to water dipole(Bentiss et al., 1999). The gradual displacement of water dipoles by the inhibitor molecules on the metal surface suppressed the rate of metal dissolution (Quraishi & Ansari, 2003).

4.2.6 Determination of inhibition efficiency by weight loss (Gravimetric) method

Gravimetry is one of the simplest and probably most widely used methods that can give the real corrosion rate. In weight loss measurements, the effect of longer immersion time up to 24 h and the effect of concentration of EHE on the inhibition of corrosion of MS sample in acidic solution were studied. Gravimetric measurements studied the inhibitive behavior of EHE by varying time, concentration, and temperature. The obtained results are compared with the electrochemical data.

4.2.6.1 Effect of immersion time

Table 4.18 : Corrosion rate of mild steel in the presence and absence of M-EHE and inhibition efficiency of M-EHE at various time of immersion.

Solution	Time (h)	Surface area (Cm^2)	Weight Loss (mg.)	Rate (mg/cm^2hr)	Inhibition efficiency (%)
Acid	3	30.11	675.00	83.30	78.98
Inhibitor		30.75	144.93	17.51	
Acid	6	29.22	1329.60	84.53	81.79
Inhibitor		30.98	256.70	15.39	
Acid	9	29.56	1984.03	83.12	73.01
Inhibitor		29.02	526.10	22.43	
Acid	12	29.96	2593.50	80.40	69.60
Inhibitor		29.42	774.03	24.44	
Acid	24	28.50	4877.27	79.49	67.91
Inhibitor		28.25	1551.57	25.51	

Inhibition behavior of EHE was studied by immersing mild steel coupon of known dimesnsion and mass in 100 mL of 1.0 M H_2SO_4 without and with EVE of 1000 ppm concentration at 298 K for different time periods viz 3 h, 6 h, 9 h, 12 h, and 24 h. Inhibition efficiency is calculated from the results of the experiments. Table 4.18.

lists the obtained results and corresponding corrosion rate and inhibition efficiency. Figure 4.2.9 (a) and (b) depict the weight loss and; corresponding IE and corrosion rate.
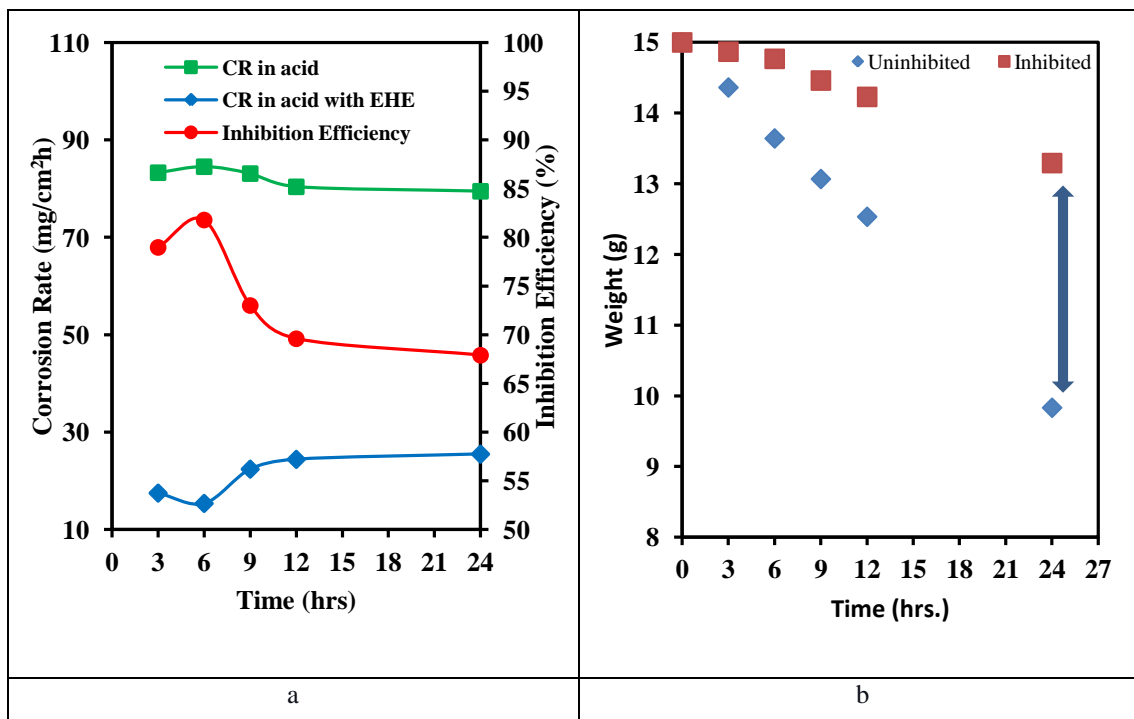
Figure 4.2. 9: a. Variation in corrosion rate in presence and absence of inhibitor and variation in inhibition efficiency with different immersion time and b. Variation in weight of mild steel in the presence and absence of inhibitor

The results show a significant reduction in weight loss in an acid solution with the addition of the EHE. The *IE* attains a maximum (82%) at 6 h of immersion and decreases to attain a steady value (70%) after 12 h of immersion. The initial increase in *IE* points to the dissolution of air formed oxide, leading to surface roughening followed by enhanced adsorption of the phytochemicals on the MS surface. The adsorbed phytochemicals blocked the active site of corrosion. However, a decrease of inhibition efficiency after 6 h of immersion in EHE solution indicated for the gradual desorption of phytochemicals. The chelation of the inhibitor molecules might have promoted desorption with the dissolved Fe^{3+} or Fe^{2+} species(Qiang et al., 2018; Sadeghi Erami et al., 2019). This is essential information concerning the application of such inhibitors in a real application where the time of immersion could be a detrimental factor. On the positive note, the inhibition efficiency after 24 h of immersion maintained at 68%.

4.2.6.2 Effect of temperature:

Table 4.19 : Corrosion rate of mild steel in the presence and absence of M-EHE and inhibition efficiency of M-EHE at various temperatures.

Solution	Temperature (K)	Surface area (Cm^2)	Weight Loss (mg.)	Corrosion Rate (mg/cm^{2}hr)	Inhibition efficiency (%)
Acid	298	31.69	1579.60	92.40	80.92
Inhibitor		29.87	283.47	17.63	
Acid	308	29.59	2180.33	136.86	70.89
Inhibitor		29.99	643.17	39.84	
Acid	318	28.66	3193.17	206.98	64.10
Inhibitor		31.02	1241.20	74.31	
Acid	328	30.29	4313.00	264.48	58.36
Inhibitor		28.43	1685.7	110.13	
Acid	338	29.97	5369.80	332.83	56.27
Inhibitor		31.67	2481.70	145.56	
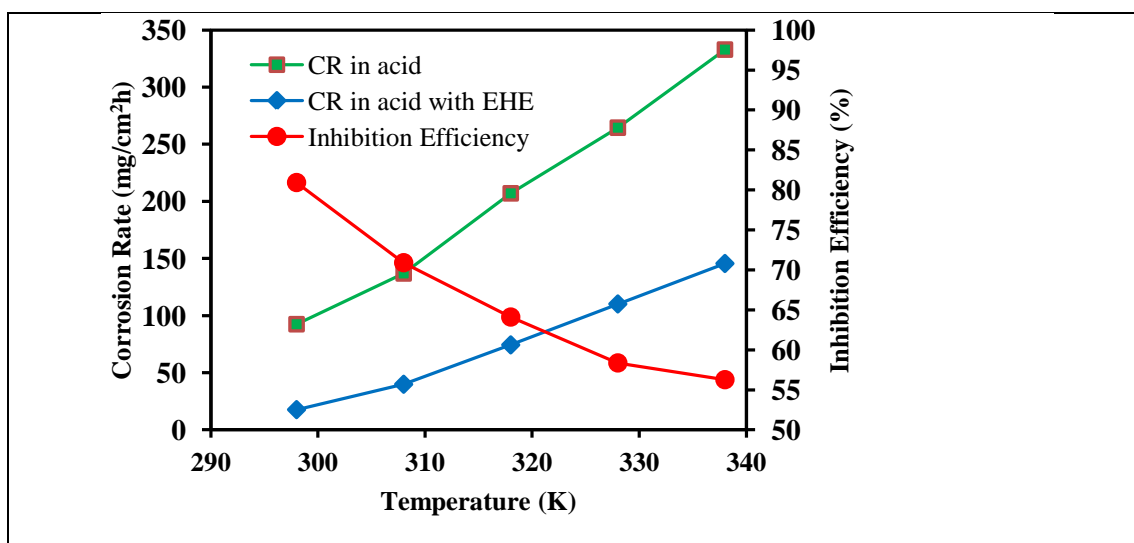
Figure 4.2. 10 : Variation of corrosion rate and inhibition efficiency with variation of temperature.

The effect of temperature on the adsorption behaviors of the phytochemical of EHE was clarified by weight loss measurement at various temperatures after immersion in 1000 ppm EHE solution for 6 h The temperature changed from 298 K to 338 K at an interval of 10 K, and results are presented in Table 4.19. The results reveal a gradual decrease in *IE* with temperature, Fig. 4.2.10. This phenomenon indicates the desorption or decomposition of inhibitor molecules at higher temperatures(Bentiss et al., 2009), and such behavior strongly hints at physical adsorption of phytochemicals.

The lower adsorption stability of the inhibitor molecules with temperature correlates with the change of *IE* with time in Fig. 4.2.10.

4.2.6.3 Effect of concentration:

The effect of concentration of EHE on inhibition efficiency and corrosion rate of MS corrosion from 200 ppm to 1000 ppm is plotted in Fig. 4.2.11(a). In all these measurements, the immersion time was 6 h at 298 K. Results are shown in Table 4.20

Table 4.20 : Corrosion rate of mild steel in the presence and absence of M-EHE and inhibition efficiency of M-EHE at various concentrations.

Concentration	Surface area (cm^2)	Weight Loss (mg)	Corrosion Rate (mg/cm^{2}hr)	Inhibition efficiency (%)	Surface coverage (θ)
0 ppm. (acid solution only)	29.22	1330.20	84.56		
200 ppm.	29.55	516.67	32.48	61.59	0.6159
400 ppm.	29.83	449.57	28.00	66.89	0.6689
600 ppm.	29.04	329.77	21.09	75.06	0.7506
800 ppm.	29.24	298.93	18.99	77.54	0.7754
1000 ppm.	30.98	257.70	15.45	81.73	0.8173

a

b
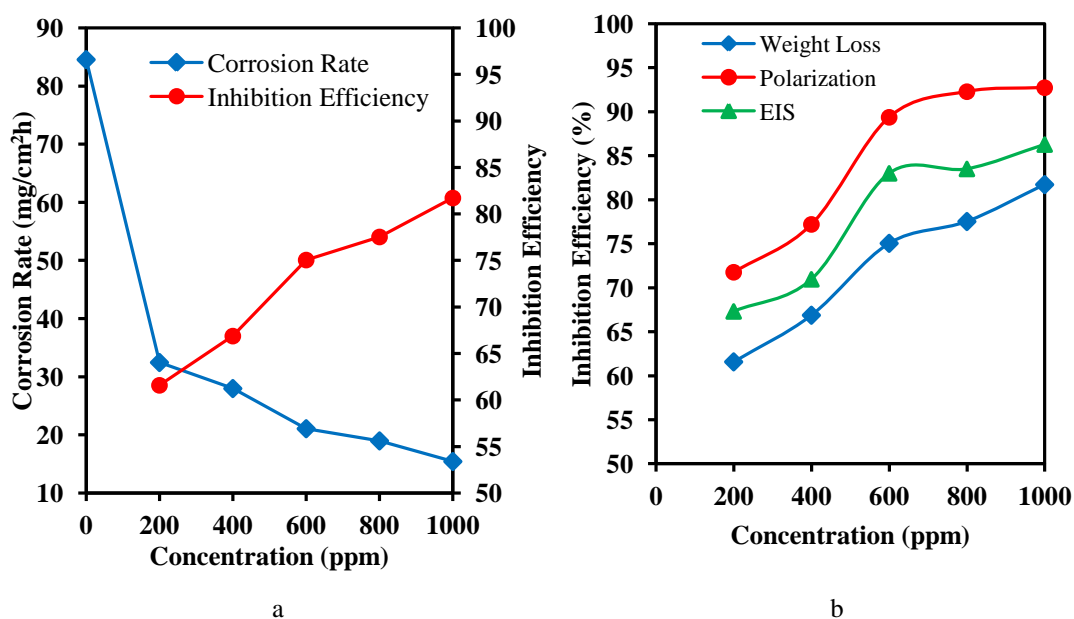
Figure 4.2. 11 : a. Variation in corrosion rate and inhibition efficiency with the variation of concentration of M-EHE and b. Inhibition efficiency of M-EHE from different methods for MS in 1.0 M H$_2$SO$_4$.

The results reveal an increase in the *IE* of EHE with concentration. A maximum *IE* of 82.0 % achieved at 1000 ppm of EHE. Accordingly, the surface coverage of the MS surface by EHE increased with its concentration due probably to the availability of a large number of inhibitor molecules for adsorption. The inhibition efficiencies estimated by all the three methods are compared in Figure 4.2.11 (b). The general features of *IE* are the same irrespective of the method used to estimate it, and values differed by about 10% among the three methods is within the range of experimental errors(Mourya et al., 2014).

4.2.7 Adsorption isotherm:

The adsorption of phytochemicals on the MS surface causes plant extracts to reduce corrosion. (Riggs Jr., 1973). Physical, chemical, or combined interactions preferentially adsorbed the polar functionalities of phytochemicals on a negatively charged metal surface. Adsorbed phytochemicals act as a barrier between the metal and the solution, reducing charge and mass transfer. (Sadeghi Erami et al., 2019). Therefore, the study of adsorption characteristics of inhibitor is an integral aspect of the analysis to know about the mechanism and extent of interaction between the inhibitor and metal surface and, to evaluate some important thermodynamic parameters like activation energy, free energy of adsorption, enthalpy of adsorption and entropy of adsorption. The adsorption of inhibitor can be considered as a quasi-substitution process between the molecules of EHE in an aqueous phase and pre-adsorbed water dipoles at the MS surface (Ahamad et al., 2010a; Cang et al., 2013; Murmu et al., 2019).

Several adsorption isotherms, like Langmuir, Tempkin, Freundlich, El-Awady, were evaluated to describe adsorption behavior of inhibitor molecules. Among them, the best fit adsorption isotherm obtained was Langmuir adsorption isotherm because when C_{inh} is plotted against C_{inh}/θ, a straight line was obtained where values of both linear correlation coefficient (R^2) and slope are almost equal to 1, Fig. 4.2.12. However, little deviation of slope from unity pointed to some interactions between adsorbed molecules on the MS surface. It may be due to mutual attraction and repulsion between differently adsorbed molecules of different functionalities. In

addition, it may also be possible that preferential adsorption of components of the extracts at cathodic and anodic sites took place(Odewunmi et al., 2015). As adsorption follows Langmuir adsorption isotherm, adsorption of inhibitor on MS surface is a monolayer where adsorbate molecules do not interact with each other.

L-uridine, quercetin, 5 methoxy fulfural, α-D-fructofuranose, rutin are a significant component of alcoholic extract of *Equisetum hyemale*(Pandey & Khatoon, 2017). So, the concentration of EHE is represented here as an average molar concentration of major compounds present in the extract to evaluate the adsorption parameter(Tiwari et al., 2019). Nevertheless, other components present in EHE might also have affected the inhibition behavior of EHE.
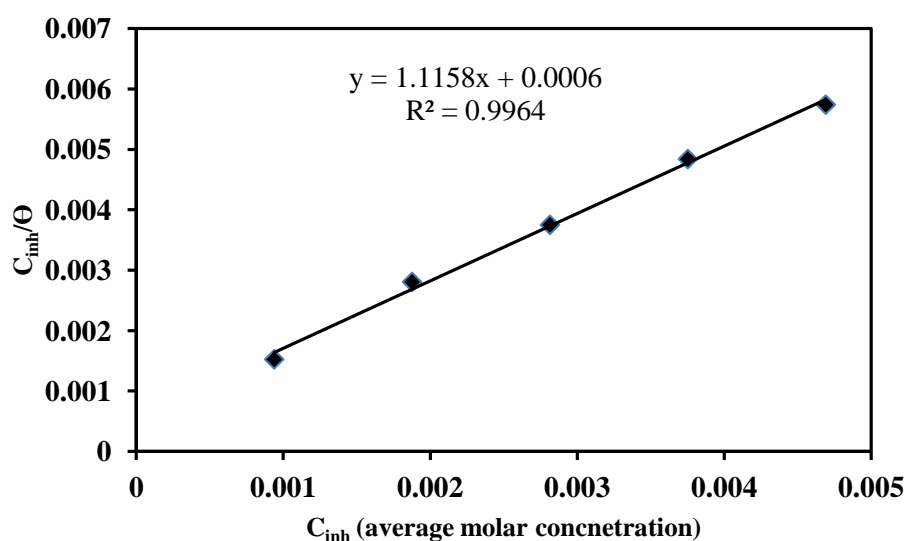
Figure 4.2. 12 : Langmuir adsorption isotherm plot for mild steel in 1.0 M H_2SO_4 with different concentration of M-EHE as the average molar concentration of some major compounds in M-EHE.

Relation of Langmuir adsorption isotherm is shown in equation [4-7],

$$\frac{C_{inh}}{\theta} = \frac{1}{K_{ads}} + C_{inh}$$ [4-7]

When C_{inh} is plotted against $\frac{C_{inh}}{\theta}$, a straight line is obtained. The value of adsorption constant K_{ads} can be calculated from the intercept of the line. This value can be used in the equation [4-8] to calculate the value of free energy of adsorption ($\Delta G°$) (Ahamad et al., 2010):

$$\Delta G_{ads}° = -RT \, ln(55.5K_{ads})$$ [4-7]

133

Where 55.5 is the molar concentration of water in solution (mol/L), and R is the universal gas constant (8.314 J/mol K). The substitution of K_{ads} and other constants values in equation [4-8] results in $\Delta G_{ads}{}^o$ of -28.34 kJ/mol. The value of $\Delta G_{ads}{}^o$ indicates that the adsorption of EHE on MS surface is a mixed type involving both physical and chemical interactions in a spontaneous manner. It is well known that physisorption is related with a value of ΔG^o less than or around -20 kJ/mol, while chemisorption is associated with a value of ΔG^o greater than or around -40 kJ/mol. (Ahamad et al., 2010; Sadeghi Erami et al., 2019). As a matter of facts, an intermediate value of $\Delta G_{ads}{}^o$ in this study suggests the adsorption process controlled by both interactions of the inhibitors molecules to the MS surface. However, the decrease of *IE* with temperature in **Fig. 4.2.10** contradicts this result of $\Delta G_{ads}{}^o$ pointing to both physical and chemical adsorptions. It may be assumed that physisorption occurred first due to the electrostatic attraction between charged inhibitor molecules and charged metal surface. Then, thermal agitation energy might be sufficient for desorption of some water dipole, which is reflected by temperature effect, and such a site may be available for chemisorption by charge transfer from inhibitor molecules to the MS surface forming a coordinate type of bond(Cang et al., 2013). Nitrogen-containing molecules have a higher potential to share electrons due to the protonation behavior of nitrogen in aqueous solution. The phytochemicals of EHE mostly contain oxygen as the heteroatom, and therefore thermal stability might be weak.

4.2.8 Calculation of activation energy and thermodynamic parameters :

The activation energy of the adsorption process is calculated in order to understand the adsorption phenomenon from the relation [4-9](Hamdy & El-Gendy, 2013a):

$$log(C.R.) = logA - \frac{E_a}{2.303\,RT} \qquad [4\text{-}8]$$

Where *C.R* refers to corrosion rate, *T* refers to the absolute temperature, and *A* refers to Arrhenius pre-exponential constant. Table 4.21 list the calculated values of E_a and *A*, and Fig. 4.2.13(a) depicts the Arrhenius plot. It is evident that the addition of EHE increased the Ea and, therefore, decreased the available metal surface for corrosion. In other words, the decrease in the corrosion rate is due to the strong adsorption of inhibitor molecules with the formation of a metal-EHE complex layer(Ostovari et al., 2009).

134
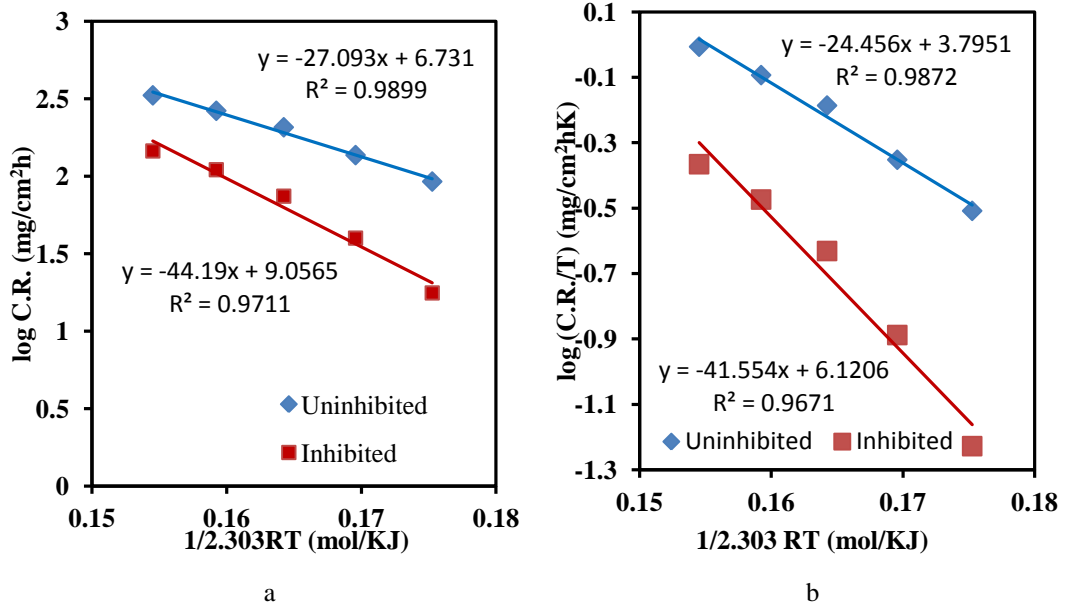
Figure 4.2. 13 : a. Arrhenius plot for mild steel in 1.0 M H$_2$SO$_4$ with and without M-EHE and b. Transition state plot for mild steel in 1.0 M H$_2$SO$_4$ with and without M-EHE.

Furthermore, Enthalpy and entropy of adsorption can be computed using transition state equation [4-10] (Hamdy & El-Gendy, 2013):

$$\log\left(\frac{C.R.}{T}\right) = \left[\log\left(\frac{R}{hN}\right) + \left(\frac{\Delta S^*}{2.303R}\right) - \frac{\Delta H^*}{2.303\,RT}\right] \qquad [4\text{-}10]$$

Where, h refers to plank's constant (6.6261×10^{-34} Js) and, N refers to Avogadro's number (6.0225×10^{23} mol^{-1}).

When $log\left[\frac{C.R.}{T}\right]$ is plotted against $\frac{1}{2.303\,RT}$, a straight line shown in Fig. 4.1.13(b) is obtained. The slope of this line is the enthalpy of activation. The intercept of the line, $\left[log\left[\frac{R}{hN}\right] + \frac{\Delta S^*}{2.303\,R}\right]$ can be used to compute the entropy of activation. Calculated values of ΔH^* and ΔS^* for 1.0 M H$_2$SO$_4$ and 1.0 M H$_2$SO$_4$ + 1000 ppm of EHE is included in Table 4.21. A positive value of ΔH^* signifies the endothermic nature of metal-EHE interaction. The value of ΔH^* increases with the addition of EHE. This reflects that the kinetic parameters of activation controls the decrease in the corrosion rate (Bhat et al., 2011). Higher value of E_a than that of ΔH^* implies the existence of a gaseous reaction, possibly the hydrogen evolution reactions. This leads to a decrease in the overall reaction volume(Ostovari et al., 2009). Furthermore, the difference in $Ea–\Delta H^*$ value nearly equals to RT shows the unimolecular nature of corrosion

135

process. Intermediate values of E_a and ΔH^* reflect a mixed type adsorption of EHE on the MS surface(Yan Li et al., 2005; Qiang et al., 2018; Sadeghi Erami et al., 2019).

As for the value of ΔS^*, a significant and negative value in 1.0 M H_2SO_4 points to an association step in the rate-determining step. However, the addition of EHE to the acid solution resulted in increasing the ΔS^* value. This may be interpreted as the phenomenon leading to the replacement of water molecules by EHE on metal surfaces. Therefore, cathodic discharge of hydrogen ion is lowered by adsorbed inhibitor molecules, and the rate-determining recombination stage produces a more randomly ordered transition state. (Hamdy & El-Gendy, 2013).

Table 4.21 : Activation parameters of the dissolution of mild steel in 1.0 M H_2SO_4 containing1000 ppm M-EHE.

Electrolyte	Ea(kJ/mol)	A (mg/cm^2)	ΔH(kJ/mol)	Ea-ΔH	ΔS(J/molK)
1.0 M H_2SO_4	27.09	5.38×10^6	24.45	2.64	-124.91
Acid with inhibitor	44.19	1.14×10^9	41.55	2.64	-80.38

4.2.9 Surface analysis

Energy dispersive X-ray (EDX) was used to get the elemental information of the MS samples immersed in 1.0 M H_2SO_4 without and with EHE for 24 h. The EDX spectra are showing the presence of elements C, N, O, P, and Fe in Figure 4.2.14. Table 4.22 shows a decrease of Fe and an increase of N and C on the MS surface immersed in an acid solution with EHE. Therefore, the formation of a protective molecular film due to the adsorption of phytochemicals on the MS surface leads to the inhibition of the Fe-dissolution.

In SEM image of MS sample immersed in 1.0 M H_2SO_4, there is a severe corrosion attack with deep furrows and large cracks, whereas MS samples immersed in 1.0 M H_2SO_4 + EHE have developed a relatively smooth surface by the adsorption of inhibitor molecules, which form a protective film on MS and inhibits the corrosion attack.
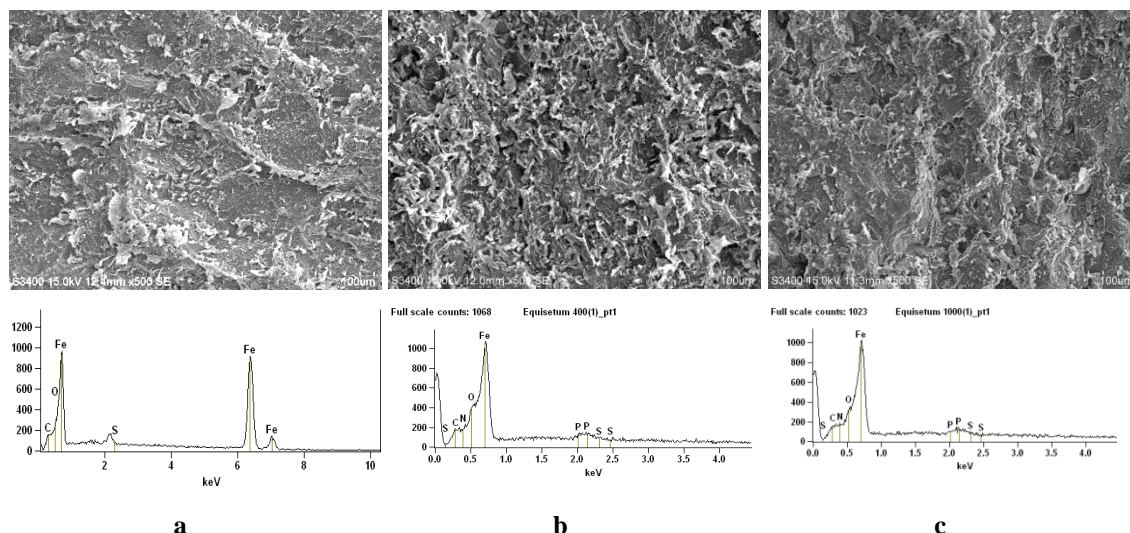
Figure 4.2. 14 : SEM images with corresponding EDX spectra of mild steel sample after 24 h of immersion in a) 1.0 M H_2SO_4, b) 1.0 M H_2SO_4 + 400 ppm M-EHE, and c) 1.0 M H_2SO_4 + 1000 ppm M-EHE.

Table 4.22 : Weight difference of different elements on the MS surface after immersion the sample in different solutions.

Surface dipped in	Iron	Carbon	Nitrogen	Oxygen	Phosphorus
Polished metal sample	100%				
In 1.0 M H_2SO_4	97.45%	1.72%		0.83%	
1.0 M H_2SO_4 + 400 ppm M-EHE	92.92	1.95	1.45	3.84	0.19
1.0 M H_2SO_4 + 1000 ppm M-EHE	87.87	5.08	3.45	3.85	0.05

4.2.10 Mechanism of inhibition:

The extent of decrease in the corrosion rate solely depends on the components present in the EHE. The calculated values of Gibb's free energy of adsorption (-28.34 kJ/mol) and energy of activation (44.19 kJ/mol) of EHE on MS in 1.0 M H_2SO_4 pointed to the involvement of both physical and chemical adsorptions.

In acidic solution, the lone pairs of electrons on N and O on the organic molecules acquire protons and become positively charged. The metal surface can become negatively charged due to the adsorption of poorly hydrated sulfate ion. Then, positively charged organic molecules of EHE can get adsorbed via electrostatic force of attraction with negatively charged MS surface. The cathodic discharge of hydrogen from protonated inhibitor molecules finally returns the organic molecules to its neutral

form. This may be followed by the interaction of vacant d-orbital of Fe with the highest occupied molecular orbital (HOMO) of organic molecules, therefore forming a coordinate bond. According to HSAB theory, the interaction between organic molecules with the metal surface is strong because large organic molecules with large polarizability accompanied with low ionization potential behaves as a soft base, metal at zero oxidation state acts as a soft acid and, there exist stronger donor-acceptor interaction between soft acid and soft base to form a stronger bond (Sadeghi Erami et al., 2019). However, to relieve Fe from accumulating an extra negative charge on its surface, electrons might be given back to lowest unoccupied molecular orbital (LUMO), which is the vacant π^* (antibonding) orbital of inhibitor molecules. This strengthens the adsorption of molecules on the metal surface.Thus, adsorption might involves an electrostatic force of attraction first (physical adsorption), which is followed by electron transfer between organic molecules and metal to form coordinate and feedback bond. Schematic representations of adsorption of two compounds L-uridine and rutin are shown in Fig. 4.1.15. This adsorption inhibits both cathodic and anodic reactions. The anodic dissolution can be inhibited by the adsorption of sulfate ion(Ma et al., 2017; Shahabi et al., 2015; Yüce & Kardaş, 2012). The reaction steps are given below:

$$H_2SO_4 \quad \rightarrow \quad H^+ + SO_4^{--}$$
$$Fe + SO_4^{--} \quad \rightarrow \quad (FeSO_4^{--})_{ads}$$
$$(FeSO_4^{--})_{ads} \quad \rightarrow \quad (FeSO_4^-)_{ads} + e^-$$
$$(FeSO_4^-)_{ads} \quad \rightarrow \quad (FeSO_4)_{ads} + e^-$$
$$(FeSO_4)_{ads} \quad \rightarrow \quad Fe^{++} + SO_4^{--}$$
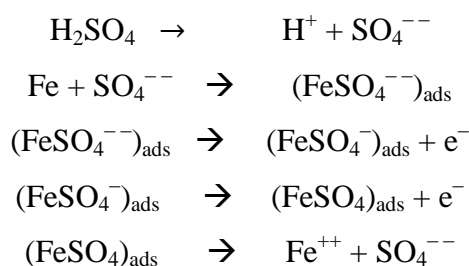
Adsorption suppress the cathodic hydrogen evolution as :

$$Fe + (EHE)H^+ \longrightarrow [Fe\text{-}(EHE)H^+]_{ads} \text{ (adsorption of protonated EHE molecules)}$$
$$[Fe\text{-}(EHE)H^+]_{ads} + e^- \longrightarrow [Fe\text{-}(EHE)H]_{ads} \quad \text{(Reduction of protonated } H^+)$$
$$[Fe\text{-}(EHE)H]_{ads} + H^+ + e^- \longrightarrow Fe + H_2 + EHE \quad \text{(Release of hydrogen)}$$
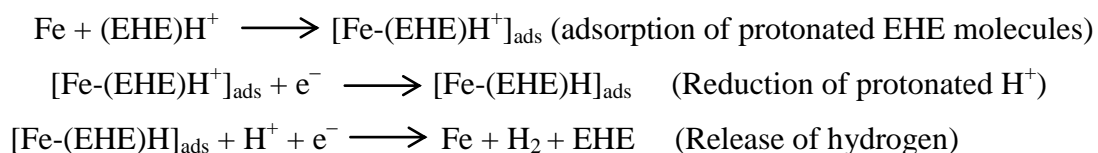
Alternatively, Hydroxy aromatic compounds present in EHE like rutin, quercetin may form stable and insoluble Fe-inhibitor complex via chelation. However, a low concentration of EHE or Fe^{2+} or Fe^{3+}, may not form a potent surface complex. Therefore dissolution of Fe may not be to the suppressed, and significant dissolution of Fe should take place. In contrast, at higher concentrations of EHE, a large number

of surface complexes with Fe should be formed covering a large surface, and hence the dissolution of Fe is suppressed. Indeed, after 600 ppm of EHE, significant corrosion inhibition is obtained (Fig. 4.2.16).

a   b
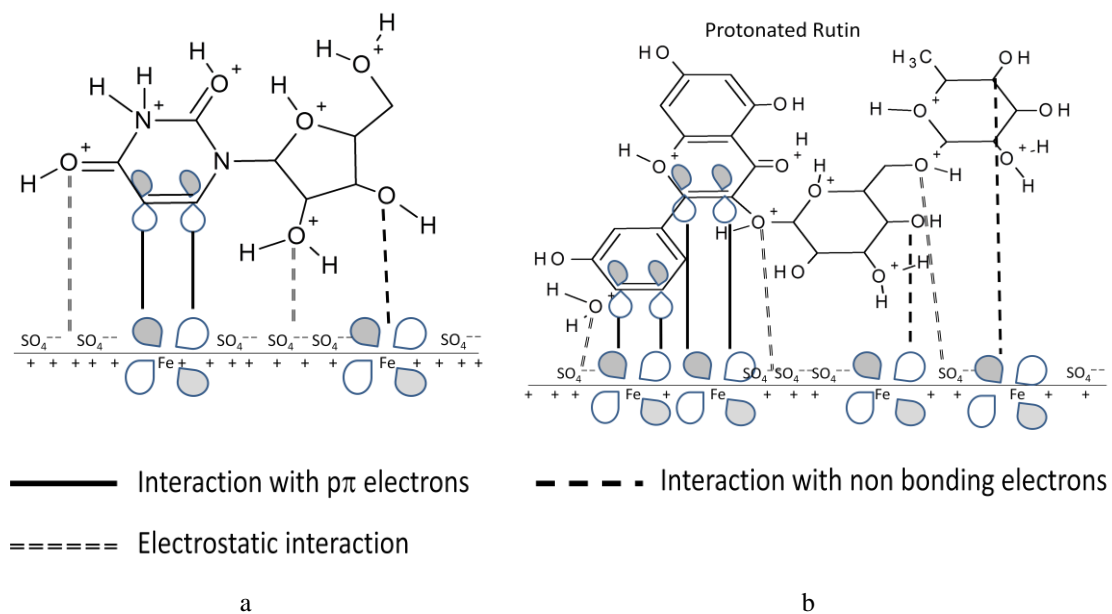
Figure 4.2. 15 : The Schematic illustration of different modes of adsorption of (a) L-Uridine and (b) Rutin molecule on mild steel/ 1.0 M H_2SO_4 interface

a   b
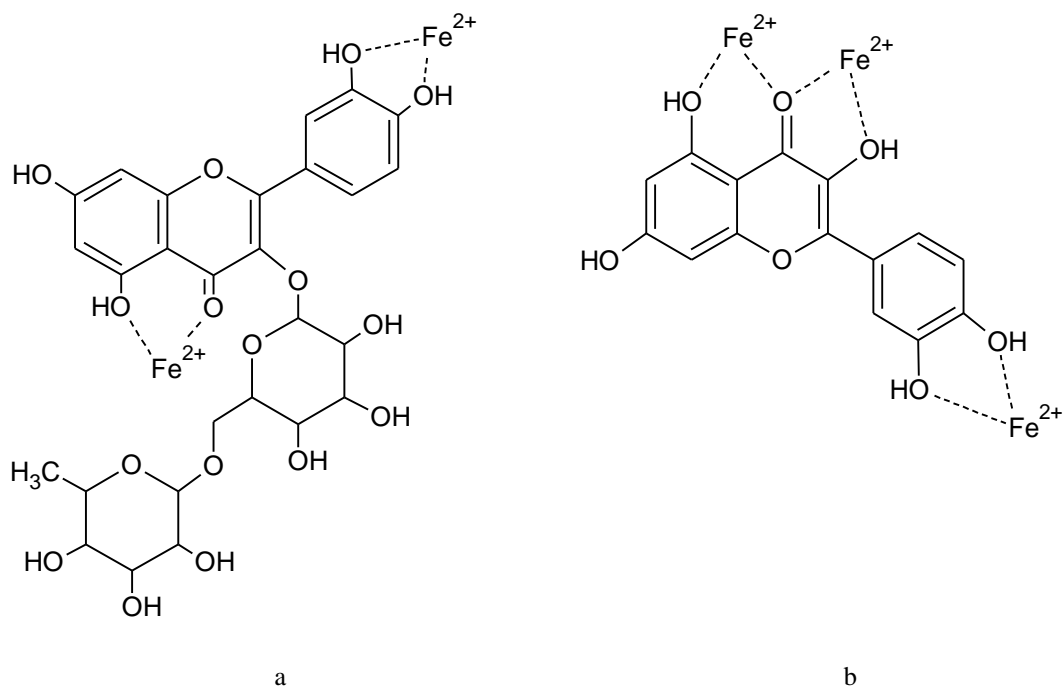
Figure 4.2. 16 : Iron-inhibitor complex formed via chelation of iron with a. rutin and b. quercetin

4.3 *Mahonia nepalensis*

Results of corrosion tests of the extract of the stem of *Mahonia nepalensis* plant are presented as follows:

4.3.1 Potentiodynamic polarization of mild steel in 1.0 M H₂SO₄ in the presence and absence of *Mahonia nepalensis* extract in methanol and n-hexane solvents

Polarization of mild steel coupon as immersed and after immersion for 24 h in the electrolyte was carried out with 1.0 M H₂SO₄ without and with inhibitor solution of different concentrations as the electrolyte. Inhibitor used in the process were n-hexane and methanol extract of *Mahonia nepalensis*. The polarization curve obtained is shown in Fig. 4.3.1a and Fig. 4.3.1b for n-hexane and methanol extract respectively. Tables 4.23 and 4.24 show the electrochemical parameters and inhibition efficiency determined from the Tafel extrapolation method of the polarization curve for n-hexane and methanol solvents, respectively.

a   b
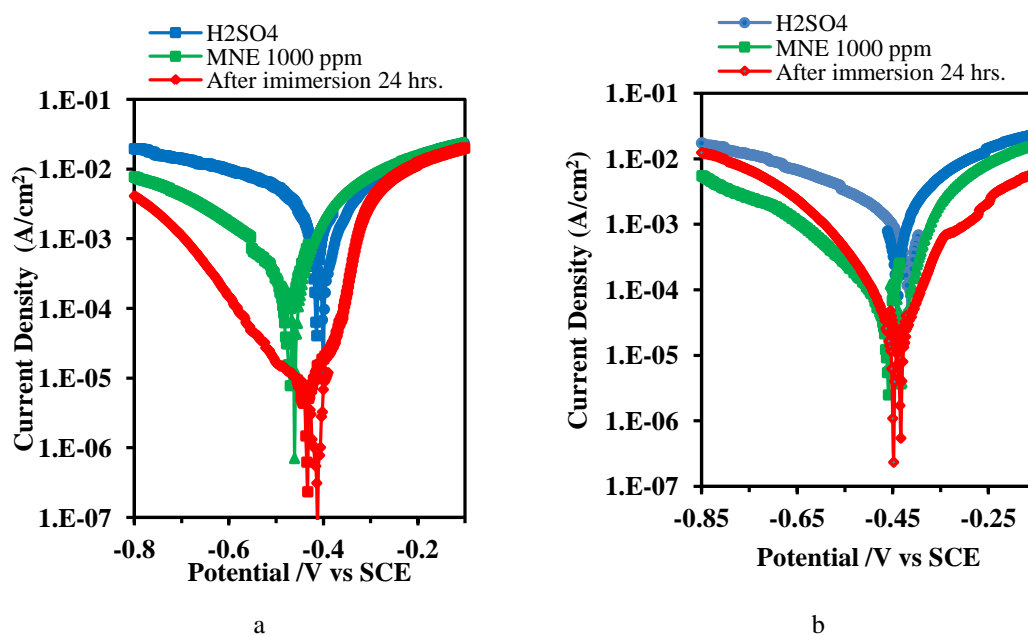
Figure 4.3. 1 : a. Polarization of Mild Steel in n-hexane extract of *Mahonia nepalensis* in 1.0 M H₂SO₄ and b. Polarization of Mild Steel in methanol extract of *Mahonia nepalensis* in 1.0 M H₂SO₄.

Data implies that the methanolic extract of *Mahonia nepalensis* is an excellent corrosion inhibitor. It shows 97.65% and 98.47% inhibition efficiency on polarization of mild steel as immersed and after immersion for 24 h. Addition of MNE supress cathodic hydrogen evolution as well as anodic metal dissolution. In the n-hexane

extract of the plant, the cathodic reaction is more suppressed and inhibition efficiency is 99.13% for the mild steel immersed for 24 h but for mild steel as immersed its efficiency 84.09%, which is less than that in methanol extract. The amount of n-hexane extract was less in amount. So, methanol extract is a good choice for detailed investigation. Both extracts behaves as a mixed inhibitor because shifting in value of corrosion potential is less than 85mV. (Riggs Jr., 1973)

Table 4.23 : Potentiodynamic polarization parameters for the corrosion of mild steel with n-hexane extract of *Mahonia nepalensis*.

Electrolyte	Sample	$-E_{corr}$ (V/SCE)	I_{corr} (A/cm^2)	βa (V/dec)	$-\beta c$ (V/dec)	I.E.%
Acid	Mild steel	0.437	8.80×10^{-4}	0.090	0.106	
Acid + H-MNE 1000 ppm	Mild Steel	0.493	1.40×10^{-4}	0.048	0.101	84.09
Acid + H-MNE 1000 ppm	Mild steel immersed in electrolyte for 24 h	0.461	7.62×10^{-6}	0.076	0.159	99.13

Table 4.24 : Potentiodynamic polarization parameters for the corrosion of mild steel with methanolic extract of *Mahonia nepalensis*.

Electrolyte	Sample	$-E_{corr}$ (V/SCE)	I_{corr} (A/cm^2)	βa (V/dec)	$-\beta c$ (V/dec)	I.E.%
Acid	Mild steel	0.435	9.12×10^{-4}	0.117	0.097	
Acid + M-MNE 1000 ppm	Mild Steel	0.444	2.13×10^{-5}	0.040	0.084	97.65
Acid + M-MNE 1000 ppm	Mild steel immersed in electrolyte for 24 h	0.417	1.40×10^{-5}	0.036	0.123	98.47

4.3.2 ATR-FTIR analysis of methanol extract of *Mahonia nepalensis*:

The *Mahonia nepalensis* is a pristine species for corrosion inhibition history, even though its chemical composition has been reported for a different purpose (Nguyen et al., 2009; Thusa & Mulmi, 2017). Fig. 4.3.2 shows the FTIR spectrum of the MNE. Several organic functional groups, such as alkaloids, flavonoids, quinones, and steroids were identified. On the FTIR plot, noteworthy absorption peaks and assigned functional groups are indicated, as well as summarized in table 4.25. The adsorbed peaks at 3657 cm^{-1}, 3202 cm^{-1}, and 1385 cm^{-1} are assigned to the O-H group. Absorptions at 3356 cm^{-1}, 1605 cm^{-1}, and 1049 cm^{-1} indicate the presence of the N-H group. The absorption band at 2963 cm^{-1} is assigned to the C-H stretch. A peak at 1223 cm^{-1} is assigned to the C-O stretching of ether. Similarly, peak at 1049 cm^{-1} is

allocated to C-O stretching of a primary alcohol, CO-O-CO stretching of anhydride, C-N stretching of amine. FTIR spectrum shows that the plant extract contained aromatic rings, oxygen, and nitrogen atoms in the functional group as main constituents, which meets the general requirements for typical corrosion inhibitors (Umoren et al., 2014).
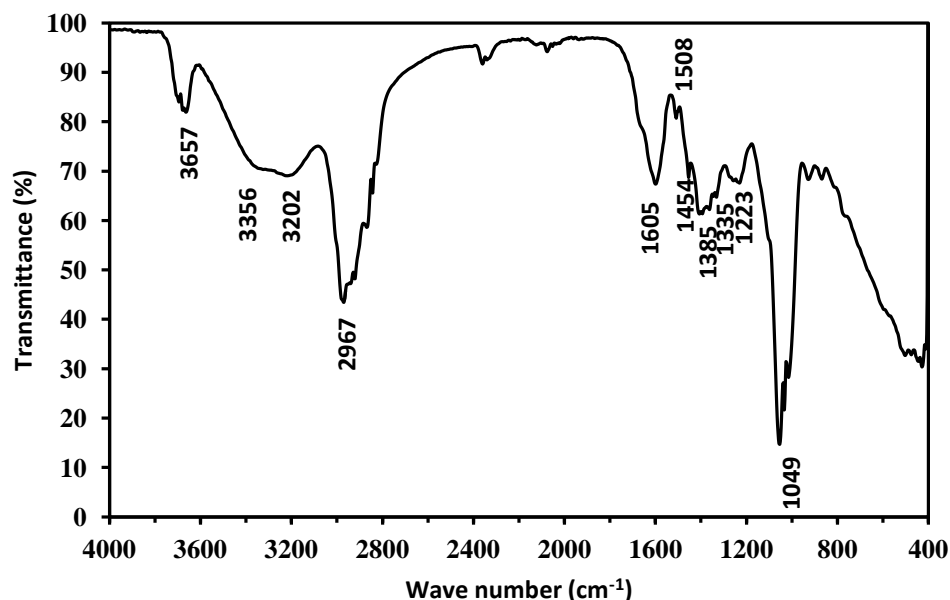
Figure 4.3. 2 : FTIR spectra of the methanolic extract of *Mahonia nepalensis*.

Table 4.25 : Some important absorption bands/ peaks from FTIR measurements of M-MNE.

Absorption Peaks	Functional groups
3657 cm^{-1}	O-H stretching of alcohol
3356 cm^{-1}	N-H stretching of amide
3202 cm^{-1}	O-H stretching of H-bonded alochols phenols
2967 cm^{-1}	C-H alkanes
1605 cm^{-1}	Aromatic C=C or N-H bending
1508 cm^{-1}	N-O stretching
1454 cm^{-1}	Phenyl C-C
1385 cm^{-1}	O-H bending alcohol, phenol
1335 cm^{-1}	C-N stretching aromatic amine
1223 cm^{-1}	C-O stretching vinyl, aryl or alkyl ether
1049 cm^{-1}	C-O stretching primary alcohol, CO-O-CO stretching anhydride, C-N stretching of amine

4.3.3 Variation of open circuit potential with time

OCP Change of the MS samples recorded in acid without and with MNE of various concentration is shown in Fig. 4.3.3. The results shows that the OCP is shifted to positive potential with addition of MNE, which reveals the adsorption of inhibitor on the metal surface to limit the contact of aggressive ions towards the surface(Sudheer & Quraishi, 2014). However, the shift is less than 85 mV implying that MNE is mixted type of inhibitor. (Riggs Jr., 1973)
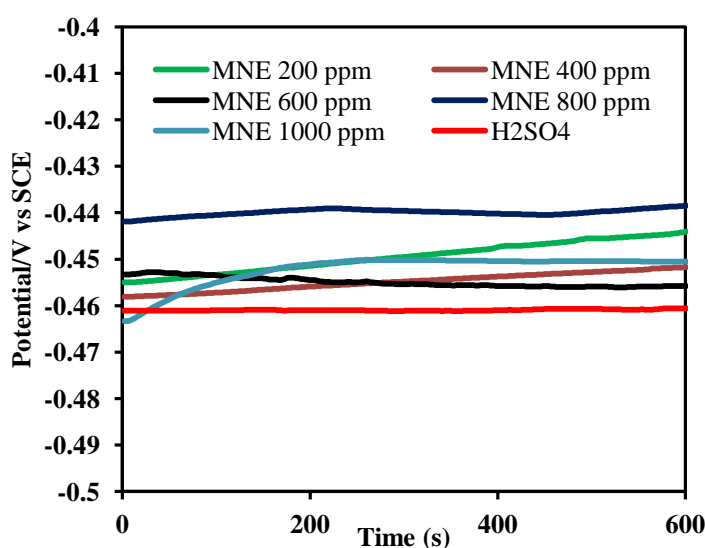
Figure 4.3. 3 : The OCP-time curves for MS specimen in 1.0 M H_2SO_4 solution without and with M-MNE of different concentrations against a SCE reference.

4.3.4 Polarization of mild steel in methanolic extract of *Mahonia nepalensis* in 1.0 M H_2SO_4

Potentiodynamic polarizations were carried out for mild steel coupon as immersed and after immersion of coupon in the electrolyte solution for 24 h and results are illustrated separately as follows:

Potentiodynamic curves for mild steel as immersed in 1.0 M H_2SO_4 were recorded in the presence and absence of MNE which is represented in Fig. 4.3.4 (a). Electrochemical parameters viz corrosion current (I_{corr}), corrosion potential (E_{corr}), Cathodic slope (βa), and anodic slope (βa) obtained from the Tafel extrapolation method of the polarization curve are presented in Table 4.26 and variation in

corrosion current and inhibition efficiency in the experiments is represented in figure 4.3.4(b).

a   b
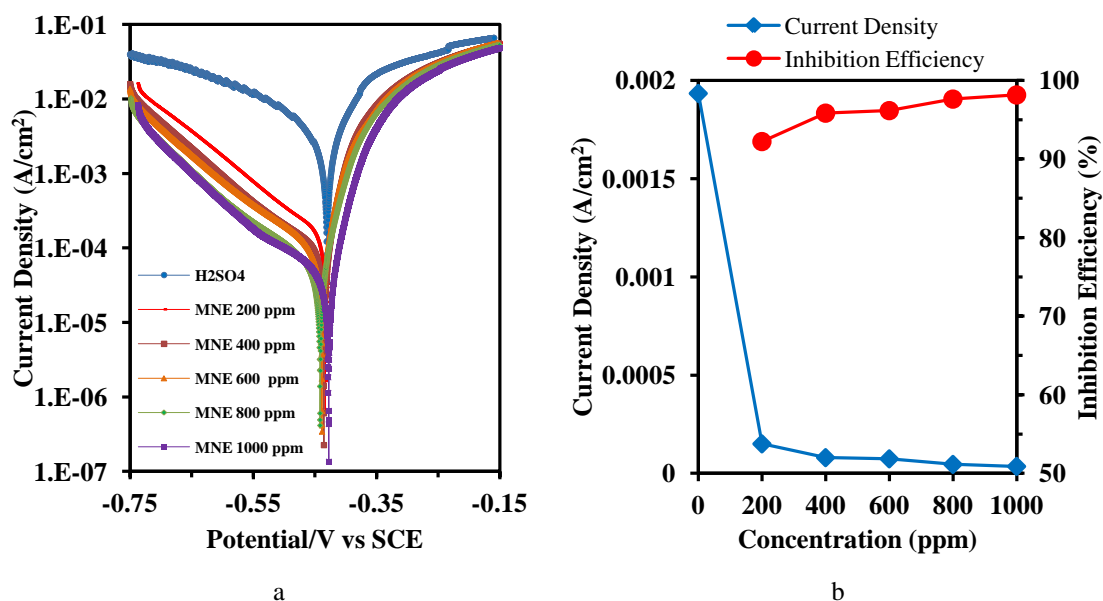
Figure 4.3. 4 : a. Polarization curve of mild steel in 1.0 M H_2SO_4 without and with M-MNE of different concentrations and b. Variation of current density and inhibition efficiency for mild steel coupon with variation of concentration of inhibitor in 1.0 M H_2SO_4.

Table 4.26 : Potentiodynamic polarization parameters for the corrosion of mild steel with various concentrations of M-MNE.

Concentration (ppm)	$-E_{corr}$ (V/SCE)	I_{corr} (A/cm^2)	βa (V/dec)	$-\beta c$ (V/dec)	I.E.%
Blank	0.428	1.93×10^{-3}	0.060	0.112	-
200	0.433	1.50×10^{-4}	0.029	0.116	92.22
400	0.437	8.05×10^{-5}	0.029	0.121	95.84
600	0.439	7.42×10^{-5}	0.029	0.118	96.16
800	0.442	4.59×10^{-5}	0.032	0.120	97.62
1000	0.429	3.57×10^{-5}	0.030	0.143	98.15

Potentiodynamic curves for mild steel in 1.0 M H_2SO_4 in the presence and absence of MNE after immersion of coupon in electrolyte for 24 h were recorded and it is represented in Fig. 4.3.5(a). Electrochemical parameters obtained from the Tafel extrapolation method of the polarization curve are presented in Table 4.27 and

variation in corrosion current and inhibition efficiency in the experiments is represented in figure 4.3.5(b).

a   b
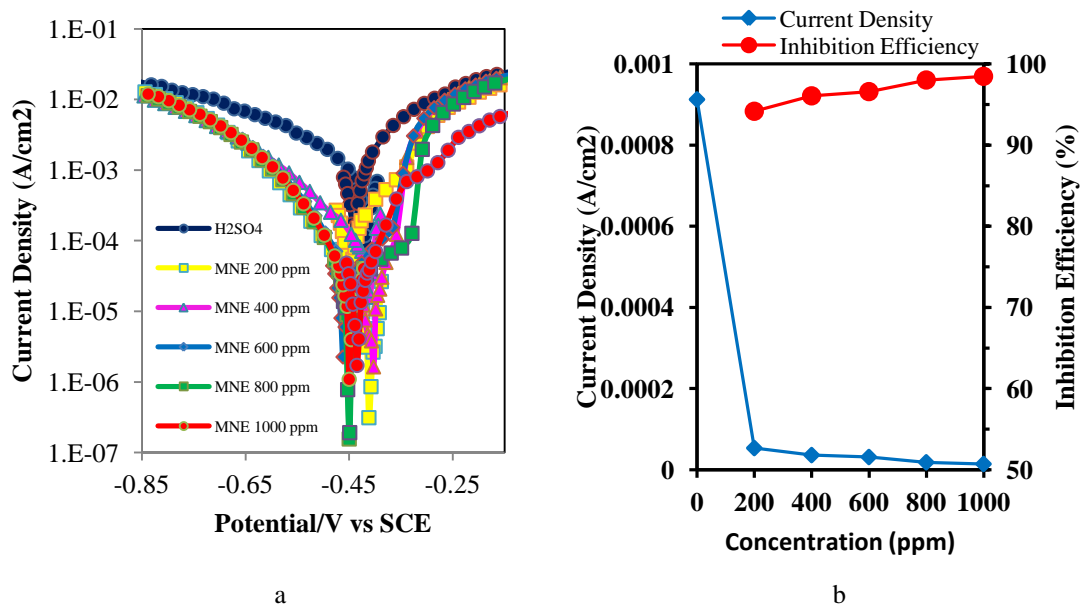
Figure 4.3. 5 : a. Polarization curve of mild steel in 1.0 M H_2SO_4 without and with M-MNE of different concentrations when mild steel coupon is immersed in electrolyte for 24 h. and b. Variation of current density and inhibition efficiency for mild steel coupon immersed in electrolyte with variation of concentration of inhibitor in 1.0 M H_2SO_4.

Table 4.27 : Potentiodynamic polarization parameters for the corrosion of mild steel immersed in electrolyte for 24 h with 1.0 M H_2SO_4 without and with various concentrations of M-MNE.

Concentration (ppm)	$-E_{corr}$ (V/SCE)	I_{corr} (A/cm^2)	βa (V/dec)	$-\beta c$ (V/dec)	I.E.%
Blank	0.435	9.12×10^{-4}	0.117	0.097	
200	0.462	5.33×10^{-5}	0.094	0.102	94.16
400	0.391	3.59×10^{-5}	0..51	0.078	96.06
600	0.446	3.12×10^{-5}	0.108	0.088	96.58
800	0.443	1.81×10^{-5}	0.147	0.055	98.01
1000	0.417	1.40×10^{-5}	0.036	0.128	98.47

It is observed from the polarization data that I_{corr} is decreases more than 50 times with addition of MNE, which implies its inhibitory nature. However, cathodic inhibition is more prominent than anodic inhibition. As the corrosion potential is shifted less than 0.85 mV, it can be concluded that it behaves as a mixed type of inhibitor. (Riggs Jr., 1973). The cathodic Tafel plots are observed parallel which indicates that the hydrogen evolution in the process is activation controlled and the

145

mechanism of reduction is unaffected by the addition of inhibitor in the acid solution (Benabdellah et al., 2006). Significant change is not observed on both slopes, indicating that inhibition is caused due to adsorption of MNE on the MS surface, which merely blocks the active sites. Such an effective inhibition of corrosion might be ascribed to the synergistic effect of interaction between different organic molecules of MNE with MS surface (Oguzie et al., 2007). The computation reveals that the inhibition efficiency increases with increase in inhibitor concentration and it reaches to 98.15% at 1000 ppm concentration for the mild steel coupon as immersed and 98.47 for coupon after immersion for 24 h. In the case of *Mahonia nepalensis* extract, inhibition efficiency for mild steel coupons as immersed and after immersion for 24 h are comparable. A comparison of inhibition efficiency is shown in Fig. 4.3.6.
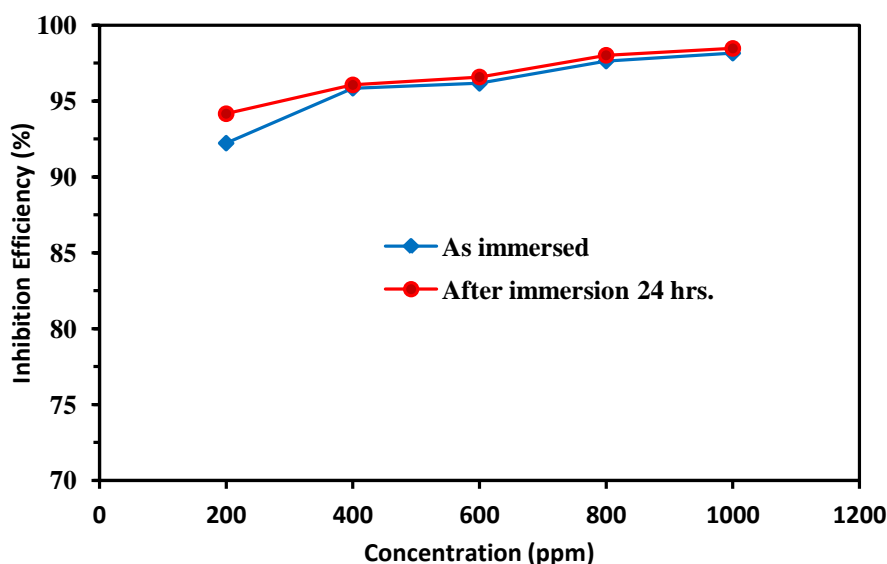
Figure 4.3. 6 : Comparison of Inhibition efficiency of M-MNE for polarization of metal as immersed and immersed for 24 h in 1.0 M H$_2$SO$_4$ without and with inhibitor of various concentrations.

4.3.5 Electrochemical impedance spectroscopy

Electrochemical impedance measurements (EIS) were used to better understand the corrosion kinetics of the mild steel sample at OCP in acid without and with MNE. Figure 4.3.7 (a-c) depicts the Nyquist and Bode plots derived from the EIS experiment, with symbols representing measured data and solid lines representing fitted data. Fitted data is obtained by employing a Randles circuit with a single time constant as illustrated in Fig 4.3.7 (d), which consists of the circuit elements R_s (solution resistance), R_{ct} (charge transfer resistance) and CPE (constant phase element). The CPE is used instead of a pure capacitor in the circuit model to take into

146

account the electrode surface non-homogeneity caused by surface roughness, adsorption of inhibitors, dislocations, grain boundaries, and the development of a porous layer. (Ahamad et al., 2010; Bammou et al., 2014; Bedair et al., 2017; Bentiss et al., 2000b; Fernandes et al., 2019a; Hosseini et al., 2003a; Jüttner, 1990; Ma et al., 2017; Murmu et al., 2019; Qiang et al., 2018; Shahabi et al., 2015; Yüce & Kardaş, 2012)
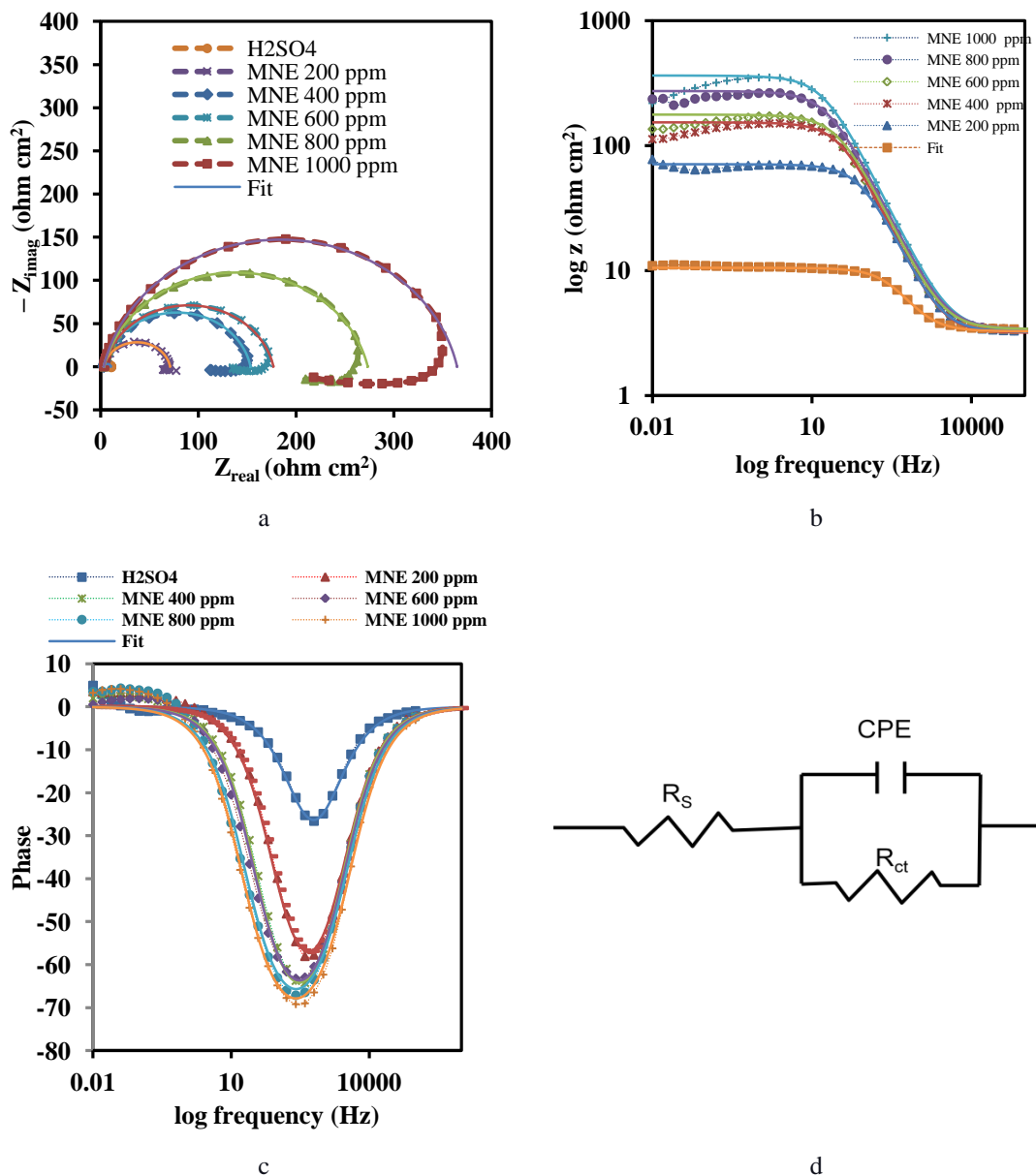
Figure 4.3. 7 : a. Nyquist plots, b. Bode modulus plots of log Z vs. frequency, c. Bode phase plots of phase angle vs. frequency for mild steel in 1.0 M H_2SO_4 with M-MNE of different concentrations and d. Equivalent circuit model used to fit the impedance spectra.

Equation [4-11] represents the impedance function of *CPE.* (Ashassi-Sorkhabi et al., 2008) :

$$ZCPE = \frac{1}{Q(j\omega)^n}$$ [4-9]

Where Q represents the magnitude of the CPE, *j,* the imaginary number ($j^2 = -1$), ω, being angular frequency ($\omega = 2\pi f$), and *n,* the CPE exponent ($-1 \leq n \leq +1$), whose value is used to evaluate the surface's non-homogeneity or roughness. (Jüttner, 1990) The CPE depicts a pure resistor when n=0, an inductor when n=-1, and a pure capacitor when n=+1. (Hosseini et al., 2003). An inductive loop is seen in Nyquist plot at low frequency which increases with the concentration of MNE. It can be ascribed to the relaxation phenomenon of adsorbed intermediates such as sulfate ions $Fe(SO_4^{2-}_{ads})$ and inhibitors molecules(Bentiss et al., 2000; Veloz & González, 2002).

Table 4.28 shows the electrochemical impedance parameters computed from the Randles circuit using Z-view software (v3.1c).

Table 4.28 : Impedance parameters for corrosion of MS in 1.0 M H_2SO_4 and 1.0 M H_2SO_4 with different concentrations of M-MNE.

Concentration (ppm)	Rs (Ωcm^2)	CPE ($\mu\Omega^{-1}S^n cm^{-2}$)	n	R_{ct} (Ωcm^2)	I.E.%
Blank (0)	3.26	180.81	0.874	7.29	
200	3.23	56.91	0.888	67.8	89.25
400	3.18	56.42	0.888	150.1	95.14
600	3.40	56.17	0.875	173.4	95.80
800	3.40	56.00	0.865	270	97.30
1000	3.35	47.09	0.871	361.4	97.98

   Corrosion of metal in acid without and with MNE is maily controlled by charge transfer process without changing mechanism which is indicated by a single capacitive loop in the Nyquist plot and single time constant in Bode plot. (Alagta et al., 2008). The charge transfer resistance (R_{ct}) of acid solution without and with MNE obtained from semicircle of Nyquist plot is used to compute inhibition efficiency. Results reveal that IE increaes with increase in concentration which is confirmed by the increase of phase angle in Bode-phase plot with addition of MNE (Hegazy et al., 2014; B. Xu et al., 2014). The increment in IE with increase in concentration of MNE

may be ascribed to more substantial surface coverage due to adsorption of MNE. It is further supported by the decrease in value of CPE caused by a decrease in dielectric constant due to an increase in the thickness of the electric double layer by adsorption of inhibitor molecules. (Bentiss et al., 2000). As the inhibitor molecules are larger in size as compared to water dipole, the gradual replacement of water dipoles by the inhibitor molecules on the metal surface reduces the rate of corrosion (Quraishi & Ansari, 2003). Figure 4.3.8 shows the variation of inhibition efficiency and constant phase element with the variation of concentration of MNE.
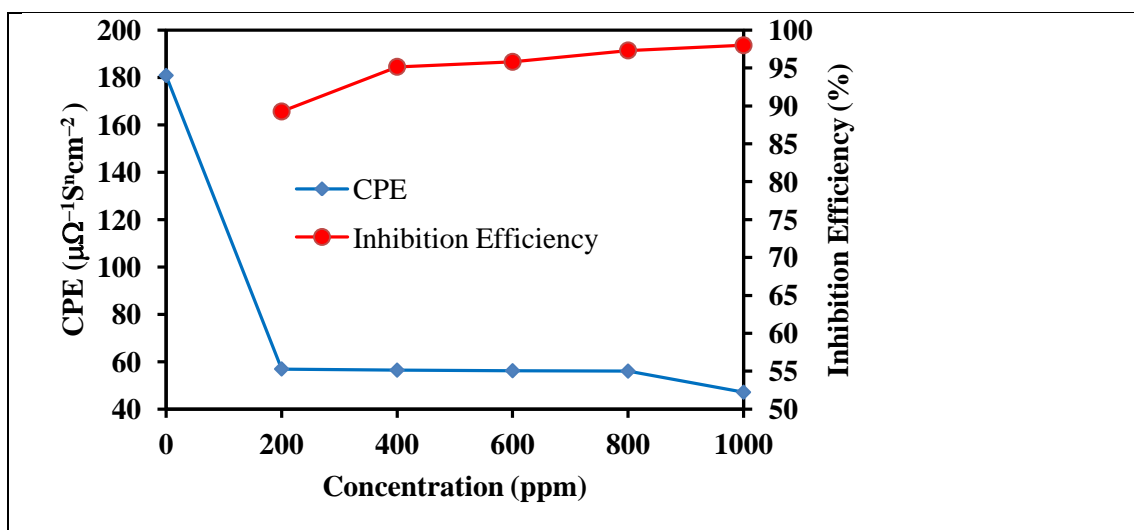
Figure 4.3. 8 : Variation of inhibition efficiency and constant phase element with the variation of concentration of M-MNE.

4.3.6 Differential pulse voltammetry and cyclic voltammetry analyses

Figure 4.3.9a shows the differential pulse voltammogram of corrosion media on a glassy carbon electrode in 0.1 M KCl as supporting electrolyte at pH 1.1 in the absence and presence of plant extract. The mild steel (MS) samples were left to corrode in 1.0M H_2SO_4 solution for 20 hrs containing different amount of MNE.
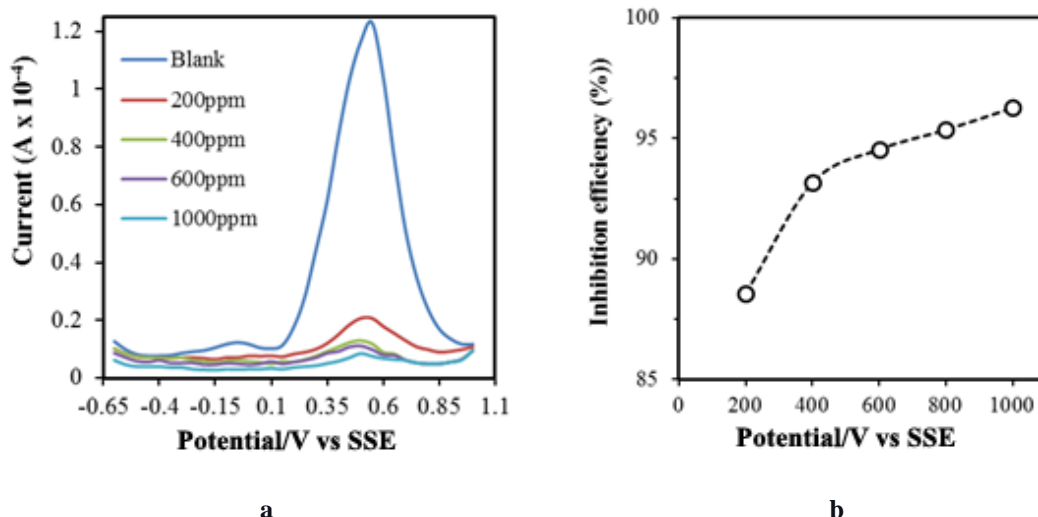
Figure 4.3. 9 : a. Differential pulse voltammogram of GCE in the presence and absence of M-MNE containing corrosion media and b. Corrosion inhibition efficiency of different amout of M-MNE on MS corrosion in acidic medium.

The DPV shows the oxidation peak resulting from the conversion of Fe^{2+} to Fe^{3+} in scanning the potential to anodic direction. The peak current, I_p, is distinctly suppressed by the addition of MNE showing the effectiveness of the plant extract in inhibiting the corrosion of MS in 1.0 M H_2SO_4 solution. More importantly, this result also signifies the adaptation of DPV as a new technique in studying corrosion inhibition effectively. The inhibition efficiency calculated from the difference in the peak current at various concentration of MNE is plotted in Fig. 3.4.9b. It can be seen that similar to other electrochemical results, DPV also shows inhibition efficiency above 96 % by 1000 ppm of MNE. The corrosion rate estimated from the peak current is tabulated in Table 4.29 together with peak potential. A significant reduction in the corrosion rate in the presence of MNE is obvious. The peak potential, on the other hand, slightly shifted to positive values with the addition of MNE. The positive shift of peak potential might be attributed to chelation of Fe^{2+} by molecules of plant extracts. However, the shift in starting potential for oxidation is very large, Fig. 4.3.9a which clearly shows the effect of chelation on the oxidation of Fe^{2+}.

Table 4.29 : Peak potential and corrosion rate ($\mu A\ cm^{-2}\ h^{-1}$) of MS in various concentrations of M-MNE obtained from Fig. 4.3.9a.

Electrolyte	Peak Potential (V)	Corrosion rate ($\mu A\ cm^{-2}\ h^{-1}$)
1.0M H_2SO_4	0.484	17.5
1.0M H_2SO_4 + 200 ppm M-MNE	0.512	2.0
1.0M H_2SO_4 + 400 ppm M-MNE	0.512	1.19
1.0M H_2SO_4 + 600 ppm M-MNE	0.504	0.95
1.0M H_2SO_4 + 800 ppm M-MNE	0.496	0.81
1.0M H_2SO_4 + 1000 ppm M-MNE	0.508	0.65

The effect of time of immersion on the peak current and inhibition efficiency was also studied in 1000 ppm MNE solution, and the results are displayed in Fig. 4.3.10. It is obvious that in the presence of MNE the peak current drastically suppressed. The inhibition efficiency after 15 min of immersion in 1000 ppm MNE solution attained to above 90% and reached to maximum value at 95% after 20 h of immersion. The result of DPV is much better in terms of reliability and reproducibility and therefore corrosion inhibition efficiency of plant extract can be well studied by this method and proposed as a new method of corrosion inhibition study giving all the important parameters such as corrosion rate, inhibition efficiency, chelation and reversibility of the redox system.
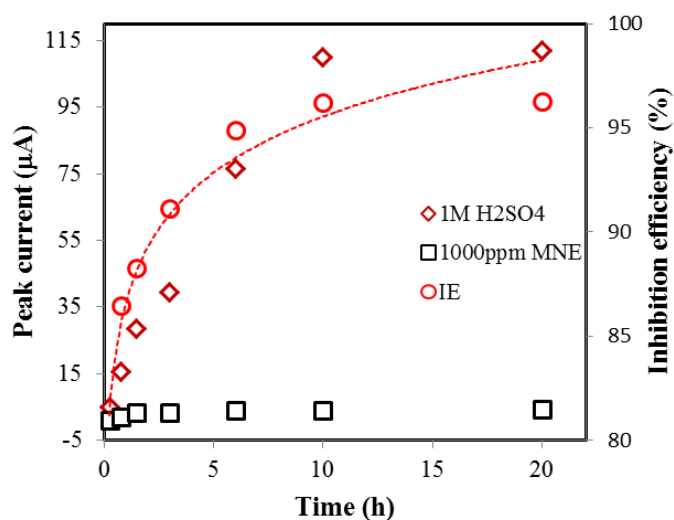
Figure 4.3. 10 : Peak current and corresponding corrosion inhibition efficiency in the presence of 1000 ppm M-MNE.

151

Furthermore, CV measurements were also performed to study corrosion inhibition of MS by MNE. Here, the main purpose was to study the effect of plant extract on peak potential so that chelation of dissolved iron with molecules of plant extract can be clarified, if any. Figure 4.3.11 shows the cyclic voltammograms of corrosion medium (1.0M H_2SO_4) in the absence and presence of 200 ppm plant extract (MNE) after 20 h immersion. A drastic inhibition of voltammetric current is an indication of inhbitory effect of MNE on metal corrosion. The results in terms of peak currents and peak potentails are shown in Table 4.30. The inhibition efficiency is similar to DPV and other electrochemical methods. However, it is interesting to observe a significant change in the cathodic peak potential to negative values with the increase in the amount of MNE, which is attributed to adsroption of oxidized Fe^{3+} on the GCE surfae which required more negative potential for reduction. On the other hand, there is negligible change of anodic peak potential the reason is probalby due to drastic reduction of redox peak with the addition of plant extract. This can be further studied using MS as working electrode in order to relate it with the formation chelation of iron with molecules of MNE.
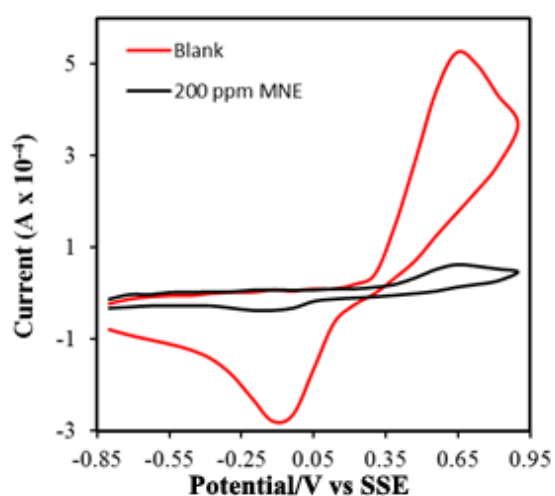
Figure 4.3. 11 : Cyclic voltammograms of GCE in corrosion medium containing M-MNE and dissolved iron from MS.

Table 4.30 : The values of peak potentials and peak currents from CV of GCE in corrosion media containing different amount of M-MNE as inhibitor.

Electrolyte	Epa (V)	Ipa (µA)	Epc (V)	Ipc (µA)	IE (%)
1.0M H_2SO_4	0.63	484	-0.07	216	
1.0M H_2SO_4+200 ppm M-MNE	0.63	41	-0.11	19	91.5
1.0M H_2SO_4+400 ppm M-MNE	0.60	26	-0.19	17	94.6
1.0M H_2SO_4+600 ppm M-MNE	0.60	25	-0.24	13	94.8
1.0M H_2SO_4+800 ppm M-MNE	0.61	26	-0.35	11	94.6
1.0M H_2SO_4+1000 ppm M-MNE	0.61	24	-0.27	10	95.0

4.3.7 Determination of inhibition efficiency by weight loss (Gravimetric) method

Gravimetry is one of the simplest and probably most widely used methods for corrosion study. It can be applied to investigate the effect of immersion of MS coupons for long time up to 24 h in comparison to short time immersion in electrochemical methods. Gravimetric measurements studied inhibitive behavior of MNE by varying time, concentration, and temperature, which are discussed as follows:

4.3.7.1 Effect of immersion time

Table 4.31 : Corrosion rate of mild steel in the presence and absence of M-MNE and inhibition efficiency of M-MNE at various time of immersion.

Solution	Time (h)	Surface area (cm^2)	Weight Loss (mg.)	Rate (mg/cm^2hr)	Inhibition efficiency (%)
Acid	0.25	21.17	28.30	59.59	90.60
Inhibitor		20.68	2.60	5.60	
Acid	0.75	20.99	88.00	62.31	91.60
Inhibitor		21.01	7.40	5.23	
Acid	1.5	21.91	187.50	63.60	92.84
Inhibitor		21.86	13.40	4.56	
Acid	3	21.90	417.60	70.84	93.01
Inhibitor		20.94	27.90	4.95	
Acid	6	21.18	916.33	80.37	93.44
Inhibitor		21.24	60.30	5.27	
Acid	9	20.80	1362.13	81.09	94.53
Inhibitor		21.11	75.63	4.44	
Acid	12	20.96	1848.60	81.93	95.12
Inhibitor		21.63	93.07	3.40	
Acid	24	21.57	3811.23	82.05	95.58
Inhibitor		21.57	168.30	3.62	

153
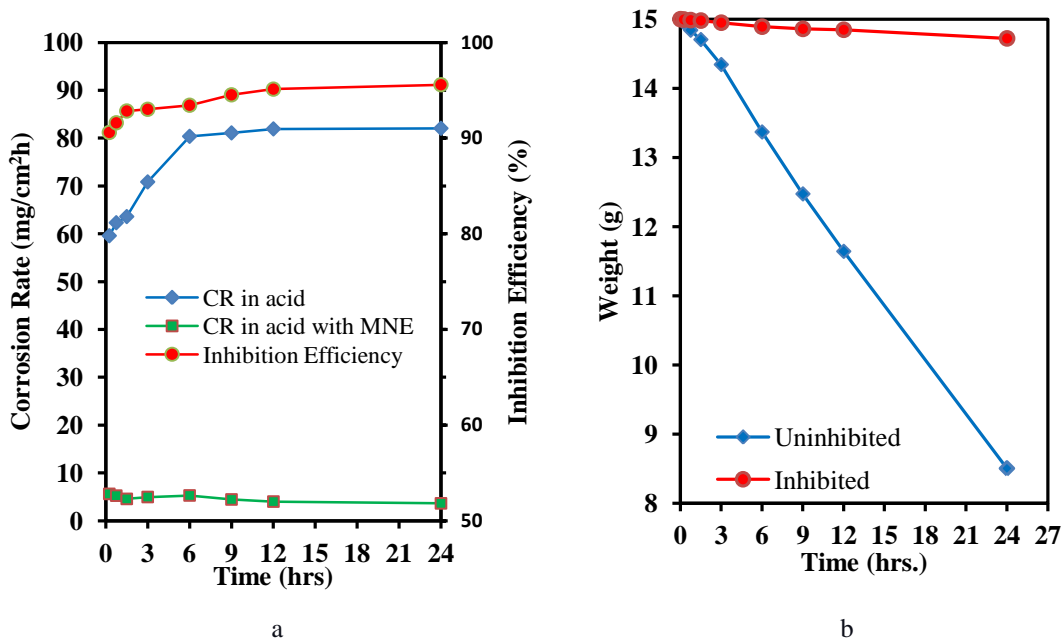
Figure 4.3. 12 : a. Variation in corrosion rate in presence and absence of inhibitor and variation in inhibition efficiency with different immersion time and b. Variation in weight of mild steel in the presence and absence of inhibitor.

The inhibition behavior of MNE was studied by immersing mild steel coupon of known dimension and mass in 100 mL of 1.0 M H_2SO_4 without and with MNE of 1000 ppm concentration at 298 K for different time periods viz 3 h, 6 h, 9 h, 12 h, and 24 h. The data is the comparison of change in weight loss of MS sample immersed in 1.0 M H_2SO_4 vs 1.0 M H_2SO_4 + 1000 ppm of MNE. The corrosion rates were computed for various time intervals. The corrosion rate is reduced about 20 times in a very short time of immersion, only 0.25 h, and reaches up to 24 after 24 h of immersion with the addition of MNE, as illustrated in Fig. 4.3.12a and table 4.31. This finding suggests that MNE adsorption on the MS surface is both efficient and quick. Similarly, the inhibition efficiency is above 90% within 0.25 h of immersion in the acid with MNE inhibitor. The inhibiton efficiency rises steadily with exposure time, reaching around 95% in 24 hours. Figure 4.3.12(b) shows the variation of weight in mild steel coupons in different time intervals in acid without and with inhibitor, which shows the significant decrease in weight loss of mild steel coupons after the addition of MNE in acid. The results show that MNE has the ability to prevent MS corrosion. The corrosion prevention appears to be driven by a protective layer formed by the effective and rapid adsorption of phytochemicals onto the metal surface.

4.3.7.2 Effect of temperature

Furthermore, the effect of temperature on the suppression of MS corrosion by MNE was investigated by immersing the MS sample in acid and acid + 1000 ppm MNE for 6 h at different temperatures. Resuts obtained and calculated inhibition efficiency are shown in Table 4.32 and Fig. 4.3.13. The data shows that *IE* reaches its peak at 328 K (54.85°C**)** on increasing the temperature from room temperature (298 K) to 65 °C (338 K). The decrease in inhibition efficiency above 54.85ºC (328 K) implies the desorption or decomposition of adsorbed molecules above that temperature. (Bentiss et al., 2009). Chemical adsorption of the inhibitors on the MS surface is indicated by the slight but consistent increase in inhibition efficacy with temperature up to 328 K. The nature and mechanism of adsorption process should be deciphered based on the preceding findings.

Table 4.32 : Corrosion rate of mild steel in the presence and absence of M-MNE and inhibition efficiency of M-MNE at various temperatures.

Solution	Temperature (K)	Surface area (cm^2)	Weight Loss (mg.)	Corrosion Rate (mg/cm^2hr)	Inhibition efficiency (%)
Acid	298	19.25	888.23	85.70	92.93
Inhibitor		19.24	62.73	6.06	
Acid	308	19.18	1488.16	144.12	93.04
Inhibitor		19.15	103.37	10.03	
Acid	318	25.19	2394.77	176.60	97.08
Inhibitor		25.74	71.43	5.16	
Acid	328	24.27	2973.90	227.65	96.60
Inhibitor		24.60	102.40	7.73	
Acid	338	21.92	4561.73	386.51	75.47
Inhibitor		22.80	1163.60	94.80	
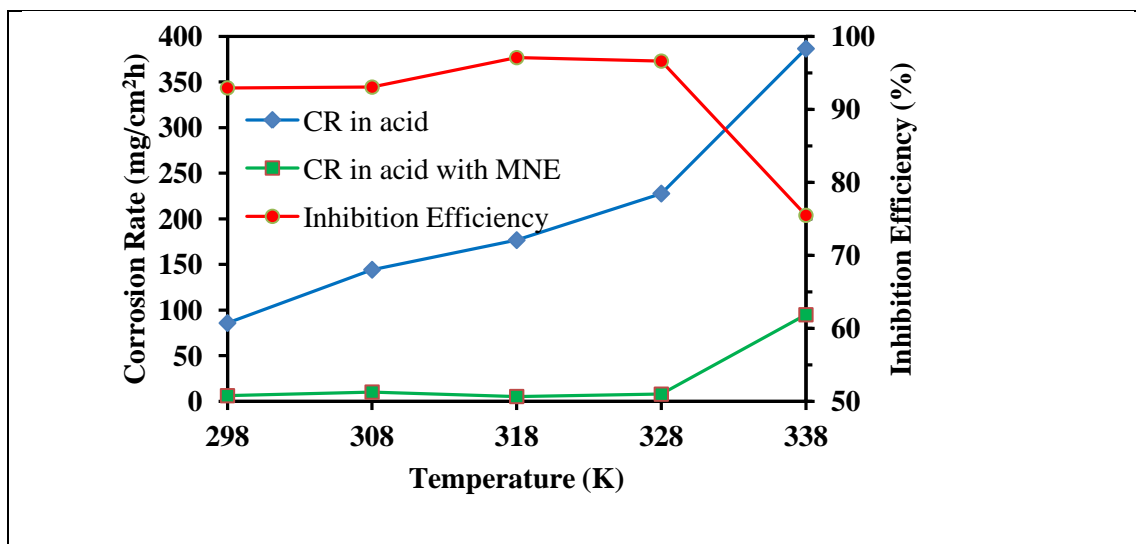
Figure 4.3. 13 : Variation of corrosion rate and inhibition efficiency with variation of temperature.

4.3.7.3 Effect of concentration:

Similary, effect of concentrations on the inhibition efficiency was studied by immersing MS sample in acid and acid with inhibitor of various concnetration for 6 h. The observed results along with computed inhibition efficiency are shown in Table 4.33 and Fig. 4.3.14(a) . The results show that the MNE concentration of 200 ppm is effective in limiting the corrosion of the MS by 90%. The increase in concentration increases the inhibition efficiency and reaches up to 95% at 1000 ppm concentration. The surface coverage of phytochemicals on the MS surface is high (0.95). Figure 4.3.14(b) shows comparison of the increase in IE with increase in concetration of inhibitor. Comparable result was observed by differential pulse voltammetry (DPV) as well.

Table 4.33 : Corrosion rate of mild steel in the presence and absence of M-MNE and inhibition efficiency of M-MNE at various concentrations.

Concentration	Surface area (cm^2)	Weight Loss (mg.)	Corrosion Rate (mg/cm^2hr)	Inhibition efficiency (%)	Surface coverage (θ)
0 ppm. (acid solution only)	19.56	868.93	82.52		
200 ppm.	19.18	86.63	8.39	89.83	0.8983
400 ppm.	19.39	61.87	5.93	92.82	0.9282
600 ppm.	19.78	58.83	5.05	93.88	0.9388
800 ppm.	18.99	48.73	4.77	94.22	0.9422
1000 ppm.	19.52	42.33	4.03	95.12	0.9512
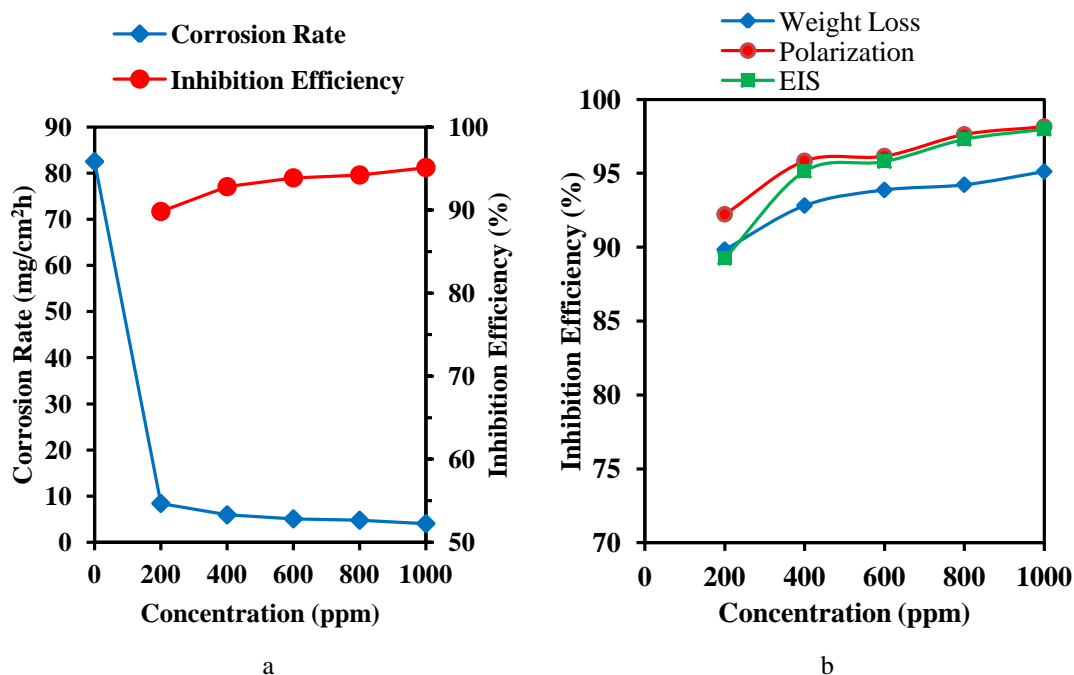
Figure 4.3. 14 : a. Variation in corrosion rate and inhibition efficiency with the variation of concentration of M-MNE and b. Inhibition efficiency of M-MNE from different methods for MS in 1.0 M H_2SO_4.

4.3.8 Adsorption isotherm

Adsorption isotherms aid in the acquisition of basic information about the inhibitor's interaction with the MS surface. Plant extracts reduce metal corrosion by adsorbing phytochemicals on their surface. Adsorption of the polar functions of phytochemicals could be physical adsorption, chemisorption or mixed of both type of adsorption. The adsorbed phytochemicals forms barrier film on metal surface to inhibit the charge and mass transfer between metal and the corrosive environment. It shows the importance of studying the adsorption behavior of inhibitor. By evaluating several important thermodynamic properties like free energy of adsorption, activation energy, enthalpy, and entropy of adsorption, it is possible to determine the mechanism and amount of inhibitor interaction with the metal surface. In aqueous solution water molecules are adsorbed on the metal surface which is replaced by large size organic molecules present in MNE during its adsorption resulting in a quasi-substitution process (Chauhan & Gunasekaran, 2007). To study the adsorption behavior, several adsorption isotherms like Langmuir, Tempkin, Freundlich, El-Awady, were evaluated were tested by plotting the degree of surface coverage (θ) obtained from the gravimetric method against the inhibitor concentration. As the inhibitor used in crude

157

extract, which is mixture of several organic compounds, all the compounds present in it might affect in the inhibition positively or negatively. However, the concentration used to fit suitable adsorption models is the average molar concentration of few essential compounds which plays a major role in inhibition. Among the several adsorption isotherm tested for the study, best fit adsorption isotherm obtained was Langmuir adsorption isotherm because when C_{inh} is plotted against C_{inh}/θ, a straight line was obtained where values of both linear correlation coefficient (R^2) and slope are almost equal to 1, Fig. 4.3.15. Little deviation of values from unity may be due to some interactions between adsorbed inhibitor molecules on the mild steel surface. Interactions may be either mutual attraction or repulsion force between different functional groups of different molecules or preferential adsorption of molecules at the cathodic and anodic site (Verma & Quraishi, 2007). As adsorption follows Langmuir adsorption isotherm, adsorption of inhibitor on MS surface is a monolayer where adsorbate molecules do not interact with each other(Sadeghi Erami et al., 2019).

Relation of Langmuir adsorption isotherm is shown in equation [4-12],

$$\frac{C_{inh}}{\theta} = \frac{1}{K_{ads}} + C_{inh} \qquad [4\text{-}12]$$

When C_{inh} is plotted against $\frac{C_{inh}}{\theta}$, a straight line is obtained. The value of adsorption constant K_{ads} can be calculated from the intercept of the line. This value can be used in the equation [4-13] to calculate the value of free energy of adsorption (ΔG°).

$$\Delta G^\circ = -RT \ln(55.5 K_{ads}) \qquad [4\text{-}110]$$

Where 55.5 refers to the concentration of water in solution in mol/L and R refers to the universal gas constant (8.314J/mol K). Calculated value of ΔG_{ads}° according to relation is -35.05 kJ/mol. Large negative value of ΔG_{ads}° implies that the AVE is adsorbed on mild steel surface spontaneously to form highly stable barrier film (Cang et al., 2013). The computed value is intermediate between physisorption (less than or around -20 kJ/mol) and chemisorption (more than or equal to -40 kJ/mol) (Sadeghi Erami et al., 2019) which indicates that the adsorption involves both physical and chemical adsorption . Generally, physisorption is related with a value of ΔG° less than or around -20 kJ/mol, while chemisorption is associated with a value of ΔG° greater than or around -40 kJ/mol. Here, the computed value is intermediate, implying the adsorption is not merely physical or chemical but involves both (Ahamad et al., 2010).

Adsorption involves physical adsorption with displacement of water molecules from the mild steel surface followed by chemisorption. (Cang et al., 2013).
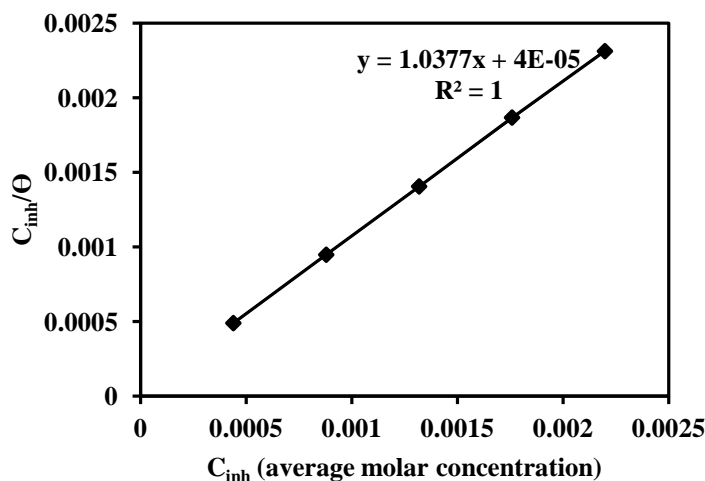
Figure 4.3. 15 : Langmuir adsorption isotherm plot for mild steel in 1.0 M H_2SO_4 with different concentration of M-MNE as the average molar concentration of some major compounds in M-MNE.

4.3.9 Calculation of activation energy and thermodynamic parameters :

The nature of the MNE adsorption is further studied by evaluating activation energy and thermodynamic parameters such as enthalpy and entropy of adsorption. Activation energy (E_a) is calculated from the slope of the Arrhenius plot obtained by plotting the computed corrosion rate at various temperatures according to the Arrhenius equation [4-14] (Ostovari et al., 2009),

$$log(CR) = log\,A - \frac{E_a}{2.303\,RT} \qquad\qquad [4\text{-}11]$$

Where, *A* refers to the Arrhenius pre-exponential constant.

E_a computed from Arrhenius plots illustrated in Fig. 4.3.16(a) is presented in Table 4.34 which shows the increment in E_a with the addition of inhibitor, implying the adsorption of MNE on the MS surface (Shukla & Ebenso, 2011). The the calculated value of activation energy for MNE adsorption is 42.55 kJ/mol, which is intermediate between physical adsorption (less than or equal to 20 kJ/mole) and chemical adsorption (greater than or equal to 80 kJ/mol) (Yan Li et al., 2005; Sadeghi Erami et al., 2019). It reflects the mixed interaction involving both physical and chemical

interaction in the adsorption of inhibitor molecule on MS surface, which is also supported by the value of free energy of adsorption.
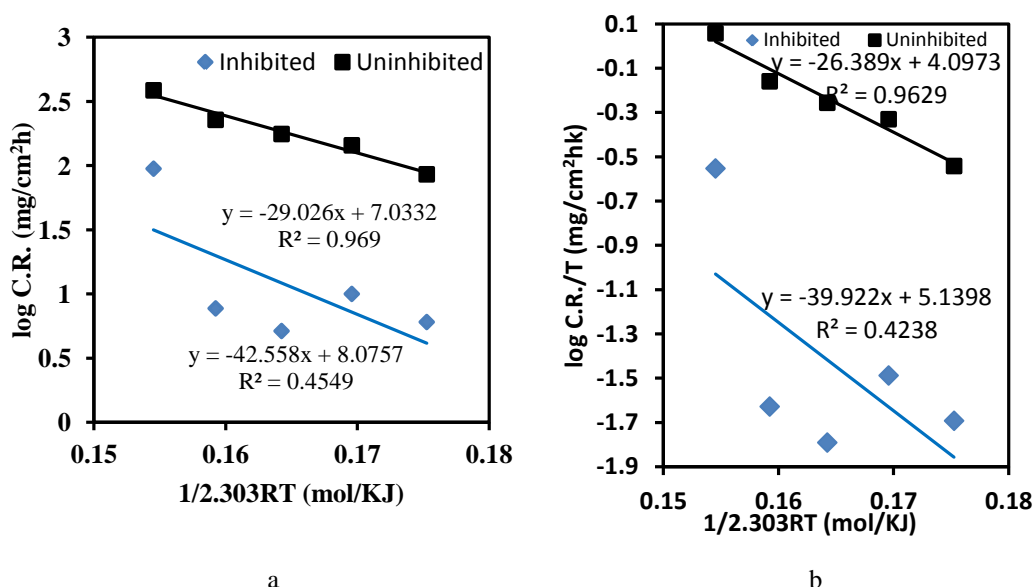
Figure 4.3. 16 : a. Arrhenius plot for mild steel in 1.0 M H_2SO_4 with and without M-MNE and b. Transition state plot for mild steel in 1.0 M H_2SO_4 with and without M-MNE.

The transition state equation [4-15] is used to evaluate entroy and enthalpy of activation, where the enthalpy of activation (ΔH^*) may be derived from the slope of a straight line generated by plotting $\log\left(\frac{C.R.}{T}\right)$ vs. $\left(\frac{1}{2.303\,RT}\right)$ as illustrated in Fig. 4.3.16(b) and the entropy of activation (ΔS^*) can be computed from the slope of the line. (Ostovari et al., 2009).

$$\log\left(\frac{C.R.}{T}\right)=\left[\log\left(\frac{R}{hN}\right)+\left(\frac{\Delta S^*}{2.303R}\right)-\frac{\Delta H^*}{2.303\,RT}\right] \qquad [4\text{-}12]$$

Where h refers to Plank's constant, 6.6261×10^{-34} Js, and N refers to the Avogadro's number, 6.0225×10^{23} mol^{-1}.

The computed values of ΔH^* and ΔS derived from Fig. 4.3.16(b) for acid without and with inhibitor are listed in Table 4.34.

A positive value of ΔH^* implies that the adsorption of inhibitor on metal surface is endothermic process. The value of ΔH^* is increased with the addition of MNE, which demonstrates that kinetic factors of activation regulate the decrease in corrosion rate (Bhat et al., 2011). (Hamdy & El-Gendy, 2013). The preceding calculations show the

greater value of Ea than ΔH*, which indicates the occurrence of gaseous reaction, namely hydrogen evolution processes, resulting in a reduction in overall reaction volume. (Ostovari et al., 2009). The difference in the value of It is inferred that the corrosion process is unimolecular in the condition, as evidenced by upholding the relation $Ea - \Delta H^* = RT$. The difference in the value of Ea and ΔH* is 2.64 kJ/mol, which is almost the same as RT. It implies the unimolar nature of corrosion process.(Yan Li et al., 2005; Qiang et al., 2018; Sadeghi Erami et al., 2019).

The association step is indicated in the rate-determining step by large and negative values of ΔS^* for mild steel in 1.0 M H₂SO₄. The result imples a decrease in disordering as the reaction progresses from reactants to the activated complex. (Hamdy & El-Gendy, 2013). Interestingly, the value of ΔS* increases with the addition of MNE, indicating an increase in disorder as the reaction progresses from reactant to the activated complex. The replacement of water molecules during the adsorption of the inhibitor on the mild steel surface causes this behavior. (Hamdy & El-Gendy, 2013). In this situation, the adsorbed inhibitor molecules may reduce the rate of discharge of hydrogen ions in the rate-determining step.

Table 4.34 : Activation parameters of the dissolution of mild steel in 1.0 M H_2SO_4 without and with an inhibitor of 1000 ppm concentration.

Electrolyte	Ea(kJ/mol)	A (mg/cm^2)	ΔH(kJ/mol)	Ea-ΔH	ΔS(J/molK)
1.0 M H₂SO₄	29.02	1.08×10^7	26.38	2.64	-119.13
Acid with inhibitor	42.56	1.19×10^8	39.92	2.64	-99.18

4.3.10 Surface analysis

The surface morphology and composition of the mild steel surface immersed in acid without and with an inhibitor for 24 hours were studied using SEM and EDX. The SEM image of the MS specimen surface immersed in acid for 24 h without inhibitor is shown in Fig 4.3.17a. The surface of the MS surface immersed in acid with MNE concentrations of 400 and 1000 ppm appears highly porous, with deep and large craks that are relatively smooth, as shown in Figs. 4.3.17(b) and 4.3.17(c), respectively. It implies the high rate of dissolution of metal in acid, but dissolution decreases with the addition of MNE due to the formation of the barrier film on the surface, which inhibits the dissolution. The formation of a protective film is also supported by the percentage composition of various elements present on the MS surface as determined by EDX, as shown in Table 4.35. It shows that the amount of

iron decreases with an increment in the amount of N, C, and O on the MS surface when the sample is immersed in acid with MNE. It is due to the adsorption of phytochemicals present in MNE that it forms a protective film to inhibit metal dissolution.

a   **b**   **c**
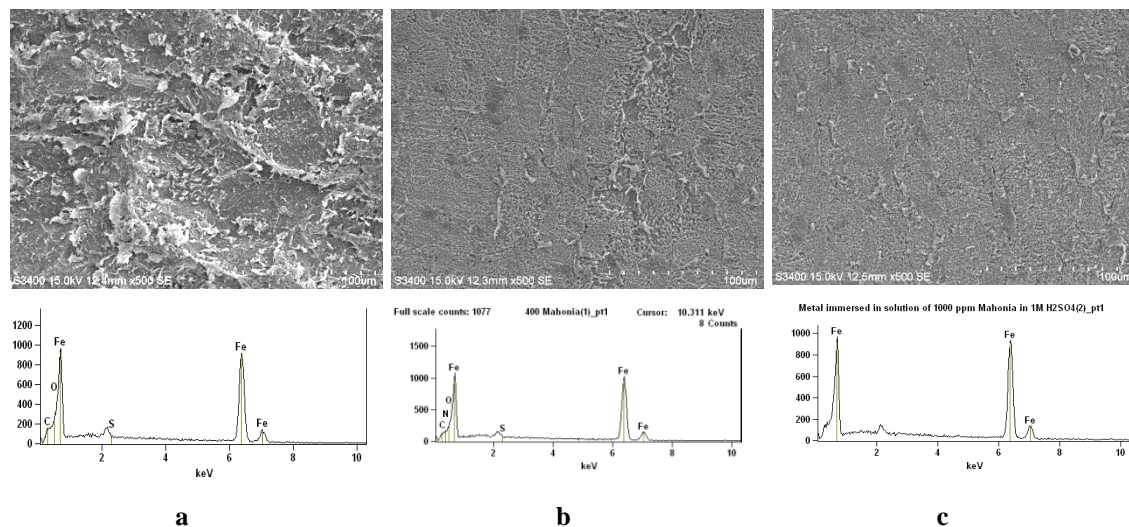
Figure 4.3. 17   : SEM images and corresponding EDX spectra of mild steel coupons after 24 h immersion in (a) 1.0 M H_2SO_4, (b) 400 ppm extract solution in 1.0 M H_2SO_4 and (c) 1000 ppm extract solution in 1.0 M H_2SO_4.

Table 4.35 : Weight difference of different elements on the MS surface after immersion the sample in different solutions.

Surface dipped in	Iron	Carbon	Nitrogen	Oxygen
Acid without inhibitor	97.45%	1.72%		0.83%
Acid with inhibitor of 400 ppm	96.94%	1.73%	0.44%	0.89
Acid with inhibitor of 1000 ppm	95.37%	3.20%	0.46%	0.95%

4.3.11 Mechanism of inhibition

It is well accepted fact that the plant extracts inhibit corrosion due to formation of barrier film on metal surface with adsorption of large size organic molecules. This barrier film blocks the active site to inhibit corrosion. Inhibition efficacy depends upon the functionality and heteroatoms present in the molecules. As discussed in earlier chapters, adsorption of MNE on mild steel surface is mixed type of adsorption involving both physical and chemical interactions.

The OCP value of MS in MNE was determined at around -0.43 V, which is greater than the potential of zero charge (PZC) of MS in sulfate solution. (Sivakumar et al.,

2018). Therefore the value of Antropov's rational corrosion potential is positive, and the net charge of MS is positive. For example, phytochemicals present in MNE like berberine, Jatrorrhizine, molecules contain quaternary nitrogen with a positive charge. Isotetrandine, thalrugosamine, 7,8 dihydro 8-methoxy berberine contains a tertiary amino group, and all the compounds have ethereal oxygen. In acidic solution, ethereal oxygen and amino nitrogen can be protonated and bears a positive charge. There will be repulsion between these phytochemicals and positively charged metal surface. But, in acidic solution, anion left by acid like sulfate ion is adsorbed first on metal surface due to small degree of hydration forming negatively charged metal surface, which makes feasible for the adsorption of positively charged inhibitor molecules to metal surface due to electrostatic force of attraction. It implies that the adsorption is made feasible due to synergism with sulfate ion (Yan Li et al., 2005; Sadeghi Erami et al., 2019).

In acid solution, positively charged inhibitor molecules may initially compete for electrons on the MS surface with H^+ ions. But, inhibitor molecules of MNE converts to its neutral form after cathodic hydrogen discharge, which is followed by the donor acceptor interaction of highest occupied molecular orbital (HOMO) of inhibitor molecules with vacant d-orbital of meta, establishing a coordinate bond (Qiang et al., 2018; Sadeghi Erami et al., 2019). This interaction forms strong bond according to HSAB theory. Because, metal in zero oxidation state behaves as a soft acid and the inhibitor molecules behave as a soft base, and interaction between soft acid and soft base is stronger and fast (Sadeghi Erami et al., 2019). To prevent Fe from acquiring a negative charge on its surface, electrons could be redirected to the lowest unoccupied molecular orbital (LUMO), which is the vacant π* (antibonding) orbital of inhibitor molecules to form feedback bond (retrodonation). The adsorption of molecules on the metal surface is strengthened by the formation of feedback bond. It shows that adsorption could start with an electrostatic force of attraction (physical adsorption), followed by electron transfer between organic molecules and metal to form a coordinate and feedback bond.

Inhibition efficiency might be enhanced by isotetrandine, thalugosamine, and 7,8 dihydro 8 methoxy berberine because electron pair of amino nitrogen can be shared

easier than by oxygen and their size is also large which can result in covering more surface area. Besides, these molecules have more methyl groups attached to ethereal oxygen, which acts as electron-rich centers, and therefore oxygen can acquire large electron density. It will, therefore, make such oxygen get protonated easily, which will help in getting easily adsorbed on a negatively charged metal surface.

Schematic representations of adsorption of two compounds berberine and isotetrandrine are illustrated in Fig. 4.3.18a and 4.3.18b.
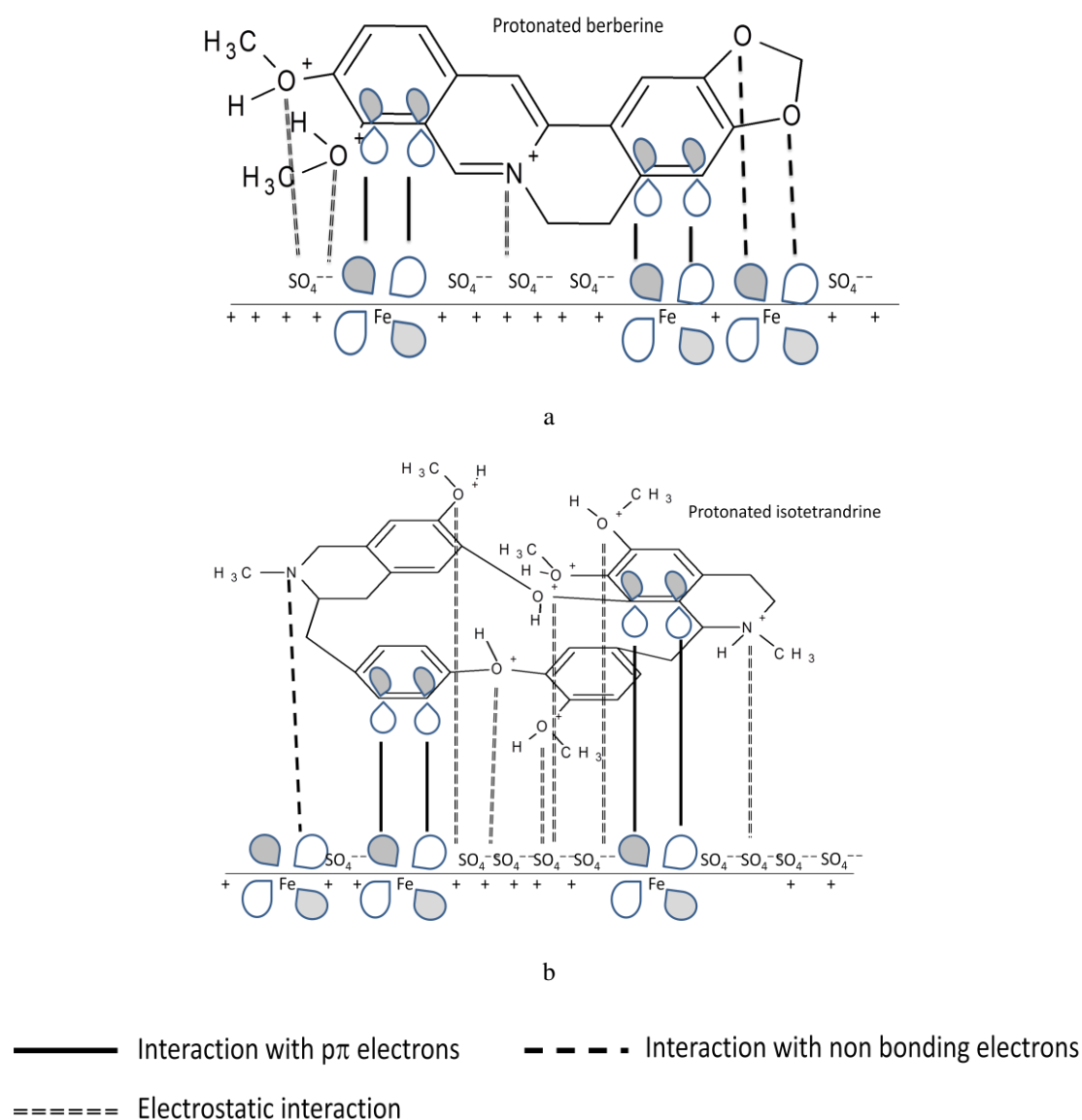
Figure 4.3. 18 : Schematic representations of adsorption of a. berberine and b. isotetrandrine.

Besides, corrosion inhibition is also due to the formation of stable and insoluble metal-inhibitor complex formed as a result of the combination of organic molecules with Fe^{+2} ions. When a number of such type of complex increases, the solubility of protective layer decrease which suppress the anodic metal dissolution and inhibits the corrosion. It explains why the inhibition efficacy increases as concentration and time increase. The possible chelate complexes of 7,8 dihydro 8 methoxy berberine and jatrorrhizine are shown in figure 4.3.19.

Chelation inhibits anodic reaction as follows :

$$Fe_{(s)} \longrightarrow Fe^{2+}_{(aq)} + 2e^-$$

$$Fe^{2+}_{(aq)} + MNE_{(ads)} \longrightarrow [Fe-MNE]^{2+}$$

a   b
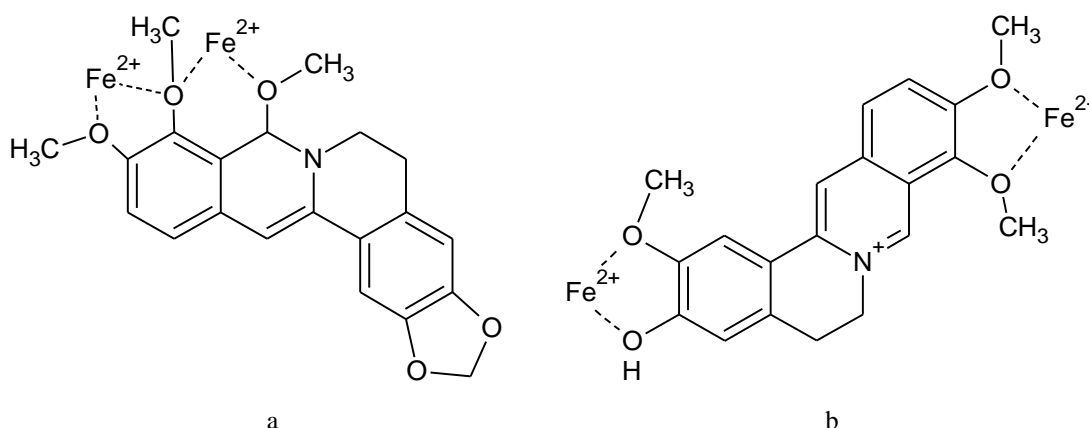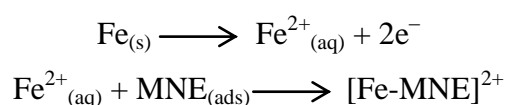
Figure 4.3. 19 : Possible complex formation between a. 7,8 dihydro 8 methoxy berberine and b. Jatrorrhizine and metallic iron on the top of the metallic surface.

Both anodic and cathodic reactions are suppressed by the adsorption of inhibitor molecules. The adsorption of sulfate ions suppresses anodic dissolution, as indicated(Karthik et al., 2014) :

$$H_2SO_4 \longrightarrow H^+ + SO_4^{--}$$

$$MNE + H^+ \longrightarrow (MNE)H^+$$

$$Fe + SO_4^{--} \longrightarrow (FeSO_4^{--})_{ads}$$

$$(FeSO_4^{--})_{ads} \longrightarrow (FeSO_4^-)_{ads} + e^-$$

$$(FeSO_4^-)_{ads} \longrightarrow (FeSO_4)_{ads} + e^-$$

$$(FeSO_4)_{ads} \longrightarrow Fe^{++} + SO_4^{--}$$
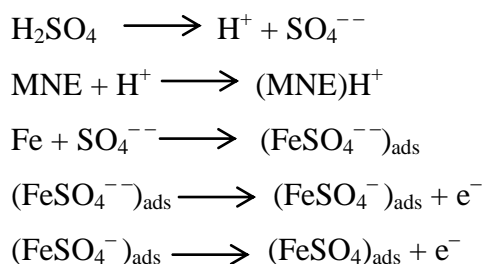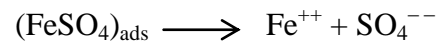
The cathodic hydrogen evolution is reduced due to adsorption of MNE on the MS surface as:

$Fe + (MNE)H^+ \rightarrow (Fe\text{-}(MNE)H^+)_{ads}$ (adsorption of protonated EHE molecules)

$(Fe\text{-}(MNE)H^+)_{ads} + e^- \rightarrow (Fe\text{-}(MNE)H)_{ads}$ (Reduction of protonated H^+)

$(Fe\text{-}(MNE)H^+)_{ads} + H^+ + e^- \rightarrow Fe + H_2 + MNE$ (release of hydrogen)
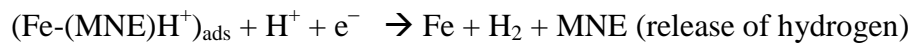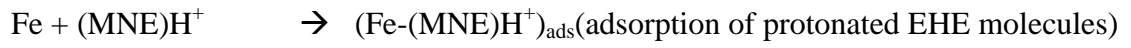
4.4 Berberis aristata:

Results of corrosion tests of extract of the stem of *Berberis aristata* plant are presented as follows:

4.4.1 Potentiodynamic polarization of mild steel in 1.0 M H_2SO_4 *Berberis aristata* extract in methanol and n-hexane solvents

a   b
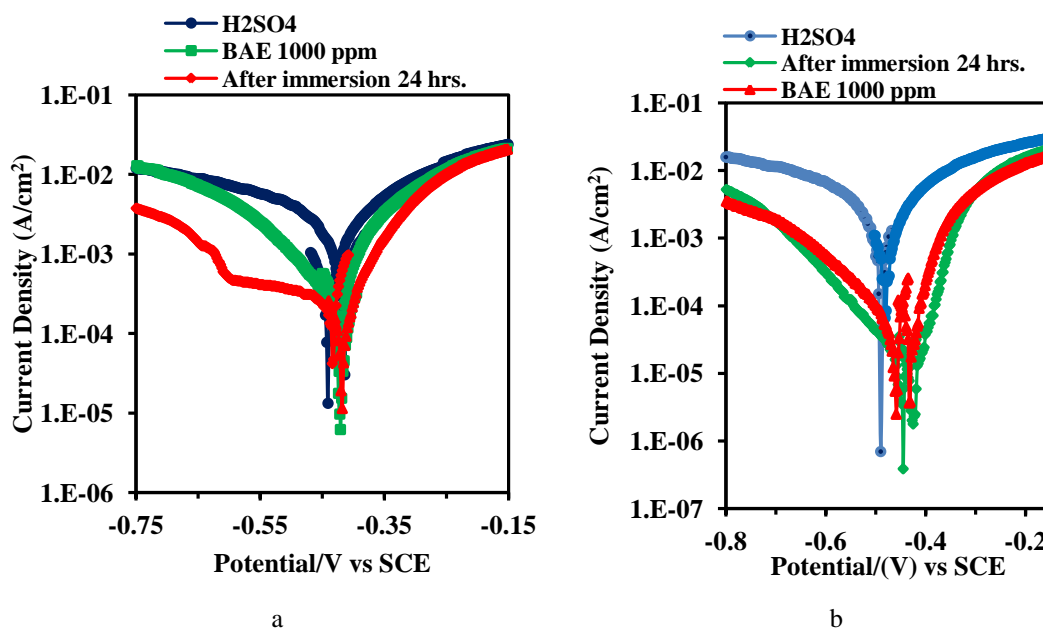
Figure 4.4. 1 : a. Polarization of Mild Steel in n-hexane extract of *Berberis aristata* in 1.0 M H_2SO_4 and b. Polarization of Mild Steel in methanol extract of *Berberis aristata* in 1.0 M H_2SO_4.

Table 4.36 : Potentiodynamic polarization parameters for the corrosion of mild steel with n-hexane extract of *Berberis aristata*.

Electrolyte	Sample	$-E_{corr}$ (V/SCE)	I_{corr} (A/cm²)	βa (V/dec)	$-\beta c$ (V/dec)	I.E.%
Acid	Mild steel	0.461	9.42×10^{-4}	0.096	0.126	
Acid + H-BAE 1000 ppm	Mild Steel	0.458	2.67×10^{-4}	0.057	0.109	71.60
Acid + H-BAE 1000 ppm	Mild steel immersed in electrolyte for 24 h	0.450	1.94×10^{-4}	0.066	0.248	79.36

Polarization of mild steel coupon as immersed and after immersion for 24 h in the electrolyte was carried out with 1.0 M H_2SO_4 without and with inhibitor solution of different concentrations as the electrolyte. Inhibitors used in the process were n-hexane and methanol extract of *Berberis aristata*. The polarization curve obtained is

shown in Fig. 4.4.1a and Fig. 4.4.1b for n-hexane and methanol extract respectively. Electrochemical parameters derived from the Tafel extrapolation method of the polarization curve along with inhibition efficiency are presented in Table 4.36 and Table 4.37 for n-hexane and methanol solvents respectively.

Table 4.37 : Potentiodynamic polarization parameters for the corrosion of mild steel with methanol extract of *Berberis aristata.*

Electrolyte	Sample	$-E_{corr}$ (V/SCE)	I_{corr} (A/cm^2)	βa (V/dec)	$-\beta c$ (V/dec)	I.E.%
Acid	Mild steel	0.473	9.57×10^{-4}	0.080	0.110	
Acid + M-BAE 1000 ppm	Mild Steel	0.425	2.16×10^{-5}	0.036	0.084	97.75
Acid + M-BAE 1000 ppm	Mild steel immersed in electrolyte for 24 h	0.423	1.31×10^{-5}	0.044	0.122	98.64

Data reflects the corrosion potential of the methanolic extract of *Berberis aristata.* Inhibition efficiency of extract for mild steel coupon as immersed is 97.75% and for a coupon after immersion for 24 h is 98.64. Inhibition is due to the suppression of both cathodic hydrogen evolution and anodic metal dissolution. Inhibition efficiency for n-hexane extract is 79.36% for coupon immersed for 24 h and 71.60% for coupons as immersed. The cathodic reaction is more suppressed for this extract. Since the efficiency of methanolic extract was more, it was selected for detailed investigation. Since the shift in E_{cor} value with the addition of BAE is less than 85mV, extracts behaves as a mixed inhibitor. (Riggs Jr., 1973)

4.4.2 ATR-FTIR analysis of methanol extract of *Berberis aristata*:

The ATR-FTIR characterization of the extract was carried out to identify the functional groups present in it. The ATR-FTIR spectra of the extract are shown in **Fig. 4.4.2**. List of absorption peaks and assigned functional groups are presented in supplementary Table 4.38. The O-H stretching of alcohol, phenol, and carbohydrate, as well as the N-H stretching of amine, results in a bandwidth in the range of 3360 cm–1 to 3209 cm^{-1}. C-H stretching of alkane causes a band at 2912 cm^{-1}. A band at 1650 cm^{-1} is attributed to C=C stretching, C=O stretching of amide or δ-lactum, C=N stretching of imine or oxime, and N-H bending of amine. The aromatic C=C bending and N-H bending of amine is shown by a sharp band at 1570 cm^{-1}. Similarly, the absorption band at 1435 cm^{-1} is associated with O-H bending of carboxylic acid, and a

sharp peak at 1384 cm^{-1} is due to C-H bending of gem dimethyl or aldehyde and, O-H bending of alcohol, phenol. The C-N stretching of aromatic amine is attributed to a band at 1284 cm^{-1}, which is corroborated by a strong peak at 1037 cm^{-1}. C-O stretching of aromatic ethers, 3° alcohol, ester, and C-N stretching of amine are associated with the absorption band at 1200 cm^{-1}, while C-O stretching of 2° alcohols, ether, and C-N stretching of amine are associated with the absorption band at 1103 cm^{-1}. There is again a band at 987 cm^{-1} attributed to the C=C bending of the alkene. The presence of functionalities such as alcohol, phenol, amine, ether, carboxylic acid, and carbohydrate with aromatic rings containing heteroatoms like N and O is revealed by these absorption bands. Therefore, the extract could be a promising candidate for green corrosion inhibitor. (Umoren et al., 2014).
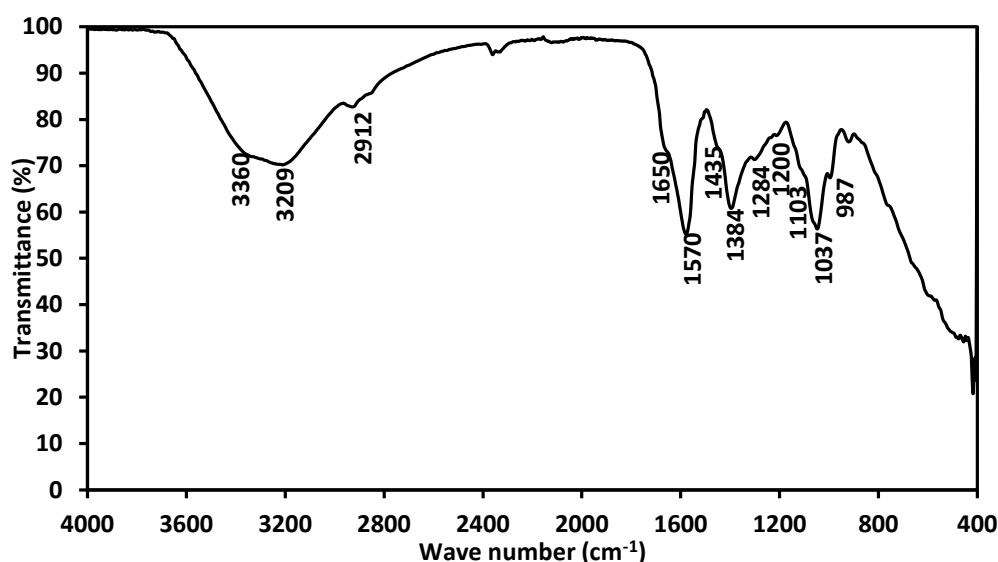
Figure 4.4. 2 : FTIR spectra of the methanolic extract of *Berberis aristata.*

Table 4.38 : Some important absorption bands/ peaks from FTIR measurements of M-BAE.

Adsorption peak (cm^{-1})	Functional groups
3360-3209	O-H stretching of alcohol, phenol, carbohydrate, N-H stretching of amine
2912	C-H stretching of alkane
1650	C=C stretching, C=N stretching of imine or oxime, C=O stretch of amide or δ-lactum, N-H bending of amine
1570	aromatic C=C bending, N-H bending of amine
1435	O-H bending of carboxylic acid
1384 (Sharp)	O-H bending of alcohol, phenol, C-H bending of gem dimethyl or aldehyde
1284	C-N stretching of aromatic amine
1200	C-O stretching of aromatic ether, 3° alcohol, ester, C-N stretching of amine
1103	C-O stretching of 2° alcohol, ether, C-N stretching of amine
1037 (Sharp)	C-N stretching of amine
987	C=C bending of monosubstituted alkene

4.4.3 Variation of open circuit potential with time

The OCP-time curves for MS specimen in 1M H_2SO_4 solution without and with BAE of different concentrations against a SCE reference are represented in Fig. 4.4.3. It is observed that the OCP increases slightly in the beginning and attains a steady potential after 1200 seconds. OCP is shifted towards positive value with the addition of BAE. This observation can be ascribed to the formation of barrier film formed on the MS surface due to the adsorption of molecules present in BAE. However potential shift is not enough to classify it as a cathodic inhibitor. Since the OCP shift is less than 80 mV, it can be said as a mixed inhibitor (Odewunmi et al., 2015).
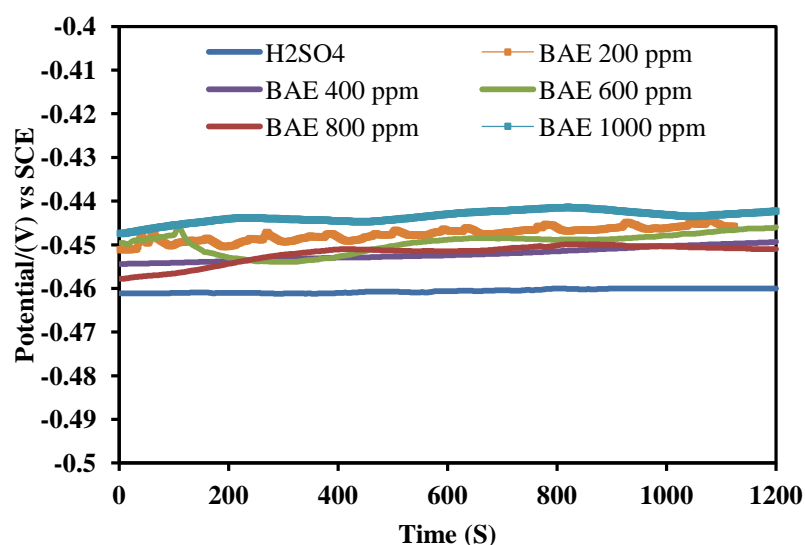
Figure 4.4. 3 : The OCP-time curves for MS specimen in 1.0 M H_2SO_4 solution without and with M-BAE of different concentrations against a SCE reference.

4.4.4 Polarization of mild steel in methanol extract of *Berberis aristata* in 1.0 M H_2SO_4

Potentiodynamic polarization was carried out for mild steel coupon as immersed and after immersion of coupon in the electrolyte solution for 24 h and results are illustrated separately as follows:

Potentiodynamic curves for mild steel as immersed in 1.0 M H_2SO_4 were recorded in the presence and absence of BAE which is represented in Fig. 4.4.4a. Electrochemical parameters viz corrosion current (I_{corr}), corrosion potential (E_{corr}), Cathodic slope (βa), and anodic slope (βa) obtained from the Tafel extrapolation method of the

170

polarization curve are presented in Table 4.39 and variation in corrosion current and inhibition efficiency in the experiments is represented in figure Fig. 4.4.4b.

a   b
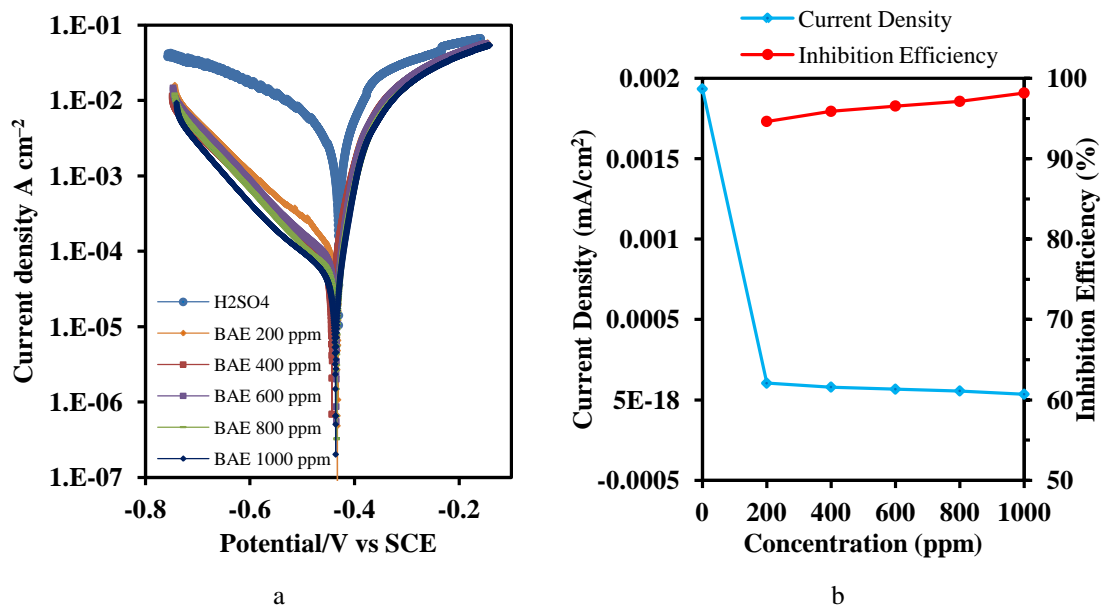
Figure 4.4. 4   : a. Polarization curve of mild steel in 1.0 M H_2SO_4 without and with M-BAE of different concentrations and b. Variation of current density and inhibition efficiency for mild steel coupon with the variation of concentration of inhibitor in 1.0 M H_2SO_4.

Table 4.39 : Potentiodynamic polarization parameters for the corrosion of mild steel with various concentrations of M-BAE.

Concentration (ppm)	$-E_{corr}$ (V/SCE)	I_{corr} (A/cm^2)	βa (V/dec)	-βc (V/dec)	I.E.%
Blank	-0.4281	1.93×10^{-3}	0.0603	0.1122	
200	-0.4327	1.04×10^{-4}	0.0276	0.1169	94.64
400	-0.4471	7.94×10^{-5}	0.0376	0.1142	95.89
600	-0.4373	6.66×10^{-5}	0.0273	0.1151	96.56
800	-0.4359	5.54×10^{-5}	0.0287	0.1348	97.13
1000	-0.4379	3.53×10^{-5}	0.0249	0.1116	98.18

Potentiodynamic curves for mild steel in 1.0 M H_2SO_4 in the presence and absence of BAE after immersion of coupon in electrolyte for 24 h were recorded and it is represented in Fig. 4.4.5a. Electrochemical parameters viz corrosion current (I_{corr}), corrosion potential (E_{corr}), Cathodic slope (βa), and anodic slope (βa) obtained from the Tafel extrapolation method of the polarization curve are presented in Table 4.40

and variation in corrosion current and inhibition efficiency in the experiments is represented in Fig. 4.4.5b.

a   b
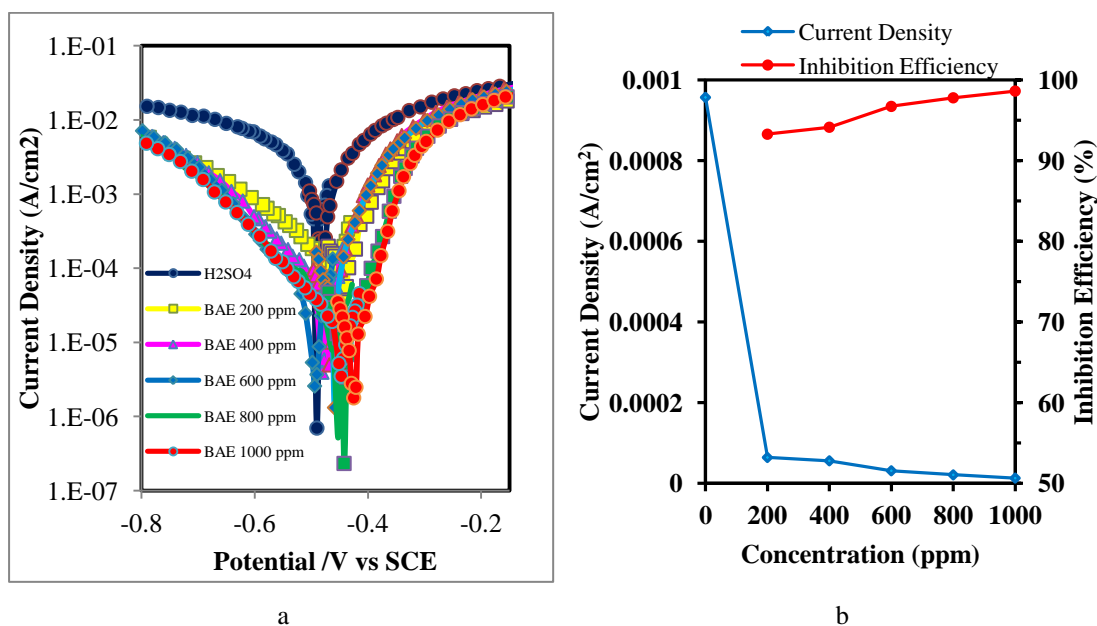
Figure 4.4. 5 : a. Polarization curve of mild steel in 1.0 M H_2SO_4 without and with M-BAE of different concentrations when mild steel coupon is immersed in the electrolyte for 24 h. and b. Variation of current density and inhibition efficiency for mild steel coupon immersed in electrolyte with the variation of concentration of inhibitor in 1.0 M H_2SO_4.

Table 4.40 : Potentiodynamic polarization parameters for the corrosion of mild steel immersed in electrolyte for 24 h with 1.0 M H_2SO_4 without and with various concentrations of M-BAE.

Concentration (ppm)	$-E_{corr}$ (V/SCE)	I_{corr} (A/cm^2)	βa (V/dec)	$-\beta c$ (V/dec)	I.E.%
Blank	0.473	9.57×10^{-4}	0.080	0.110	
200	0.443	6.42×10^{-5}	0.050	0.110	93.29
400	0.461	5.60×10^{-5}	0.054	0.122	94.15
600	0.475	3.12×10^{-5}	0.056	0.104	96.74
800	0.444	2.10×10^{-5}	0.060	0.122	97.80
1000	0.423	1.31×10^{-5}	0.044	0.122	98.64

The potentiodynamic polarization curves presented in Fig. 4.4.4 and Fig. 4.4.5 for mild steel coupons as immersed and after immersion for 24 h show a significant reduction of cathodic current in presence of BAE. Curves reflect that both cathodic and anodic currents are decreased by the addition of BAE, but decrease in more in the cathodic branch Slopes of the curve are not much more affected by BAE, which

172

implies that inhibition is due to adsorption of organic molecules present in the extract to form a barrier film on metal surface which reduces active sites of corrosion. The synergistic effect of various organic compounds present in the BAE might have improved the extent of adsorption, which will be addressed further in a later section.

It can be observed from Table 4.39 that the corrosion current decreases with an increase in the concentration of inhibitor. Suppression is maximum (about 55 times) in 1000 ppm solution where inhibition efficiency is 98.18%. Data shows that even small concentration of inhibitor can suppress the I_{corr} by about 19 times where inhibition efficiency is approximately 95% for mild steel sample as immersed (Fouda et al., 2014; Muthukrishnan et al., 2014; Qiang et al., 2018). These values Show the excellent inhibition efficacy of BAE for inhibition of MS corrosion in acidic medium by adsorbing effectively on the metal surface. In case of *Berberis aristata* extract, inhibition efficiency for mild steel coupon as immersed and after immersion for 24 h are comparable. A comparison of inhibition efficiency is shown in Fig. 4.4.6.
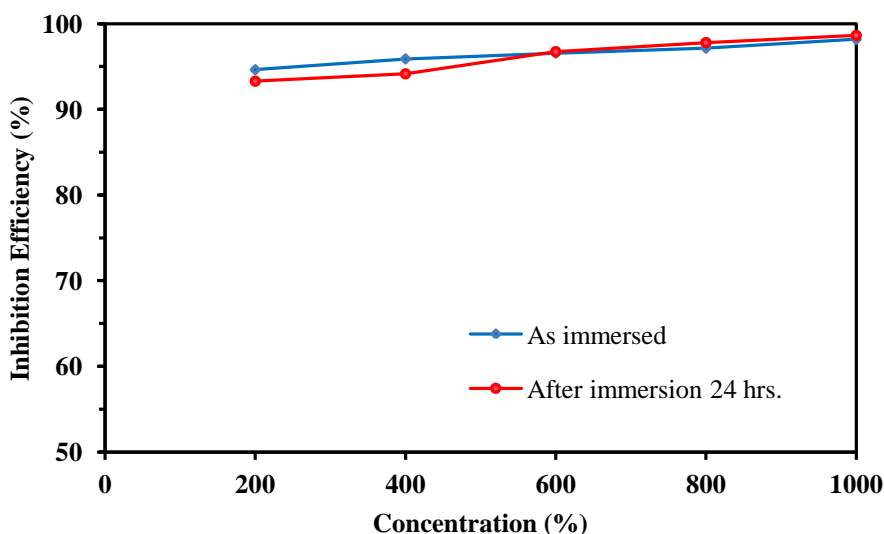
Figure 4.4. 6 : Comparison of inhibition efficiency of M-BAE for polarization of metal as immersed and immersed for 24 h in 1.0 M H$_2$SO$_4$ without and with inhibitor of various concentrations.

4.4.5 Electrochemical impedance spectroscopy

The corrosion behaviour of MS in the presence and absence of BAE was investigated by EIS measurement at OCP in a wide range of frequency. Impedance method was implemented to get information about the surface properties of the investigated system and kinetics of the electrode process. Nyquist, Bode modulus, and Bode phase plots

for MS electrodes immersed in 1M H_2SO_4 solution in the absence and presence of various concentrations of BAE are shown in Fig. 4.4.7a-c respectively. In the plots, curves with symbols represent the measured data, and solid lines represent the fitting data using Z-view (3.1c version) software.
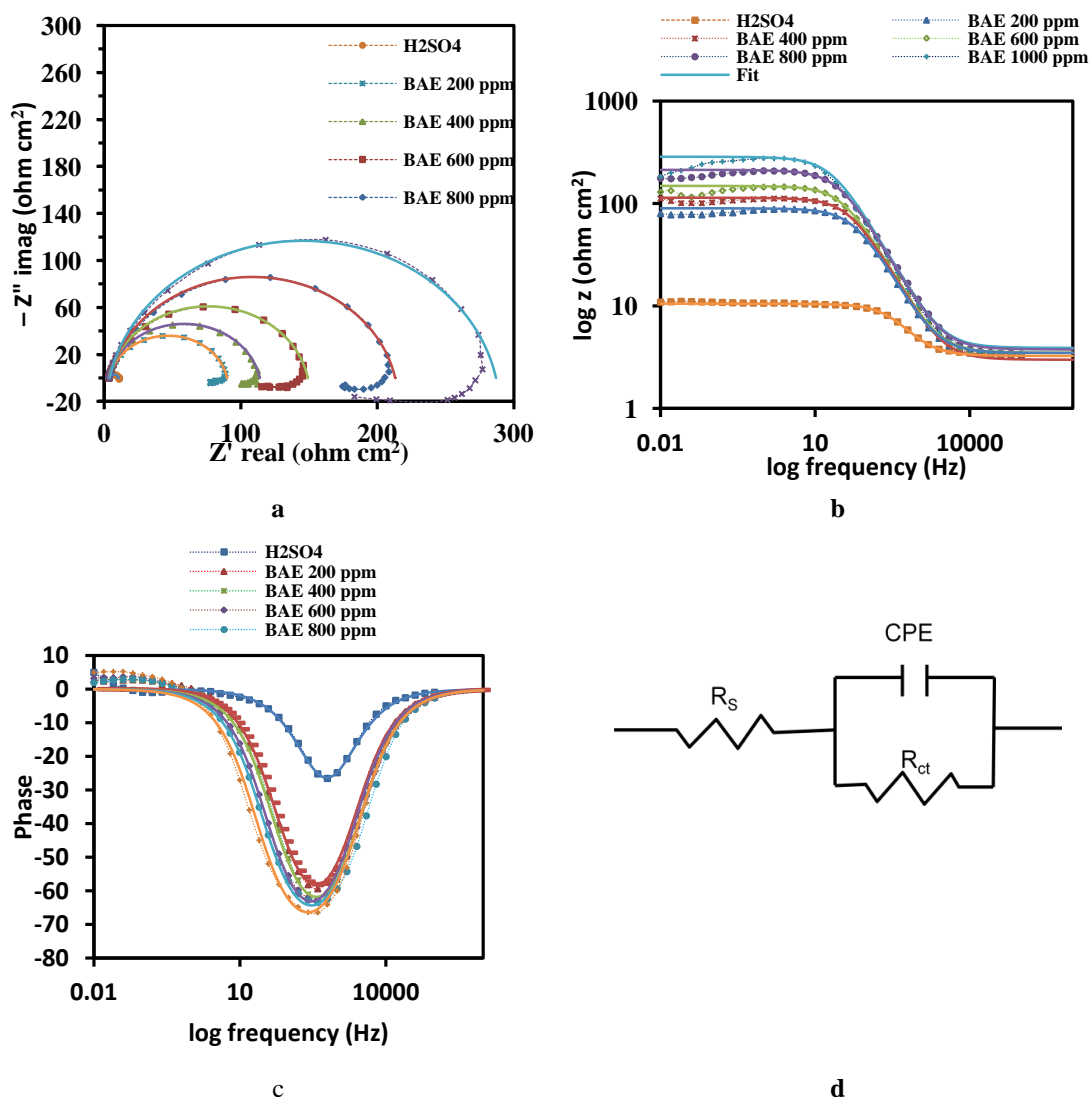
Figure 4.4. 7 : a. Nyquist plots, b. Bode modulus plots of log Z vs. frequency, c. Bode phase plots of phase angle vs. frequency for mild steel in 1.0 M H_2SO_4 with M-BAE of different concentrations and d. Equivalent circuit model used to fit the impedance spectra.

The shape of EIS plot is not changed with addition of inhibitor, which shows that the addition of inhibitor does not change the mechanism of corrosion. A single depressed capacitive loop is observed at high frequency in Nyquist plot which can be ascribed to the time constant of the electric double layer and charge transfer resistance. Such behaviour is typical of solid electrodes which often shows frequency dispersion and

ascribed to the roughness and other non-homogeneity of structural or interfacial origin, such as those found in adsorption processes (Verma & Quraishi, 2014). An inductive loop is appeared in Nyquist plot at low frequency region in presence of BAE and diameter of loop increases with increase in concentration of BAE. The inductive behaviour at low frequency can be attributed to the relaxation process obtained by adsorption of inhibitor on the electrode surface or to the re-dissolution of the passivated surface at low frequencies. It may be due to the effects of the layer stabilization by corrosion products on electrode surface such as [FeSO4^{-2}$_{(ads)}$], [FeOH], [FeH] involving inhibitor molecules.

The diameter of capacitive loops in Nyquist plot, which indicates charge transfer resistance, is increased with addition of inhibitor and it increases with increase in concentration. It indicates that corrosion is inhibited with addition of BAE and inhibition efficiency increases with increase in concentration of BAE. An increment in phase angle in the Bode-phase plot and an increment in the value of impedance at low frequencies in the Bode-modulus plot with the concentration of BAE also confirm the inhibitive behaviour of BAE increases with increase in concentration of BAE. Increase in inhibition efficiency with increase in concentration of inhibitor is presumably due to more coverage of the MS surface by inhibitor molecules.

Single phase peak observed in Bode-phase plot indicates that there is one time constant for the system under study, related to the electrical double layer. So, the equivalent circuit consisting of one-time constant depicted in Fig. 4.4.7d was employed to analyze the impedance spectra. The circuit consists of solution resistance (R_s), charge transfer resistance (R_{ct}) and constant phase element (CPE) instead of a pure capacitor represents the interfacial capacitance. The CPE is used in the circuit model to take into account the electrode surface non-homogeneity arising from surface roughness, adsorption of inhibitors, dislocations, grain boundaries, and the formation of a porous layer . (Ahamad et al., 2010; Bammou et al., 2014; Bedair et al., 2017; Bentiss et al., 2000b; Fernandes et al., 2019a; Hosseini et al., 2003a; Jüttner, 1990; Ma et al., 2017; Murmu et al., 2019; Qiang et al., 2018; Shahabi et al., 2015; Yüce & Kardaş, 2012).

The impedance of CPE is described by equation [4-16](Ashassi-Sorkhabi et al., 2008):

$$\mathbf{Z_{CPE}} = Y_0^{-1}(j\omega)^{-n} \qquad \text{[4-13]}$$

Where Y_0 is the magnitude of the CPE, j is the imaginary number ($j^2 = -1$), ω is angular frequency ($\omega = 2\pi f$), and n is the CPE exponent ($-1 \leq n \leq +1$), whose value is used to gauge the non-homogeneity or roughness of the surface (Jüttner, 1990). The CPE depicts a pure resistor when n=0, an inductor when n=-1, and a pure capacitor when n=+1 (Hosseini et al., 2003).

Electrochemical parameters obtained by fitting impedance data along with calculated IE is presented in table 4.41.

Table 4.41 : Impedance parameters for corrosion of MS in 1.0 M H_2SO_4 and 1.0 M H_2SO_4 with different concentrations of M-BAE.

Concentration (ppm)	Rs (Ωcm^2)	CPE $(\mu\Omega^{-1}S^ncm^{-2}$	n	R_{ct} (Ωcm^2)	I.E.%
Blank (0)	3.26	180.81	0.874	7.29	
200	3.48	63.60	0.882	86.40	91.56
400	3.00	59.28	0.882	110.80	93.42
600	3.50	56.81	0.887	145.50	94.99
800	3.75	49.24	0.876	209.30	96.52
1000	3.90	47.00	0.879	283.00	97.42

It can be observed from Table 4.41 that value CPE decreases decreases drastically with the addition of BAE, which is due to a decrease in local dielectric constant. The result can be ascribed to the increase in the thickness of the electric double layer, which is due to adsorption of large size inhibitor molecule on the metal surface with the gradual displacement of water molecule leading to the formation of protective film or complex from an acidic solution. The value of CPE decreases with an increase in the concentration of BAE, which implies that the adsorption increases with an increase in the concentration of BAE increasing the thickness of the electric double layer. Hence inhibition efficiency increases with an increase in the concentration of inhibitor.

Variation in IE and CPE with the variation of concentration of BAE is shown in Fig 4.4.8.
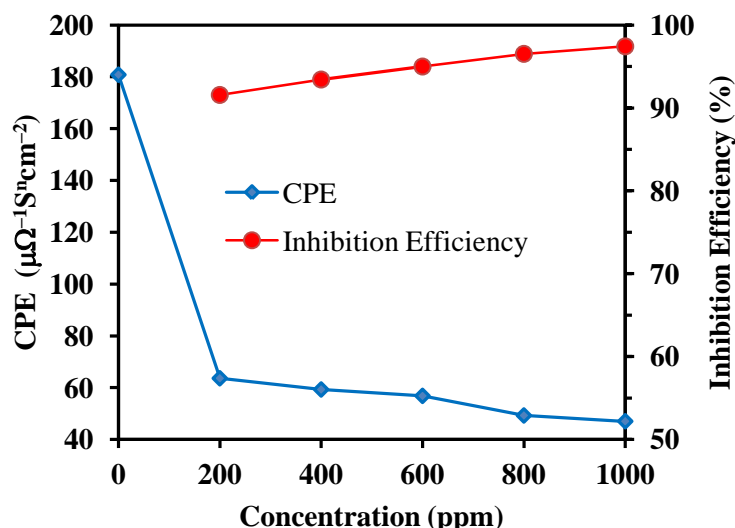
Figure 4.4. 8 : Variation of inhibition efficiency and constant phase element with the variation of concentration of M-BAE.

4.4.6 Differential pulse voltammetry and cyclic voltammetry analyses

Figure 4.4.9a shows the differential pulse voltammogram of corrosion media on a glassy carbon electrode in 0.1 M KCl as supporting electrolyte at pH 1.1 in the absence and presence of BAE. The results depicted for the voltammograms of corrosion medium after 20 h immersion of MS sample in 1.0M H_2SO_4 solution containing different amount of BAE.

a   b
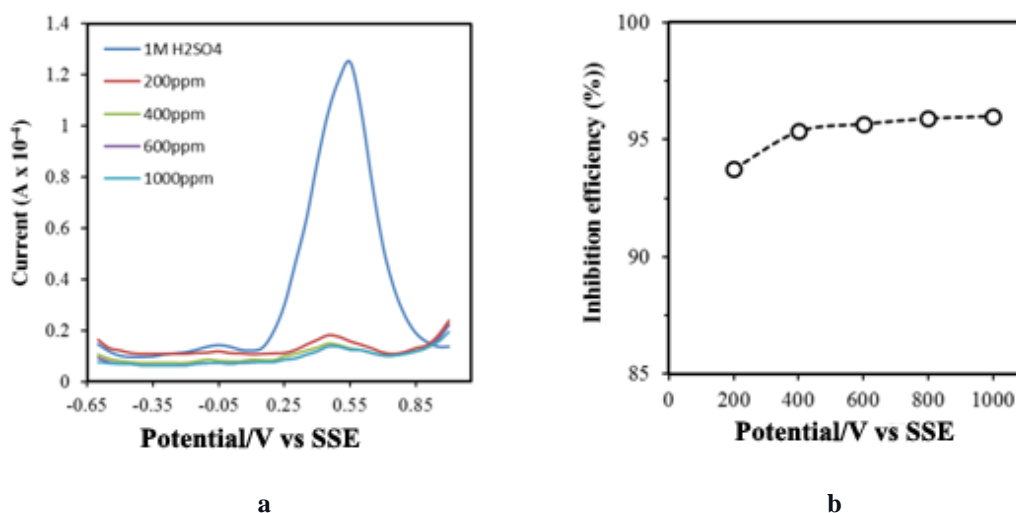
Figure 4.4. 9 : a. Differential pulse voltammogram of GCE in the presence and absence of M-BAE containing corrosion media and b. Corrosion inhibition efficiency of different amount of M-BAE on MS corrosion in acidic media.

The potential was scanned from cathodic limit of -0.6 V toward anodic direction and therefore oxidation voltammogram was recorded for Fe^{2+} to Fe^{3+} conversion. The

drastic suppression of peak current, I_p, is obvious by the addition of BAE showing the effectiveness of the plant extract in inhibiting the corrosion of MS in 1.0M H_2SO_4 solution as in the case of MNE. More importantly, this result like in the case of MNE again signifies the adaptation of DPV as a new technique in studying corrosion inhibition effectively. From the difference in the peak currents between the voltammograms of corrosion medium in the absence and presence of plant extracts, the inhibition efficiency was calculated at various concentration of BAE and is plotted in Fig. 4.4.9b. The inhibition efficiency above 96 % by 1000 ppm of BAE is indicative of the effectiveness of the DPV method for the corrosion inhibition study. The corrosion rate in terms of amount of current per unit area per hour estimated from the peak current is tabulated in Table 4.42 together with peak potential. A significant decrease in the corrosion rate in the presence of BAE is obvious. The peak current remains almost constant, which seems to be due to difficulty in analysis of the peak due to small current values. However, this needs to be further studied by employing MS as working electrode which can yield more information on such aspect.

Table 4.42 : Peak potential and corrosion rate (μA cm-2h-1) of MS in various concentrations of M-BAE obtained from Fig. 4.4.9 a.

Electrolyte	Peak Potential (V)	Corrosion rate (μA cm^{-2} h^{-1})
1.0M H_2SO_4	0.484	17.5
1.0M H_2SO_4 + 200 ppm M-BAE	0.480	1.09
1.0M H_2SO_4 + 400 ppm M-BAE	0.482	0.81
1.0M H_2SO_4 + 600 ppm M-BAE	0.488	0.76
1.0M H_2SO_4 + 800 ppm M=BAE	0.484	0.72
1.0M H_2SO_4 + 1000 ppm M-BAE	0.484	0.70

Fig. 4.4.10 shows the time variation of peak current and corresponding inhibition efficiency in 1000 ppm BAE solution. The result clearly shows the drastic lowering of peak current by the addition of plant extracts. After 15 min of immersion in 1000 ppm BAE solution the inhibition efficiency reached to above 93% and attained a maximum value of 98% after 20 h of immersion proving effectiveness of this method in corrosion inhibition study.
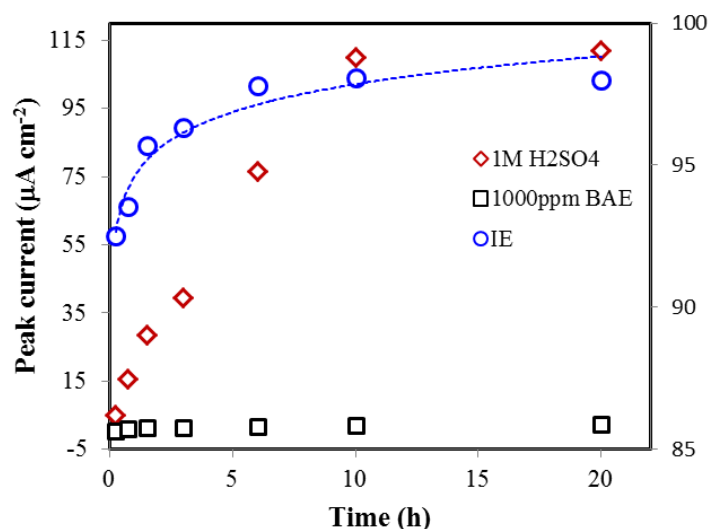
Figure 4.4. 10 : Peak current and corresponding corrosion inhibition efficiency in the presence of 1000 ppm M-BAE.

Figure 4.4.11 shows cyclic voltammograms of GCE electrode in corrosion medium (0.1M H_2SO_4) in the absence and presence of 200 ppm plant extract (BAE) after 20 h immersion. The peak currents are drastically supressed by the addition of plant extract giving an inhibition efficiency of 96% in in 200 ppm BAE. The results in terms of peak currents and peak potentails are shown in Table 4.43. The BAE produced better inhibition efficiency comapred to MNE. However, like in the case of MNE, a significant change in the cathodic peak potential to negative values with the increase in the amount of BAE is attributed to adsorption of Fe^{3+} on GCE.
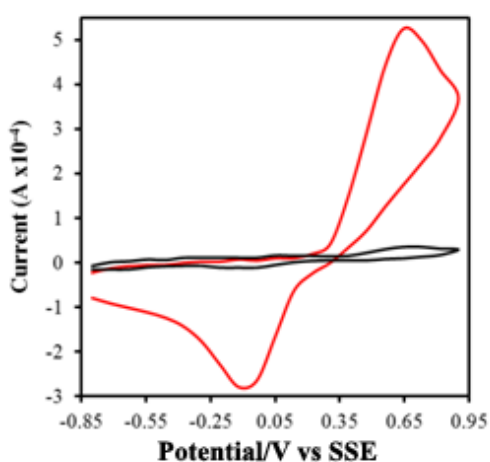
Figure 4.4. 11 : Cyclic voltammograms of GCE in corrosion medium containing M-BAE and dissolved iron from MS.

Table 4.43 : The values of peak potentials and peak currents from CV of GCE in corrosion media containing different amount of M-BAE as inhibitor.

Electrolyte	Epa (V)	Ipa (μA)	Epc (V)	Ipc (μA)	IE (%)
1.0M H_2SO_4	0.630	484	-0.070	216	
1.0M H_2SO_4 + 200 ppm M-BAE	0.657	20	-0.120	6.44	95.9
1.0M H_2SO_4 + 400 ppm M-BAE	0.623	13	-0.179	4.80	97.3
1.0M H_2SO_4 + 600 ppm M-BAE	0.644	12	-0.216	5.16	97.5
1.0M H_2SO_4 + 800 ppm M-BAE	0.623	12	-0.254	4.60	97.5
1.0M H_2SO_4 + 1000 ppm M-BAE	0.593	10.9	-0.240	4.17	97.7

4.4.7 Determination of inhibition efficiency by weight loss (Gravimetric) method

Gravimetry is one of the simplest and extensively used methods for corrosion study. It can be applied to evaluate the effect of long time exposure of MS coupons up to 24 h in comparison to short time exposure in electrochemical methods. Gravimetric measurements studied inhibitive behavior of BAE by varying time, concentration, and temperature, which are discussed as follows:

4.4.7.1 Effect of immersion time

a   b
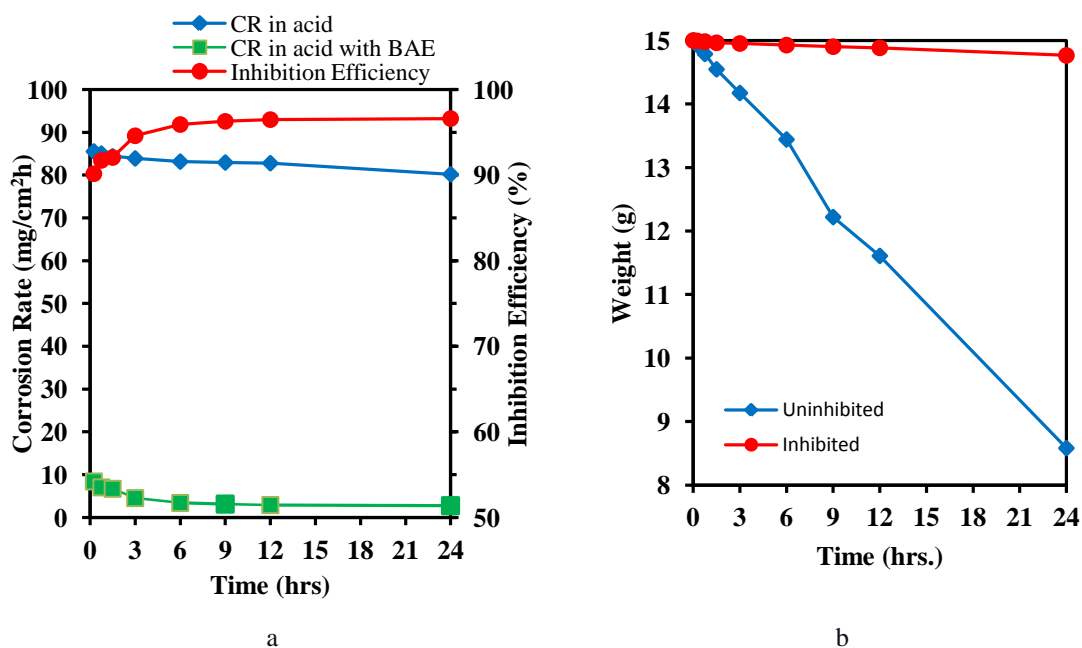
Figure 4.4. 12 : a. Variation in corrosion rate in presence and absence of inhibitor and variation in inhibition efficiency with different immersion time and b. Variation in weight of mild steel in the presence and absence of inhibitor.

Gravimetric measurements were used to investigate the inhibitory behavior of BAE by immersing MS coupons in 1000 ppm solution for various time periods (0.25 h, 0.75 h, 1.5 h, 3 h, 6 h, 9 h, 12 h, and 24 h) at 298 K.Corrosion rate and inhibition efficiency calculated from the obtained results are presented in Fig. 4.4.12(a) and Table 4.44. Data implies that corrosion is inhibited with the addition of BAE as an inhibitor, and inhibition increases with an increase in time and reaches up to 96.62% in immersion for 24 hrs. Data suggests that it is an effective inhibitor that is adsorbed quickly and whose inhibition efficiency is above 90% only after 15 minutes. Such a fast inhibition of corrosion is important for practical applications of the inhibitor (Yadav et al., 2004). Fig. 4.4.12(b) depicts the weight of mild steel coupons over time when immersed in acid with and without inhibitor.This data reveals that loss of metal in acidic media is retarded by using an inhibitor.

Table 4.44 : Corrosion rate of mild steel in the presence and absence of M-BAE and inhibition efficiency of M-BAE at various time of immersion.

Solution	Time (h)	Surface area (cm^2)	Weight Loss (mg.)	Rate (mg/cm^{2}hr)	Inhibition efficiency (%)
Acid	0.25	21.73	41.70	85.55	90.17
Inhibitor		21.73	4.10	8.41	
Acid	0.75	22.40	128.20	85.05	91.73
Inhibitor		22.40	10.60	7.03	
Acid	1.5	21.08	239.50	84.42	92.07
Inhibitor		21.08	19.00	6.70	
Acid	3	23.96	541.13	83.91	94.60
Inhibitor		22.76	27.73	4.53	
Acid	6	24.94	1116.87	83.18	95.92
Inhibitor		22.42	40.93	3.39	
Acid	9	22.24	1489.67	82.96	96.29
Inhibitor		23.23	57.70	3.06	
Acid	12	23.19	2067.03	82.80	96.50
Inhibitor		23.52	73.50	2.90	
Acid	24	23.82	4113.70	80.21	96.62
Inhibitor		22.31	130.30	2.71	

4.4.7.2 Effect of temperature:

Gravimetric analysis at various temperatures (298 K, 308 K, 318 K, 328 K, 338 K) were carried out for 6 h in 1000 ppm BAE solution to study activation parameters as as the stability of protective film formed due to adsorption of inhibitor on the metal

surface. Corrosion rate and inhibition efficiency computed from the results shown in Table 4.45 and represented in Fig. 4.4.13 (a). The IE remains almost same until 308 K, then declines marginally and remaims constant at 80% at 338 K. This is a promising outcome for plant extracts as corrosion inhibitors, because in most of the other studies, the IE has been observed to fall below 40% at higher temperatures (Choudhary et al., 2015; El-Etre, 2007; Ostovari et al., 2009). Owing to higher IE at higher temperatures, BAE can be useful for a variety of purposes, such as in the removal of corrosion products for weight loss determination. (Yadav et al., 2004). Similarly, by carrying out the procedure at a higher temperature, it can be applied in industries to accelerate the removal of scales and oxide layer for the surface finishing of metal. Temperature stability of BAE is even better than berberine isolated from *Coptis chinesis* (Yan Li et al., 2005; Na et al., 2019). The decrease in IE of plant extract at higher temperatures is attributed to the decomposition or desorption of organic compounds present in it (Bentiss et al., 2009). But, the significant IE of BAE at higher temperatures indicates the higher temperature stability of its components. Therefore, individual components of BAE should be isolated and further studied.

Table 4.45 : Corrosion rate of mild steel in the presence and absence of M-BAE and inhibition efficiency of M-BAE at various temperatures.

Solution	Temperature (K)	Surface area (Cm^2)	Weight Loss (mg.)	Corrosion Rate (mg/cm^2hr)	Inhibition efficiency (%)
Acid	298	22.74	916.60	74.87	95.13
Inhibitor		22.97	45.13	3.65	
Acid	308	23.61	1642.47	129.21	95.92
Inhibitor		23.61	67.00	5.27	
Acid	318	25.77	2774.13	199.99	88.12
Inhibitor		24.93	318.80	23.75	
Acid	328	25.18	3711.67	273.77	81.39
Inhibitor		25.04	686.67	50.94	
Acid	338	21.92	4561.73	386.51	80.53
Inhibitor		23.69	959.90	75.27	
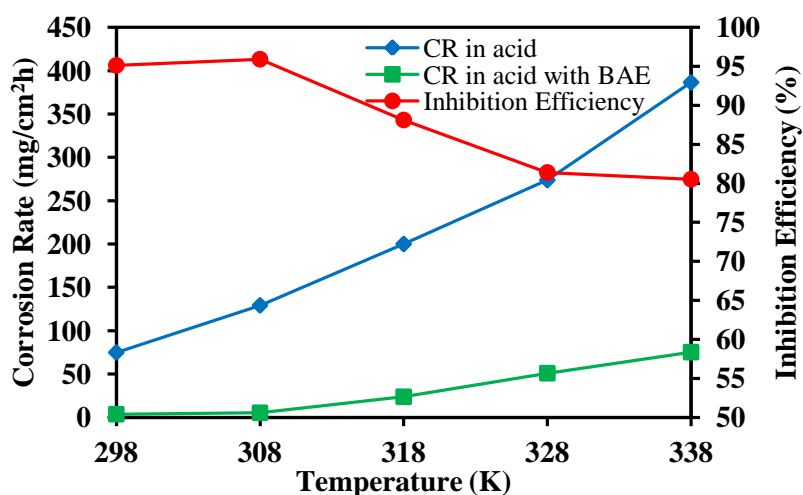
Figure 4.4. 13 : Variation of corrosion rate and inhibition efficiency with variation of temperature.

4.4.7.3 Effect of concentration:

Table 4.46 : Corrosion rate of mild steel in the presence and absence of M-BAE and inhibition efficiency of M-BAE at various concentrations.

Concentration	Surface area (cm^2)	Weight Loss (mg.)	Corrosion Rate (mg/cm^{2}hr)	Inhibition efficiency (%)	Surface coverage (θ)
0 ppm. (acid solution only)	22.74	916.60	74.87		
200 ppm.	22.99	89.70	7.25	90.32	0.9032
400 ppm.	21.84	57.10	4.86	93.51	0.9351
600 ppm.	22.66	50.03	4.10	94.52	0.9452
800 ppm.	22.47	45.17	3.73	95.01	0.9501
1000 ppm.	22.97	37.77	3.05	95.92	0.9592

Corrosion rate and inhibition efficiency by BAE at various concentrations (200 ppm, 400 ppm, 600 ppm, 800 ppm, and 1000 ppm) at 298 K for 6 hours are computed from weight loss data is shown in Table 4.46 and represented in Fig. 4.4.14. Results reveal that BAE is an effective corrosion inhibitor that inhibits corrosion rate by 90.32% even at 200 ppm concentration, and IE increases with an increase in concentration, which reaches up to 96% at 1000 ppm. It shows fast adsorption on BAE, which is not reported in various other plant extracts (Fouda et al., 2014; Muthukrishnan et al., 2014; Qiang et al., 2018). The increased surface covering of mild steel, as well as the increased adsorption of phytochemical substances on it, can be attributed to an

183

increase in IE with concentration. Electrochemical studies, such as potentiodynamic polarization, EIS, and DPV, have all produced similar results. Fig. 4.4.14(b) shows a comparison of inhibitory efficiency acquired using various approaches.

a

b
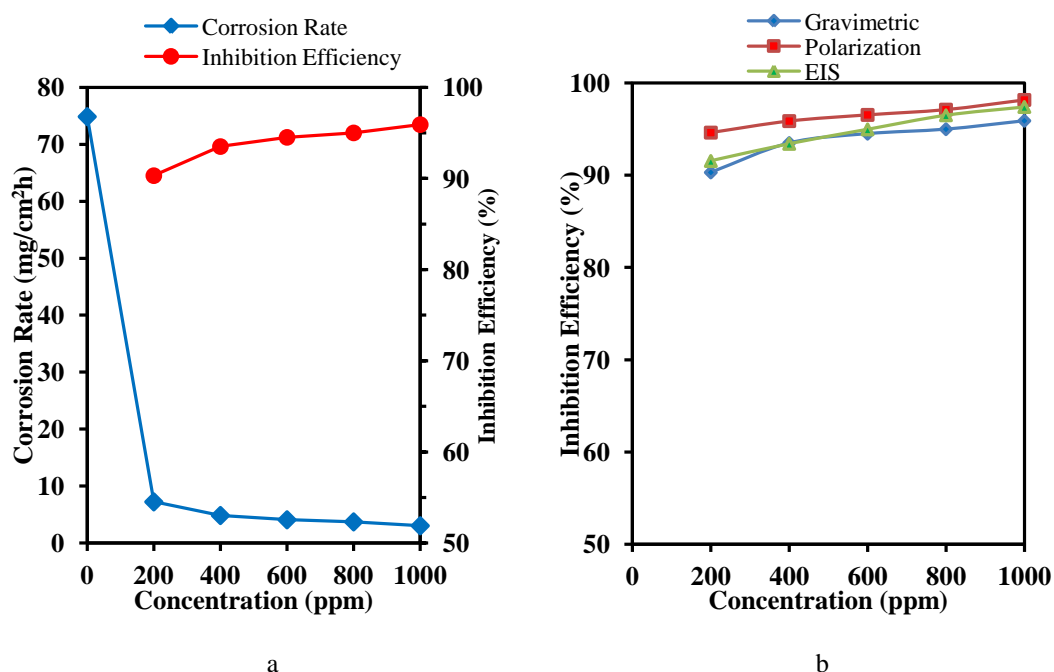
Figure 4.4. 14   : a. Variation in corrosion rate and inhibition efficiency with the variation of concentration of M-BAE and b. Inhibition efficiency of M-BAE from different methods for MS in 1.0 M H_2SO_4.

4.4.8 Adsorption isotherm:

Adsorption isotherm of inhibitor on MS is more informative in understanding the mechanism of corrosion inhibition. Basic information on mode and interaction degree between an inhibitor and MS surface have been investigated with the aid of adsorption isotherm. The interaction energy between the inhibitor and a MS surface is higher than that between water molecules and MS surface, which makes adsorption of inhibitor molecules feasible. The molecular structures of molecules in chemical composition, temperature, and the electrochemical potential at the metal/solution interface all influence adsorption of inhibitor. The adsorption process of BAE is considered as a quasi-substitution process because water molecules, which were adsorbed at the electrode surface [H_2O(ads)] in aqueous phase is displaced by inhibitor molecules [org(sol)] in the process (Cang et al., 2013; Verma & Quraishi, 2007).

184

Org (sol) + nH$_2$O (ads) $\longrightarrow$ Org(ads) + nH$_2$O (sol)
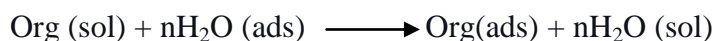
Where, n is the number of water molecules displaced by one inhibitor molecule.

Several adsorption isotherms like Langmuir, El-Awady, Flory-Huggins, Tempkin, Freundlich were tested by plotting the degree of surface coverage (θ) against inhibitor concentration. In this study, the inhibitor used is a crude plant extract, which is a mixture of several organic compounds. All these compounds might affect the inhibitive action of an inhibitor either positively or negatively. However, the concentration used to fit suitable adsorption models is the average molar concentration of a few important compounds shown in Fig. 3.6, which play a vital role in inhibition (El-Etre, 2008). Among all the adsorption isotherms, the Langmir adsorption isotherm was obtained as the best fit isotherm in which a straight was obtained when C_{inh} was plotted against C_{inh}/θ, where the value of the linear correlation coefficient (R^2) was 1 and the value of the slope was almost equal to 1 as shown in Fig. 4.4.15. Some interactions between adsorbed molecules on the MS surface, such as mutual attraction or repulsion between different functional groups of molecules or preferential adsorption of molecules at the cathodic and anodic sites, can be attributed to the small deviation of slope from unity (Odewunmi et al., 2015; Verma & Quraishi, 2014). As the best fit adsorption isotherm is the Langmuir adsorption isotherm, it can be concluded that the adsorption is monolayer without interaction of adsorbed molecules.
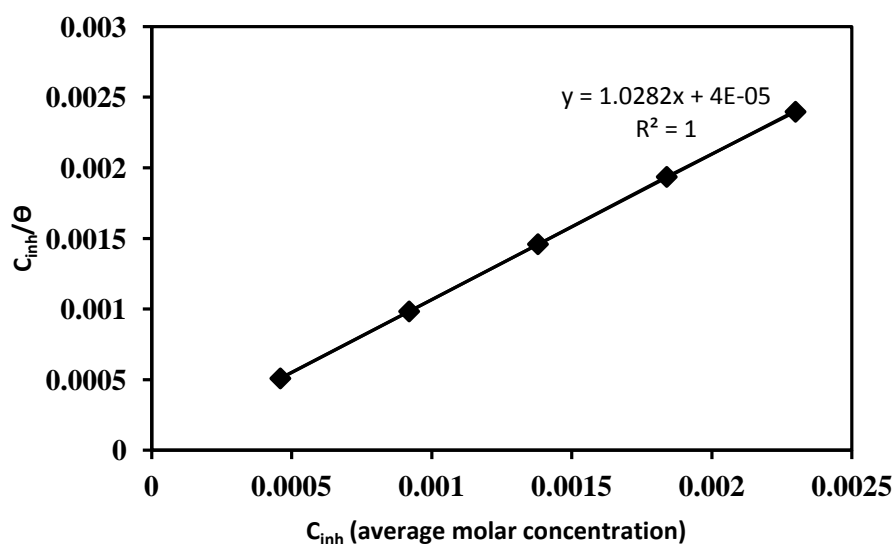
Figure 4.4. 15 : Langmuir adsorption isotherm plot for mild steel in 1.0 M H$_2$SO$_4$ with different concentrations of M-BAE as the average molar concentration of some major compounds in M-BAE.

Langmuir adsorption isotherm is given in equation [4-17] (Ostovari et al., 2009),

$$\frac{C_{inh}}{\theta} = \frac{1}{K_{ads}} + C_{inh}$$ [4-14]

The slope of the Langmuir adsorption isotherm plot in Fig. 4.4.15 can be used to compute the value of adsorption constant (K_{ads}), which can then be used to calculate the value of free energy of adsorption (ΔG^o) using equation [4-18] (Cang et al., 2013).

$$\Delta G^o = - \text{RT} \ln(55.5 K_{ads})$$ [4-15]

Where, R refers to the universal gas constant (8.314J/mol K), and 55.5 refers to the concentration of water in solution in mol/L. The value of free energy of adsorption is calculated as -35.05 kJ/mol, which is in between -20 kJ/mol and -40 kJ/mol and higher than intermediate. So, it can be concluded that adsorption is not merely physical or chemical but involves both with domination of chemisorption. The adsorption process begins with physical adsorption followed by chemisorption (Bentiss et al., 2007; Cang et al., 2013). Large negative value of ΔG_{ads}^o can be attributed to spontaneous adsorption of inhibitor on metal surface with the formation of highly stable adsorbed layer (Bentiss et al., 2007; Cang et al., 2013).

4.4.9 Calculation of activation energy and thermodynamic parameters :

Arrhenius equation [4-19] gives the temperature dependency of corrosion rate, which can be applied to calculate activation energy (Ostovari et al., 2009):

$$\textbf{log (CR)} = \textbf{log A} - \frac{\textbf{E}_\textbf{a}}{\textbf{2.303RT}}$$ [4-16]

Where E_a refers to the activation energy, A refers to the Arrhenius pre-exponential constant, T refers to the absolute temperature. E_a is the slope of Arrhenius plot obtained by plotting log CR against 1/2.3.3RT shown in Fig. 4.4.16(a). The value of E_a for acid and inhibited acid is tabulated in Table 4.47, which shows a significant increase in the value when BAE is added. It can be attributed to the strong adsorption of inhibitor molecules on the mild steel surface (Hamdy & El-Gendy, 2013). The E_a value of several plant extracts has been reported in the literature to be in the range of 40 kJ/mol. (Bammou et al., 2014; Cang et al., 2013; Desai, 2015; El-Etre, 2008; Hamdy & El-Gendy, 2013). Therefore, it is reasonable to predict that the higher thermal stablility of BAE observed in gravimetric temperature effect is attributable to its higher activation energy. However, as mentioned earlier, the reason for its higher

thermal stablility can be studied further by isolating various compounds from it and following their individual studies.
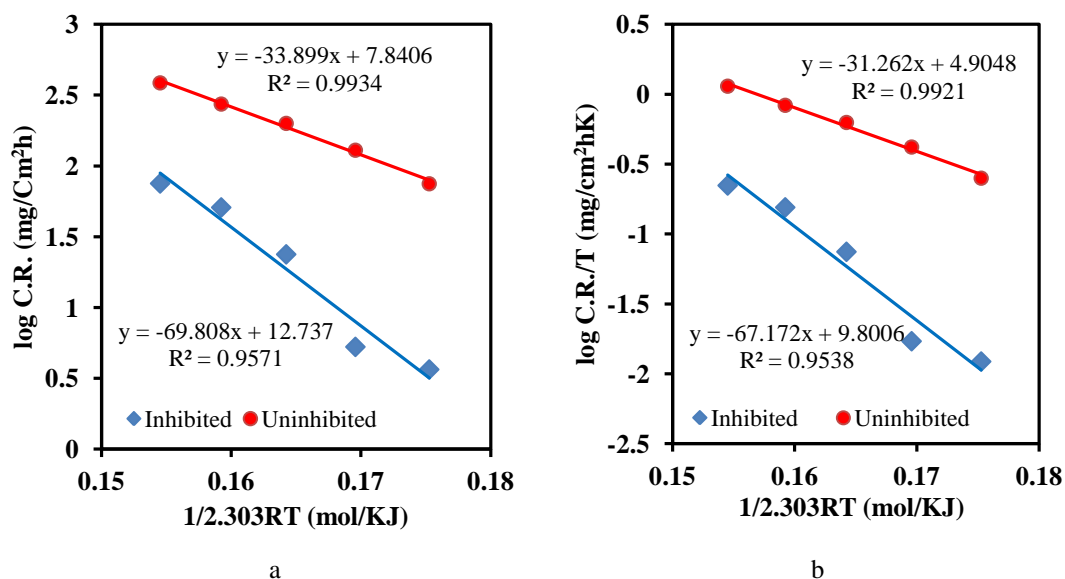
Figure 4.4. 16 : a. Arrhenius plot for mild steel in 1.0 M H_2SO_4 with and without M-BAE and b. Transition state plot for mild steel in 1.0 M H_2SO_4 with and without M-BAE

The transition state equation [4-20] can be applied to find the change in entropy and enthalpy of the adsorption (Ostovari et al., 2009). When log (CR/T) is plotted against 1/2.303, the slope of the plot is enthalpy and the intercept can be used to compute entroypy.

$$\log\left(\frac{CR}{T}\right)=\left[\log\left(\frac{R}{hN}\right)+\left(\frac{\Delta S^*}{2.303R}\right)-\frac{\Delta H^*}{2.303\,RT}\right] \qquad [4\text{-}17]$$

Where h stands for plank's constant, 6.6261×10^{-34} Js and N stands for the Avogadro's number, 6.0225×10^{23} mol^{-1}

The calculated values of ΔH^* and ΔS^* for acid and inhibited acid are illustrated in Table 4.47. An intermediate value of ΔH^* (67.17 kJ/mol) again supports the mixed type of adsorption involving both physical and chemical adsorption (Khadom et al., 2018). Furthermore, the positive and higher values of ΔH^* indicate that the corrosion is controlled by the kinetic factors. The value of Ea is higher than that of ΔH^*, which shows the reduction in total reaction volume. It is due to the involvement of gaseous reactions, namely hydrogen evolution reactions (Ostovari et al., 2009). E_a is greater

than ΔH^* by 2.64, which isnearly equal to RT, implying that the corrosion process is unimolecular.

The addition of BAE in acid shifts the value of ΔS^* towards positive, indicating an increase in system disorder as the system transitions from reactant to activated complex. This behavior can be ascribed to the displacement of water molecules by inhibitor molecules during adsorption. (Hamdy & El-Gendy, 2013). Such type of significant increase in the value of ΔS^* is unusual to observe as the increment is smaller in most of the plant extracts (Kairi & Kassim, 2013; Singh et al., 2010; Ulaeto et al., 2012; Umoren et al., 2014). It should be further investigated to understand the better thermal stability of BAE so that such types of inhibitor can be developed or isolated in the future.

Table 4.47 : Activation parameters of the dissolution of mild steel in 1.0 M H_2SO_4 in the presence of 1000 ppm concentration.

Electrolyte	Ea(kJ/mol)	A (mg/cm^2)	ΔH(kJ/mol)	Ea-ΔH	ΔS(J/molK)
1.0 M H_2SO_4	33.9	6.93×10^7	31.26	2.64	-103.66
Acid with inhibitor (1000 ppm)	69.81	5.46×10^{12}	67.17	2.64	-9.93

4.4.10 Surface analysis

Energy dispersive X-ray (EDX) was carried out to estimate the percentage of heteroelements present on the surface of the MS coupon in the absence and presence of inhibitor when the coupons were retrieved after 24 h of immersion in the test solution. EDX spectra and SEM micrograph of the surface of MS coupons immersed in acid in the absence and presence of inhibitor solutions of 400 ppm and 1000 ppm are shown in Fig 4.4.17 and the percentage of different elements present on the surface is presented in supplementary Table 4.48. The figure and data show the increase in the amount of nitrogen on the surface, which supports the formation of a protective film on the surface due to the adsorption of organic compounds on the surface. It can be seen from the SEM image that severe damage with deep furrows and large cracks is seen on the surface of MS coupons immersed in acid in the absence of inhibitor. On the surface immersed in acid with inhibitor, these cracks and furrows are relatively rare, and a relatively smooth surface with protective film can be seen.This

observation can be attributed to the adsorption of inhibitor molecules on the MS surface.
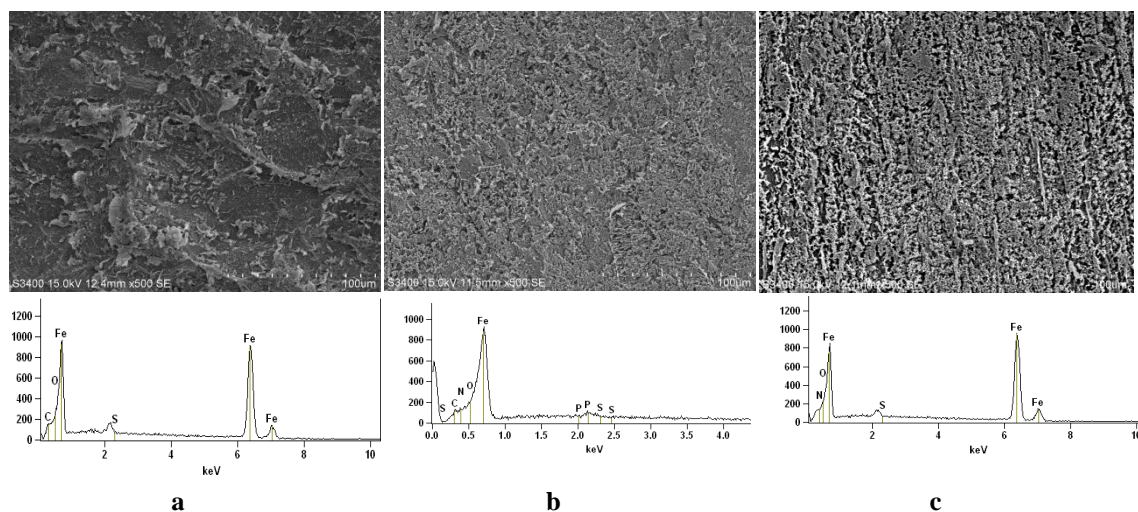
Figure 4.4. 17 : SEM images and corresponding EDX spectra of mild steel coupons after 24 h immersion in (a) 1.0 M H_2SO_4, (b) 400 ppm extract solution in 1.0 M H_2SO_4 and (c) 1000 ppm extract solution in 1.0 M H_2SO_4.

Table 4.48 : Weight difference of different elements on the MS surface after immersion the sample in different solutions.

Surface dipped in	Iron	Carbon	Nitrogen	Oxygen
Acid without inhibitor	89.94%	7.39%		2.76%
Acid with inhibitor of 400 ppm	94.41%		2.73%	2.86%
Acid with inhibitor of 1000 ppm	95.06%		1.75%	3.19%

4.4.11 Mechanism of inhibition

It is well recognized that organic inhibitors inhibit corrosion due to the adsorption of the molecules on the metal/solution interface. The charge on the metal surface, chemical structure, dipole moment of inhibitor molecules, and the role of additional ions that are adsorbed on the metal surface are the factors that govern the adsorption of the molecules. The large-sized aromatic organic molecules with heteroatoms present in BAE can be adsorbed on the metal surface. Thermodynamic parameters such as free energy of adsorption (-35.05 KJ/mol) and energy of activation (69.81 KJ/mol) studied in this study indicate that the adsorption of inhibitors on the metal surface is comprehensive adsorption involving both physisorption followed by

189

chemisorption, but predominantly chemical adsorption. So, the mechanism of inhibition by BAE can be assumed to be as follows.

BAE contains organic molecules such as berberine and jatrorhizine, which have quaternary nitrogen with a positive charge. Protonation of amino nitrogen, phenolic or etheral oxygen in an acidic solution makes inhibitor molecules positively charged. The observed value of the OCP of MS in BAE (-0.44V) is greater than the potential of zero charge (PZC) of MS in sulfate solution (Sivakumar et al., 2018), which suggests the positive value of Antropov's rational corrosion, indicating the net positive charge on the metal surface. In such conditions, positively charged inhibitor molecules cannot be adsorbed due to electrostatic repulsion. However, adsorption is made feasible by synergism between inhibitor molecules and sulfate ions derived from sulfuric acid due to a small degree of hydration. Negatively charged sulfate ions are first adsorbed onto a positively charged metal surface. As a result, there will be excessive negative charge near the interface, which will cause inhibitor molecules to be adsorbed. This adsorption of BAE molecules suppresses the adsorption of H^+ ions on the cathodic site of mild steel, resulting in the inhibition of cathodic hydrogen evolution.

Physisorption is then followed by chemisorption with the displacement of water molecules from the metal surface by inhibitor molecules. Chemisorption is the donor acceptor interaction between vacant d-orbital of metal and HOMO (orbital with a larger electron density like a non bonded pair of electrons or π-orbital) of inhibitor molecules. This interaction is strong according to the HSAB theory, where large sized inhibitor molecules behave as soft bases and metal atoms act as soft acids, resulting in a strong interaction between soft acid and soft base (Sadeghi et al., 2019). Extra negative charges accumulate on the metal surface as a result of this interaction, which is relived by retrodonation. Retrodonation is the formation of feedback bonds as a result of the transference of electron density from 4s or 3d orbitals of the metal atom to the LUMO (orbitals with a larger electron density, such as a vacant antibonding π^* orbital) of inhibitor molecules. Figure 4.4.18 shows a schematic illustration of the adsorption of two molecules, berberine and berberamine.

Figure content labels:

Protonated berberine

Interaction with pπ electrons — — — Interaction with non bonding electrons

a. - - - - - Electrostatic interaction

Protonated Berberamine

Interaction with pπ electrons — — — Interaction with non bonding electrons

b. - - - - - Electrostatic interaction
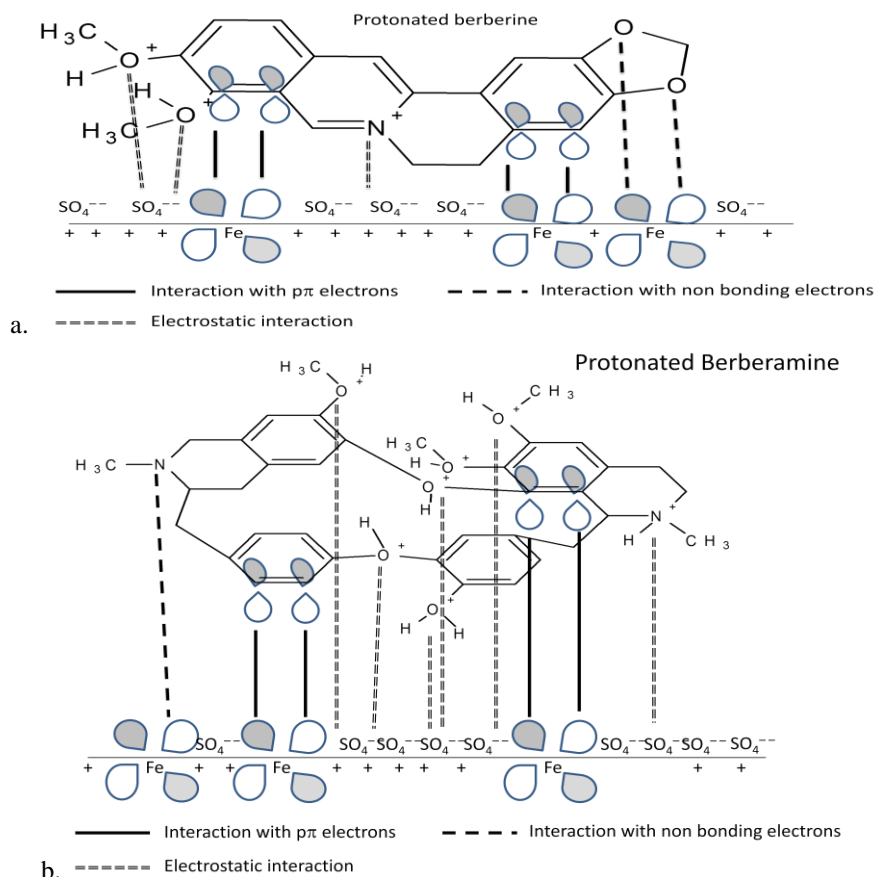
Figure 4.4. 18 : The Schematic illustration of different modes of adsorption of (a) Berberine and (b) Berberamine molecule on mild steel/ 1.0 M H_2SO_4 interface.

Furthermore, chelation of Fe^{+2} with the organic molecules to form a stable and insoluble complex also explains the corrosion inhibition by BAE. The solubility of the protective layer reduces once a number of these chelate complex molecules form, which reduces anodic metal dissolution and so prevents corrosion. It explains why the IE increases as concentration and time increase. Figure 4.4.19 depicts the possible chelate complexes of two organic molecules.

The anodic reaction is inhibited by chelation in the following way:
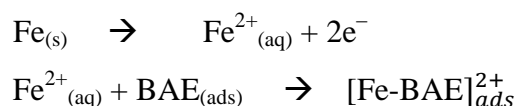
$$Fe_{(s)} \quad \rightarrow \quad Fe^{2+}_{(aq)} + 2e^-$$
$$Fe^{2+}_{(aq)} + BAE_{(ads)} \quad \rightarrow \quad [Fe\text{-}BAE]^{2+}_{ads}$$

Both anodic and cathodic reactions are suppressed by the adsorption of inhibitor molecules. The adsorption of sulfate ions inhibits anodic dissolution, as depicted below (Karthik et al., 2014):

$$H_2SO_4 \quad \rightarrow \quad H^+ + SO_4^{--}$$
$$Fe + SO_4^{--} \quad \rightarrow \quad (FeSO_4^{--})_{ads}$$

$$(FeSO_4^{--})_{ads} \quad \rightarrow \quad (FeSO_4^{-})_{ads} + e^{-}$$

$$(FeSO_4^{-})_{ads} \quad \rightarrow \quad (FeSO_4)_{ads} + e^{-}$$

$$(FeSO_4)_{ads} \quad \rightarrow \quad Fe^{++} + SO_4^{--}$$
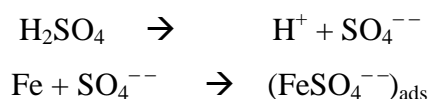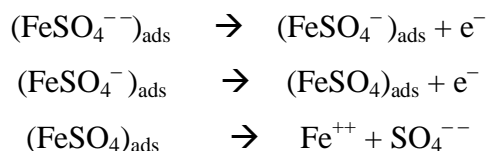
Adsporption of BAE inhibits the cathodic hydrogen as follows :

$$BAE + H^{+} \quad \rightarrow \quad (BAE)H^{+} \text{ (protonation of inhibitor molecules)}$$

$$Fe + (BAE)H^{+} \quad \rightarrow \quad [Fe\text{-}(BAE)H^{+}]_{ads} \text{ (adsorption of protonated BAE molecules)}$$

$$[Fe\text{-}(BAE)H^{+}]_{ads} + e^{-} \quad \rightarrow \quad [Fe\text{-}(BAE)H]_{ads} \quad \text{(Reduction of protonated } H^{+})$$

$$[Fe\text{-}(BAE)H]_{ads} + H^{+} + e^{-} \quad \rightarrow \quad Fe + H_2 + BAE \quad \text{(Release of hydrogen)}$$
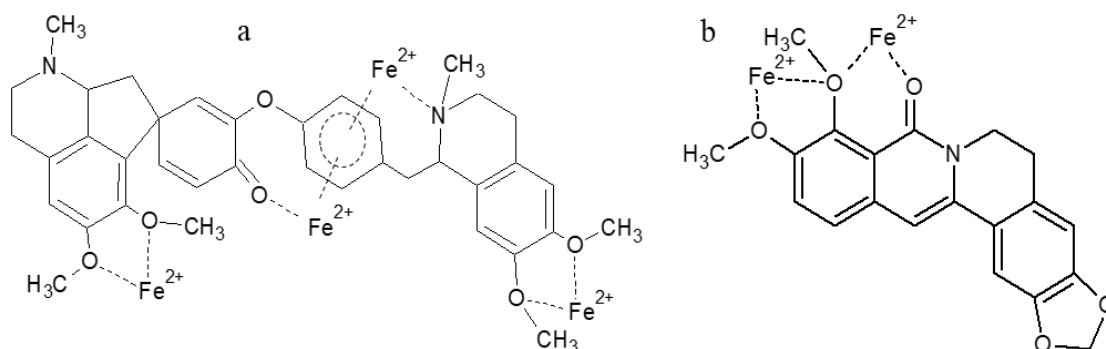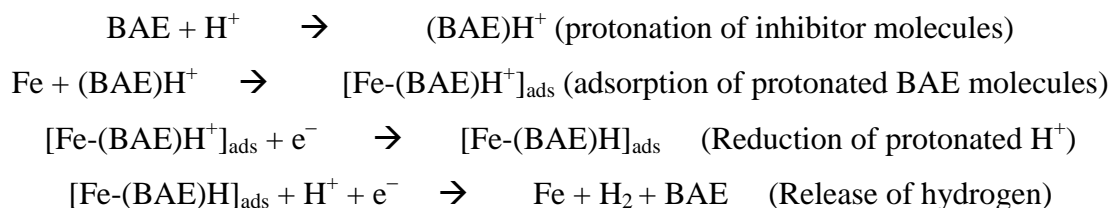
Figure 4.4. 19: Metal inhibitor chelate complex formed by iron with (a) Pakistanamine and (b) Oxyberbeine

Part of this work is published in Analytical and Bioanalytical electrochemistry, volume 12, 970-988 (2020)(Karki et al., 2020).

The results of four plants are summarized as follows :

In n-hexane extract, adsorption of extract seems slow, because IE at less time is less and after 24 hours, it shows significant inhibition. The difference in the inhibition properties of non-polar and polar solvent can be explained on the basis of solubility properties of polar inhibitor molecules. When a polar solute molecule interacts with a polar solvent, the attraction between the solute and solvent molecules is generally greater than the solute-solute attraction or the solvent-solvent attraction. So, polar compound can usually dissolve in polar solvents. (Even if the attractive forces are about the same, the increase in entropy that results from the substances mixing generally drives the process in forward direction).

When extraction is carried out using non-polar solvent like hexane, the molecules such as alkaloids having long lipophilic tail with polar head are obtained. It is because lipophilic tail interacts with non-polar solvent forming micelles structure with lipophobic head at its interior. So, when such extracted compound is added to a polar solvent, such as H_2SO_4, the polar lipophobic head at its interior in the non-polar hexane must reorient out of the micelle structure of the extract to interact with polar solvent molecules. So, the intermixing of hexane extract with polar solvent occurs slowly with the inversion of micelles and overcoming of van der walls force of attraction between the molecules. Thus, the micelles like structure of the extract having lipophobic tail in contact with polar solvent will be formed.

Hence, hexane extract takes a time to adsorb over metal surface passing through positively charge metal-solvent interface. As a result the adsorption of non-polar inhibitor compound takes slowly and surface coverage of metal proceeds with time. This gives higher inhibition efficiency with progress of time.

Due to slower adsoprtion and less yield of n-hexane extract, methanolic extract of plants were selected for further study. Results from potentiodynic polarization shows that MNE and BAE containing berberine and other alkaloids are found more effective corrosion inhibitor than AVE and EHE. Shift of Ecor is less than 85 mV in all extract which reveals that all extracts are found mixed inhibitor. Result of EIS also shows that BAE and MNE are more effective inhibitor.

Decrease in weight in weight loss experiment, decrease in current density in potentiodynamic polarization and increase in charge transfer resistance with increase in concentration show that inhibition efficiency increases with increase in concentration.

IE increases with increase in time in BAE and MNE, where IE is high in short time as well, but in case in AVE and MNE, IE is low at longer time, and, in potentidynamic polarization, it seems that IE increases with increase in time in all extracts, which can be explained on the basis of chelation of dissolved metal ion with inhibitor molecules. In the polarization experiment, the sample was immersed for 24 hours in inhibitor solution, and polarization was carried out in fresh inhibitor solution. The inhibition

efficiency increases with time due to enough adsorption. But, in the weight-loss experiment, the sample was dipped continuously for 24 hours and weighted afterward. In the case of MNE and BAE, inhibition efficiency increases with time, where inhibition efficiency is a maximum in a short time as compared to AVE and EHE. In AVE and EHE, inhibition efficiency is less at the beginning of immersion which means more metal ions are dissolved out in the solution. These disolved ions chelate with inhibitor molecules. As the time of immersion increases, available inhibitor molecules decrease for inhibition. Hence, inhibition decreases with an increase in time when the sample is continuosly immersed.

IE of EHE and AVE is less at higher temperature, where as IE of MNE is very hight even upto 55ºC and that of BAE is more than 80% even at 65ºC. Such type of corrosion inhibition behaviour of MNE and BAE is more benificial to apply to remove rust and corrosion produts in weight loss estimation as well as in acid pickling as the pickling is done at higher temperature to accelerate the process.

CHAPTER 5

5. CONCLUSION AND RECOMMENDATIONS

5.1 Conclusions

Based on the study of corrosion inhibition properties of methanolic extracts of four plants viz *Artemisia vulgaris, Equisetum hyemale, Berberis aristata* and *Mahonia nepalensis* on mild steel in acidic media by a different technique such as OCP measurement, electrochemical spectroscopy, Potentiodynamic polarization, weight-loss method, SEM image, FTIR and, calculation of kinetic and thermodynamic parameters, conclusions are drawn for different plant extract are presented here in the separate heading.

5.1.1 Conclusion for *Artemisia vulgaris*

1. The methanol extract of *Artemisia vulgaris* acts as an effective green corrosion inhibitor for mild steel in 1.0 M H_2SO_4.

2. IE increases with an increase in concentration and it is calculated 94.22% for 1000 ppm solution by potentiodynamic polarization. IE increases up to 308 K and decreases beyond this temperature.

3. IE increases up to 6 h and decreases onwards.

4. Inhibition is due to monolayer adsorption without interaction of adsorbed molecules, which follows the Langmuir adsorption isotherm. Values of ΔG^o and Ea imply that the adsorption of molecules on the mild steel surface is a mixed type of adsorption involving both physical and chemical interaction.

5. Values of ΔH^* and Ea indicate that the process of corrosion is unimolecular, and kinetic parameters of activation control the rate. Values of ΔH^*, ΔS^* imply that the adsorption process is spontaneous and endothermic.

6. Based on electrochemical parameters, it can be concluded that it is a mixed type of inhibitor that inhibits both cathodic hydrogen evolution and anodic metal dissolution.

7. The formation of a protective barrier film of AVE on the mild steel surface is confirmed by EDX and SEM, which inhibits corrosion.

5.1.2 Conclusion for *Equisetum hyemale*

1. Methanoic extract of *Equisetum hyemale* acts as an effective green corrosion inhibitor for mild steel in 1.0 M H_2SO_4 solution.

2. The weight-loss method confirms that the IE of EHE is more than 85% at 1000 ppm. The *IE* increases with an increase in concentration and decreases with an increase in temperature. *IE* increases until 6 h, and decreases to maintain a steady-state value after 12 h of immersion.

3. The thermodynamic parameters calculation also supports the weight-loss results. The adsorption of the extract on the mild steel (MS) follows the Langmuir adsorption isotherm, which indicates the monolayer adsorption of inhibitor on MS surface.

4. Values of ΔG^o and E_a indicate the adsorption of molecules on the MS surface involves both physical and chemical interaction, but a decrease in *IE* with an increase in temperature reveals the physical adsorption dominant. Similarly, the values of ΔH^* and E_a explain the corrosion process is unimolecular, and kinetic parameters of activation control the rate. Also, they indicate that the adsorption process is spontaneous and endothermic.

5. Electrochemical measurement points out as the inhibition behavior of EHE is a mixed type by showing a parallel Tafel slope. This result is further supported by only one time constant in EIS.

6. EDX and SEM confirm the suppression of corrosion attack by adsorbed extract on the MS surface.

5.1.3 Conclusion for *Mahonia nepalensis*

1. Extract of *Mahonia nepalensis* is found as an efficient and thermally stable green corrosion inhibitor. The inhibition efficiency (*IE*) increases with an increase in MNE concentration. About 90% IE is computed in 200 ppm only and IE increases to approximately 98% in 1000 ppm for macroscale corrosion of MS in 1.0 M H_2SO_4 solution.

2. IE increases with an increase in time of immersion. The inhibition efficiency of the extract is high and quick. The extract shows above 90% IE only in 15 minute immersion time.

3. The *IE* also increases with temperature up to 328 K and decreases afterward due to the desorption MNE.

4. Corrosion inhibition by MNE is due to monolayer adsorption following the Langmuir adsorption isotherm. The values of ΔG^o and Ea imply that the adsorption involves physisorption and chemisorption, with the domination of chemisorption.

5. Values of ΔH^* and Ea indicate that the corrosion process is unimolecular and the rate is controlled by the kinetic parameters of activation. Values of ΔH^*, ΔS^* indicate that the adsorption process is spontaneous and endothermic and occurs through increasing randomness in a transition state in the presence of MNE.

6. Electrochemical parameters show that the inhibitor is a mixed type. Parallel cathodic slopes of acids without and with different concentrations of MNE indicate that there is no change in corrosion mechanism and the inbition is due to adsorption of inhibitor molecules onto the barrier film. The only time constant in acid without and with MNE of varying concentrations indicates that the corrosion mechanism is unaffected by the addition of inhibitor.

7. The development of a protective MNE film on the MS surface and the suppression of corrosion are confirmed by EDX and SEM.

5.1.4 Conclusion for *Berberis aristata*

1. Methanolic extract of *Berberis aristata* is investigated as a highly effective and thermally stable corrosion inhibitor for MS in 1.0 M H_2SO_4.

2. At 200 ppm of BAE, the inhibition efficiency is greater than 90%. The IE increases with increasing concentration, with a maximum IE of 98.14 % recorded through potentiodynamic polarization for a 1000 ppm solution.

3. At 338 K, the thermal stability of the BAE on MS surface is remarkable, with an IE of 80%. The BAE was discovered to be a highly effective inhibitor, with 90% efficacy in 0.25 hours in a 1000 ppm solution.

4. The corrosion inhibition is due to the monolayer adsorption of inhibitor molecules on the metal surface following the Langmuir adsorption isotherm. Values of ΔG^o and Ea imply that the adsorption is of mixed adsorption, whereas chemical adsorption is dominant. Meanwhile, the difference in values of ΔH^* and Ea is nearly equal to RT, indicating a unimolecular and endothermic adsorption process.

5. OCP changes in acid in the absence and presence of BAE show that BAE is a mixed inhibitor. Cathodic parallel Tafel slope and only one time constant of acid in the absence and presence of BAE varying concentrations in EIS show that the mechanism of corrosion is not affected. Corrosion is inhibited due to adsorption of inhibitor molecules by the formation of barrier film onto the metal surface.

6. The formation of the barrier film of BAE on the MS surface to inhibit corrosion is confirmed by EDX and SEM analysis.

To sum up, all plant extracts are good inhibitor. However, MNE and BAE have higher IE in less concentration and time of immersion and they have thermal stability as well. Inhibitor with higher efficiency at higher temperature is more applicable for removing corrosion products for weight loss estimation, faster removal of scales and oxide layer in the industrial procedure used for surface finish. Acid pickling is carried out generally above 60ºC, so, MNE and BAE could be suitable alternative corrosion inhibitor for the process. As mentioned earlier, the global corrosion inhibitors market size is valued at US$ 7.4 billion in 2019 and expected to reach US$ 9.9 billion by 2027, production of efficient and applicable inhibitors such as MNE, BAE helps to generate revenue for the country and contributes to promote GDP of the nation.

5.2 Recommendations and Limitations :

From the study of plant extract as corrosion inhibitor, the following recommendations are suggested for further research

1. Surface characterization of metal sample could be done by XPS method to ensure the adsorbed compounds on metal surface.

2. Crude extract was tested as the inhibitor in the study. This study is not able to mention the particular compound present in the extract which plays a vital role in the corrosion inhibitor. Different compounds can be separated and isolated from the extract and can be studied as corrosion inhibition.

3. Inhibition may be due to the synergistic effect of two or more compounds present in the compounds, which can be studied in the future.

4. Synergistic effect by adding some other compounds may enhance the inhibition efficiency which can be studied in the future.

CHAPTER 6

6. SUMMARY

Mild steel has wild spread applications in large a variety of structures and industries due to its mechanical properties, availability, and low cost. On exposure to aggressive media during its use such as acid pickling, descaling, etc, it is suffered from corrosion. Corrosion is a potent force that devastates economies, depletes resources, and causes expensive and untimely plant, equipment, and component failures. Although corrosion is inevitable, its cost and risk could be reduced if proper corrosion management system is used. Among several methods adopted to reduce corrosion, the best and cost-effective method is the use of inhibitors. The the global corrosion inhibitors market was worth \$7.4 billion in 2019. Unfortunately, several traditionally used inhibitors are found hazardous to humans and the environment. Due to environmental legislation, a new research trend is going to develop cost-effective, green corrosion inhibitor. Researchers are fascinated to the plant products such as essential oil, crude extract for the alternative as the phytochemicals present in them are similar to conventional organic inhibitors in electronic and molecular structure. This work is an effort to develop green corrosion inhibitors from high altitude plants of Nepal. The achievements of the work presented in the thesis can be summarized chapter wise as follows.

A general background of the corrosion and its control are presented in chapter 1. The impacts of corrosion and economic importance of corrosion study is discussed. Different types of methods used to control corrosion such as surface coating, proper material design are also represented. Chapter 1 discusses types of inhibitors, industrial use, and factors in applying inhibitors. As the conventional inhibitors are found hazardous and expensive, plant extracts are introduced as the alternative non-toxic, environment-friendly, cheap green inhibitor. Inhibitors inhibit the corrosion rate due to their adsorption on metal surface. The mechanism of corrosion inhibition by inhibitor is discussed in terms of adsorption. Chapter also discuss about the different types of corrosion monitoring technique such as weight loss, EIS, LPR, potentiodynamic polarization techniques.

Different types of research works and the development of different inhibitors are discussed in chapter 2. In the beginning several organic compounds were developed as the corrosion inhibitors. Later on, after development environmental awareness research works seems diverted to the synthesis of green inhibitors. Since, synthetic green inhibitors are expensive, new research trend is growing to develop cheap green inhibitors from plant products. In a few research works, pure compounds isolated from extract are also tested for inhibition, but there is no improvement in the inhibition efficiency.

Chapter 3 discusses the materials and methods. General introduction plants selected for the work (*Artemisia vulgaris, Equisetum hyemale, Berberis aristata* and *Mahonia nepalensis*) and chemical compounds isolated from these plants by natural product chemist that could be responsible for inhibition are discussed. It includes the methods of preparation metal coupons, plant extract, inhibitor solution. In this thesis, Gravimetric and electrochemical techniques such as potentiodynamic polarization, EIS in combination with surface analytical tools such as SEM, EDX were applied to characterize the corrosion processes of mild steel in 1.0 M H_2SO_4. ATR-FTIR is used to analyze different functional groups present in the extract.

Results obtained by different methods are discussed in chapter 4. Corrosion rate and IE are calculated from different methods. Effect of temperature, exposure time and concentration of inhibitor are studied in the inhibition efficiency. Adsorption kinetics is studied using polarization and impedance measurements, as well as adsorption isotherm investigations to derive thermodynamic parameters to support the adsorption mechanism. Mechanism of the inhibition is discussed at the end of this chapter.

Conclusions regarding corrosion inhibition properties of different plant extracts are listed in chapter 5. It was concluded that all plants extracts could be used as an effective corrosion inhibitor. Extracts of *Artemisia vulgaris* and *Equisetum hyemale* are effective as an inhibitor for a short time, low temperature and higher concentration, where as extracts of *Mahonia nepalensis* and *Berberis aristata* are thermally stable inhibitors which are effective in a short time, low concentration and high temperature as well. Finally, the whole thesis is summarized in chapter 6.

REFERENCES

Abdel-Gaber, A. M., Abd-El-Nabey, B. A., & Saadawy, M. (2009). The role of acid anion on the inhibition of the acidic corrosion of steel by lupine extract. *Corrosion Science*, *51*(5), 1038–1042. https://doi.org/10.1016/j.corsci.2009.03.003

Abdel-Gaber, A. M., Abd-El-Nabey, B. A., Sidahmed, I. M., El-Zayady, A. M., & Saadawy, M. (2006). Inhibitive action of some plant extracts on the corrosion of steel in acidic media. *Corrosion Science*, *48*(9), 2765–2779. https://doi.org/10.1016/j.corsci.2005.09.017

Abdul Rahiman, A. F. S., & Sethumanickam, S. (2017). Corrosion inhibition, adsorption and thermodynamic properties of poly(vinyl alcohol-cysteine) in molar HCl. *Arabian Journal of Chemistry*, *10*, S3358–S3366. https://doi.org/10.1016/j.arabjc.2014.01.016

Abu-Shandi, K., & Al-Marahleh, H. (2017). Isolation and Characterization of the Phytoconstituents in the Aerial Parts of Wild and Home Planted *Artemisia vulgaris* by Gas Chromatography-Mass Spectrometry. *Journal of Chemical and Pharmaceutical Research*, *9*(4), 126.

Adejo, S. O., Ekwenchi, M. M., Gbertyo, J. A., Menengea, T., & Ogbodo, J. O. (2014). Determination of Adsorption Isotherm model best fit for methanol leaf extract of *Securinega virosa* as corrosion inhibitor for corrosion of mild steel in HCl. *Journal of Advances in Chemistry, 10*(5), 2737–2742. https://doi.org/10.24297/jac.v10i5.891

Adewuyi, A., Göpfert, A., & Wolff, T. (2014). Succinyl amide gemini surfactant from *Adenopus breviflorus* seed oil: A potential corrosion inhibitor of mild steel in acidic medium. *Industrial Crops and Products*, *52*, 439–449. https://doi.org/10.1016/j.indcrop.2013.10.045

Afia, L, Benali, O., Salghi, R., Ebenso, E. E., Jodeh, S., Zougagh, M., & Hammouti, B. (2014). Steel corrosion inhibition by acid garlic essential oil as a green corrosion inhibitor and sorption behavior. *Int. J. Electrochem. Sci.*, *9*, 8392-8406.

Afia, Leila, Salghi, R., Bazzi, E. H., Zarrouk, A., Hammouti, B., Bouri, M., Zarrouk, H., Bazzi, L., & Bammou, L. (2012). Argan hulls extract: Green inhibitor of

mild steel corrosion in 1 M HCl solution. *Research on Chemical Intermediates*, *38*(8), 1707–1717. https://doi.org/10.1007/s11164-012-0496-y

Ahamad, I., Prasad, R., & Quraishi, M. A. (2010). Adsorption and inhibitive properties of some new Mannich bases of Isatin derivatives on corrosion of mild steel in acidic media. *Corrosion Science*, *52*(4), 1472–1481. https://doi.org/10.1016/j.corsci.2010.01.015

Ahmad, Z. (2006). *Principles of corrosion engineering and corrosion control* (1st ed). Elsevier/BH.

Aiad, I., & Negm, N. A. (2009). Some corrosion inhibitors based on schiff base surfactants for mild steel equipments. *Journal of Dispersion Science and Technology*, *30*(8), 1142–1147. https://doi.org/10.1080/01932690802701598

Alagta, A., Felhösi, I., Bertoti, I., & Kálmán, E. (2008). Corrosion protection properties of hydroxamic acid self-assembled monolayer on carbon steel. *Corrosion Science*, *50*(6), 1644–1649. https://doi.org/10.1016/J.CORSCI.2008.02.008

Al-Amiery, A., Kadhum, A., Kadihum, A., Mohamad, A., How, C., & Junaedi, S. (2014). Inhibition of mild steel corrosion in sulfuric acid solution by new Schiff base. *Materials*, *7*(2), 787–804. https://doi.org/10.3390/ma7020787

Alaneme, K. K., Olusegun, S. J., & Adelowo, O. T. (2016). Corrosion inhibition and adsorption mechanism studies of *Hunteria umbellata* seed husk extracts on mild steel immersed in acidic solutions. *Alexandria Engineering Journal*, *55*(1), 673–681. https://doi.org/10.1016/j.aej.2015.10.009

Alkhathlan, H. Z., Khan, M., Abdullah, M. M. S., Al-Mayouf, M., Mousa, A. A., & Al-Othman, Z. A. M. (2014). *Launaea nudicaulis* as a source of new and efficient green corrosion inhibitor for mild steel in acidic medium: A comparative study of two solvent extracts. *Int. J. Electrochem. Sci.*, *9*, 870-889.

Al-Senani, G., Al-Saeedi, S., & Almufarij, R. (2015). Green corrosion inhibitors for carbon steel by green leafy vegetables extracts in 1 M HCl. *Oriental Journal of Chemistry*, *31*(4), 2077–2086. https://doi.org/10.13005/ojc/310428

Amira, W. A. W. E., Rahim, A. A., Osman, H., Awang, K., & Raja, P. B. (2011). Corrosion Inhibition of Mild Steel in 1 M HCl Solution by *Xylopia Ferruginea* Leaves from Different Extract and Partitions. *Int. J. Electrochem. Sci.*, *6*, 2998–3016.

Anbarasi, C. M., Rajendran, S., Pandiarajan, M., & Krishnaveni, A. (2013). An encounter with corrosion inhibitors. *Eur. Chem. Bull*, *2*(4), 197–205. https://doi.org/10.17628/ECB.2013.2.197

Anupama, K. K., Ramya, K., & Joseph, A. (2016). Electrochemical and computational aspects of surface interaction and corrosion inhibition of mild steel in hydrochloric acid by *Phyllanthus amarus* leaf extract (PAE). *Journal of Molecular Liquids*, *216*, 146–155. https://doi.org/10.1016/j.molliq.2016.01.019

Anuradha, K., Vimala, R., Narayanasamy, B., Arockia Selvi, J., & Rajendran, S. (2007). Corrosion inhibition of carbon steel in low chloride media by an aqueous extract of *Hibiscus rosa-* Sinensis linn. *Chemical Engineering Communications*, *195*(3), 352–366. https://doi.org/10.1080/00986440701673283

Arab, S. T., & Noor, E. A. (1993). Inhibition of Acid Corrosion of Steel by Some S-Alkylisothiouronium Iodides. *Corrosion*, *49*(2), 122–129. https://doi.org/10.5006/1.3299206

Aramaki, K. (2004). Historical and Future Perspectives on Corrosion Inhibitor Studies. *Zairyo-to-Kankyo*, *53*(7), 348–351. https://doi.org/10.3323/jcorr1991.53.348

Arthur, D., Adedayo, A., Igelige, G., & Ogwuche, E. (2014). Corrosion Inhibition of Mild Steel in 0.1M H2SO4 Solution by *Anacardium occidentale* Gum. *American Chemical Science Journal*, *4*(6), 847–854. https://doi.org/10.9734/ACSJ/2014/9499

Asegbeloyin, J., Ejikeme, P., Olasunkanmi, L., Adekunle, A., & Ebenso, E. (2015). A Novel Schiff Base of 3-acetyl-4-hydroxy-6-methyl-(2H)pyran-2-one and 2,2'-(ethylenedioxy)diethylamine as Potential Corrosion Inhibitor for Mild Steel in Acidic Medium. *Materials*, *8*(6), 2918–2934. https://doi.org/10.3390/ma8062918

Ashassi-Sorkhabi, H., Seifzadeh, D., & Hosseini, M. G. (2008). EN, EIS and polarization studies to evaluate the inhibition effect of 3H-phenothiazin-3-one, 7-dimethylamin on mild steel corrosion in 1 M HCl solution. *Corrosion Science*, *50*(12), 3363–3370. https://doi.org/10.1016/j.corsci.2008.09.022

Avci, G., & Keleş, Y. (2011). Aqueous extract of *Acacia cyanophylla* leaves as environmentally friendly inhibitor for mild steel corrosion in 1 M H_2SO_4

solution. *Surface and Interface Analysis*, *43*(10), 1311–1317. https://doi.org/10.1002/sia.3714

Awad, M. I. (2006). Eco friendly corrosion inhibitors: Inhibitive action of quinine for corrosion of low carbon steel in 1 m HCl. *Journal of Applied Electrochemistry*, *36*(10), 1163–1168. https://doi.org/10.1007/s10800-006-9204-1

Awasthi, L. (2018). Corrosion inhibition of mild steel in acidic medium by *Eucalyptus globulus* as green inhibitor *[M.Sc. Project]*. Tri Chandra Multiple Campus, Tribhuvan University.

Bajpai, V., Singh, A., Arya, K. R., Srivastava, M., & Kumar, B. (2015). Rapid screening for the adulterants of *Berberis aristata* using direct analysis in real-time mass spectrometry and principal component analysis for discrimination. *Food Additives & Contaminants: Part A*, *32*(6), 799–807. https://doi.org/10.1080/19440049.2015.1022885

Bammou, L., Belkhaouda, M., Salghi, R., Benali, O., Zarrouk, A., Zarrok, H., & Hammouti, B. (2014). Corrosion inhibition of steel in sulfuric acidic solution by the *Chenopodium Ambrosioides* extracts. *Journal of the Association of Arab Universities for Basic and Applied Sciences*, *16*, 83–90. https://doi.org/10.1016/j.jaubas.2013.11.001

Bedair, M. A., El-Sabbah, M. M. B., Fouda, A. S., & Elaryian, H. M. (2017). Synthesis, electrochemical and quantum chemical studies of some prepared surfactants based on azodye and Schiff base as corrosion inhibitors for steel in acid medium. *Corrosion Science*, *128*(September), 54–72. https://doi.org/10.1016/j.corsci.2017.09.016

Behpour, M., Ghoreishi, S. M., Khayatkashani, M., & Soltani, N. (2012). Green approach to corrosion inhibition of mild steel in two acidic solutions by the extract of *Punica granatum* peel and main constituents. *Materials Chemistry and Physics*, *131*(3), 621−633. https://doi.org/10.1016/j.matchemphys.2011.10.027

Benabdellah, M., Aouniti, A., Dafali, A., Hammouti, B., Benkaddour, M., Yahyi, A., & Ettouhami, A. (2006). Investigation of the inhibitive effect of triphenyltin 2-thiophene carboxylate on corrosion of steel in 2 M H_3PO_4 solutions. *Applied Surface Science*, *252*(23), 8341–8347. https://doi.org/10.1016/J.APSUSC.2005.11.037

Bentiss, F., Bouanis, M., Mernari, B., Traisnel, M., Vezin, H., & Lagrene, M. (2007). Understanding the adsorption of 4 H -1 , 2 , 4-triazole derivatives on mild steel surface in molar hydrochloric acid. *Applied surface Science, 253*, 3696–3704. https://doi.org/10.1016/j.apsusc.2006.08.001

Bentiss, F., Lagrenee, M., Traisnel, M., & Hornez, J. C. (1999). The corrosion inhibition of mild steel in acidic media by a new triazole derivative. *Corrosion Science*, *41*(4), 789–803. https://doi.org/10.1016/S0010-938X(98)00153-X

Bentiss, F., Lebrini, M., Vezin, H., Chai, F., Traisnel, M., & Lagrené, M. (2009). Enhanced corrosion resistance of carbon steel in normal sulfuric acid medium by some macrocyclic polyether compounds containing a 1,3,4-thiadiazole moiety: AC impedance and computational studies. *Corrosion Science*, *51*(9), 2165–2173. https://doi.org/10.1016/J.CORSCI.2009.05.049

Bentiss, F., Traisnel, M., & Lagrenee, M. (2000). The substituted 1,3,4-oxadiazoles: A new class of corrosion inhibitors of mild steel in acidic media. *Corrosion Science*, *42*(1), 127–146. https://doi.org/10.1016/S0010-938X(99)00049-9

Bhat, J. I., Vijaya, D. P., & Alva, V. (2011). Meclizine hydrochloride as a potential non-toxic corrosion inhibitor for mild steel in hydrochloric acid medium. *Arch. Appl. Sci. Res.*, *3*, 343.

Bhawsar, J., Jain, P. K., & Jain, P. (2015). Experimental and computational studies of Nicotiana tabacum leaves extract as green corrosion inhibitor for mild steel in acidic medium. *Alexandria Engineering Journal*, *54*(3), 769–775. https://doi.org/10.1016/j.aej.2015.03.022

Bist, B. B. (2019). Effect of *Cassia tora* (Tapre Jhar) Stem Extracts on the Corrosion Inhibition of Mild Steel in 1M Sulphuric Acid Solution *[M.Sc. Dissertation]*. Amrit Campus, Tribhuvan University.

Bohara, D. S. (2019). Effect of *Crotalaria spectabilis* Stem Extracts on the Corrosion Inhibition of Mild Steel in 1M Sulphuric Acid Solution *[M.Sc. Dissertation]*. Amrit Campus, Tribhuvan University.

Bothi Raja, P., & Sethuraman, M. G. (2010). Studies on the Inhibition of Mild Steel Corrosion by *Rauvolfia serpentina* in Acid Media. *Journal of Materials Engineering and Performance*, *19*(5), 761–766. https://doi.org/10.1007/s11665-009-9541-4

Boudalia, M., Fernández-Domene, R. M., Tabyaoui, M., Bellaouchou, A., Guenbour, A., & García-Antón, J. (2019). Green approach to corrosion inhibition of

stainless steel in phosphoric acid of *Artemesia herba* albamedium using plant extract. *Journal of Materials Research and Technology*, *8*(6), 5763–5773. https://doi.org/10.1016/j.jmrt.2019.09.045

Boumhara, K., Tabyaoui, M., Jama, C., & Bentiss, F. (2015). *Artemisia Mesatlantica* essential oil as green inhibitor for carbon steel corrosion in 1M HCl solution: Electrochemical and XPS investigations. *Journal of Industrial and Engineering Chemistry*, *29*, 146–155. https://doi.org/10.1016/j.jiec.2015.03.028

Bouyanzer, A., Hammouti, B., & Majidi, L. (2006). Pennyroyal oil from Mentha pulegium as corrosion inhibitor for steel in 1M HCl. *Materials Letters*, *60*(23), 2840–2843. https://doi.org/10.1016/j.matlet.2006.01.103

Cang, H., Fei, Z., Shao, J., Shi, W., & Xu, Q. (2013). Corrosion Inhibition of Mild Steel by Aloes Extract in HCl Solution Medium. *Int. J. Electrochem. Sci.*, *8*, 720-734.

Chander, V., Aswal, J. S., Dobhal, R., & Uniyal, D. P. (2017). A review on Pharmacological potential of Berberine; an active component of Himalayan Berberis aristata. *The Journal of Phytopharmacology*, *6*(1), 58–58.

Chapagain, A. (2019). Inhibitory Action of the Alkaloid Extracts of *Rhynchostylis Retusa* on the Mild Steel in 1 M H_2SO_4 *[M.Sc. Dissertation]*. Amrit Campus, Tribhuvan University.

Chaudhari, H., & Vashi, R. (2016). The study of henna leaves extract as green corrosion inhibitor for mild steel in acetic acid. *Journal of Fundamental and Applied Sciences*, *8*(2), 280. https://doi.org/10.4314/jfas.v8i2.8

Chaudhary, Y., Karki, N., & Yadav, A. P. (2016). Study of the corrosion inhibition behavior of *Pogostemon benghalensis* (Rudilo) for mild steel in acidic medium by weight loss method. *J. Nepal Chem. Soc.*, *35*, 139.

Chauhan, L. R., & Gunasekaran, G. (2007). Corrosion inhibition of mild steel by plant extract in dilute HCl medium. *Corrosion Science*, *49*(3), 1143–1161. https://doi.org/10.1016/J.CORSCI.2006.08.012

Chetouani, A., Hammouti, B., & Benkaddour, M. (2004). Corrosion inhibition of iron in hydrochloric acid solution by jojoba oil. *Pigment & Resin Technology*, *33*(1), 26–31. https://doi.org/10.1108/03699420410512077

Chevalier, M., Robert, F., Amusant, N., Traisnel, M., Roos, C., & Lebrini, M. (2014). Enhanced corrosion resistance of mild steel in 1M hydrochloric acid solution

by alkaloids extract from *Aniba rosaeodora* plant: Electrochemical, phytochemical and XPS studies. *Electrochimica Acta*, *131*, 96–105. https://doi.org/10.1016/j.electacta.2013.12.023

Chigondo, M., & Chigondo, F. (2016). Recent Natural Corrosion Inhibitors for Mild Steel: An Overview. *Journal of Chemistry*, *2016*, 1–7. https://doi.org/10.1155/2016/6208937

Choudhary, G., Sharma, A., Bangar, R. K., & Sharma, A. (2015). Eco-friendly Inhibition by Weed (*Bidens biternata*) Extract towards Acid Corrosion of AA6063 INTRODUCTION *: International Journal of Innovative Research in Advanced Engineering, 2*(12), 112–119.

Dahmani, M., Et-Touhami, A., Al-Deyab, S. S., Hammouti, B., & Bouyanzer, A. (2010). Corrosion Inhibition of C38 Steel in 1 M HCl: A Comparative Study of Black Pepper Extract and Its Isolated Piperine. *Int. J. Electrochem. Sci.*, *5*, 1060-1069.

Dariva, C. G., & Galio, A. F. (2014). Corrosion Inhibitors – Principles, Mechanisms and Applications. In M. Aliofkhazraei (Ed.), *Developments in Corrosion Protection*. InTech. https://doi.org/10.5772/57255

Das, A., & Chhetry, T. K. (2016). Evaluation of Anti-Diabetic Activity of *Mahonia nepalensis* in STZ Induced Rat Model. *International Journal of Pharmacognosy and Phytochemical Research*, *8*(7), 1104-1110.

Davis, J. R. (2000). *Corrosion: Understanding the basics*. A.S.M. International.

Desai, P. S. (2015). *Hibiscus rosa-sinensis* (Jasud) leaves extracts used as corrosion inhibitors for mild steel in hydrochloric acid. *European Journal of Pharmaceutical and Medical Research*, *2*(1), 470–485.

Desai, P. S. (2015). Inhibitory action of extract of ankado (*Calotropis gigantea*) leaves on mild steel corrosion in hydrochloric acid solution. *International Journal of Current Microbiology and Applied Sciences*, *4*(1), 437.

Desai, P. S., & Indorwala, N. S. (2015). Triazoles used as a Corrosion inhibitor for mild steel in Hydrochloric Acid. *International Journal of Current Microbiology and Applied Sciences*, 928–938.

Eddy, N. O., & Mamza, P. A. P. (2009). Inhibitive and Adsorption Properties of Ethanol Extract of Seeds and Leaves of *Azadirachta Indica* on the Corrosion of Mild Steel in H_2SO_4: *Portugaliae Electrochimica Acta*, *27*(4), 443–456. https://doi.org/10.4152/pea.200904443

Eddy, N. O., Odoemelam, S. A., & Mbaba, A. J. (2008). Inhibition of the corrosion of mild steel in HCl by sparfloxacin. *African Journal of Pure and Applied Chemistry*, *2*(12), 132–138.

Eddy, N. O., Odoemelam, S. A., & Odiongenyi, A. O. (2009). Joint effect of halides and ethanol extract of *Lasianthera africana* on inhibition of corrosion of mild steel in H_2SO_4. *Journal of Applied Electrochemistry*, *39*(6), 849–857. https://doi.org/10.1007/s10800-008-9731-z

Ekanem, U. F., Umoren, S. A., Udousoro, I. I., & Udoh, A. P. (2010). Inhibition of mild steel corrosion in HCl using pineapple leaves (*Ananas comosus* L.) extract. *Journal of Materials Science*, *45*(20), 5558–5566. https://doi.org/10.1007/s10853-010-4617-y

El Bribri, A., Tabyaoui, M., Tabyaoui, B., El Attari, H., & Bentiss, F. (2013). The use of *Euphorbia falcata* extract as eco-friendly corrosion inhibitor of carbon steel in hydrochloric acid solution. *Materials Chemistry and Physics*, *141*(1), 240–247. https://doi.org/10.1016/j.matchemphys.2013.05.006

El-Etre, A. Y. (2007). Inhibition of acid corrosion of carbon steel using aqueous extract of olive leaves. *Journal of Colloid and Interface Science*, *314*(2), 578–583. https://doi.org/10.1016/j.jcis.2007.05.077

El-Etre, A. Y. (2008). Inhibition of C-steel corrosion in acidic solution using the aqueous extract of zallouh root. *Materials Chemistry and Physics*, *108*(2–3), 278–282. https://doi.org/10.1016/j.matchemphys.2007.09.037

El-Etre, A. Y., & El-Tantawy, Z. (2006). Inhibition of metallic corrosion using Ficus extract. *Portugaliae Electrochemica Acta*, *24*, 347–356.

El-Meligi, A.A. (2010). Corrosion Preventive Strategies as a Crucial Need for Decreasing Environmental Pollution and Saving Economics. *Recent Patents on Corrosion Science, 2,* 22-33. https://doi.org/10.2174/1877610801002010022

Evans, U. R. (1972). *An introduction to metallic corrosion* (2nd Ed.). Edward Arnold Ltd.

Fernandes, C. M., Alvarez, L. X., dos Santos, N. E., Maldonado Barrios, A. C., & Ponzio, E. A. (2019). Green synthesis of 1-benzyl-4-phenyl-1H-1,2,3-triazole, its application as corrosion inhibitor for mild steel in acidic medium and new approach of classical electrochemical analyses. *Corrosion Science*, *149*(January), 185–194. https://doi.org/10.1016/j.corsci.2019.01.019

Finšgar, M., & Jackson, J. (2014). Application of corrosion inhibitors for steels in acidic media for the oil and gas industry: A review. *Corrosion Science*, *86*, 17–41. https://doi.org/10.1016/j.corsci.2014.04.044

Fiori-Bimbi, M. V., Alvarez, P. E., Vaca, H., & Gervasi, C. A. (2015). Corrosion inhibition of mild steel in HCL solution by pectin. *Corrosion Science*, *92*, 192–199. https://doi.org/10.1016/j.corsci.2014.12.002

Fouda, A. S., Abousalem, A. S., & EL-Ewady, G. Y. (2017). Mitigation of corrosion of carbon steel in acidic solutions using an aqueous extract of *Tilia cordata* as green corrosion inhibitor. *International Journal of Industrial Chemistry*, *8*(1), 61–73. https://doi.org/10.1007/s40090-016-0102-z

Fouda, A. S., Elewady, G. Y., Shalabi, D., & Habouba, S. (2014). Anise Extract as Green Corrosion Inhibitor for Carbon Steel in Hydrochloric Acid Solution. *International Journal of Innovative Research in Science, Engineering and Technology*, *3*, 11210.

Fouda, A. S., Etaiw, S. H., & Elnggar, W. (2014). Punica Plant extract as Green Corrosion inhibitor for C-steel in Hydrochloric Acid Solutions. *Int. J. Electrochem. Sci.*, *9*, 4866-4883.

Garai, S., Garai, S., Jaisankar, P., Singh, J. K., & Elango, A. (2012). A comprehensive study on crude methanolic extract of *Artemisia pallens* (Asteraceae) and its active component as effective corrosion inhibitors of mild steel in acid solution. *Corrosion Science*, *60*, 193–204. https://doi.org/10.1016/j.corsci.2012.03.036

Gentil, V. (2003). *Corrosao* (4th ed.). Rio de Jenerio:LTC.

Gerengi, H., & Sahin, H. I. (2012). *Schinopsis lorentzii* Extract As a Green Corrosion Inhibitor for Low Carbon Steel in 1 M HCl Solution. *Industrial & Engineering Chemistry Research*, *51*(2), 780–787. https://doi.org/10.1021/ie201776q

Ghali, E., Sastri, V. S., & Elboujdaini, M. (2007). *Corrosion Prevention and Protection: Practical Solution*. John Wiley & Sons, Inc., England.

Gilani, A. H., Yaeesh, S., Jamal, Q., & Ghayur, M. N. (2005). Hepatoprotective activity of aqueous-methanol extract of *Artemisia vulgaris*. *Phytotherapy Research*, *19*(2), 170–172. https://doi.org/10.1002/ptr.1632

Grand View Research. (2020, May). *Corrosion Inhibitors Market Size, Share & Trends Analysis Report By Product (Organic, Inorganic), By Type (Water Based, Oil Based), By End Use, By Region, And Segment Forecasts, 2020—*

2027 [Market Analysis Report]. https://www.grandviewresearch.com/industry-analysis/corrosion-inhibitors-market

Gunasekaran, G., & Chauhan, L. R. (2004). Eco friendly inhibitor for corrosion inhibition of mild steel in phosphoric acid medium. *Electrochimica Acta*, *49*(25), 4387–4395. https://doi.org/10.1016/j.electacta.2004.04.030

Gupta, D. K., Kafle, K. A., Das, A. K., Neupane, S., Ghimire, A., Yadav, B. D., Chaudhari, Y., Karki, N., & Yadav, A. P. (2020). Study of *Jatropha Curcas* Extract as a Corrosion Inhibitor in Acidic Medium on Mild Steel by Weight Loss and Potentiodynamic Methods. *Journal of Nepal Chemical Society*, *41*(1), 87-93. https://doi.org/tps://doi.org/10.3126/jncs.v41i1.30493

Hackerman, N., Hurd, R. M., & Kenworthy, L. (1962). *1st International Congress on Metallic Corrosion*. Butterworth.

Hamdy, A., & El-Gendy, N. S. (2013). Thermodynamic, adsorption and electrochemical studies for corrosion inhibition of carbon steel by henna extract in acid medium. *Egyptian Journal of Petroleum*, *22*(1), 17–25. https://doi.org/10.1016/j.ejpe.2012.06.002

Hegazy, M. A., Abdallah, M., Awad, M. K., & Rezk, M. (2014). Three novel di-quaternary ammonium salts as corrosion inhibitors for API X65 steel pipeline in acidic solution. Part I: Experimental results. *Corrosion Science*, *81*, 54–64. https://doi.org/10.1016/J.CORSCI.2013.12.010

Heusler, K. E., Landolt, D., & Trasatti, S. (1989). Electrochemical Corrosion Nomenclature. *Pure and Applied Chemistry*, *61*, 19–22.

Hmamou, D. B., Salghi, R., Bazzi, L., Hammouti, B., Al-Deyab, S. S., Bammou, L., Bazzi, L., & Bouyanzer, A. (2012). Prickly Pear Seed Oil Extract: A Novel Green Inhibitor for Mild Steel Corrosion in 1 M HCl Solution. *Int. J. Electrochem. Sci.*, *7*, 1303-1318.

Hosseini, M., Mertens, S. F. L., Ghorbani, M., & Arshadi, M. R. (2003). Asymmetrical Schiff bases as inhibitors of mild steel corrosion in sulphuric acid media. *Materials Chemistry and Physics*, *78*(3), 800–808. https://doi.org/10.1016/S0254-0584(02)00390-5

Hussin, M. H., & Kassim, M. J. (2011). The corrosion inhibition and adsorption behavior of *Uncaria gambir* extract on mild steel in 1M HCl. *Materials Chemistry and Physics*, *125*(3), 461–468. https://doi.org/10.1016/j.matchemphys.2010.10.032

Hussin, M. H., Rahim, A. A., Mohamad Ibrahim, M. N., & Brosse, N. (2016). The capability of ultrafiltrated alkaline and organosolv oil palm (*Elaeis guineensis*) fronds lignin as green corrosion inhibitor for mild steel in 0.5 M HCl solution. *Measurement*, *78*, 90–103. https://doi.org/10.1016/j.measurement.2015.10.007

Ji, G., Anjum, S., Sundaram, S., & Prakash, R. (2015). *Musa paradisica* peel extract as green corrosion inhibitor for mild steel in HCl solution. *Corrosion Science*, *90*, 107–117. https://doi.org/10.1016/j.corsci.2014.10.002

Ji, G., Dwivedi, P., Sundaram, S., & Prakash, R. (2013). Inhibitive Effect of *Chlorophytum borivilianum* Root Extract on Mild Steel Corrosion in HCl and H $_2$ SO $_4$ Solutions. *Industrial & Engineering Chemistry Research*, *52*(31), 10673–10681. https://doi.org/10.1021/ie4008387

ji, G., Shukla, S. K., Dwivedi, P., Sundaram, S., & Prakash, R. (2011). Inhibitive Effect of *Argemone mexicana* Plant Extract on Acid Corrosion of Mild Steel. *Industrial & Engineering Chemistry Research*, *50*(21), 11954–11959. https://doi.org/10.1021/ie201450d

Jin, M., Zhang, C., Zheng, T., Yao, D., Shen, L., Luo, J., Jiang, Z., Ma, J., Jin, X.-J., Cui, J., Lee, J. J., & Li, G. (2014). A new phenyl glycoside from the aerial parts of *Equisetum hyemale*. *Natural Product Research*, *28*(21), 1813–1818. https://doi.org/10.1080/14786419.2014.947491

John, S., Jeevana, R., Aravindakshan, K. K., & Joseph, A. (2017). Corrosion inhibition of mild steel by N(4)-substituted thiosemicarbazone in hydrochloric acid media. *Egyptian Journal of Petroleum*, *26*(2), 405–412. https://doi.org/10.1016/j.ejpe.2016.05.012

Jones, D. A. (1996). *Principles and prevention of corrosion* (2nd ed). Prentice Hall.

Joshi, P. V., Shirkhedkar, A. A., Prakash, K., & Maheshwari, V. L. (2011). Antidiarrheal activity, chemical and toxicity profile of *Berberis aristata*. *Pharmaceutical Biology*, *49*(1), 94–100. https://doi.org/10.3109/13880209.2010.500295

Joshi, T. P. (2018). Corrosion inhibition of mild steel by *Magnifera indica* bark extracts *[M.Sc. Project]*. Tri Chandra Multiple Campus, Tribhuvan University.

Ju, H., Ju, Y., & Li, Y. (2012). Berberine as an Environmental-Friendly Inhibitor for Hot-Dip Coated Steels in Diluted Hydrochloric Acid. *Journal of Materials*

Science and Technology, *28*(9), 809–816. https://doi.org/10.1016/S1005-0302(12)60135-2

Jüttner, K. (1990). Electrochemical impedance spectroscopy (EIS) of corrosion processes on inhomogeneous surfaces. *Electrochimica Acta*, *35*(10), 1501–1508. https://doi.org/10.1016/0013-4686(90)80004-8

Kairi, N. I., & Kassim, J. (2013). The Effect of Temperature on the Corrosion Inhibition of Mild Steel in 1 M HCl Solution by *Curcuma Longa* Extract. *Int. J. Electrochem. Sci.*, 8, *7138–7155*.

Kamal, C., & Sethuraman, M. G. (2012). *Spirulina platensis* – A novel green inhibitor for acid corrosion of mild steel. *Arabian Journal of Chemistry*, *5*(2), 155–161. https://doi.org/10.1016/j.arabjc.2010.08.006

Kamal, Chennappan, & Sethuraman, M. G. (2012). Caulerpin—A bis-Indole Alkaloid As a Green Inhibitor for the Corrosion of Mild Steel in 1 M HCl Solution from the Marine Alga *Caulerpa racemosa*. *Industrial & Engineering Chemistry Research*, *51*(31), 10399–10407. https://doi.org/10.1021/ie3010379

Karki, N., Chaudhary, Y., & Yadav, A. P. (2018). Thermodynamic, Adsorption and Corrosion Inhibition Studies of Mild Steel by Artemisia vulgaris Extract from Methanol as Green Corrosion Inhibitor in Acid Medium. *Journal of Nepal Chemical Society*, *39*, 76. https://doi.org/10.3126/jncs.v39i0.27041

Karki, N., Neupane, S., Chaudhary, Y., Gupta, D. K., & Yadav, A. (2020). *Berberis Aristata*: A Highly Efficient and Thermally Stable Green Corrosion Inhibitor for Mild Steel in Acidic Medium. *Analytical and Bioanalytical Electrochemistry*, *12*(7), 970–988.

Karthik, R., Muthukrishnan, P., Elangovan, A., Jeyaprabha, B., & Prakash, P. (2014). Extract of *Cassia senna* as Green Inhibitor for the Corrosion of Mild Steel in 1M Hydrochloric Acid Solution. *Advances in Civil Engineering Materials*, *3*(1), 20140010. https://doi.org/10.1520/ACEM20140010

Karthikaiselvi, R., & Subhashini, S. (2014). Study of adsorption properties and inhibition of mild steel corrosion in hydrochloric acid media by water soluble composite poly (vinyl alcohol-omethoxy aniline). *Journal of the Association of Arab Universities for Basic and Applied Sciences*, *16*(1), 74–82. https://doi.org/10.1016/j.jaubas.2013.06.002

Khadom, A. A., Abd, A. N., & Ahmed, N. A. (2018). *Xanthium strumarium* leaves extracts as a friendly corrosion inhibitor of low carbon steel in hydrochloric

acid: Kinetics and mathematical studies. *South African Journal of Chemical Engineering*, *25*, 13–21. https://doi.org/10.1016/j.sajce.2017.11.002

Khamis, E., & Al-Andis, N. (2002). *Mat.-wiss.u.werkstofftech*.

Khan, G., Newaz, K. Md. S., Basirun, W. J., Ali, H. B. Md., Faraj, F. L., & Khan, G. M. (2015). Application of Natural Product Extracts as Green Corrosion Inhibitors for Metals and Alloys in Acid Pickling Processes-A review. *Int. J. Electrochem. Sci*, *10*, 6120.

Krishnaveni, K., & Ravichandran, J. (2014). Effect of aqueous extract of leaves of *Morinda tinctoria* on corrosion inhibition of aluminium surface in HCl medium. *Transactions of Nonferrous Metals Society of China*, *24*(8), 2704–2712. https://doi.org/10.1016/S1003-6326(14)63401-4

Lahhit, N., Bouyanzer, A., Desjobert, J.-M., Hammouti, B., Salghi, R., Costa, J., Jama, C., Bentiss, F., & Majidi, L. (2011). Fennel (*Foeniculum Vulgare*) Essential Oil as Green Corrosion Inhibitor of Carbon Steel in Hydrochloric Acid Solution: *Portugaliae Electrochimica Acta*, *29*(2), 127–138. https://doi.org/10.4152/pea.201102127

Lama, P. C., Chaudhary, Y., Karki, N., & Yadav, A. P. (2016). Study of the Corrosion Inhibition Behavior of *Pogostemon benghalensis* (Rudilo) for Mild Steel in acidic medium by Potentiodynamic Method. *J. Nepal Chem. Soc.*, *34*, 120.

Lama, R., Das, A. K., Yadav, B., Chaudhary, Y., Lama, P. C., Shrestha, S. L., Gupta, D. K., Karki, N., & Yadav, A. P. (2018). Corrosion Inhibition of Mild Steel in Acidic Medium using High Altitude Plant Extract. *J. Nepal Chem. Soc.*, *38*, 48.

Lebrini, M., Robert, F., Blandinières, P. A., & Roos, C. (2011). Corrosion Inhibition by *Isertia coccinea* Plant Extract in Hydrochloric Acid Solution. *Int. J. Electrochem. Sci.*, *6*, 2443-2460.

Lebrini, M., Robert, F., & Roos, C. (2011). Alkaloids Extract from *Palicourea guianensis* Plant as Corrosion Inhibitor for C38 Steel in 1 M Hydrochloric Acid Medium. *Int. J. Electrochem. Sci.*, *6*, 847-859.

Leelavathi, S., & Rajalakshmi, R. (2013). *Dodonaea viscosa* (L.) Leaves extract as acid Corrosion inhibitor for mild Steel – A Green approach. *J. Mater. Environ. Sci.*, *4*(5), 625–638.

Li, W., Zhao, X., Liu, F., & Hou, B. (2008). Investigation on inhibition behavior of S-triazole-triazole derivatives in acidic solution. *Corrosion Science*, *50*(11), 3261–3266. https://doi.org/10.1016/j.corsci.2008.08.015

Li, Yan, Zhao, P., Liang, Q., & Hou, B. (2005). Berberine as a natural source inhibitor for mild steel in 1 M H 2 SO 4. *Applied Surface Science*, *252*(5), 1245–1253. https://doi.org/10.1016/j.apsusc.2005.02.094

Li, Yongxin, Zhang, Y., Jungwirth, S., Seely, N., Fang, Y., & Shi, X. (2014). Corrosion inhibitors for metals in maintenance equipment: Introduction and recent developments. *Corrosion Reviews*, *32*(5–6), 163–181. https://doi.org/10.1515/corrrev-2014-0002

Lynes, W. (1951). Some Historical Developments Relating to Corrosion. *Journal of The Electrochemical Society*, *98*(1), 3C-10C. https://doi.org/10.1149/1.2778101

Ma, Q., Qi, S., He, X., Tang, Y., & Lu, G. (2017). 1,2,3-Triazole derivatives as corrosion inhibitors for mild steel in acidic medium: Experimental and computational chemistry studies. *Corrosion Science*, *129*(September), 91–101. https://doi.org/10.1016/j.corsci.2017.09.025

Mai, T. H., Tuan, T. A., Huong, H. T., Minh, C. V., Ban, N. K., & Kiem, P. V. (2009). Bisbenzylisoquinoline Alkaloids from Mahonia Nepalensis. *Journal of Chemistry*, *47*(3), 368.

Manske, R. H. F. (1955). Chapter 48 Minor Alkaloids of Unknown Structure. In *The Alkaloids: Chemistry and Physiology* (Vol. 5, pp. 301–332). Elsevier. https://doi.org/10.1016/S1876-0813(08)60091-3

McCafferty, E. (2005). Validation of corrosion rates measured by the Tafel extrapolation method. *Corrosion Science*, *47*(12), 3202–3215. https://doi.org/10.1016/j.corsci.2005.05.046

Michael, N. C. (2014). The Corrosion Inhibition of Mild Steel in Sulphuric Acid Solution by Flavonoid (Catechin) Separated from *Nypa Fruticans Wurmb* Leaves Extract. *Science Journal of Chemistry*, *2*(4), 27-32. https://doi.org/10.11648/j.sjc.20140204.11

Mohammadi, A., Hosseini, S. M. A., Bahrami, M. J., & Shahidi, M. (2016). Corrosion Inhibition of Mild Steel in Acidic Solution by Apricot Gum as a Green Inhibitor. *Prog. Color Colorants Coat.*, *9*, 117–134.

Mohd, N., & Ishak, A. S. (2015). Thermodynamic Study of Corrosion Inhibition of Mild Steel in Corrosive Medium by *Piper nigrum* Extract. *Indian Journal of Science and Technology*, *8*(17). https://doi.org/10.17485/ijst/2015/v8i17/63478

Morad, M. S., & El-Dean, A. M. K. (2006). 2,2′-Dithiobis(3-cyano-4,6-dimethylpyridine): A new class of acid corrosion inhibitors for mild steel. *Corrosion Science*, *48*(11), 3398–3412. https://doi.org/10.1016/j.corsci.2005.12.006

Mourya, P., Banerjee, S., & Singh, M. M. (2014). Corrosion inhibition of mild steel in acidic solution by *Tagetes erecta* (Marigold flower) extract as a green inhibitor. *Corrosion Science*, *85*, 352–363. https://doi.org/10.1016/j.corsci.2014.04.036

Murmu, M., Saha, S. K., Murmu, N. C., & Banerjee, P. (2019). Effect of stereochemical conformation into the corrosion inhibitive behaviour of double azomethine based Schiff bases on mild steel surface in 1 mol L−1 HCl medium: An experimental, density functional theory and molecular dynamics simulation study. *Corrosion Science*, *146*(September 2018), 134–151. https://doi.org/10.1016/j.corsci.2018.10.002

Murthy, H. C. A., & Karungamye, P. N. (2017). Highly Efficient Baobab (*Adansonia digitata*) Fruit Seeds and Pulp Extracts as Potential Green Corrosion Inhibitors for Mild Steel in 0.5M HCl Solution. *International Journal of Research in Chemistry and Environment*, *6*(4), 32–42.

Muthukrishnan, P., Jeyaprabha, B., & Prakash, P. (2014). Mild steel corrosion inhibition by aqueous extract of *Hyptis Suaveolens* leaves. *International Journal of Industrial Chemistry*, *5*(1), 1–11. https://doi.org/10.1007/s40090-014-0005-9

Muthukrishnan, P., Prakash, P., Jeyaprabha, B., & Shankar, K. (2019). Stigmasterol extracted from *Ficus hispida* leaves as a green inhibitor for the mild steel corrosion in 1 M HCl solution. *Arabian Journal of Chemistry*, *12*(8), 3345–3356. https://doi.org/10.1016/j.arabjc.2015.09.005

Muto, I., Saito, E., & Ito, S. (1994). *Application of accelerated corrosion tests to service life prediction of materials*. ASTM STP.

Na, L., Hui, G., Peng, Z., Xin, Z., Lihua, Z., & Singh, A. (2019). The extraction of a natural dye berberine and evaluation of its corrosion inhibition properties for

P110SS steel. *International Journal of Electrochemical Science*, *14*(2), 1830–1842. https://doi.org/10.20964/2019.02.62

NACE International Institute IMPACT PLUS. (2020, May 7). https://www.nace-impact.org/

Nair-IJTIMES, R. (2018). Kinetic, Thermodynamic, adsorption and electrochemical studies for Corrosion Behaviour of Aluminium AA6063 Alloy in Ethanolic Extract of *Lawsonia alba* Lam. Leaves. *International Journal of Technical Innovation in Modern Engineering & Science (IJTIMES)*, *4*(12), 170.

Naqvi, I., Saleemi, A. R., & Naveed, S. (2011). Cefixime: A drug as Efficient Corrosion Inhibitor for Mild Steel in Acidic Media. Electrochemical and Thermodynamic Studies. *Int. J. Electrochem. Sci.*, *6*, 146-161.

Nguyen, T. M., Tran, A. T., Hoang, T. H., Chau, V. M., Ninh, K. B., & Phan, V. K. (2009). Bisbenzylisoquinoline Alkaloid From *Mahonia nepalensis*. *Journal of Chemistry*, *47*, 368.

Nnanna, L. A., Owate, I. O., & Oguzie, E. E. (2014). Inhibition of Mild Steel Corrosion in HCl Solution by *Pentaclethra macrophylla Bentham* Extract. *International Journal of Materials Engineering*, 4(5) 171-179.

Noor, E. A. (2007). Temperature Effects on the Corrosion Inhibition of Mild Steel in Acidic Solutions by Aqueous Extract of Fenugreek Leaves. *Int. J. Electrochem. Sci.*, *2*, 996-1017.

Nwabanne, J. T., & Okafor, V. N. (2012). Adsorption and Thermodynamics Study of the Inhibition of Corrosion of Mild Steel In H_2SO_4 Medium Using *Vernonia Amygdalina*. *Journal of Minerals and Materials Characterization and Engineering*, *11*(09), 885.

Nwankwo, M. O., Offor, P. O., Neife, S. I., Oshionwu, L. C., & Idenyi, N. E. (2014). *Amaranthus cordatus* as a Green Corrosion Inhibitor for Mild Steel in H_2SO_4 and NaCl. *Journal of Minerals and Materials Characterization and Engineering*, *02*(03), 194–199. https://doi.org/10.4236/jmmce.2014.23024

Obot, I. B., Obi-Egbedi, N. O., & Umoren, S. A. (2009). Antifungal drugs as corrosion inhibitors for aluminium in 0.1M HCl. *Corrosion Science*, *51*(8), 1868–1875. https://doi.org/10.1016/j.corsci.2009.05.017

Odewunmi, N. A., Umoren, S. A., & Gasem, Z. M. (2015). Watermelon waste products as green corrosion inhibitors for mild steel in HCl solution. *Journal*

of Environmental Chemical Engineering, *3*(1), 286–296. https://doi.org/10.1016/j.jece.2014.10.014

Odewunmi, Nurudeen A., Umoren, S. A., Gasem, Z. M., Ganiyu, Saheed. A., & Muhammad, Q. (2015). l-Citrulline: An active corrosion inhibitor component of watermelon rind extract for mild steel in HCl medium. *Journal of the Taiwan Institute of Chemical Engineers*, *51*, 177–185. https://doi.org/10.1016/j.jtice.2015.01.012

Odusote, J. K., Owalude, D. O., Olusegun, S. J., & Yahya, R. A. (2016). Inhibition Efficiency of *Moringa Oleifera* Leaf Extract on the Corrosion of Reinforced Steel Bar in HCl Solution. *The West Indian Journal of Engineering*, *38*, 64-70.

Oguzie, E. E., Li, Y., & Wang, F. H. (2007). Effect of surface nanocrystallization on corrosion and corrosion inhibition of low carbon steel: Synergistic effect of methionine and iodide ion. *Electrochimica Acta*, *52*(24), 6988–6996. https://doi.org/10.1016/j.electacta.2007.05.023

Oguzie, E.E., Enenebeaku, C. K., Akalezi, C. O., Okoro, S. C., Ayuk, A. A., & Ejike, E. N. (2010). Adsorption and corrosion-inhibiting effect of *Dacryodis edulis* extract on low-carbon-steel corrosion in acidic media. *Journal of Colloid and Interface Science*, *349*(1), 283–292. https://doi.org/10.1016/j.jcis.2010.05.027

Oguzie, Emeka E. (2006). Studies on the inhibitive effect of *Occimum viridis* extract on the acid corrosion of mild steel. *Materials Chemistry and Physics*, *99*(2–3), 441–446. https://doi.org/10.1016/j.matchemphys.2005.11.018

Oguzie, Emeka E. (2008). Evaluation of the inhibitive effect of some plant extracts on the acid corrosion of mild steel. *Corrosion Science*, *50*(11), 2993–2998. https://doi.org/10.1016/j.corsci.2008.08.004

Okafor, P. C., Ikpi, M. E., Uwah, I. E., Ebenso, E. E., Ekpe, U. J., & Umoren, S. A. (2008). Inhibitory action of *Phyllanthus amarus* extracts on the corrosion of mild steel in acidic media. *Corrosion Science*, *50*(8), 2310–2317. https://doi.org/10.1016/j.corsci.2008.05.009

Okafor, P. C., Osabor, V. I., & Ebenso, E. E. (2007). Eco-friendly corrosion inhibitors: Inhibitive action of ethanol extracts of *Garcinia kola* for the corrosion of mild steel in H_2SO_4 solutions. *Pigment & Resin Technology*, *36*(5), 299–305. https://doi.org/10.1108/03699420710820414

217

Olajire, A. A. (2017). Corrosion inhibition of offshore oil and gas production facilities using organic compound inhibitors—A review. *Journal of Molecular Liquids*, *248*, 775–808. https://doi.org/10.1016/j.molliq.2017.10.097

Ostovari, A., Hoseinieh, S. M., Peikari, M., Shadizadeh, S. R., & Hashemi, S. J. (2009). Corrosion inhibition of mild steel in 1 M HCl solution by henna extract: A comparative study of the inhibition by henna and its constituents (Lawsone, Gallic acid, α-d-Glucose and Tannic acid). *Corrosion Science*, *51*(9), 1935–1949. https://doi.org/10.1016/j.corsci.2009.05.024

Oukhrib, R., Issami, E., Ibrahimi, B., Mouaden, K., & Bazzi, L. (2017). Ziziphus lotus as Green Inhibitor of Copper Corrosion in Natural Sea Water: *Portugaliae Electrochimica Acta*, *35*(4), 187–200. https://doi.org/10.4152/pea.201704187

Pandey, B. P., Thapa, R., & Upreti, A. (2017). Chemical composition, antioxidant and antibacterial activities of essential oil and methanol extract of *Artemisia vulgaris* and *Gaultheria fragrantissima* collected from Nepal. *Asian Pacific Journal of Tropical Medicine*, *10*(10), 952–959. https://doi.org/10.1016/j.apjtm.2017.09.005

Pandey, G., & Khatoon, S. (2017). Evaluation of Phytochemical Profile and Antioxidant Activity of *Equisetum hyemale* L. *World Journal of Pharmaceutical Research*, *6*(03), 723-737.

Park, B.-J., & Tomohiko, M. (2011). Feruloyl, caffeoyl, and flavonol glucosides from *Equisetum hyemale*. *Chemistry of Natural Compounds*, *47*(3), 363–365. https://doi.org/10.1007/s10600-011-9934-0

Parthipan, P., Narenkumar, J., Elumalai, P., Preethi, P. S., Usha Raja Nanthini, A., Agrawal, A., & Rajasekar, A. (2017). Neem extract as a green inhibitor for microbiologically influenced corrosion of carbon steel API 5LX in a hypersaline environments. *Journal of Molecular Liquids*, *240*, 121–127. https://doi.org/10.1016/j.molliq.2017.05.059

Patel, N. S., Hadlicka, J., Beranek, P., Salghi, R., Bouya, H., Ismat, H. A., & Hammouti, B. (2014). Corrosion Inhibition of Steel by Various Parts of *Rotula Aquatica* Plant Extracts in H_2SO_4 Solutions: *Portugaliae Electrochimica Acta*, *32*(6), 395–403. https://doi.org/10.4152/pea.201406395

Patel, N. S., Jauhariand, S., Mehta, G. N., Al-Deyab, S. S., Warad, I., & Hammouti, B. (2013). Mild Steel Corrosion Inhibition by Various Plant Extracts in 0.5 M Sulphuric acid. *Int. J. Electrochem. Sci.*, *8*, 2635-2655.

Pierre, R. R. (2008). *Corrosion Engineering: Principles and Practice* (1st ed.). McGraw-Hill Inc.

Prabakaran, M., Kim, S.-H., Kalaiselvi, K., Hemapriya, V., & Chung, I.-M. (2016). Highly efficient *Ligularia fischeri* green extract for the protection against corrosion of mild steel in acidic medium: Electrochemical and spectroscopic investigations. *Journal of the Taiwan Institute of Chemical Engineers*, *59*, 553–562. https://doi.org/10.1016/j.jtice.2015.08.023

Pushpanjali, M., Rao, S. A., & Padmalatha. (2014). *Carica papaya* seeds—Green inhibitor for corrosion control of aluminium in acid medium. *Journal of Applicable Chemistry*, *3*(1), 310–323.

Qiang, Y., Zhang, S., Tan, B., & Chen, S. (2018). Evaluation of Ginkgo leaf extract as an eco-friendly corrosion inhibitor of X70 steel in HCl solution. *Corrosion Science*, *133*(September 2017), 6–16. https://doi.org/10.1016/j.corsci.2018.01.008

Queiroz, G. M., Souza-Moreira, T. M., Salgado, H. R. N., Moreira, R. R. D., Utrera, S. H., Martins, C. H. G., & Pietro, R. C. L. R. (2014). Antimicrobial activity and toxicity in vitro and in vivo of *Equisetum hyemale* extracts. *Rev Cienc Farm Basica Apl*, *35*(4), 559–563.

Quraishi, M. A., & Ansari, F. A. (2003). Corrosion inhibition by fatty acid triazoles for mild steel in formic acid. *Journal of Applied Electrochemistry*, *33*(3), 233–238. https://doi.org/10.1023/A:1024106123577

Quraishi, M. A., Singh, A., Singh, V. K., Yadav, D. K., & Singh, A. K. (2010). Green approach to corrosion inhibition of mild steel in hydrochloric acid and sulphuric acid solutions by the extract of *Murraya koenigii* leaves. *Materials Chemistry and Physics*, *122*(1), 114–122. https://doi.org/10.1016/j.matchemphys.2010.02.066

Rahim, A. A., Rocca, E., Steinmetz, J., Kassim, M. J., Adnan, R., & Sani Ibrahim, M. (2007). Mangrove tannins and their flavanoid monomers as alternative steel corrosion inhibitors in acidic medium. *Corrosion Science*, *49*(2), 402–417. https://doi.org/10.1016/j.corsci.2006.04.013

Raja, B., & Sethuraman, M. G. (2009). *Solanum Tuberosum* as an Inhibitor of Mild Steel Corrosion in Acid Media. *Iran. J. Chem. Chem. Eng.*, *28*(1), 77-84.

Raja, Pandian Bothi, Fadaeinasab, M., Qureshi, A. K., Rahim, A. A., Osman, H., Litaudon, M., & Awang, K. (2013). Evaluation of Green Corrosion Inhibition

by Alkaloid Extracts of *Ochrosia oppositifolia* and Isoreserpiline against Mild Steel in 1 M HCl Medium. *Industrial & Engineering Chemistry Research*, *52*(31), 10582–10593. https://doi.org/10.1021/ie401387s

Raja, Pandian Bothi, Qureshi, A. K., Abdul Rahim, A., Osman, H., & Awang, K. (2013). *Neolamarckia cadamba* alkaloids as eco-friendly corrosion inhibitors for mild steel in 1M HCl media. *Corrosion Science*, *69*, 292–301. https://doi.org/10.1016/j.corsci.2012.11.042

Raja, Pandian Bothi, & Sethuraman, M. G. (2008). Natural products as corrosion inhibitor for metals in corrosive media—A review. *Materials Letters*, *62*(1), 113–116. https://doi.org/10.1016/j.matlet.2007.04.079

Raja, P.B., & Sethuraman, M. G. (2009). Inhibition of corrosion of mild steel in sulphuric acid medium by *Calotropis procera*. *Pigment & Resin Technology*, *38*(1), 33–37. https://doi.org/10.1108/03699420910923553

Rani, B. E. A., & Basu, B. B. J. (2012). Green Inhibitors for Corrosion Protection of Metals and Alloys: An Overview. *International Journal of Corrosion*, *2012*, 1–15. https://doi.org/10.1155/2012/380217

Riggs Jr., O. L. (1973). *Corrosion Inhibitors* (2nd Editio). C.C. Nathan, Houston.

Roberge, P. R. (2012). *Handbook of Corrosion Engineering*. McGraw-Hill Inc.

Roy, P., Karfa, P., Adhikari, U., & Sukul, D. (2014). Corrosion inhibition of mild steel in acidic medium by *polyacrylamide grafted Guar* gum with various grafting percentage: Effect of intramolecular synergism. *Corrosion Science*, *88*, 246–253. https://doi.org/10.1016/j.corsci.2014.07.039

Saadawy, M. (2015). An important world crop – barley – as a new green inhibitor for acid corrosion of steel. *Anti-Corrosion Methods and Materials*, *62*(4), 220–228. https://doi.org/10.1108/ACMM-12-2013-1333

Sadeghi Erami, R., Amirnasr, M., Meghdadi, S., Talebian, M., Farrokhpour, H., & Raeissi, K. (2019). Carboxamide derivatives as new corrosion inhibitors for mild steel protection in hydrochloric acid solution. *Corrosion Science*, *151*(February), 190–197. https://doi.org/10.1016/j.corsci.2019.02.019

Saedah, R. A.-M. (2014). Inhibition of mild steel corrosion using Juniperus plants as green inhibitior. *African Journal of Pure and Applied Chemistry*, *8*(1), 9–22. https://doi.org/10.5897/AJPAC2013.0497

Saidi, N., Elmsellem, H., Ramdani, M., Chetouani, A., Azzaoui, K., Yousfi, F., & Hammouti, B. (2015). Using pectin extract as eco-friendly inhibitor for steel corrosion in 1M HCl media. *Der Pharma Chemica*, *7*(5), 87–94.

Saleh, R. M., Ismall, A. A., & El Hosary, A. A. (1982). Corrosion Inhibition by Naturally Occurring Substances: VII. The effect of aqueous extracts of some leaves and fruit-peels on the corrosion of steel, Al, Zn and Cu in acids. *British Corrosion Journal*, *17*(3), 131–135. https://doi.org/10.1179/000705982798274345

Sanyal, B. (1981). Organic compounds as corrosion inhibitors in different environments—A review. *Progress in Organic Coatings*, *9*(2), 165–236. https://doi.org/10.1016/0033-0655(81)80009-X

Sastri, V. S. (1998). *Corrosion Inhibitors: Principles and Applications*. J. Wiley.

Sastri, V. S. (2011). *Green Corrosion Inhibitors: Theory and Practice* (1st Ed.). John, Wiley & Sons, Inc. England.

Satapathy, A. K., Gunasekaran, G., Sahoo, S. C., Amit, K., & Rodrigues, P. V. (2009). Corrosion inhibition by *Justicia gendarussa* plant extract in hydrochloric acid solution. *Corrosion Science*, *51*(12), 2848–2856. https://doi.org/10.1016/j.corsci.2009.08.016

Sethuraman, M. G., & Bothi Raja, P. (2005). Corrosion inhibition of mild steel by *Datura metel* in acidic medium. *Pigment & Resin Technology*, *34*(6), 327–331. https://doi.org/10.1108/03699420510630345

Shahabi, S., Norouzi, P., & Ganjali, M. R. (2015). Theoretical and Electrochemical Study of Carbon Steel Corrosion Inhibition in the Presence of Two Synthesized Schiff Base Inhibitors: Application of Fast Fourier Transform Continuous Cyclic Voltammetry to Study the Adsorption Behavior. *Int. J. Electrochem. Sci.*, *10*, 2646-2662.

Sharma, S. K., Peter, A., & Obot, I. B. (2015). Potential of *Azadirachta indica* as a green corrosion inhibitor against mild steel, aluminum, and tin: A review. *Journal of Analytical Science and Technology*, *6*(1), 26. https://doi.org/10.1186/s40543-015-0067-0

Sherif, E. M., & Park, S.-M. (2006). Effects of 2-amino-5-ethylthio-1,3,4-thiadiazole on copper corrosion as a corrosion inhibitor in aerated acidic pickling solutions. *Electrochimica Acta*, *51*(28), 6556–6562. https://doi.org/10.1016/j.electacta.2006.04.047

Shrestha, P. R., Oli, H. B., Thapa, B., Chaudhary, Y., Gupta, D. K., Das, A. K., Nakarmi, K. B., Singh, S., Karki, N., & Yadav, A. P. (2019). Bark Extract of *Lantana camara* in 1M HCl as Green Corrosion Inhibitor for Mild Steel. *Engineering Journal*, *23*(4), 205–211. https://doi.org/10.4186/ej.2019.23.4.205

Shrestha, R. L., & Shrestha, P. (2016). Phytochemicalscreening, Antioxidant study and GC-MS analysis of *Mahonia nepalensis*. *J. Nepal Chem. Soc.*, *34*(1), 132–138.

Shukla, S. K., & Ebenso, E. E. (2011). Corrosion inhibition, adsorption behavior and thermodynamic properties of streptomycin on mild steel in hydrochloric acid medium. *International Journal of Electrochemical Science*, *6*(8), 3277–3291.

Singh, A., Ahamad, I., & Quraishi, M. A. (2012). *Piper longum* extract as green corrosion inhibitor for aluminium in NaOH solution. *Arabian Journal of Chemistry*, *9*, S1584–S1589. https://doi.org/10.1016/j.arabjc.2012.04.029

Singh, A., Singh, V. K., & Quraishi, M. A. (2010). Aqueous Extract of Kalmegh (*Andrographis paniculata*) Leaves as Green Inhibitor for Mild Steel in Hydrochloric Acid Solution. *International Journal of Corrosion*, *2010*, 1–10. https://doi.org/10.1155/2010/275983

Singh, A.K., Mohapatra, S., & Pani, B. (2016). Corrosion inhibition effect of Aloe Vera gel: Gravimetric and electrochemical study. *Journal of Industrial and Engineering Chemistry*, *33*, 288–297. https://doi.org/10.1016/j.jiec.2015.10.014

Singh, Ashish Kumar, Shukla, S. K., & Quraishi, M. A. (2011). Corrosion Behaviour of Mild Steel in Sulphuric Acid Solution in Presence of Ceftazidime. *Int. J. Electrochem. Sci.*, *6*, 5802-5814.

Singh, M.R., Gupta, P., & Gupta, K. (2019). The litchi (*Litchi Chinensis*) peels extract as a potential green inhibitor in prevention of corrosion of mild steel in 0.5 M H_2SO_4 solution. *Arabian Journal of Chemistry*, *12*(7), 1035–1041. https://doi.org/10.1016/j.arabjc.2015.01.002

Sivakumar, V., Velumani, K., & Rameshkumar, S. (2018). Colocid Dye—A Potential Corrosion Inhibitor for the Corrosion of Mild Steel in Acid Media. *Materials Research*, *21*(4), 1–10. https://doi.org/10.1590/1980-5373-mr-2017-0167

Soltani, N., & Khayatkashani, M. (2015). *Gundelia tournefortii* as a Green Corrosion Inhibitor for Mild Steel in HCl and H_2SO_4 Solutions. *Int. J. Electrochem. Sci.*, 10, 46-62.

Soltani, N., Tavakkoli, N., & Ghasemi, M. (2016). Corrosion Inhibition of Low Carbon Steel by *Strychnos nux- vomica* Extract as Green Corrosion Inhibitor in Hydrochloric Acid Solution. *International Journal of Electrochemical Science*, *11*, 8827–8847. https://doi.org/10.20964/2016.10.22

Soltani, N., Tavakkoli, N., Khayat Kashani, M., Mosavizadeh, A., Oguzie, E. E., & Jalali, M. R. (2014). *Silybum marianum* extract as a natural source inhibitor for 304 stainless steel corrosion in 1.0 M HCl. *Journal of Industrial and Engineering Chemistry*, *20*(5), 3217–3227. https://doi.org/10.1016/j.jiec.2013.12.002

Sood, H., Kumar, Y., Gupta, V. K., & Arora, D. S. (2019). Scientific validation of the antimicrobial and antiproliferative potential of *Berberis aristata* DC root bark, its phytoconstituents and their biosafety. *AMB Express*, *9*(1), 143. https://doi.org/10.1186/s13568-019-0868-4

Srivastava, K., & Srivastava, P. (1981). Studies on plant materials as corrosion inhibitors. *Br. Corros. J.*, *16*, 221–223.

Stern, M., & Geary, A. L. (1957). Electrochemical Polarization. *Journal of the Electrochemical Society*, *104*, 56.

Sudheer, & Quraishi, M. A. (2014). 2-Amino-3,5-dicarbonitrile-6-thio-pyridines: New and Effective Corrosion Inhibitors for Mild Steel in 1 M HCl. *Industrial & Engineering Chemistry Research*, *53*(8), 2851–2859. https://doi.org/10.1021/ie401633y

Tebbji, K., Hammouti, B., Oudda, H., Ramdani, A., & Benkadour, M. (2005). The inhibitive effect of bipyrazolic derivatives on the corrosion of steel in hydrochloric acid solution. *Applied Surface Science*, *252*(5), 1378–1385. https://doi.org/10.1016/j.apsusc.2005.02.097

Thapa, B., Gupta, D. K., & Yadav, A. P. (2019). Corrosion Inhibition of Bark Extract of *Euphorbia royleana* on Mild Steel in 1M HCl. *Journal of Nepal Chemical Society*, *40*, 25–29. https://doi.org/10.3126/jncs.v40i0.27274

Thusa, R., & Mulmi, S. (2017). Analysis of Phytoconstituents and Biological Activities of Different Parts of *Mahonia nepalensis* and *Berberis aristata*. *Nepal Journal of Biotechnology*, *5*(1), 5–13. https://doi.org/10.3126/njb.v5i1.18864

Tiwari, A., Uprety, Y., & Rana, S. K. (2019). Plant endemism in the Nepal Himalayas and phytogeographical implications. *Plant Diversity*, *41*(3), 174–182. https://doi.org/10.1016/j.pld.2019.04.004

Trabanelli, G., Zucci, F., Zucchini, G. L., & Carassiti, V. (1967). *Electrochim. Met.* (Vol. 2).

Trabelsi, W., Cecilio, P., Ferreira, M. G. S., & Montemor, M. F. (2005). Electrochemical assessment of the self-healing properties of Ce-doped silane solutions for the pre-treatment of galvanised steel substrates. *Progress in Organic Coatings*, *54*(4), 276–284. https://doi.org/10.1016/j.porgcoat.2005.07.006

Tuaweri, T. J., Ogbonnaya, E. A., & Onyemaobi, O. O. (2015). Corrosion Inhibition of Heat Treated Mild Steel with Neem Leave Extract in a Chloride Medium. *International Journal of Research in Engineering and Technology*, *04*(06), 404–409. https://doi.org/10.15623/ijret.2015.0406069

Uhlig, H. H., & Revie, R. W. (2008). *Corrosion and Corrosion Control: An Introduction to Corrosion Science and Engineering* (4th ed.). Wiley and Sons, Inc. Publication.

Ulaeto, S. B., Ekpe, U. J., Chidiebere, M. a, & Oguzie, E. E. (2012). Corrosion Inhibition of Mild Steel in Hydrochloric Acid by Acid Extracts of *Eichhornia Crassipes*. *International Journal of Materials and Chemistry*, *2*(4), 158–164. https://doi.org/10.5923/j.ijmc.20120204.08

Umoren, S. A. (2008). Inhibition of aluminium and mild steel corrosion in acidic medium using Gum Arabic. *Cellulose*, *15*(5), 751–761. https://doi.org/10.1007/s10570-008-9226-4

Umoren, S. A., Obot, I. B., Israel, A. U., Asuquo, P. O., Solomon, M. M., Eduok, U. M., & Udoh, A. P. (2014). Inhibition of mild steel corrosion in acidic medium using coconut coir dust extracted from water and methanol as solvents. *Journal of Industrial and Engineering Chemistry*, *20*(5), 3612–3622. https://doi.org/10.1016/j.jiec.2013.12.056

Umoren, S. A., Obot, I. B., & Obi-Egbedi, N. O. (2009). *Raphia hookeri* gum as a potential eco-friendly inhibitor for mild steel in sulfuric acid. *Journal of Materials Science*, *44*(1), 274–279. https://doi.org/10.1007/s10853-008-3045-8

Umoren, S., Obot, I. B., Gasem, Z., & Odewunmi, N. A. (2015). Experimental and Theoretical Studies of Red Apple Fruit Extract as Green Corrosion Inhibitor

for Mild Steel in HCl Solution. *Journal of Dispersion Science and Technology*, *36*(6), 789–802. https://doi.org/10.1080/01932691.2014.922887

Umoren, S.A., Eduok, U. M., Solomon, M. M., & Udoh, A. P. (2016). Corrosion inhibition by leaves and stem extracts of *Sida acuta* for mild steel in 1M H_2SO_4 solutions investigated by chemical and spectroscopic techniques. *Arabian Journal of Chemistry*, *9*(7), S209–S224. https://doi.org/10.1016/j.arabjc.2011.03.008

Umoren, Saviour A., Gasem, Z. M., & Obot, I. B. (2013). Natural Products for Material Protection: Inhibition of Mild Steel Corrosion by Date Palm Seed Extracts in Acidic Media. *Industrial & Engineering Chemistry Research*, *52*(42), 14855–14865. https://doi.org/10.1021/ie401737u

Ur Rashid, M., Alamzeb, M., Ali, S., Ullah, Z., Shah, Z. A., Naz, I., & Khan, M. R. (2019). The chemistry and pharmacology of alkaloids and allied nitrogen compounds from *Artemisia* species: A review. *Phytotherapy Research*, *33*(10), 2661–2684. https://doi.org/10.1002/ptr.6466

Veloz, M. A., & González, I. (2002). Electrochemical study of carbon steel corrosion in buffered acetic acid solutions with chlorides and H_2S. *Electrochimica Acta*, *48*(2), 135–144. https://doi.org/10.1016/S0013-4686(02)00549-2

Verma, C. B., & Quraishi, M. A. (2014). *Schiff ' s Bases of Glutamic Acid and Aldehydes as Green Corrosion Inhibitor for Mild Steel: Weight- Loss , Electrochemical and Surface Analysis*. *3*(7), 14601–14613.

Verma, C. B., Quraishi, M. A., & Singh, A. (2015). 2-Aminobenzene-1,3-dicarbonitriles as green corrosion inhibitor for mild steel in 1 M HCl: Electrochemical, thermodynamic, surface and quantum chemical investigation. *Journal of the Taiwan Institute of Chemical Engineers*, *49*(June 2018), 229–239. https://doi.org/10.1016/j.jtice.2014.11.029

Verma, C., Singh, P., & Quraishi, M. A. (2016). A thermodynamical, electrochemical and surface investigation of Bis (indolyl) methanes as Green corrosion inhibitors for mild steel in 1 M hydrochloric acid solution. *Journal of the Association of Arab Universities for Basic and Applied Sciences*, *21*(1), 24–30. https://doi.org/10.1016/j.jaubas.2015.04.003

Vimala, J. R., Rose, A. L., & Raja, S. (2011). *Cassia auriculata* Extract as Corrosion Inhibitor for Mild Steel in Acid Medium. *International Journal of ChemTech Research*, *3*, 1791–1801.

Vinod Kumar, K. P., Sankara Narayanan Pillai, M., & Rexin Thusnavis, G. (2011). Green corrosion inhibitor from seed extract of *Areca catechu* for mild steel in hydrochloric acid medium. *Journal of Materials Science*, *46*(15), 5208–5215. https://doi.org/10.1007/s10853-011-5457-0

Wu, X., Wiame, F., Maurice, V., & Marcus, P. (2020). 2-Mercaptobenzothiazole corrosion inhibitor deposited at ultra-low pressure on model copper surfaces. *Corrosion Science*, *166*, 108464. https://doi.org/10.1016/j.corsci.2020.108464

Xu, B., Yang, W., Liu, Y., Yin, X., Gong, W., & Chen, Y. (2014). Experimental and theoretical evaluation of two pyridinecarboxaldehyde thiosemicarbazone compounds as corrosion inhibitors for mild steel in hydrochloric acid solution. *Corrosion Science*, *78*, 260–268. https://doi.org/10.1016/J.CORSCI.2013.10.007

Xu, X., Singh, A., Sun, Z., Ansari, K. R., & Lin, Y. (2017). Theoretical, thermodynamic and electrochemical analysis of biotin drug as an impending corrosion inhibitor for mild steel in 15% hydrochloric acid. *Royal Society Open Science*, *4*(12), 170933. https://doi.org/10.1098/rsos.170933

Yadav, A. P., Suzuki, F., Nishikata, A., & Tsuru, T. (2004). Investigation of atmospheric corrosion of Zn using ac impedance and differential pressure meter. *Electrochimica Acta*, *49*(17), 2725–2729. https://doi.org/10.1016/j.electacta.2004.01.033

Yaro, A. S., Khadom, A. A., & Wael, R. K. (2013). Apricot juice as green corrosion inhibitor of mild steel in phosphoric acid. *Alexandria Engineering Journal*, *52*(1), 129–135. https://doi.org/10.1016/j.aej.2012.11.001

Yıldırım, A., & Çetin, M. (2008). Synthesis and evaluation of new long alkyl side chain acetamide, isoxazolidine and isoxazoline derivatives as corrosion inhibitors. *Corrosion Science*, *50*(1), 155–165. https://doi.org/10.1016/j.corsci.2007.06.015

Yüce, A. O., & Kardaş, G. (2012). Adsorption and inhibition effect of 2-thiohydantoin on mild steel corrosion in 0.1M HCl. *Corrosion Science*, *58*, 86–94. https://doi.org/10.1016/j.corsci.2012.01.013

Yurt, A., Balaban, A., Kandemir, S. U., Bereket, G., & Erk, B. (2004). Investigation on some Schiff bases as HCl corrosion inhibitors for carbon steel. *Materials Chemistry and Physics*, *85*(2–3), 420–426. https://doi.org/10.1016/j.matchemphys.2004.01.033

Zhang, S. H., & Lyon, S. B. (1994). Anodic processes on iron covered by thin, dilute electrolyte layers (I)—Anodic polarisation. *Corrosion Science*, *36*(8), 1289–1307. https://doi.org/10.1016/0010-938X(94)90182-1

Zheng, X., Gong, M., Li, Q., & Guo, L. (2018). Corrosion inhibition of mild steel in sulfuric acid solution by loquat (*Eriobotrya japonica Lindl*.) leaves extract. *Scientific Reports*, *8*(1), 9140. https://doi.org/10.1038/s41598-018-27257-9

Znini, M., Cristofari, G., Majidi, L., Ansari, A., Bouyanzer, A., Paolini, J., Costa, J., & Hammouti, B. (2012). Green Approach to Corrosion Inhibition of Mild Steel by Essential Oil Leaves of *Asteriscus Graveolens* (Forssk.) in Sulphuric Acid Medium. *Int. J. Electrochem. Sci.*, *7*, 3959-3981.

Znini, M., Majidi, L., Bouyanzer, A., Paolini, J., Desjobert, J.-M., Costa, J., & Hammouti, B. (2012). Essential oil of *Salvia aucheri mesatlantica* as a green inhibitor for the corrosion of steel in 0.5M H_2SO_4. *Arabian Journal of Chemistry*, *5*(4), 467–474. https://doi.org/10.1016/j.arabjc.2010.09.017

APPENDIX

<u>**Subjective Research Papers :**</u>

1. *Berberis aristata* : A highly Efficienct and Thermally Stable Green Corrosion Inhibitor for Mild Steel in Acidic Medium, **Nabin Karki**, Shova Neupane, Yogesh Chaudhary, Dipak Kumar Gupta, Amar Prasad Yadav, Analytical and Bioanalytical Electrochemistry, Vol. 12 (2020) Page 970-988

   Analytical and Bioanalytical Electrochemistry is **indexed and abstracted** by Chemical Abstracts, Scopus, and Web of Science (ESCI). Also, the journal is approved by Journals Survey Commission of Persian Sciences, Researches, SjR, Technologies Ministry and indexed by Islamic world Science Citation Center (ISC) and others.

2. *Equisetum hyemale*: a new candidate for green corrosion inhibitor family, **N. Karki,** S. Neupane, Y. Chaudhary, D.K. Gupta, A.P. Yadav, International Journal of Corrosion and Scale Inhibition, Vol. 12 (2021) Page 206-227
   DOI : 10.17675/2305-6894-2021-10-1-12

   The International Journal of Corrosion and Scale Inhibition is **indexed and abstracted** by the Emerging Sources Citation Index (Web of Science), Scopus (Q3) and Chemical Abstracts. It is listed in the Directory of Open Access Journals (DOAJ).

3. *Thermodynamic, Adsorption and Corrosion Inhibition Studies of Mild Steel by Artemisia Vulgaris Extract from Methanol as Green Corrosion Inhibitor in Acid Medium,* **Nabin Karki**, Yogesh Chaudhary, Amar Prasad Yadav, Journal of N epal Chemical Society, vol. 39, (2018), Page 76-85,
   DOI : https://doi.org/10.3126/jncs.v39i0.27041

4. *Effects of Anions on the Polarization Behavior of Galvanized Steel of Nepal,* **Nabin Karki**, Journal of Nepal Chemical Society vol. 32 (2013), page 89-91

5. *Effects of Anions on the Polarization Behavior of Zn-55Al Alloy coated Steel,* **Nabin Karki**, Journal of Nepal Chemical Society vol. 33 (2014), Page 101-103

6. *Study of the corrosion behavior of Pogostemon benghalensis for mild steel in acidic medium by potentiodynamic method,* Prakash Chandra Lama, Yogesh

Chaudhary, **Nabin Karki**, Amar Prasad Yadav, Journal of Nepal Chemical Society Vol. 34 (2016), Page 120-126

7. *Study of corrosion Inhibitor behavior of Pogostemon benghalensis (Rudilo) for mild steel in acidic medium by weight loss method,* Yogesh Chaudhary, **Nabin Karki**, Amar Prasad Yadav, Journal of Nepal Chemical Society Vol 35 (2016), Page 139-144,

8. *Bark Extract of Lanata Camara in 1M HCl as Green Corrosion Inhibitor for Mild Steel,* Prem Raj Shrestha, Hari Bhakta Oli, Bishal Thapa, Yogesh Chaudhary, Dipak K. Gupta, Anju Kumari Das, Krishna Badan Nakarmi, Sanjay Singh, **Nabin Karki**, Amar Prasad Yadav Engineering Journal Vol. 23 (2019) Page 205-211. DOI : https://doi.org/10.4186/ej.2019.23.4.205

EJ ranks in the 2nd Quartile (Cr. Scopus) in the General Engineering subject category, and is currently indexed in Emerging Sources Citation Index (ESCI) - (ISI) Web of Science, Scopus, IET Inspec, Chemical Abstracts Service (CAS), Asean Citation Index (ACI), Thai-Journal Citation Index (TCI), Directory of Open Access Journals (DOAJ)

9. *Corrosion Inhibition of Mild Steel in Acidic Medium using High Altitude Plant Extract,* Roshan Lama, Anju Kumar Das, Brahamdeo Yadav, Yogesh Chaudhar, Prakash Chandra Lama, Suman Lal Shrestha, Dipak K Gupta, **Nabin Karki**, Amar P Yadav, Journal of Nepal Chemical Society, Vol. 38 (2018) Page 48 https://doi.org/10.3126/jncs.v38i0.27787

10. *Study of Jatropha curcas Extract as a corrosion Inhibitor in Acidic Medium on Mild Steel by Weight Loss and Potentiodynamic Methods,* Dipak Kumar Gupta, KM Anita Kafle, Anju Kumar Das, Shova Neupane, Anita Ghimire, Braham Dev Yadav, Yogesh Chaudhari, **Nabin Karki,** Amar Prasad Yadav, Journal of Nepal Chemical Society, vol. 41 (2020) Page 87-93

DOI : https://doi.org/10.3126/jncs.v41i1.30493

11. *The effect of electrolytes on the coating of polyaniline on mild steel by electrochemical methods and its corrosion behavior,* Dipak Kumar Gupta, Shova Neupane, Sanjay Singh, Nabin Karki, Amar Prasad Yadav, Progress in Organic Coating, vol. 152 (2021) page 106127

DOI : *10.1016/j.porgcoat.2020.106127*

Progress in organic coating is Q1 journal which is indexed and abstracted in Science Citation Index, Cambridge Scientific Abstracts, Chemical Abstracts,

Current Contents, Engineering Index, Metals Abstracts, Pascal Francis, Physikalische Berichte, World Surface Coatings Abstracts, Research Alert, Applied Polymers Literature, Scopus, INSPEC.

12. *Dataset for the selection of electrolytes for Electropolymerization of aniline*, Dipak Kumar Gupta, Shova Neupane, Sanjay Singh, Nabin Karki, Amar Prasad Yadav, Data in Brief, Vol. 35 (2021) Page 106875

DOI : https://doi.org/10.1016/j.dib.2021.106875

Data in brief is Q4 Journal which is indexed and abstracted in PubMed Central, PubMed/Medline, Scopus, Emerging Sources Citation Index (ESCI), Directory of Open Access Journals (DOAJ).

Full Paper

Berberis Aristata: A Highly Efficient and Thermally Stable Green Corrosion Inhibitor for Mild Steel in Acidic Medium

Nabin Karki,[1, 2] Shova Neupane,[1, *] Yogesh Chaudhary,[1] Dipak Kumar Gupta,[1, 3] and Amar Prasad Yadav[1,*]

[1]Central Department of Chemistry, Tribhuvan University, Kathmandu, Nepal
[2]Bhaktapur Multiple Campus, Tribhuvan University, Bhaktapur, Nepal
[3]Trichandra Multiple Campus, Tribhuvan University, Kathmandu, Nepal

*Corresponding Author, Tel.: +9779851124444

E-Mail: amar2y@yahoo.com

Abstract- Plant extracts are extensively researched as a source of green corrosion inhibitors. Herein, we report on a highly efficient and thermally stable corrosion inhibitor from the stem extract of high-altitude shrub *Berberis aristata*. The corrosion inhibition efficiency (*IE*) of the extract was tested in 1.0 M H_2SO_4 for the corrosion protection of mild steel (MS) by using gravimetric and electrochemical measurements. It displayed a remarkable *IE* of 90% at 200 ppm and reached to 98.18% at high concentration (1000 ppm) at room temperature. The thermal stability of the adsorbed extract was uncommon among the recently reported plant extracts, giving an *IE* of 80% at 338K. Besides, the adsorption of the extract was extremely efficient, producing an *IE* of 90% in 15 min. The thermodynamic parameters (ΔG and *Ea*) showed a chemisorption dominated behavior of the extract. Electrochemical measurements indicated a mixed type of inhibitor, and the extract suppressed the corrosion rate by blocking the active surface of the MS.

Keywords- Corrosion inhibitor; *Berberis aristata*; Weight loss; Potentiodynamic polarization; Electrochemical impedance spectroscopy

1. INTRODUCTION

The study of corrosion of mild steel (MS) is vital for academics and industrialists since it is an excellent material in a wide range of industries and machinery due to its mechanical properties, ease of fabrication, weldability, availability, and low cost. However, corrosion of MS is a major concern, and there have been tremendous efforts in minimizing the corrosion loss by adopting various strategies depending on the application areas [1]. Various acidic compositions are used to remove corrosion products, scales, or chalky deposits from the MS surface [2–5]. However, the used acidic medium also attacks the bare MS surface resulting in a reduction in materials strength. The effective remedy for this problem is the use of inhibitors. A recent trend of inhibitor is to explore environmentally friendly, non-toxic, and renewal component of plant sources [4, 6–8]. Plant sources contain large size organic molecules having active centers containing heteroatoms like N, S, O, and P in conjugation with multiple bonds or aromatic rings [9]. Such electron-releasing centers do a strong interaction with the MS surface to protect from aggressive corrosion medium.

Alkaloids containing phytochemicals present in plant extract are mainly responsible for corrosion inhibitive action. The common ways to characterize the inhibitive behavior of the plant extracts are to make weight loss and electrochemical polarization measurements [3, 7, 8, 10]. The effects of parameters like concentration of inhibitor, adsorption time, and temperature are found to be the prime focus of most studies.

In the recent past, plenty of plant sources have been studied as corrosion inhibitors for MS corrosion in acidic medium, and the inhibitive ability of their extracts have been found to be satisfactory to excellent [4, 6–26]. However, a primary concern for such inhibitors is their thermal stability, in most cases, desorption of the inhibitor molecules occurs at around 45°C (318 K), and inhibition efficiency drops below 40% [4, 8, 12]. As a matter of fact, this limits the applicability of the plant extracts at elevated temperature, which is necessary to remove the oxide layer or scale at shorter immersion time, and therefore, it requires a slightly elevated temperature, such as 50-60°C [5]. The thermodynamic calculations have shown that most of the plant extracts act as inhibitors due to mixed adsorption on metal surface involving both physical and chemical adsorption [8–10, 13–15]. Formation of coordinate covalent bond is attributed to the transfer of lone pair of electrons of heteroatoms or π electrons present in inhibitor molecules to vacant d-orbital of metal. The pairing efficiency of the molecule present in the plant extract as corrosion inhibitors depends upon the stability of formed chelate, corrosion medium, and possible steric effects [2, 4, 27].

In this study, we report the corrosion inhibition efficiency (*IE*) of high altitude (altitude: 1511 m) plant *Berberis aristata* of Nepalese origin. Nepal is rich in high altitude endemic plants, and many of them have been investigated as corrosion inhibitors for MS in acidic medium [28–33]. *Berberis aristata* is widely distributed from the northern Himalayan region to Sri Lanka, Bhutan, and hilly areas of Nepal. The main chemical constituent of this plant is

berberine. Berberine extracted from *coptis chinesis* has been reported as an effective inhibitor for MS and galvanized steels in acidic medium with temperature stability up to 45ºC [34, 35].

Similarly, berberine in *Mahonia neplensis* was found as mostly responsible for producing excellent inhibition efficiency for MS in acidic medium [36]. This research also showed the *IE* dominated by chemical adsorption and thermal stability up to 55°C. The stem extract of *Berberis aristata* chosen in this study is never tested for corrosion inhibition purpose to date. Therefore, the methanolic extract of *Berberis aristata* was evaluated as a highly efficient, thermally stable, and eco-friendly corrosion inhibitor for MS in acidic medium by electrochemical and gravimetric methods. The prime focus of this research was to analyze the effect of temperature, plant extract concentration, and adsorption time. Electrochemical evidences were complimented by estimating thermodynamic parameters of adsorption.

2. EXPERIMENTAL

2.1. Solution and specimen preparation

The stem of *Berberis aristata*, collected from Sipadol (latitude: 27º38'6.2" N, longitude: 85º25'58.7" E and altitude: 1511 m), Nepal were washed with distilled water, cut into smaller pieces and dried in the shade for one month. It was ground into a fine powder, dipped in methanol, shaken occasionally, and macerated for 72 hours at room temperature. After that, the supernatant liquid was collected by repeated filtration until a clear supernatant liquid, which was concentrated using IKA RV-10 digital rotary evaporator. The suspension was further dried using a water bath to obtain a solid residue, which is *Berberis aristata* extract (BAE). 1.0 g of BAE was dissolved in 1000 mL of warm 1.0 M H_2SO_4 to prepare a stock solution (1000 ppm), and the undissolved residue was discarded by filtration. The stock solution was further diluted with 1.0 M H_2SO_4 to prepare 800, 600, 400, and 200 ppm solutions.

A flat sheet of commercial mild steel (MS) available in the local market of Nepal was used in this study. The MS sample of dimensions of 3.25 cm×3.25 cm×0.15 cm and 2 cm×2 cm×0.15 cm were used for gravimetric and electrochemical experiments, respectively. Each sample was mechanically polished with silicon carbide (SiC) paper till #1200 grit size. The abraded samples were cleaned ultrasonically with anhydrous ethanol for 15 min to remove residual particles, dried with air blower, and stored in a desiccator.

2.2. Characterization of extract and metal surface

A Fourier transform infrared (FTIR) spectrum in attenuated total reflectance (ATR) mode of the BAE was recorded using a Shimadzu FTIR spectrophotometer. The obtained spectra were analyzed to ensure the presence of different functional groups in the BAE extract. A Bio-Logic M470 Ac-SECM scanning electron microscope (SEM) in conjugation with an energy dispersive X-ray (EDX) was used to observe the morphological changes of MS surface

immersed in 1.0 M H_2SO_4 and 1.0 M H_2SO_4+ BAE for 24 h. The surface analyses of the MS sample were performed at three different locations to ensure reproducibility. Similarly, EDX analysis was carried out employing a beam of accelerating voltage of 15 KV for elemental analysis.

2.3. Electrochemical measurements

Electrochemical measurements involved open circuit potential (OCP), potentiodynamic polarization and electrochemical impedance spectroscopy (EIS) measurements in different concentrations of BAE. A gamry reference 600 potentiostat was used to perform these measurements. A three-electrode cylindrical glass cell with a saturated calomel electrode (SCE) as a reference electrode and a platinum wire as a counter electrode were used. The potential value mentioned hereafter is referred to as SCE. OCP was measured for 20 min to let the MS sample attain a steady-state condition before running potentiodynamic polarization. The polarization was started from a cathodic potential limit of -0.30 V vs. OCP to anodic limit of +0.30 V vs. OCP at a scan rate of 0.5 mV/s. Corrosion potential (E_{corr}), corrosion current (I_{corr}), and Tafel slopes were estimated to evaluate the *IE* of the BAE on MS corrosion in 1.0 M H_2SO_4 with the following equation (1) [10],

$$IE\% = \left(1 - \frac{I_{corr}}{I_{corr}^0}\right) \times 100\% \qquad (1)$$

where corrosion current densities with and without inhibitor are I_{corr} and I_{corr}^0, respectively.

For *EIS* measurements, a sinusoidal voltage of 10 mV peak to peak at frequencies between 100 kHz to 0.01 Hz was applied at OCP. A simple Randles circuit consisting of a single time constant was used to fit the data. The R_{ct} value thus obtained was used to estimate the *IE* by the equation (2) [10],

$$IE\% = \left(1 - \frac{R_{ct}^0}{R_{ct}}\right) \times 100\% \qquad (2)$$

where charge transfer resistances with and without inhibitor are R_{ct} and R_{ct}^0, respectively.

2.4. Gravimetric measurements

Gravimetric analyses were carried out with triplicates samples to study the effect of time, concentration, and temperature. Weight of the clean MS sample was taken before and after corrosion in 1.0 M H_2SO_4 solution containing different amounts of BAE. The sample was thoroughly rinsed in the running distilled water after each immersion measurements, dried with compressed air, and preserved in a desiccator. An Ohaus E1RR80 analytical balance was used to take the weight of samples before and after immersion. The measurement temperature was varied from 298 to 338 at 10 K interval, and the temperature-control was achieved by a Clifton water bath (NE2-4D). From the temperature effect, the thermodynamic parameters and

adsorption isotherms were calculated. The concentration of BAE solution used were 1000, 800, 600, 400, and 200 ppm. The effect of time on corrosion inhibition efficiency of BAE was estimated at 1000 ppm of BAE.

The equation (3) was used to calculate the corrosion rate (*CR*) of MS sample in each set of experiment [10]:

$$CR = \frac{87.6W}{AtD} \qquad (3)$$

where *W* is weight loss (mg), *A* is the surface area (cm^2), *t* = time of immersion (h) and *D* is the density of the MS sample (g/cm^3)

The inhibition efficiency (*IE*) and surface coverage (*θ*) were calculated by equations (4) and (5), respectively [10]:

$$IE\% = \left(1 - \frac{CR_2}{CR_1}\right) \times 100 \qquad (4)$$

where, *CR$_1$* and *CR$_2$* are the corrosion rates in the absence and presence of inhibitor, respectively.

$$\theta = \left(1 - \frac{W_2}{W_1}\right) \qquad (5)$$

Where, *W$_1$* and *W$_2$* are the weight loss in the absence and presence of inhibitor, respectively.

3. RESULTS AND DISCUSSION

3.1. ATR-FTIR analysis

Fig. 1a shows the ATR-FTIR spectra of the BAE extract with representative functional groups. Broadband in the range of 3360 cm^{-1} to 3209 cm^{-1} is attributed to O-H stretching of alcohol, phenol, carbohydrate, and N-H stretching of amine. A band at 2912 cm^{-1} is due to C-H stretching of alkane while the band at 1650 cm^{-1} represents C=C stretching, C=N stretching of imine or oxime, C=O stretching of amide or δ-lactum and N-H bending of amine. A sharp band at 1570 cm^{-1} is associated with aromatic C=C bending and N-H bending of amine. Similarly, the absorption band at 1435 cm^{-1} is due to O-H bending of carboxylic acid, and a sharp peak at 1384 cm^{-1} is for O-H bending of alcohol, phenol, and C-H bending of gem dimethyl or aldehyde. A band at 1284 cm^{-1} is ascribed to C-N stretching of aromatic amine which is further supported by a sharp peak at 1037 cm^{-1}. The absorption band at 1200 cm^{-1} is attributed to C-O stretching of aromatic ether, 3° alcohol, ester, C-N stretching of amine, and band at 1103 cm^{-1} is related to C-O stretching of 2° alcohols, ether, C-N stretching of amine. There is again a band at 987 cm^{-1} due to C=C bending of the alkene. These absorptions bands divulge that extract contains functionalities like alcohol, phenol, amine, ether, carboxylic acid,

carbohydrate with aromatic rings. Aromatic rings with heteroatoms like N, O make the BAE extract as a promising candidate for corrosion inhibitor of MS[16]. The major compounds in the methanolic extract of Berberis aristata are Berberine, Jatrorrhizine, 7,8-dihydro-8-hydroxy berberine, Berbamine, Oxyberberine, Pakistanamine, as shown in Fig. 1b[37–39].
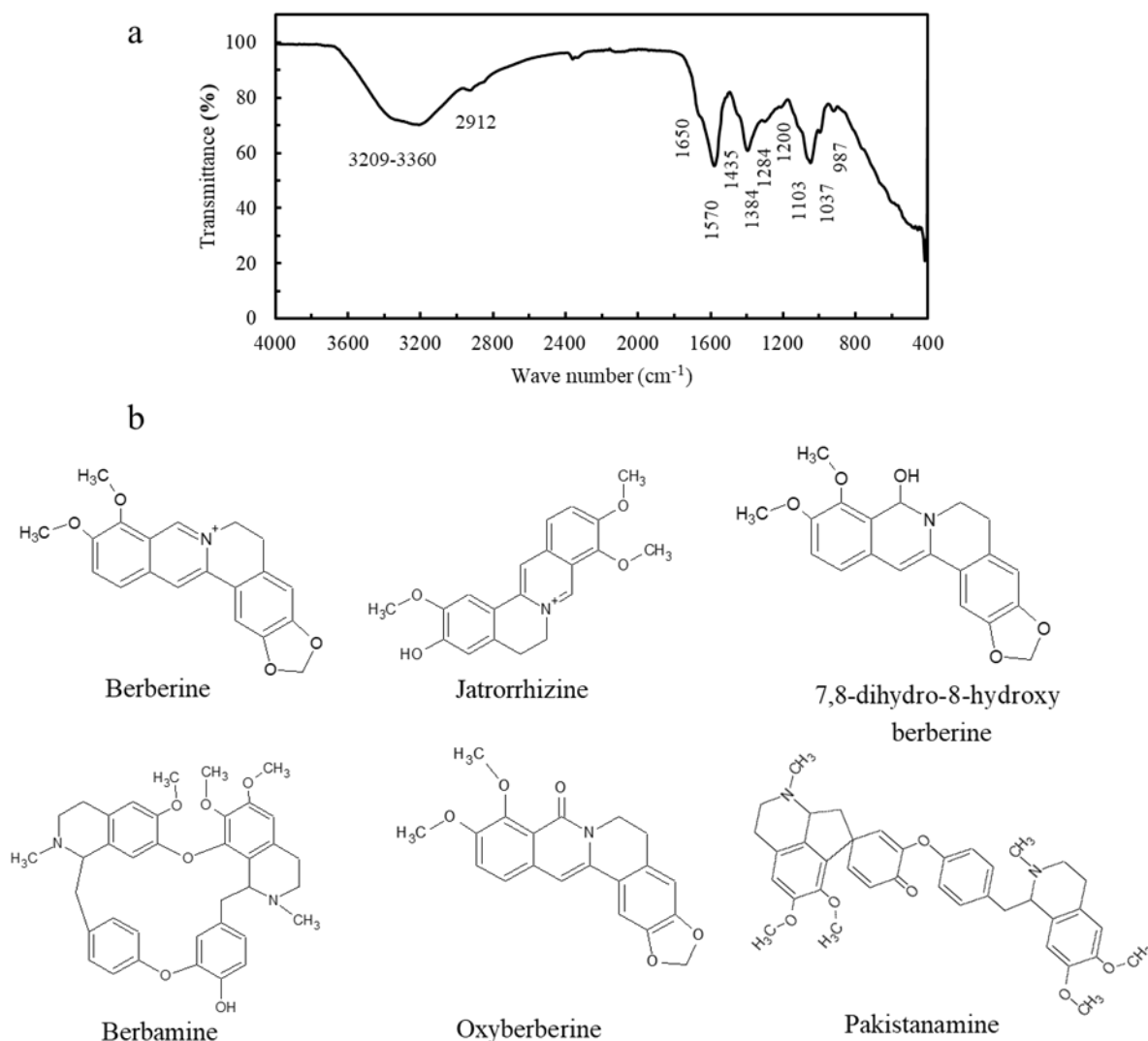
Fig. 1. a) FTIR spectra of the extract of *Berberis aristata*, b) Structure of a few compounds isolated from methanol extract of *Berberis aristata*

3.2. Electrochemical measurements

Fig. 2a shows the variation of OCP of MS in 1.0 M H_2SO_4 containing different amounts of BAE. There is a negligible change of OCP with BAE solution as compared to 1.0 M H_2SO_4 solution. This phenomenon shows that the BAE acts as a mixed type of inhibitor [17]. The marginal shift of OCP towards positive value is due to the adsorption of molecules present in BAE.
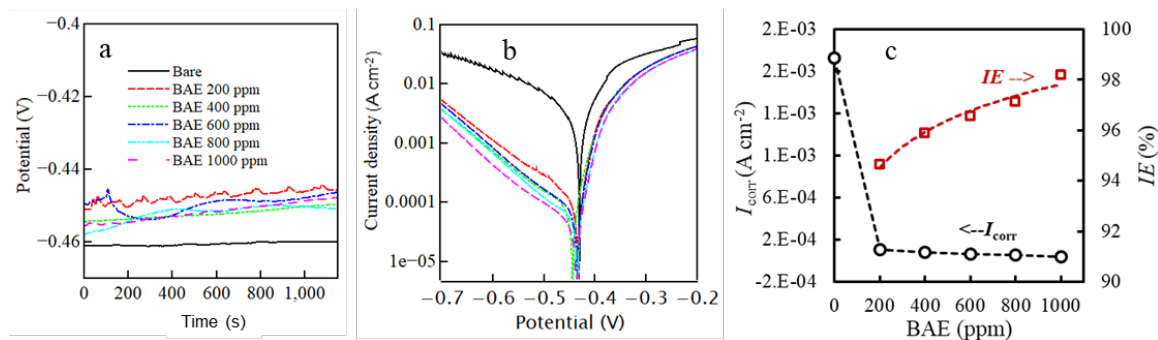
Fig. 2. a) Variation of OCP b) Polarization curve of MS sample in 1.0 M H₂SO₄ with different concentrations of BAE. c) the variation of I$_{corr}$ and IE with the concentration of BAE

The potentiodynamic polarization curves presented in Fig. 2b shows a significant suppression of cathodic current with the addition of BAE. The cathodic and anodic Tafel slopes remain in the range of 0.114 V/decade and 0.028 V/decade, respectively. These values are typical for hydrogen evolution and Fe-dissolution reactions [40].

Fig. 2c shows the variation of I_{corr} with the concentration of BAE and corresponding *IE*. It can be seen that a 1000 ppm BAE solution lowered the I_{corr} value by 55 times, enlisting an *IE* of 98.18%. The lowest concentration of the BAE, 200 ppm, also significantly suppressed the I_{corr} by about 19 times and producing an *IE* of approximately 95%, which is an excellent efficiency shown by a lower concentration of the extract [9, 18, 19]. These values of *IE* indicate that BAE by adsorbing effectively on the MS surface acts as an excellent inhibitor for corrosion protection of MS in acidic medium. Adsorption might be enhanced due to the synergistic effect of different organic compounds present in the BAE, which will be discussed further in a later section.

EIS was also used to study the effect of BAE on steady-state corrosion behavior of MS in 1.0 M H₂SO₄ at OCP in a wide range of frequencies. Fig. 3a and 3b show the Nyquist and Bode phase plots at various concentrations of BAE. The symbols represent the measured data, and solid lines represent the fitting data using Z-View (3.1c version) software using a simple equivalent circuit, as shown in Fig. 3c.

A similar shape of EIS plots in the presence of BAE inhibitor of different concentrations implies a single relaxation process with similar corrosion mechanisms as the bare counterparts. High-frequency dispersion in the capacitive loop is typical of solid electrodes following surface roughness [41]. Furthermore, non-homogeneity of structural or interfacial origin prevalent in the adsorption processes also contributes to high-frequency dispersion [41]. The presence of inductive loop at low-frequency region, whose diameter increases with the concentration of BAE, is indicative of the relaxation process associated with adsorption-desorption of inhibitor molecules on the electrode surface accompanied by re-dissolution of the inhibited surface. It may be due to the consequence of the layer stabilization by intermediate products on electrode surface such as $[FeSO_4^{-2}]_{ads}, [FeOH]_{ads}^-, [FeH]_{ads}^+$ involving inhibitor molecules. The effect of

adsorption of inhibitor molecules of BAE on MS surface is reflected in the Bode-phase plot. The adsorption of BAE has significantly increased the phase angle.
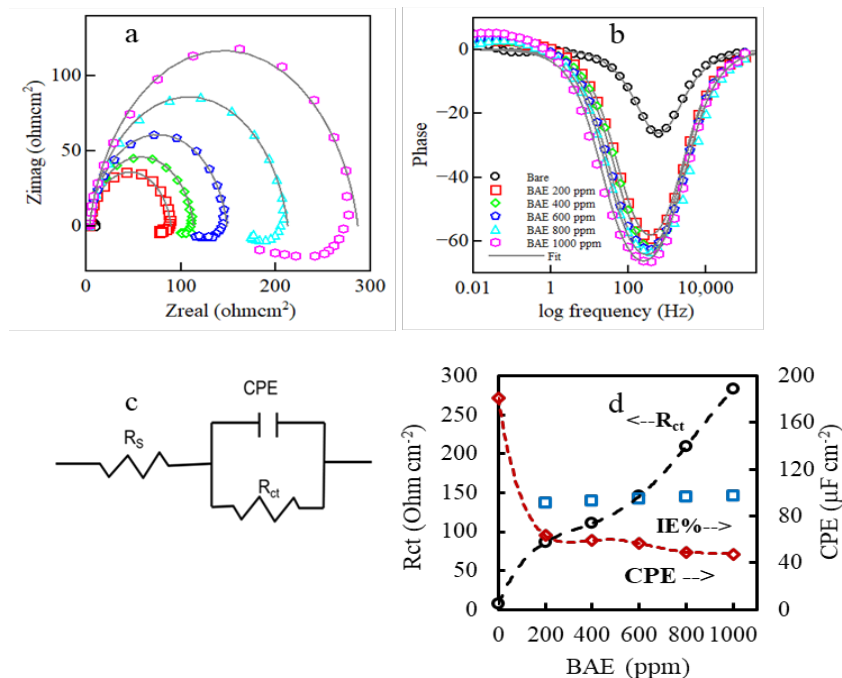
Fig. 3. a) Nyquist plots b) Bode phase plots of phase angle vs. frequency for MS in 1.0 M H_2SO_4 with BAE of different concentrations c) The equivalent circuit model used to fit the impedance spectra. d) The change of R_{ct}, C_{dl} and IE with concentration

Fig. 3d shows the variation of R_{ct} and CPE values estimated from fitting the Nyquist plot in Fig. 3a. There is a gradual increase of R_{ct} with the concentration of BAE due to more considerable surface coverage as more inhibitor molecules are available. Oppositely, the CPE value drastically decreased with the addition of BAE and almost remains constant at higher concentrations. The decrease of CPE with BAE is attributed to decrease in the local dielectric constant of the double-layer with an increase in the thickness of the electric double layer. This might be due to the large size of the inhibitor molecule, which gradually replaces water molecules. The IE estimated from the R_{ct} values is also depicted in Fig. 3d, which shows values above 92% at 200 ppm to 98% at 1000 ppm. This again indicates that the BAE acts as a promising inhibitor for the corrosion protection of MS in acidic medium.

3.3. Gravimetric Measurement

Gravimetry was used to study the effect of long time immersion of MS samples in BAE acidic solutions. Fig. 4a shows the results of gravimetric measurements in 1000 ppm BAE solution for 0.25 h, 0.75 h, 1.5 h, 3 h, 6 h, 9 h, 12 h, and 24 h at 298 K and the corresponding *IE* calculated from the obtained results. The plot implies that the corrosion of MS is significantly inhibited by the addition of BAE as an inhibitor, and inhibition increases with

time, reaching a value of approximately 97.0% after 24 h of immersion in 1.0 M H_2SO_4 solution. The result is clear evidence that BAE is effective and efficient inhibitor acting promptly by adsorbing on MS surface, thereby producing an *IE* of above 90% in just 0.25 h after immersion in acidic solution. Such a fast inhibition of corrosion is essential for practical applications of the inhibitor[5].
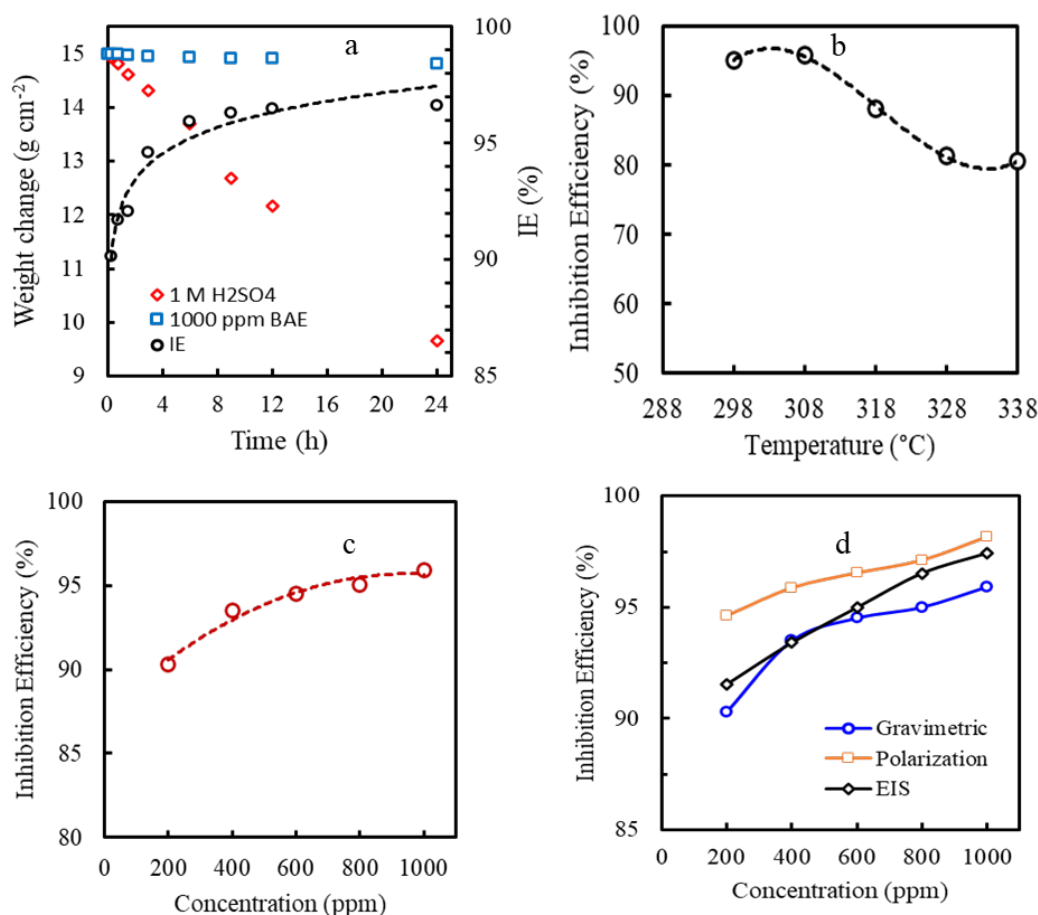
Fig. 4. a) Variation in weight of MS sample immersed in the presence and absence of BAE together with the variation of *IE* with immersion times. Variation of inhibition efficiency of BAE on mild steel surface at b) different temperatures, c) different concentrations and d) from different methods

The stability of barrier film formed due to adsorption of inhibitor on MS surface as well as activation parameters of the corrosion process of MS in acidic media was studied by gravimetric at various temperatures (298 K, 308 K, 318 K, 328 K, 338 K) for 6 h in 1000 ppm BAE solution. The effect of temperature on the corrosion rate and inhibition efficiency is shown in table 1 and represented in Fig. 4b. The *IE* remains the same till 308 K, and after that decreases marginally and stays constant at 80% after 12 h. This result is very encouraging for plant extracts as a corrosion inhibitor as in most cases the *IE* has been reported to fall below

40% at such temperature [4, 11, 12]. Such a higher *IE* at 338 K (65 ˚C) can be beneficial for other applications as well, such as for removing corrosion products for weight loss estimation [5]. Similarly, this will allow for faster removal of scales and oxide layers in the industrial process used for surface finish. Berberine extracted from *Coptis chinesis,* though showed similar *IE* to this study, but temperature stability was not like BAE [34, 35]. Therefore, isolation of the various components of BAE should be done to understand the higher temperature stability of the extract of *Berberis aristata*. The study should clarify the desorption characteristics of various components of BAE at higher temperatures.

Table 1: Corrosion rate of mild steel and inhibition efficiency of BAE for mild steel corrosion at various temperatures.

Temperature (K)	Corrosion Rate (mg/cm^{2}h)		Inhibition Efficiency (*IE*) (%)
	Only acid	Acid with inhibitor	
298	74.87	3.65	95.13
308	129.21	5.27	95.92
318	199.99	23.75	88.12
328	273.77	50.94	81.39
338	386.51	75.27	80.53

The effect of BAE concentrations on *IE* is shown in Fig. 4c. The MS sample was immersed in several BAE solutions for 6 h at 298 K. The effectiveness of the BAE can be seen from the figure, where 200 ppm of the extract is enough to inhibit with the corrosion of MS by 90.32%, and maximum *IE* reaches a value of 96.0% at 1000 ppm. There are not many plant extracts giving in *IE* of 90% at 200 ppm [9, 18, 19]. An increase in *IE* with the concentration of extract can be ascribed to the more surface coverage of MS by the extract molecules. The result is in agreement with electrochemical tests such as potentiodynamic polarization and EIS. A comparison of inhibition efficiency obtained by different methods is shown in Fig. 4d, showing similar *IE* by all the methods.

3.4. Adsorption isotherm

Adsorption isotherm of BAE on MS is necessary to understand the interaction degree between inhibitor molecules and MS surface. A spontaneous adsorption of inhibitor molecules is feasible if the interaction energy between the molecules and the MS surface is higher than that of water molecules and MS surface. Adsorption depends upon chemical composition, the molecular structure of inhibitor, temperature, and the electrochemical potential at the metal/solution interface. In the process, the solvent water molecules could also adsorb-desorb at the metal/solution interface. So, this adsorption can be considered as a quasi-substitution

process between the inhibitor molecules in aqueous phase [org(sol)] and water molecules at the electrode surface [$H_2O(ads)$]:

$$Org(sol) + nH_2O(ads) \longrightarrow Org(ads) + nH_2O(sol)$$
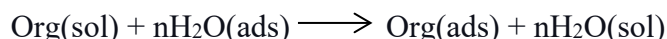
where, n is the number of water molecules replaced by one inhibitor molecule.

The degree of surface coverage (θ) obtained by the gravimetric method was plotted as a function of inhibitor concentration to evaluate the best isotherm that fits the data obtained in the present study. As for the inhibitor concentration used for fitting the suitable adsorption model, an average molar concentration of few important compounds listed in Fig. 1(b), which plays a vital role in inhibition, is used [8]. Several adsorption isotherms, such as Langmuir, Tempking, Freundlich, El-Awady, were tested to describe the adsorption behavior of inhibitor, in which best fit was obtained in Langmuir adsorption isotherm. A plot of C_{inh} against C_{inh}/θ in Fig. 5 shows a straight line with values of linear correlation coefficient (R^2) and slope equal to about 1. Little deviation of slope from unity can be attributed to some interactions between adsorbed molecules on MS surface, which may be mutual attraction or repulsion between different functional groups of molecules or preferential adsorption of molecules at the cathodic and anodic site[17,41]. According to Langmuir's assumption, adsorption of inhibitor molecules on MS surface in the present study leads to monolayer formation where adsorbate molecules do not interact with each other.
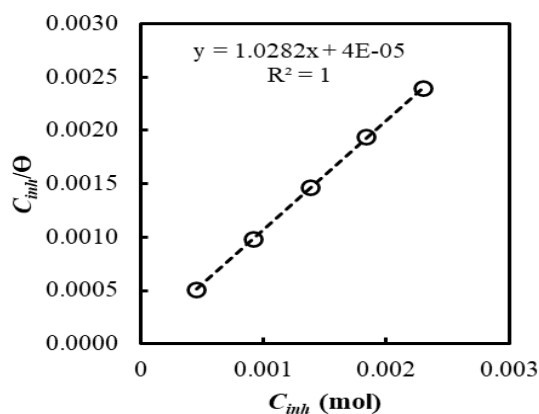
Fig. 5. Langmuir adsorption isotherm plot for mild steel in 1.0 M H_2SO_4 with different concentrations of BAE as the average molar concentration of some major compounds in BAE

Adsorption isotherm given by Langmuir is given in equation (6) [4].

$$\frac{C_{inh}}{\theta} = \frac{1}{K_{ads}} + C_{inh} \qquad (6)$$

Value of adsorption constant (K_{ads}) can be obtained from the slope of Langmuir adsorption isotherm plot in Fig. 5 and this value can be used to compute the value of free energy of adsorption (ΔG^o) according to equation (7) [10]:

$$\Delta G^o = -\text{RT} \ln(55.5 K_{ads}) \tag{7}$$

where, R is the universal gas constant (8.314J/mol K), and 55.5 is the concentration of water in solution in mol/L. The calculated value of ΔG^o according to relation (7) is -35.05 KJ/mol. A significant negative value of ΔG_{ads}^o indicates that adsorption of BAE on MS surface is spontaneous with the formation of a highly stable adsorbed layer [10, 42]. Generally, the value of ΔG^o less than or around -20 KJ/mol is associated with physisorption, and more than or around -40 KJ/mol is associated with chemisorption. Since the calculated value ΔG^o is more than the intermediate value, it can be concluded that adsorption is mainly dominated by chemisorption [10, 42]. The adsorption of inhibitors molecules is due to the electrostatic interaction between charged BAE molecules and charged MS surface with replacement of water molecules from the MS surface. This is further followed by chemisorption with the formation of a coordinate type of bond due to charge transfer from organic molecule to vacant d-orbital of Fe [10].

3.5. Calculation of activation energy and thermodynamic parameters

Corrosion rate depends upon the temperature and temperature dependency is given by Arrhenius equation (8) [4]:

$$\log(\text{CR}) = \log\text{A} - \frac{E_a}{2.303\,RT} \tag{8}$$

where E_a is the activation energy, A is the Arrhenius pre-exponential constant, T is the absolute temperature. From the Arrhenius plot in Fig. 6a, the value of E_a is calculated and tabulated in table 2. A significant increase in E_a with the addition of BAE reflects a strong adsorption of inhibitor molecules on the metal surface [20]. The literature values of some of the plant extracts show the E_a value in the range of 40 KJ/mol [8, 10, 14, 20, 21]. Therefore, it can be plausibly assumed that higher thermal stability of BAE is due to the higher energy of activation of molecules in BAE. However, as mentioned above, it is necessary to isolate the various compounds in BAE and check the *IE* of individual molecules so that higher thermal stability of BAE can be explained.
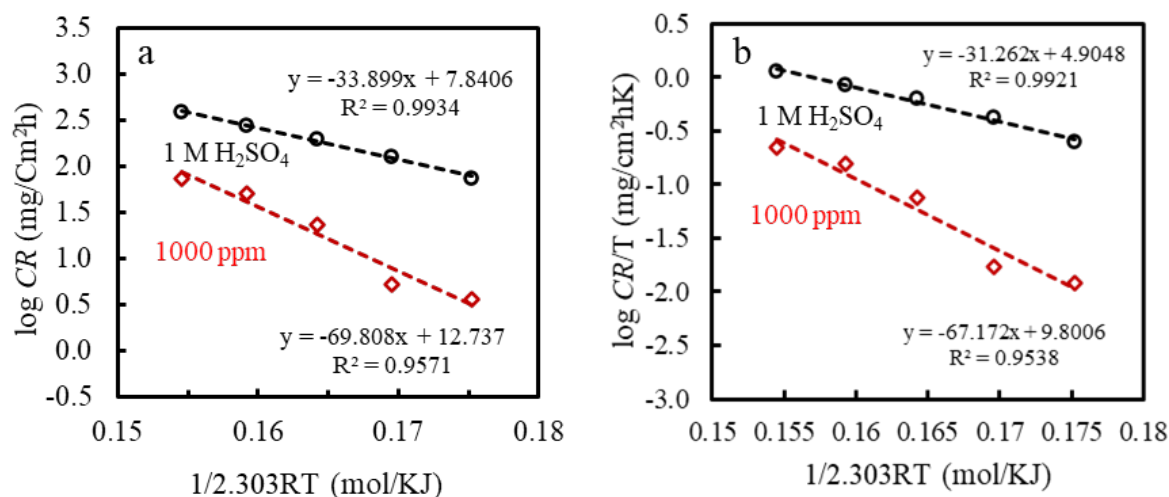
Fig. 6. a) Arrhenius plot for mild steel in 1.0 M H₂SO₄ with and without BAE, b) Transition state plot for mild steel in 1.0 M H₂SO₄ with and without BAE

The change in entropy and enthalpy of the adsorption can be calculated from transition state equation (9), where the slope of line obtained by plotting log(*CR/T*) vs. 1/2.303*RT* is enthalpy and entropy can be calculated from intercept [4]:

$$\log\left(\frac{CR}{T}\right) = \left[\log\left(\frac{R}{hN}\right) + \left(\frac{\Delta S^*}{2.303R}\right) - \frac{\Delta H^*}{2.303\,RT}\right] \tag{9}$$

where *h* is plank's constant, 6.6261×10^{-34} Js and *N* is the Avogadro's number, 6.0225×10^{23} mol^{-1}.

The values of Δ*H** and Δ*S** for acid without and with inhibitor are compared in table 2. An intermediate value of Δ*H** (67.17 KJ/mol) reflects a mixed type of adsorption of BAE molecules involving physisorption and chemisorption[22]. In addition, the positive and relatively more tremendous value of Δ*H** implies the control of corrosion by the kinetic factors. Similarly, the higher value of *Ea* than that of *ΔH** indicates a decrease in the total reaction volume due to the involvement of a gaseous reaction, merely the hydrogen evolution reactions[4]. The difference in the value of *Ea* and *ΔH** is nearly equal to *RT*, which divulges that the corrosion process is unimolecular.

The shift of Δ*S** towards positive value by the addition of BAE indicates an increase in disorder of the system on going from reactant to activated complex. This behavior can be explained due to the replacement of water molecules during the BAE adsorption on the metal surface [20]. However, it is not common to get such a significant increase in *ΔS** value with the addition of plant extracts, and many plant extracts have shown a lower change in *ΔS** value [16, 23–25]. This again needs to be investigated further so that higher thermal stability of BAE can be understood and more such inhibitor molecules can be designed or isolated.

Table 2. Activation parameters of the dissolution of mild steel in 1.0 M H_2SO_4 in the presence of 1000 ppm concentration

Electrolyte	Ea (KJ/mol)	ΔH (KJ/mol)	Ea-ΔH	ΔS (J/molK)
1.0 M H_2SO_4	33.9	31.26	2.64	–103.66
Acid with inhibitor (1000 ppm)	69.81	67.17	2.64	–9.93
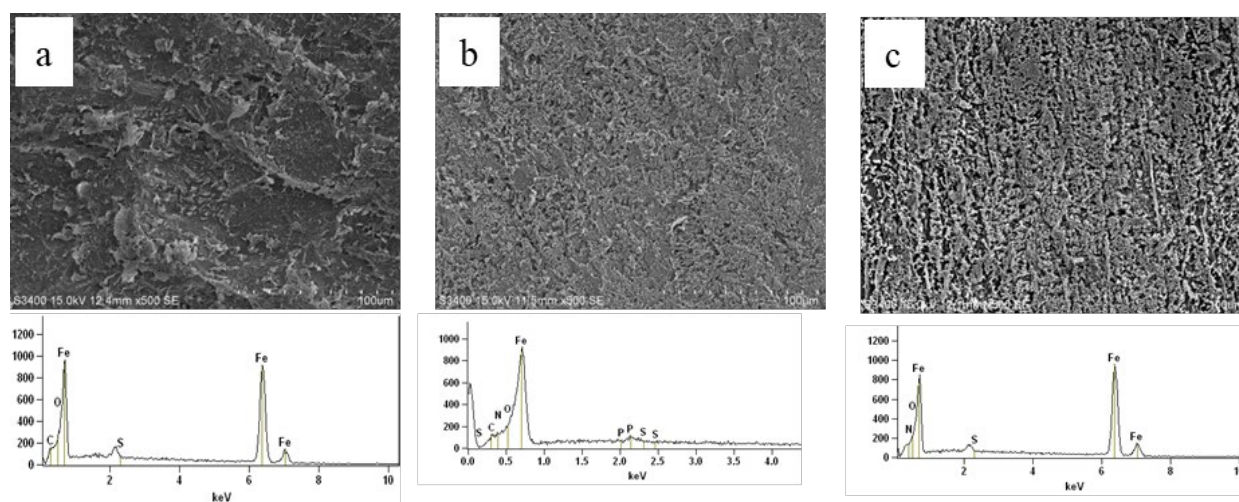
Fig. 7. SEM images and corresponding EDX spectra of mild steel coupons after 24 hrs immersion in (a) 1.0 M H_2SO_4 (b) 400 ppm extract solution in 1.0 M H_2SO_4 (c) 1000 ppm extract solution in 1.0 M H_2SO_4

3.6. Surface analysis

SEM and EDX measurements were carried out to observe the surface morphological changes and presence of heteroelements on the MS surface after 24 h immersion in the BAE solutions. Fig. 7 shows some severe surface damage with deep furrows, and large cracks on the sample immersed in acid. These cracks and furrows are not seen in the surface immersed in acid with BAE. It displays a relatively smooth surface with the formation of a protective film. EDX shows the amount of nitrogen increased on the BAE covered surface, which indicates the molecular presence of nitrogen containing species in BAE.

3.7. Mechanism of inhibition

The molecular adsorption on the MS surface depends on the surface charge, chemical structure, dipole moment of inhibitor molecules, and the role of additional ions. Extract of *Berberis aristata* contains large size aromatic organic molecules with heteroatoms; prominent among them are berberine family molecules. These molecules can be adsorbed on the metal surface and inhibit corrosion either by physical adsorption due to electrostatic force of attraction between the charged metal surface and inhibitor molecules or by chemical

adsorption due to the sharing of π-electrons or lone pair of electrons of heteroatoms. These features will be further supported by electron-releasing centers such as the methyl group. Thermodynamic parameters such as the free energy of adsorption (-35.05 KJ/mol) and energy of activation (69.81 KJ/mol) point to the chemisorption dominated behavior of BAE on the MS.

BAE contains berberine family molecules with quaternary nitrogen with a positive charge. In acidic medium, amino nitrogen, phenolic or ethereal oxygen gets protonated. So, inhibitor molecules will be positively charged. The OCP of MS in BAE is measured around -0.44 V, which is positive than the potential of zero charge (PZC) of MS in sulfate solution [43]. When the value of PZC is less than that of OCP, the value of Antropov's rational corrosion potential becomes positive, and the net charge on MS gets positive. In such conditions, there will be electrostatic repulsion between the protonated inhibitor molecule and the metal surface. However, sulfate ions derived from H_2SO_4 are adsorbed on the metal surface due to a small degree of hydration, which results in the excessive negative charge close to the interface and favors the adsorption of positively charged protonated inhibitor molecules. Thus, inhibitor molecules get adsorbed on the metal surface through the sulfate bridge. In other words, there is a synergism between sulfate ion and inhibitor molecules for physical adsorption. This adsorption of BAE molecules will compete with adsorption of H^+ ion on the cathodic site of MS leading to suppression of cathodic hydrogen evolution.

In addition to physisorption, neutral or cationic inhibitor molecules may be adsorbed by chemisorption as well with replacement of water from MS surface by inhibitor molecules. Chemisorption is due to the interaction of the highest occupied molecular orbital (HOMO) of organic molecules with vacant d-orbital of iron to form a coordinate bond (donor-acceptor interaction). HOMO is the orbital with larger electron density, such as bonding π-orbital or lone pair of electrons. Due to electron pair on heteroatoms, the large organic molecules in BAE acts as a soft base with large polarizability accompanied with low ionization potential. The bulk metal or metal at zero oxidation state behaves as a soft acid. According to Hard and Soft Acid and Base (HSAB) theory, soft acid reacts faster and forms a strong bond with a soft base. So, stronger donor-acceptor interaction is expected between electrons of the inhibitor to the metal atom [44]. This interaction results in the accumulation of extra negative charges on the metal surface. To relieve this extra charge, electrons may be given back from 4s or 3d orbital of the metal atom to lowest unoccupied molecular orbital (LUMO) of BAE molecules to form a feedback bond. LUMO is a vacant antibonding π^* orbital of organic molecules with larger orbital density. The presence of two tertiary nitrogen centers together with electron- releasing methyl groups seems to be making the adsorption of BAE very useful.
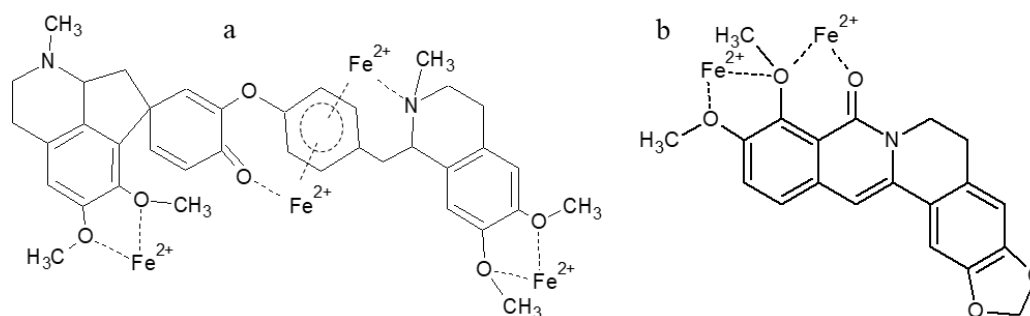
Fig. 8. Metal inhibitor chelate complex formed by iron with (a) Pakistanamine (b) Oxyberbeine

Besides, inhibition can also be explained by the chelation of Fe^{2+} with BAE molecules leading to the formation of a stable insoluble metal-inhibitor complex. After the formation of a number of such types of complex molecules, the solubility of the protective layer decreases, which suppresses the anodic metal dissolution and hence prevents the corrosion. It explains the increase in inhibition efficiency with the increase in concentration and time. The possible chelate complexes of two organic molecules are shown in Fig. 8.

Chelation inhibits the anodic reaction as follows:

$$Fe_{(s)} \quad \rightarrow \quad Fe^{2+}_{(aq)} + 2e^-$$

$$Fe^{2+}_{(aq)} + BAE_{(ads)} \quad \rightarrow \quad [Fe\text{-}BAE]^{2+}_{ads}$$
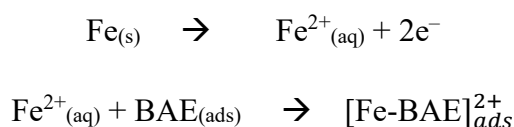
The adsorption of inhibitor molecules inhibits both anodic and cathodic reactions. Anodic dissolution is suppressed by the adsorption of sulfate ions which is shown as follows [26]:

$$H_2SO_4 \quad \rightarrow \quad H^+ + SO_4^{--}$$

$$Fe + SO_4^{--} \quad \rightarrow \quad (FeSO_4^{--})_{ads}$$

$$(FeSO_4^{--})_{ads} \quad \rightarrow \quad (FeSO_4^-)_{ads} + e^-$$

$$(FeSO_4^-)_{ads} \quad \rightarrow \quad (FeSO_4)_{ads} + e^-$$

$$(FeSO_4)_{ads} \quad \rightarrow \quad Fe^{++} + SO_4^{--}$$
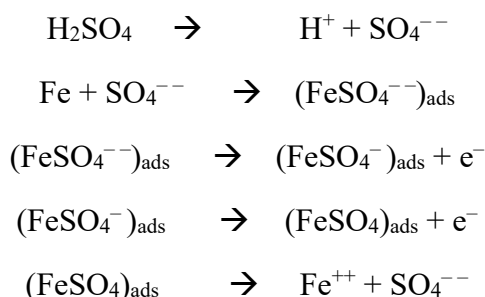
The cathodic hydrogen evolution is suppressed due to adsorption as:

$$BAE + H^+ \quad \rightarrow \quad (BAE)H^+ \text{ (protonation of inhibitor molecules)}$$

$$Fe + (BAE)H^+ \quad \rightarrow \quad [Fe\text{-}(BAE)H^+]_{ads} \text{ (adsorption of protonated BAE molecules)}$$

$$[Fe\text{-}(BAE)H^+]_{ads} + e^- \quad \rightarrow \quad [Fe\text{-}(BAE)H]_{ads} \quad \text{(Reduction of protonated } H^+)$$

$$[Fe\text{-}(BAE)H]_{ads} + H^+ + e^- \quad \rightarrow \quad Fe + H_2 + BAE \quad \text{(Release of hydrogen)}$$
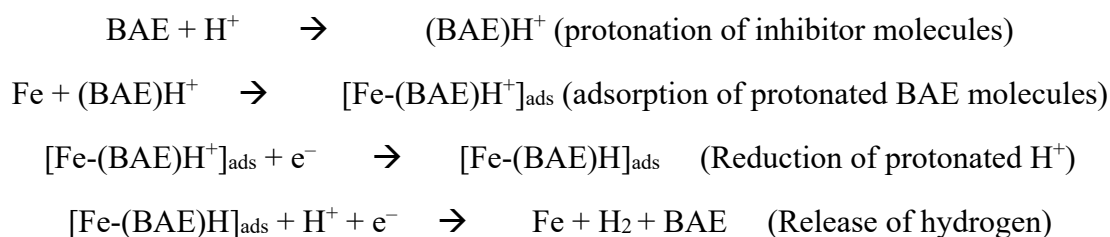
4. CONCLUSION

The methanol extract of *Berberis aristata* is found to be an effective corrosion inhibitor for MS in 1.0 M H_2SO_4. Inhibition efficiency is above 90% at 200 ppm concentration of BAE. The *IE* increases with an increase in concentration, and maximum *IE* of 98.14% is obtained for 1000 ppm solution by potentiodynamic polarization. The thermal stability of the BAE on MS surface is exceptionally high, giving an *IE* of 80% at 338 K. The BAE is found to be a highly efficient inhibitor giving 90% efficiency in 0.25 h in 1000 ppm solution. The inhibition of corrosion of MS is due to monolayer adsorption of inhibitor molecules on the metal surface, and the adsorption follows the Langmuir adsorption isotherm. Values of ΔG^o and Ea indicate the adsorption of molecules on the MS is dominated by chemical adsorption.

Meanwhile, values of ΔH^* and Ea indicate that the adsorption process is unimolecular and endothermic. Electrochemical parameters show that it is a mixed type of inhibitor which significantly suppresses the cathodic reaction. EDX and SEM analysis confirm the formation of the surface film of BAE on the MS surface and inhibit the corrosion by barrier layer action.

Acknowledgments

Conflicts of interest: The author declares no conflicts of interest.

Supplementary material: The corresponding author provides supplementary material upon a reasonable request.

REFERENCES

[1]   E. E. Oguzie, Y. Li, and F. H. Wang, Electrochimica Acta 52 (2007) 6988.

[2]   M. Murmu, S. K. Saha, N. C. Murmu, and P. Banerjee, Corros. Sci. 146 (2019) 134.

[3]   M. A. Hegazy, A. S. El-Tabei, A. H. Bedair, and M. A. Sadeq, RSC Adv. 5 (2015) 64633.

[4]   A. Ostovari, S. M. Hoseinieh, M. Peikari, S. R. Shadizadeh, and S. J. Hashemi, Corros. Sci. 51 (2009) 1935.

[5]   A. P. Yadav, F. Suzuki, A. Nishikata, and T. Tsuru, Electrochim. Acta 49 (2004) 2725.

[6]   M. Dahmani, A. Et-Touhami, S. S. Al-Deyab, B. Hammouti, and A. Bouyanzer, Int. J. Electrochem. Sci. 5 (2010) 1060.

[7]   P. Mourya, S. Banerjee, and M. M. Singh, Corros. Sci. 85 (2014) 352.

[8]   A.Y. El-Etre, Mater. Chem. Phys. 108 (2008) 278.

[9]   Y. Qiang, S. Zhang, B. Tan, and S. Chen, Corros. Sci. 133 (2018) 6.

[10] H. Cang, Z. Fei, J. Shao, W. Shi, and Q. Xu, Int. J. Electrochem. Sci. 8 (2013) 720.

[11] A.Y. El-Etre, J. Colloid Interface Sci. 314 (2007) 578.

[12] G. Choudhary, A. Sharma, R. K. Bangar, and A. Sharma, IJIRAE. 2 (2015) 112.

[13] N. Soltani, N. Tavakkoli, M. K. Kashani, and A. Mosavizadeh, Journal of Industrial and Engineering Chemistry 20 (2014) 3217.

[14] P. S. Desai, Eur. J. Pharm. Med. Res. 2 (2015) 470.

[15] N. A. Odewunmi, S. A. Umoren, Z. M. Gasem, S. A. Ganiyu, and Q. Muhammad, J. Taiwan Inst. Chem. Eng. 51 (2015) 177.

[16] S. A. Umoren, I. B. Obot, A. U. Israel, P. O. Asuquo, M. M. Solomon, U. M. Eduok, and A. P. Udoh, J. Ind. Eng. Chem. 20 (2014) 3612.

[17] N. A. Odewunmi, S. A. Umoren, and Z. M. Gasem, J. Environ. Chem. Eng. 3 (2015) 286.

[18] A. S. Fouda, G. Y. Elewady, D. Shalabi, and S. Habouba, Int. J. Innov. Res. Sci. Eng. Technol. 3 (2014) 11210.

[19] P. Muthukrishnan, B. Jeyaprabha, and P. Prakash, Int. J. Ind. Chem. 5 (2014) 1.

[20] A. Hamdy, and N. S. El-Gendy, Egypt. J. Pet. 22 (2013) 17.

[21] L. Bammou, M. Belkhaouda, R. Salghi, O. Benali, A. Zarrouk, H. Zarrok, and B. Hammouti, J. Assoc. Arab Univ. Basic Appl. Sci. 16 (2014) 83.

[22] A. A. Khadom, A. N. Abd, and N. Arif, South Afr. J. Chem. Eng. 25 (2018) 13.

[23] N. I. Kairi, and J. Kassim, Int. J. Electrochem. Sci. 8 (2013) 7138.

[24] S. B. Ulaeto, U. J. Ekpe, M. A. Chidiebere, and E. E. Oguzie, Int. J. Mater. Chem. 2 (2012) 158.

[25] A. Singh, V. K. Singh, and M. A. Quraishi, Int. J. Corr. 2010 (2010)

[26] R. Karthik, P. Muthukrishnan, A. Elangovan, and B. Jeyaprabha, Adv. Civil Eng. Mater. 3 (2014) 413.

[27] A. Aytac, U. Ozmen, and M. Kabasakaloglu, Mater. Chem. Phys. 89 (2005) 176.

[28] P. R. Shrestha, H. B. Oli, B. Thapa, Y. Chaudhary, D. K. Gupta, A. K. Das, K. B. Nakarmi, S. Singh, N. Karki, and A. P. Yadav, Eng. J. 23 (2019) 205.

[29] B. Thapa, D. K. Gupta, and A. P. Yadav, J. Nepal Chem. Soc. 40 (2019) 25.

[30] N. Karki, Y. Chaudhary, and A. P. Yadav, J. Nepal Chem. Soc. 39 (2018) 76.

[31] P. C. Lama, Y. Chaudhary, N. Karki, and A. P. Yadav, J. Nepal Chem. Soc. 34 (2016) 120.

[32] R. Lama, A. K. Das, B. Yadav, Y. Chaudhary, P. C. Lama, S. L. Shrestha, D. K. Gupta, N. Karki, and A. P. Yadav, J. Nepal Chem. Soc. 38 (2018) 48.

[33] Y. Chaudhary, N. Karki, and A. P. Yadav, J. Nepal Chem Soc. 35 (2016) 139.

[34] Y. Li, P. Zhao, Q. Liang, and B. Hou, Appl. Surf. Sci. 252 (2005) 1245.

[35] L. Na, G. Hui, Z. Peng, Z. Xin, Z. Lihua, and A. Singh, Int. J. Electrochem. Sci. 14 (2019) 1830.

[36] N. Karki.,S. Neupane, Y. Choudhary, U. Singh, and A. P. Yadav, Surf. Interfaces. (2020). https://www.journals.elsevier.com/surfaces-and-interfaces, in press.

[37] R. Thusa, and S. Mulmi, Nepal J. Biotechnol. 5 (2017) 5.

[38] V. Chander, J. S. Aswal, R. Dobhal, and D. P. Uniyal, The Journal of Phytopharmacology 6 (2017) 53.

[39] P. Taylor, V. Bajpai, A. Singh, K. R. Arya, M. Srivastava, and B. Kumar, Food Additives & Contaminants: Part A 32 (2015) 37.

[40] W. Li, X. Zhao, F. Liu, and B. Hou, Corros. Sci. 50 (2008) 3261.

[41] C. B. Verma, and M. A. Quraishi, Electrochem. Surface Anal. 3 (2014) 14601.

[42] F. Bentiss, M. Bouanis, B. Mernari, M. Traisnel, H. Vezin, and M. Lagrene, Applied Surface Sci. 253 (2007) 3696.

[43] V. Sivakumar, K. Velumani, and S. Rameshkumar, Mate. Res. 21 (2018) 1.

[44] R. Sadeghi, M. Amirnasr, S. Meghdadi, and M. Talebian, Corros. Sci. 151 (2019) 190.

Equisetum hyemale: a new candidate for green corrosion inhibitor family

N. Karki,[1,2] S. Neupane,[1]* Y. Chaudhary,[1] D.K. Gupta[1,3] and A.P. Yadav[1]*

[1]Central Department of Chemistry, Tribhuvan University, 44613, Kathmandu, Nepal
[2]Bhaktapur Multiple Campus, Tribhuvan University, 44800, Bhaktapur, Nepal
[3]Tri-Chandra Multiple Campus, Tribhuvan University, 44605, Ghantaghar, Kathmandu, Nepal
E-mail: amar2y@yahoo.com, shova_n@yahoo.com

Abstract

Plant extracts are a possible better alternative source of eco-friendly corrosion inhibitors for metallic materials. Herein, methanol extract of *Equisetum hyemale* (*EHE*) has been studied as an eco-friendly inhibitor for the corrosion protection of mild steel (MS) in 1.0 M H_2SO_4. The corrosion inhibition effects of *Equisetum hyemale* were evaluated by weight loss, potentiodynamic polarization, electrochemical impedance spectroscopy (EIS), and surface analyses. The weight loss results divulged a decrease in corrosion inhibition efficiency (*IE*) with temperature. Moreover, *IE* increased until six hours of immersion, then decreased afterward. Similarly, EIS studies showed an increase in charge transfer resistance together with a decrease in double-layer capacitance. The current density decreased with an increment of the inhibitor concentration without affecting the reaction mechanism. Surface characterization indicated the surface coverage of the MS by the phytochemicals present in the *EHE*. Thermodynamic parameters such as free energy, enthalpy, entropy of adsorption, and activation energy calculations supported a mixed type of adsorption involving both physical and chemical interactions. The molecular adsorption of the phytochemicals showed a spontaneous and consistent behavior with the Langmuir adsorption isotherm model.

Keywords: Equisetum hyemale, eco-friendly inhibitor, weight loss, potentiodynamic polarization, electrochemical impedance spectroscopy (EIS).

1. Introduction

Corrosion is a universal phenomenon responsible for the losses and failures of the structural materials. The economic losses due to corrosion account for 3–4% of GDP, of which 30–40% can be saved with proper use of corrosion expertise [1]. The metallic corrosion due to the use of acid for removing rust, scales, or chalky deposits from mild steel is a common problem in industrial process such as acid pickling, cleaning of boilers, oil well acidizing, *etc*. [2–5]. The corrosive acid solution starts to attacks at the defect or at the kink part of the

surface causing enormous a significant loss of material properties leading to failure [6]. Therefore, corrosion protection of such metallic materials from acidic atmosphere is an essential step in mitigating the corrosion loss. The use of inhibitors for mitigating corrosion of materials used in acid solution are well practiced with different levels of success [7]. Inhibitor molecules retard the rate of corrosion due to their adsorption on the metal surface, and even a small amount of inhibitor significantly suppress the rate of corrosion [8].

The factors that can define the efficiency of inhibitors are stability of formed chelate, type of corrosion medium, possible steric effects, availability of lone pairs/π-electrons, aromaticity, type of hetero elements, and interaction between *p*-orbital of inhibitor to *d*-orbital of metal [9−14]. Most effective and efficient inhibitors are natural or synthetic organic compounds [15−25], and inorganic compounds like chromate, dichromate, arsenate, *etc*. [26, 27]. Nevertheless, the environmental concerns have limited the use of these effective industrial inhibitors [28, 29]. Increasing environmental legislation and ecological awareness motivates researchers to develop eco-friendly, non-toxic, and readily available inhibitor adopting green methods [20, 22].

Natural products like essential oil from plants or crude plant extracts have been extensively studied and promoted as alternative inhibitors. These plant extracts are the rich source of naturally synthesized organic compounds, which are biodegradable, renewable, and can be extracted with low cost adopting green methods. They contain complex organic species such as alkaloids, flavonoids, polyphenol, tannins, nitrogen bases, carbohydrates, and protein as well as hydrolysis products in their composition [25]. These compounds contain heteroatoms such as nitrogen (N), oxygen (O), sulfur (S) having high electron negativity, which forms double or triple bonds in their structure with available lone pair of electrons [21]. Therefore, they have a high tendency for adsorption on the metal surface, and hence they function as a corrosion inhibitor [30−32]. Adsorption of inhibitor molecules block the active sites on the metal surface and reduce the corrosion by affecting cathodic and/or anodic reactions. Such a phenomenon also affects the ingress of aggressive species to the metal surface and alters the electrical resistance of the metal surface [33]. The different functional groups present in the extract can produce a synergistic effect in enhancing the inhibition efficiency (*IE*) [34].

There is no dearth of research reports on the plant extracts as effective corrosion inhibitors such as *Eichhornia Crassipes* [3], *Curcuma Longa* [7], *Henna* [13, 26], *Moringa Oleifera* [19], Aloes [24], Coconut [27], *Chenopodium Ambrosioides* [28], *Ginko* [29], Watermelon [30], Zallouh [31]. Nepal is blessed with large varieties of endemic high altitude plants [32]. Extract of these plants have potent to be corrosion inhibitor. There is on-going research on screening of the high-altitude plants of Nepal as a possible good source of corrosion inhibitors. The corrosion test results have shown the extract of *Artemisia vulgaris* [33], *Lanata camara* [34], *Euphorbia royleana* [35], *Pogostemon benghalesis* [36, 37], *Gaultheria fragrantisima* [38], *Berberis aristata* [39] as a good inhibitor for corrosion of mild steel (MS) in an acidic environment. The IE of these plant extracts for corrosion

protection of MS have been over 95%. The present work reports on the corrosion inhibition efficiency of the plant *Equisetum hyemale* (phylum: *Sphenophyta*, family: *Equisetaceae*, and common name: horsetail), which is one of the perennial herbs [40]. Phytochemical screening of alcoholic extract of aerial parts of the plants has shown the presence of phytochemicals like rutin, 2-(sophorosyl)-1-(4-hydroxyphenyl)ethanone, α-*D*-fructofuranose, *L*-uridine, quercetin, 5-hydroxymethylfurfural, containing some falvonol, and phenyl glycosides [41–43]. Figure 1 shows the molecular structure of these compounds. These plant extracts have not yet been tested for corrosion inhibition properties, and therefore, it is a pristine plant extract for corrosion study. This study was undertaken to evaluate the methanolic extract of *Equisetum hyemale* as an eco-friendly corrosion inhibitor for MS in 1.0 M H_2SO_4. The IE of the extract was determined using weight loss, potentiodynamic polarization, electrochemical impedance spectroscopy (EIS), and surface analyses. Effect of temperature on IE and corresponding thermodynamics parameters were used to evaluate the adsorption phenomenon.
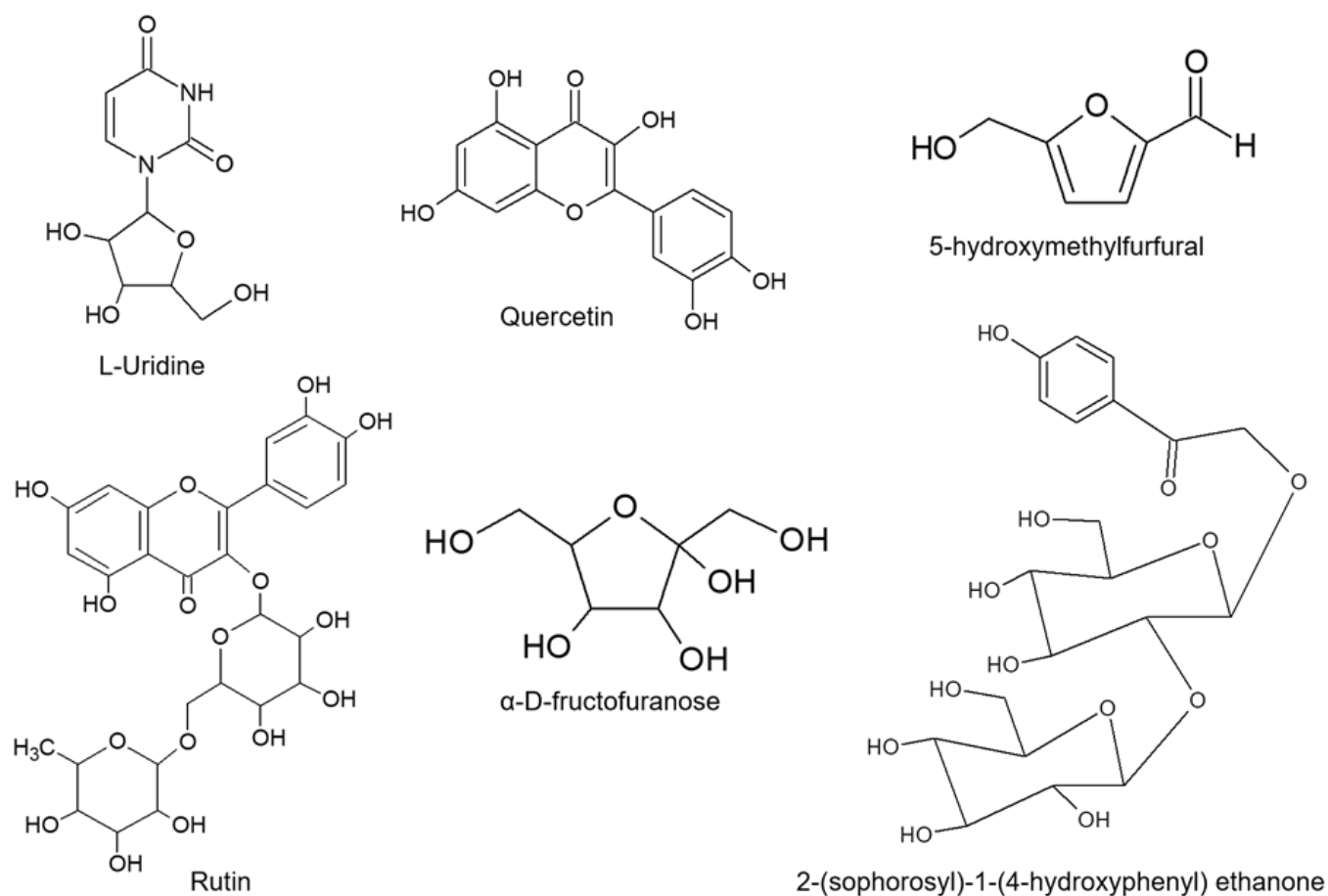
Figure 1. Structure of various compounds isolated from the alcoholic extract of *Equisetum hyemale* [41–43].

2. Experimental

2.1 Preparation of MS samples

MS samples were cut from a flat sheet collected from the local market of Nepal. The coupons of dimensions $3.25 \times 3.25 \times 0.15$ cm were design for weight loss measurements whereas $2.0 \times 2.0 \times 0.15$ cm size coupons with the exposed surface area of 0.608 cm^2 was used for electrochemical measurements. The coupons were abraded with silicon carbide (SiC) paper till #1200 grits. The abraded samples were cleaned ultrasonically in ethanol for 15 min for the removal of residual particles, washed with ethanol, and dried with compressed air.

2.2 Equisetum hyemale extract and inhibitor solution preparation

Aerial part of *Equisetum hyemale,* collected from Gundu (latitude: 27°39′2.5″N, longitude: 85°24′59.6″E and altitude: 1402 m), Bhaktapur, Nepal, was dried in the shade and pulverized into a fine powder. 200 g of powder was soaked in 1000 mL methanol for 72 h with occasional shaking followed by filtration. The process was repeated until colorless effluent was obtained. Then, the collected filtrate was initially concentrated using IKA RV-10 digital rotary evaporator. It was further dried on a water bath to get a solid residue named as *Equisetum hyemale* extract (*EHE*). 1.0 gm of *EHE* was dissolved in 1000 mL warm 1.0 M H$_2$SO$_4$. Undissolved extract residue was removed by filtration using standard filter paper. The filtrate constituted an *EHE* stock solution of 1000 ppm. It was further diluted to 800, 600, 400, and 200 ppm using 1.0 M H$_2$SO$_4$. All chemicals were of reagent grade, and laboratory-grade solvents were procured from Fisher Scientific, India.

2.3 FTIR analysis of EHE

The presence of different functional groups in *EHE* was confirmed by making Fourier transform infrared (FTIR) analysis in attenuated total reflectance (ATR) mode using a Shimadzu FTIR spectrophotometer.

2.4 Electrochemical Measurements

A Gamry reference 600 potentiostat running on Gamry framework software was used to perform electrochemical measurements. Measurements were carried out in a 300 mL test solution using a three-electrode cylindrical glass cell. The MS sample was used as a working electrode, a saturated calomel electrode (SCE) as a reference electrode and a platinum wire as an auxiliary electrode. All the potential mentioned in this paper are referred to as SCE. Before each electrochemical measurement, the MS sample was immersed in the test solution for 20 min to attain a steady-state open circuit potential (OCP). Potentiodynamic polarization was carried out in the range of ±0.3 V from OCP with a scan rate of 0.5 mV/s, and the polarization started from a cathodic limit to anodic limit. The corrosion potential (E_{corr}), corrosion current (I_{corr}), and Tafel slopes were estimated to evaluate the *IE* of the *EHE* on MS corrosion in 1.0 M H$_2$SO$_4$. The *IE* was calculated by the equation (1) [13].

$$IE\% = \frac{I_{corr}^0 - I_{corr}}{I_{corr}^0} \times 100\% \tag{1}$$

Where I_{corr} and I_{corr}^0 represent corrosion current densities with and without inhibitor, respectively.

EIS was used to measure the AC response of the MS in 1.0 M H_2SO_4 containing *EHE* of varying concentrations. A superimposing sine wave signal of 10 mV peak to peak at frequencies between 100 kHz to 0.01 Hz was applied at OCP. The response of the AC signal in terms of charge transfer resistance (R_{ct}) and double layer capacitance was analyzed by fitting the response with the help of an equivalent circuit. The R_{ct} value thus obtained was used to estimate the *IE* by the equation 2 [13]:

$$IE\% = \frac{R_{ct} - R_{ct}^0}{R_{ct}} \times 100\% \tag{2}$$

Where R_{ct} and R_{ct}^0 are charge transfer resistances with and without inhibitor, respectively.

2.5 Weight loss measurements

The weight loss measurements were used to evaluate the performance of the inhibitor, and the nature of adsorption isotherms. Two measurements were performed in a row. On the one hand, pre-weighed MS samples were immersed in 100 mL 1.0 M H_2SO_4 and 1.0 M H_2SO_4+*EHE* for different time intervals of 3, 6, 9, 12, and 24 h. A 1000 ppm *EHE* solution at RT was used as an inhibitor. The MS samples were taken out, washed thoroughly with distilled water, dried, preserved in a desiccator overnight, and weighed again. On the other hand, a series of samples immersed in 1000, 800, 600, 400, and 200 ppm *EHE* at RT for 6 h to observe the effect of the *EHE* concentration. Similarly, the effect of temperature on *IE* and thermodynamic parameters were estimated by performing measurements at 298 K, 308 K, 318 K, 328 K, and 338 K using 1000 ppm *EHE*. The immersion time was 6 h, and the temperature was adjusted by using a Clifton water bath (model no. NE2–4D).
From the above experimental setup, corrosion rate (*CR*), surface coverage (θ), and inhibition efficiency (*IE%*) determined using equations 3, 4, and 5 [24].

$$CR = \frac{87.6W}{AtD} \tag{3}$$

Where *W* is weight loss (mg) of MS sample, *A* is surface area (cm²) of the coupon, *t* is time (hours) of immersion, and *D* is density (g/mL) of MS. From the weight loss data, the geometric surface coverage (θ) of MS due to blocking action of the inhibitor can be expressed as:

$$\theta = \frac{W_1 - W_2}{W_1} \tag{4}$$

Where, W_1 and W_2 are the weight loss in the absence and presence of inhibitor, respectively. The inhibition efficiency can then be estimated as:

$$IE\% = \left(\frac{W_1 - W_2}{W_1}\right) \times 100 \qquad (5)$$

All the measurements were made in triplicate to assure the reproducibility of the results, and illustrated data are the mean values of three measurements.

2.6 Surface analysis

Scanning electron microscope (SEM, Bio-Logic M470 Ac-SECM) in conjugation with an energy dispersive spectrometer (EDX, accelerating voltage 15 kV) was used for surface study of MS surface under different experimental conditions. The MS samples were immersed in the *EHE* solutions of 400 ppm and 1000 ppm for 24 h to make the surface characterization. The SEM images of the MS samples were taken at several locations to ensure reproducibility. Similarly, EDX analysis was carried out for elemental information.

## 3. Results and Discussion

3.1 FTIR analysis of EHE

Figure 2 shows an ATR mode FTIR spectrum of crude *EHE*. The various adsorption peaks are indicative of the presence of different bonds and functional groups in the *EHE*. Broad peaks at 3367 to 3232 cm^{-1} are representative of the O–H group. A peak at 2935 is due to C–H stretching of alkane. The peak confirms the presence of C=O of amine and carboxylic acid at 1635 cm^{-1}. Similarly, peaks at 1570 and 1400 cm^{-1} are due to the presence of the C=C bond. The peaks at 1570 and 1400 cm^{-1} attributed to N–H and C–O–H bending, respectively. Another peak at 1292 cm^{-1} indicates the C–O stretching of ether, alcohol, or carboxylic acid. The C–O of polysaccharide and C–N stretching confirmed by the presence of a peak at 1026 cm^{-1}. FTIR result shows that the main constituents of plant extract contained an aromatic ring, oxygen, and nitrogen atoms as main constituents. Phytochemical studies of *Equisetum hyemale* have reported the presence of similar FTIR bands [41–43]. The presence of such functionality is a prerequisite for typical corrosion inhibitors [25]. Therefore, its effect on corrosion inhibition of MS in acidic medium has to be clarified [27].

3.2 Electrochemical measurements

OCP variation of MS samples recorded in the presence of *EHE* extract of different concentrations in 1.0 M H$_2$SO$_4$ solution with its bare counterpart is shown in Figure 3a. The result shows an increment of OCP in the beginning and attaining a steady potential after 15 min. The addition of *EHE* shifted the OCP towards positive value compared to 1.0 M H$_2$SO$_4$ solution without *EHE*. However, the shift in OCP is less than 10 mV, which proves

that the *EHE* acts as a mixed type of inhibitor [14]. The positive shift of OCP indicated the formation of an adsorb layer of *EHE* on the MS surface [44].

The inhibition effect of *EHE* was further studied by potentiodynamic polarization of MS samples in 1.0 M H_2SO_4 and 1.0 M H_2SO_4+*EHE* of different concentrations. Figure 3b represents the polarization curves in various concentrations of *EHE*. The values of corrosion current (I_{corr}) and corrosion potential (E_{corr}) were used to interpret the effect of *EHE* on inhibition of the MS corrosion in acidic solution. Table 1 summarizes the I_{corr}^0, E_{corr}^0, and *IE* values estimated form the polarization curves for various concentrations of *EHE*.
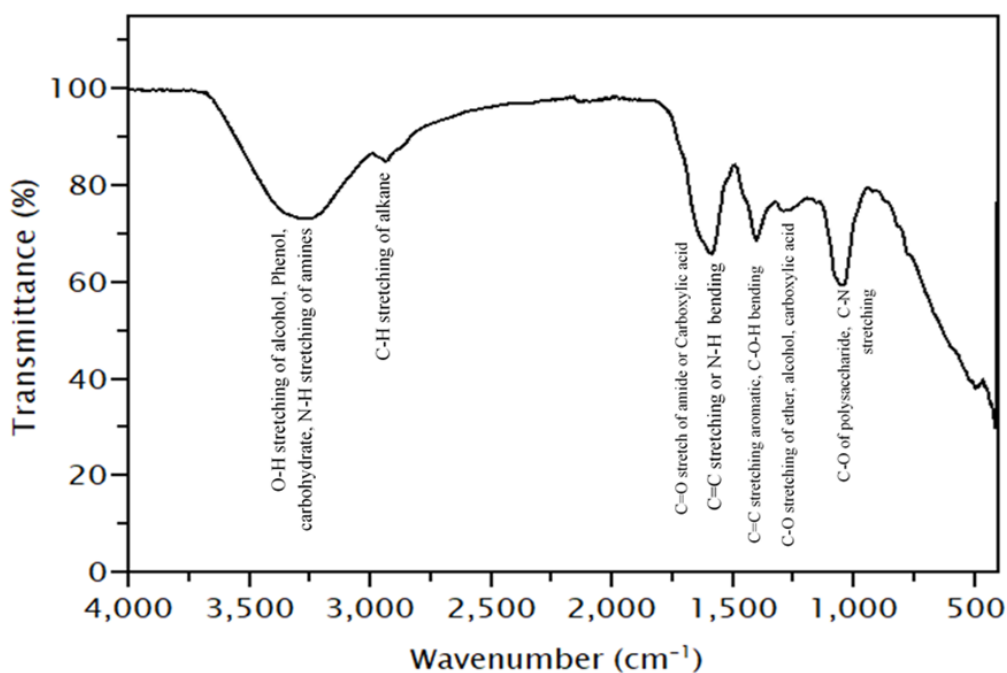
Figure 2. FTIR spectra of methanol extract of *Equisetum hyemale* (*EHE*).

Table 1. Potentiodynamic polarization parameters for the corrosion of MS samples at various *EHE* concentrations.

Concentration (ppm)	$-E_{corr}$ (V/SCE)	I_{corr} (A/cm²)	IE%
Blank	0.428	1.93×10^{-3}	–
200	0.432	5.47×10^{-4}	71.77
400	0.432	4.41×10^{-4}	77.21
600	0.432	2.05×10^{-4}	89.38
800	0.426	1.49×10^{-4}	92.29
1000	0.428	1.40×10^{-4}	92.74

The addition of 1000 ppm of *EHE* inhibitor has resulted in significantly suppressing the corrosion current by about 14 times. This confirms the fact that *EHE* has worked as a suitable inhibitor for the protection of MS. The addition of *EHE* has mainly suppressed the cathodic current, and a marginal increase of slope with the concentration of inhibitor is found. Therefore, the cathodic reduction of hydrogen is suppressed by merely blocking the MS surface by organic molecules present in the *EHE* [45]. Shift in value of E_{corr} is almost negligible, which reveals that *EHE* worked as a mixed type of inhibitor [14]. The calculation shows that the *IE* increases with the concentration of *EHE* in acid solution, reaching a value of approximately 93.0% at 1000 ppm. Adsorption phenomenon ascribed to the synergistic effect of different organic molecules with different functionalities facilitating the formation of an inhibiting film [6].
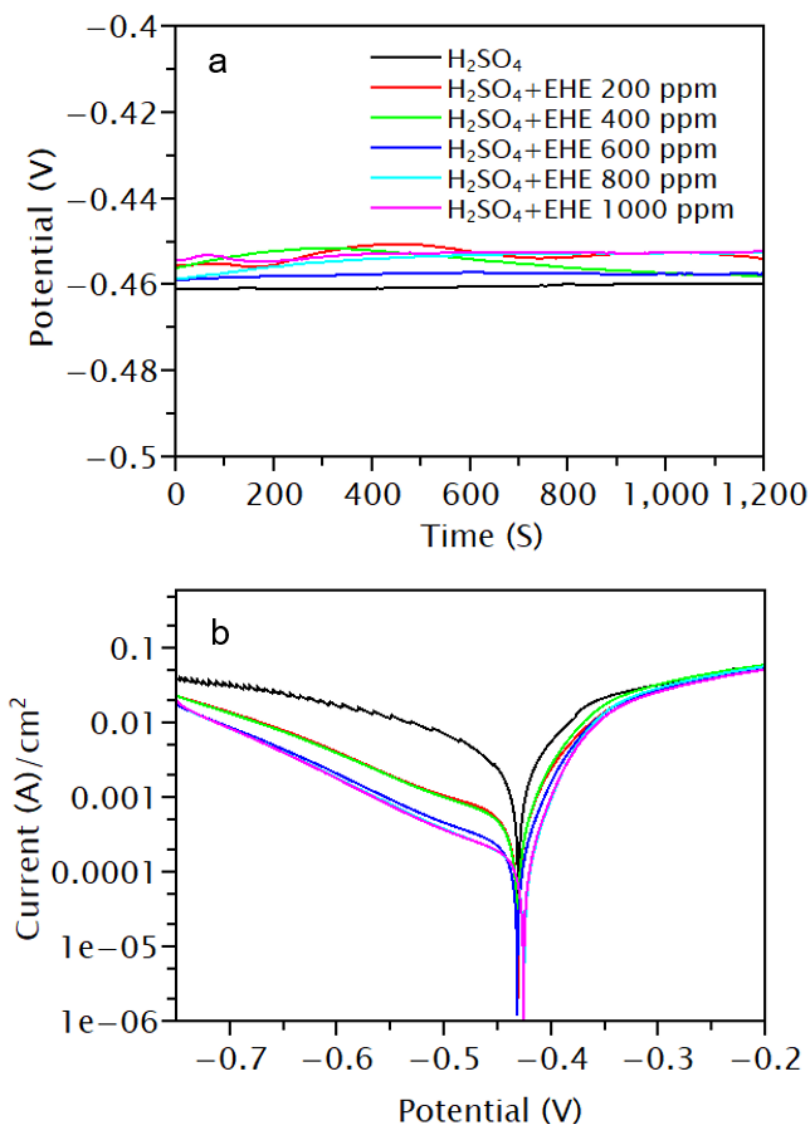
Figure 3. a. Variation of OCP of MS sample with different *EHE* concentrations;
b. Polarization curve of mild steel in 1.0 M H_2SO_4 + *EHE* of different concentrations.

The effect of *EHE* was further studied at steady-state conditions by impedance measurements of the MS in 1.0 M H_2SO_4+*EHE* of different concentrations at OCP. Figure 4a, 4b, and 4c represent the Nyquist, Bode modulus, and phase plots, respectively. Here the symbols represent the measured data, and solid lines represent the fitting data using Z-view software (V3.2b). A simple Randles circuit consisting of a one-time constant is used to fit the impedance spectra, as shown in Figure 4d. The R_s, R_{ct}, and *CPE* represent the solution resistance, charge transfer resistance, and constant phase element, respectively. The fitted parameters, along with *IE*, are tabulated in Table 2. Several publications have explained the use of *CPE* for depressed semicircle by taking into account the surface inhomogeneity and related relaxation process [5, 17, 28, 29, 46–53]. The impedance function of *CPE* is represented by the expression 6 [24]:

$$Z_{CPE}=\frac{1}{Q(j\omega)^n} \tag{6}$$

Where Q represents the magnitude of the *CPE*, *j*, the imaginary number ($j^2=-1$), ω, being angular frequency ($\omega=2\pi f$), and *n,* the *CPE* exponent ($-1\leq n\leq+1$), whose value is used to gauge the non-homogeneity or roughness of the surface [47]. At $n=0$, the *CPE* represents a pure resistor; at $n=-1$, an inductor; and at $n=+1$, a pure capacitor [48].

Table 2. Impedance parameters for corrosion of mild steel in 1.0 M H_2SO_4 at various *EHE* concentrations.

Concentration (ppm)	R_s (Ω cm^2)	*CPE* (F s$^{(1-a)}$ cm^{-2})	*n*	R_{ct} (Ω cm^2)	*IE%*
Blank (0)	3.26	180.81	0.878	7.29	–
200	3.527	104.36	0.865	22.31	67.32
400	3.06	112.50	0.843	25.11	70.97
600	2.89	81.10	0.845	42.9	83.01
800	3.099	78.49	0.849	44.22	83.51
1000	3.161	52.54	0.882	53.15	86.28

Nyquist plot showing a single depressed capacitive loop at high frequency is indicative of a single charge transfer process of Fe-dissolution. The Nyquist curve shape remains the same with the addition of *EHE*, which implies that the addition of *EHE* does not change the MS corrosion mechanism in 1.0 M H_2SO_4. Nevertheless, the diameter of the capacitive loops increases with the concentration of *EHE*. Therefore, inhibition effect increases with the concentration of the *EHE*. The increment of the inductive loop observed in the lower frequency with the concentration of *EHE* might be attributed to the relaxation phenomenon of adsorbed intermediates such as sulfate ions Fe($SO_{4\,ads}^{2-}$) and inhibitor molecules [49, 54].

The increment of phase angle in a Bode-phase plot [55, 56] and the value of impedance at low frequencies in the Bode-modulus plot [46] with the concentration of *EHE* also confirm the inhibitive behavior of *EHE* with its concentration. The increase of phase angle with the concentration of inhibitor is presumably due to more coverage of the MS surface by inhibitor molecules. A similar behavior is reported elsewhere [15, 57, 58].

The fitting results show a decrease in *CPE* with the concentration of *EHE*, indicating that the adsorption of inhibitor molecules results in decreasing the dielectric constant of the double layer. It may also be attributed to an increase in the thickness of the electric double layer due to the large size of inhibitor molecules compared to water dipole, which is substituted in the adsorption process. It is noteworthy that inhibitor molecules have a larger size compared to water dipole [59]. The gradual replacement of water dipoles by the inhibitor molecules on the metal surface suppressed the rate of metal dissolution [60].
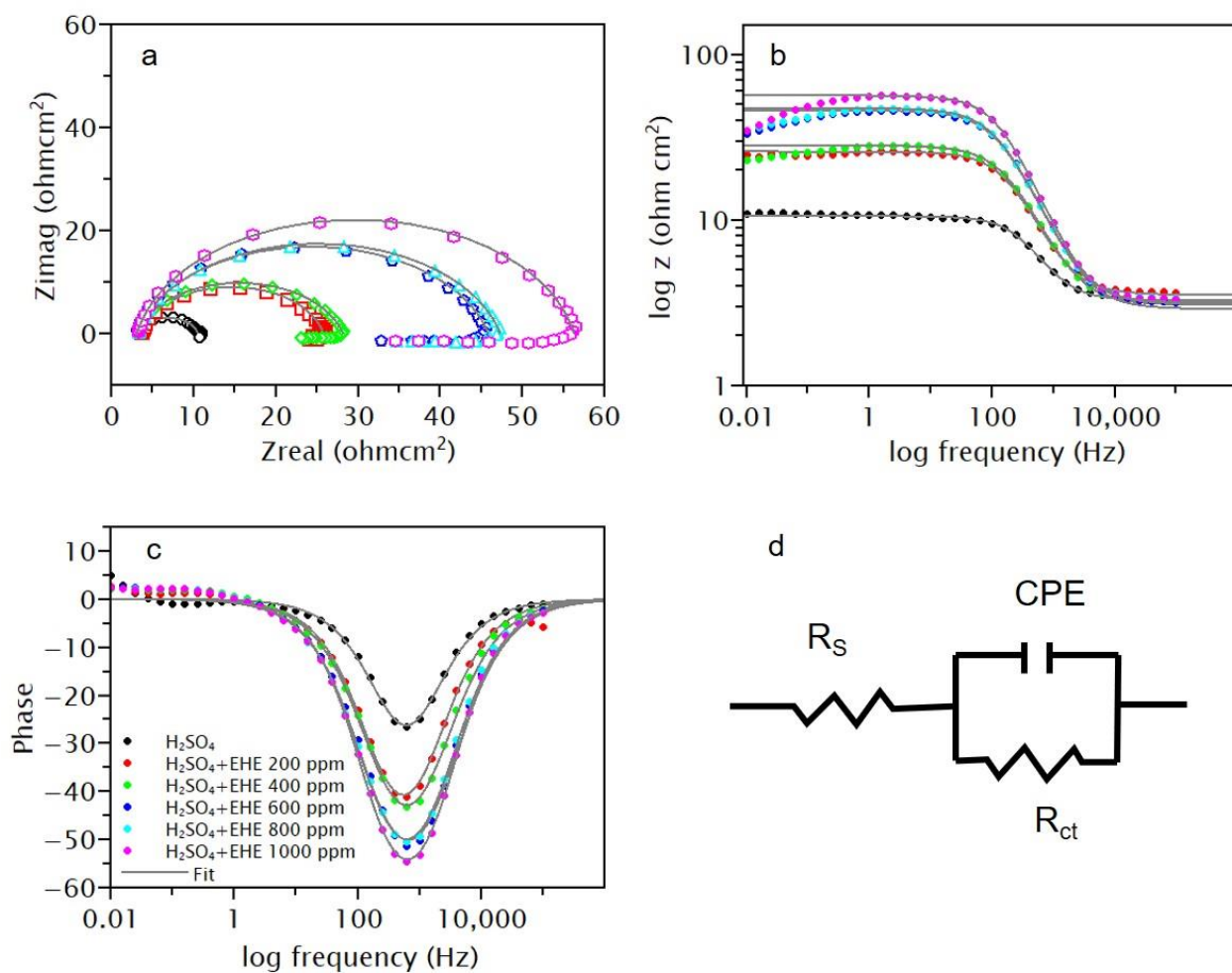
Figure 4. a. Nyquist plots, b. Bode modulus plots of log *Z* vs. frequency, c. Bode phase plots of phase angle vs. frequency for mild steel in 1.0 M H₂SO₄ with *EHE* of different concentrations, and d. Equivalent circuit model used to fit the impedance spectra.

3.3 Weight Loss Measurement

Only weight loss measurements can give a real corrosion rate. In weight loss measurements, the effect of longer immersion time up to 24 h and the effect of concentration of *EHE* on the inhibition of corrosion of MS sample in acidic solution were studied. The obtained results are compared with the electrochemical data. Figure 5a and 5b depict the weight loss and corresponding *IE*. The results show a significant reduction in weight loss in an acid solution with the addition of the *EHE*. The *IE* attains a maximum (82%) at 6 h of immersion and decreases to attain a steady value (70%) after 12 h of immersion. The initial increase in *IE* points to the dissolution of air formed oxide, leading to surface roughening followed by enhanced adsorption of the phytochemicals on the MS surface. The adsorbed phytochemicals blocked the active site of corrosion. However, a decrease of inhibition efficiency after 6 h of immersion in *EHE* solution indicated for the gradual desorption of phytochemicals. The chelation of the inhibitor molecules might have promoted desorption with the dissolved Fe^{3+} or Fe^{2+} species [29, 57]. This is essential information concerning the application of such inhibitors in a real application where the time of immersion could be a detrimental factor. On the positive note, the inhibition efficiency after 24 h of immersion maintained at 70%.
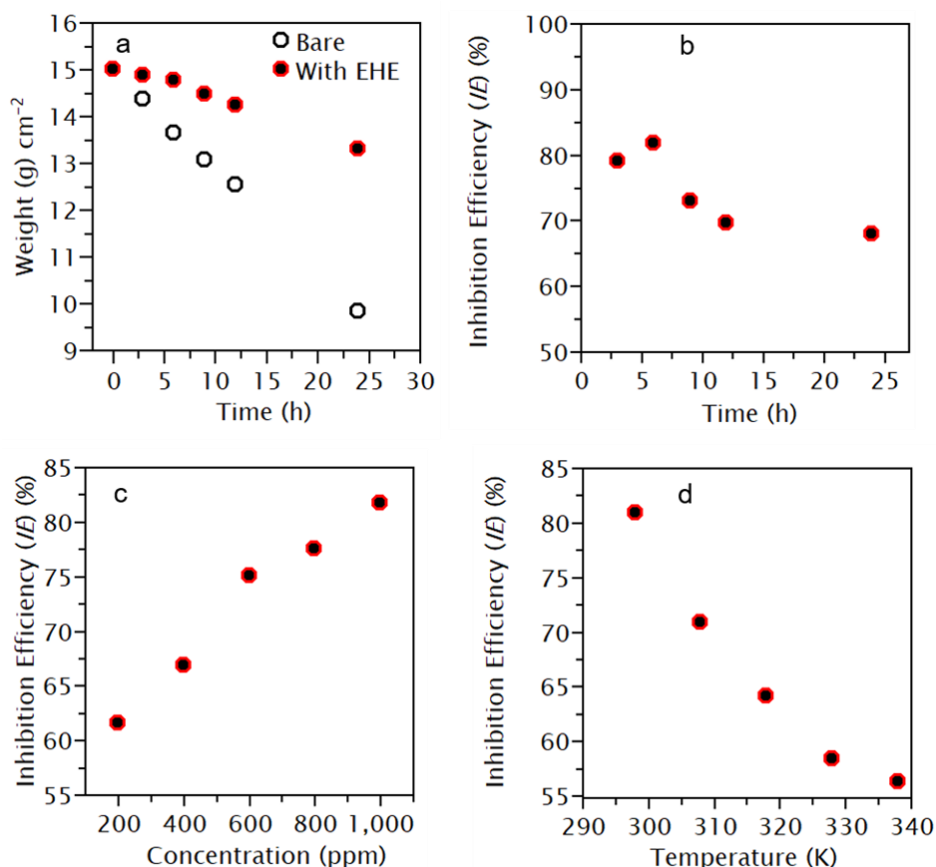

Figure 5. a. Variation in a weight loss of mild steel immersed in 1.0 M H_2SO_4 with *EHE*, and inhibition efficiency (*IE*) of *EHE* with: b, immersion time; c, concentration; and d, temperature.

The effect of concentration of *EHE* on MS corrosion from 200 ppm to 1000 ppm is plotted in Figure 5c. In all these measurements, the immersion time was 6 h at 298 K. The results reveal an increase in the *IE* of *EHE* with concentration. A maximum *IE* of 82.0% achieved at 1000 ppm of *EHE*. Accordingly, the surface coverage of MS surface by *EHE* increased with its concentration due probably to the availability of a large number of inhibitor molecules for adsorption.

The effect of temperature on the adsorption behaviors of the phytochemical of *EHE* was clarified by weight loss measurement at various temperatures after immersion in 1000 ppm *EHE* solution for 6 h. The temperature changed from 298 K to 338 K at an interval of 10 K, and results are presented in Figure 5d. The results reveal a gradual decrease in *IE* with temperature. This phenomenon indicates the desorption or decomposition of inhibitor molecules at higher temperatures [61], and such behavior strongly hints at physical adsorption of phytochemicals. The lower adsorption stability of the inhibitor molecules with temperature correlates with the change of *IE* with time in Figure 5b.

The inhibition efficiencies estimated by all the three methods are compared in Figure 6. The general features of *IE* are the same irrespective of the method used to estimate it, and values differed by about 10% among the three methods is within the range of experimental errors [58].
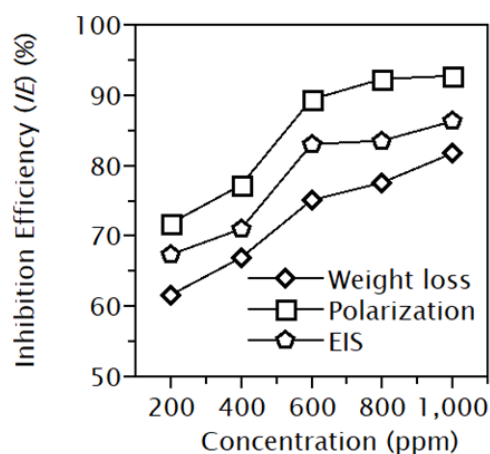
Figure 6. Comparison of variation in inhibition efficiency with the variation of concentration by different methods.

3.4 Adsorption isotherms

The inhibition of corrosion by plant extracts is due to the adsorption of phytochemicals on the MS surface [14]. The polar functions of phytochemicals preferentially get adsorbed on a negatively charged metal surface by either physical or chemical interactions or both. The adsorbed phytochemicals function as a barrier for charge and mass transfer between metal and the solution [57]. Therefore, the study of adsorption behavior of inhibitor is an integral part of the study to know about the mode and extent of interaction between the inhibitor and metal surface by evaluating some important thermodynamic parameters such as free energy,

activation energy, enthalpy and entropy of adsorption. The adsorption of inhibitor molecules can be considered as a quasi-substitution process between the organic molecules of *EHE* in aqueous phase and pre-adsorbed water dipoles at the MS surface [5, 17, 24].

The adsorption isotherms are determined by working on a linear relation between θ (surface coverage) value and C_{inh} (concentration of inhibitor). The testing of various isotherms revealed that the best fit could only be achieved in Langmuir adsorption isotherm

$$\frac{C_{inh}}{\theta} = \frac{1}{K_{ads}} + C_{inh} \tag{7}$$

The result is shown in Figure 7a. A linear correlation coefficient ($R^2=0.9964$) and a slope of 1.1158 are obtained. The adsorption of *EHE* led to monolayer formation. However, little deviation of slope from unity pointed to some interactions between adsorbed molecules on the MS surface. It may be due to mutual attraction and repulsion between differently adsorbed molecules of different functionalities. In addition, it may also be possible that preferential adsorption of components of the extracts at cathodic and anodic sites took place [30].

L-uridine, quercetin, 5 methoxy fulfural, α-*D*-fructofuranose, rutin are a significant component of alcoholic extract of *Equisetum hyemale* [43]. So, the concentration of *EHE* is represented here as an average molar concentration of major compounds present in the extract to evaluate the adsorption parameter [32]. Nevertheless, other components present in *EHE* might also have affected the inhibition behavior of *EHE*.
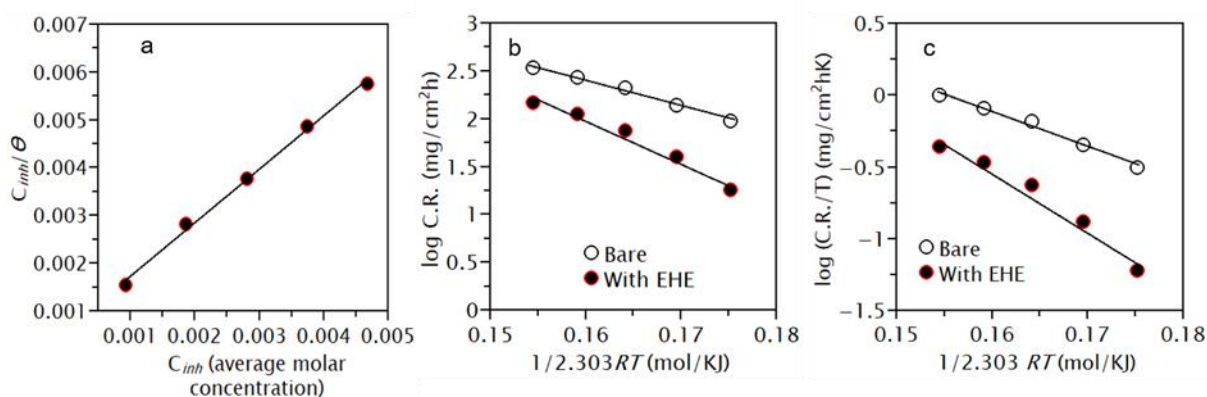
Figure 7. a. Langmuir adsorption isotherm plot for mild steel in 1.0 M H_2SO_4 with different concentration of *EHE* as the average molar concentration of major compounds b. Arrhenius plot, and c. Transition state plot for mild steel in 1.0 M H_2SO_4 with *EHE*.

From the Langmuir adsorption isotherm plot in Figure 7a, the value of adsorption equilibrium constant (K_{ads}) is obtained from the intercept, which is then used to calculate the standard free energy of adsorption (ΔG^0_{ads}) from the equation (8) [17]:

$$\Delta G^0_{ads} = -RT \, Ln(55.5 K_{ads}) \tag{8}$$

Where 55.5 is the molar concentration of water in solution (mol/L), and R is the universal gas constant (8.314 J/mol K). The substitution of K_{ads} and other constants values in equation (8) results in ΔG_{ads}^{0} of –28.34 kJ/mol. The value of ΔG_{ads}^{0} indicates that the adsorption of *EHE* on MS surface is a mixed type involving both physical and chemical interactions a spontaneous manner. It is well known that physical adsorption results in ΔG_{ads}^{0} value of less than or equal to –20 kJ/mol, while ΔG_{ads}^{0} equals to or more than –40 kJ/mol hints to chemical adsorption [17, 57]. As a matter of fact, an intermediate value of ΔG_{ads}^{0} in this study suggests the adsorption process controlled by both interactions of the inhibitors molecules to the MS surface. However, the decrease of *IE* with temperature in Figure 5d contradicts this result of ΔG_{ads}^{0} pointing to both physical and chemical adsorptions. It may be assumed that physisorption occurred first due to the electrostatic interaction between charged inhibitor molecules and charged metal surface. Then, thermal agitation energy might be sufficient for desorption of some water dipole, which is reflected by temperature effect, and such a site may be available for chemisorption by charge transfer from organic molecules to the MS surface to form a coordinate type of bond [24]. Nitrogen-containing molecules have a higher potential to share electrons due to the protonation behavior of nitrogen in aqueous solution. The phytochemicals of *EHE* mostly contain oxygen as the heteroatom, and therefore thermal stability might be weak. Further, the activation energy of the adsorption process is calculated in order to understand the adsorption phenomenon from the relation (9) [26]:

$$\log(C.R.) = \log A - \frac{E_a}{2.303RT} \tag{9}$$

Where *C.R.* is corrosion rate, T is the absolute temperature, and A is Arrhenius pre-exponential constant. Table 3 list the calculated values of E_a and A, and Figure 7b depicts the Arrhenius plot. The increase in the energy barrier in the presence of *EHE* as inhibitor reflects decrease in corrosion rate.

Furthermore, the change of enthalpy (ΔH^{*}) and entropy (ΔS^{*}) of activation for the formation of the activation complex in the transition state could be obtained from the transition state equation 10 [26]:

$$\log\left(\frac{C.R.}{T}\right) = \left[\log\left(\frac{R}{hN}\right) + \left(\frac{\Delta S^{*}}{2.303R}\right) - \frac{\Delta H^{*}}{2.303RT}\right] \tag{10}$$

Where enthalpy of activation (ΔH^{*}) is the slope of straight line obtained by plotting $\log(C.R./T)$ vs. $1/2.303RT$ and entropy of activation (ΔS^{*}) can be calculated from the intercept of the line, Figure 7c. In the equation, h is plank's constant, 6.6261×10^{-34} Js, and N is the Avogadro's number, 6.0225×10^{23} mol^{-1}.

Table 3. Activation parameters of the dissolution of mild steel in 1.0 M H_2SO_4 containing 1000 ppm *EHE*.

| Electrolyte	E_a (kJ/mol)	*Constant (A)* (mg/cm^2)	ΔH (kJ/mol)	$E_a - \Delta H$	ΔS (J/mol K)
1.0 M H_2SO_4	27.09	5.38×10^6	24.45	2.64	−124.91
1.0 M H_2SO_4 + *EHE* (1000 ppm)	44.19	1.13×10^9	41.55	2.64	−80.38

Calculated values of ΔH^* and ΔS^* for 1.0 M H_2SO_4 and 1.0 M H_2SO_4+1000 ppm of *EHE* are included in Table 3. A positive value of ΔH^* signifies the endothermic nature of metal-*EHE* interaction. The value of ΔH^* increases with the addition of *EHE*. This reflects the decrease in the corrosion rate is controlled by kinetic parameters of activation [62]. The value of E_a is higher than that of ΔH^*, which implies the involvement of a gaseous reaction, possibly the hydrogen evolution reactions. This leads to a decrease in the total reaction volume [13]. Furthermore, the difference in $E_a - \Delta H^*$ value nearly equals to RT shows that the corrosion process is unimolecular. Intermediate values of E_a and ΔH^* reflect a mixed type adsorption of *EHE* on the MS surface [15, 29, 57]. In Table 3, *A* is the Arrhenius pre-exponential factor or frequency factor, representing the affinity of ions to get adsorbed on the metal surface. An increase in the value of *A* in inhibitor solution indicates the higher adsorption affinity of inhibitor molecules to the MS surface. The values of *A* and E_a are related to each other; therefore an increment of *A* increases the value of E_a in the inhibitor solution.

As for the value of ΔS^*, a significant and negative value in 1.0 M H_2SO_4 points to an association step in the rate-determining step. However, the addition of *EHE* to the acid solution resulted in increasing the ΔS^* value. This may be interpreted as the phenomenon leading to the replacement of water molecules by *EHE* on metal surfaces. Therefore, cathodic discharge of hydrogen ion is lowered by adsorbed inhibitor molecules, and a more randomly arranged transition state in the rate-determining recombination step is formed [26].

3.5 Surface analysis

Energy dispersive X-ray (EDX) was used to get the elemental information of the MS samples immersed in 1.0 M H_2SO_4 and 1.0 M H_2SO_4+*EHE* for 24 h. The EDX spectra are showing the presence of elements C, N, O, P, and Fe in Figure 8. Table 4 shows a decrease of Fe and an increase of N and C on the MS surface immersed in an acid solution with *EHE*. Therefore, the formation of a protective molecular film due to the adsorption of phytochemicals containing N, C, and O on the MS surface leads to the inhibition of the Fe dissolution.

In SEM image of MS sample immersed in 1.0 M H_2SO_4, there is a severe corrosion attack with deep furrows and large cracks (Figure 8a), whereas MS samples immersed in 1.0 M H_2SO_4+*EHE* have developed a relatively smooth surface by the adsorption of inhibitor molecules, which form a protective film on MS and inhibits the corrosion attack (Figure 8b and 8c).
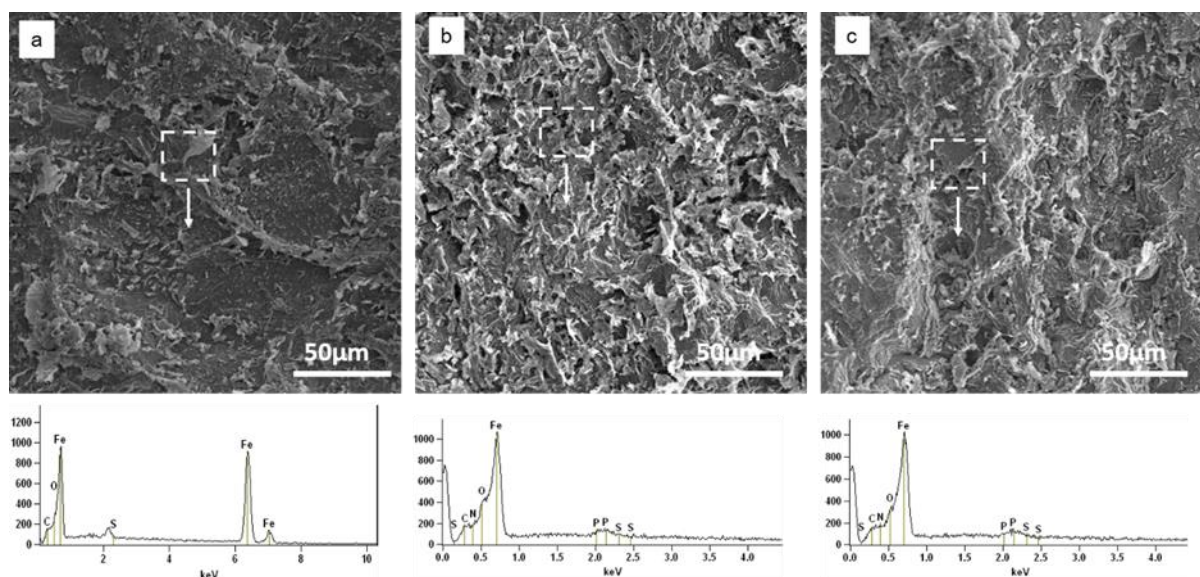
Figure 8. SEM images with corresponding EDX spectra of mild steel sample after 24 h of immersion in a. 1.0 M H_2SO_4 b. 1.0 M H_2SO_4+400 ppm *EHE* and c. 1.0 M H_2SO_4+1000 ppm *EHE*.

Table 4. Weight of different elements on the MS surface after immersion in the sample in different solutions.

Surface	Iron (%)	Carbon (%)	Nitrogen (%)	Oxygen (%)	Phosphorus (%)
Polished metal sample	100	–	–	–	–
In 1.0 M H_2SO_4	97.45	1.72	–	0.83	–
1.0 M H_2SO_4+400 ppm *EHE*	92.92	1.95	1.45	3.84	0.19
1.0 M H_2SO_4+1000 ppm *EHE*	87.87	5.08	3.45	3.85	0.05

Conclusion

Extract of stem of *Equisetum hyemale* acts as a suitable inhibitor for corrosion of mild steel in 1.0 M H_2SO_4 solution. Three processes, such as weight loss, thermodynamic parameter, and electrochemical method, are used to calculate the *IE* of *EHE*. The weight-loss method confirms that the IE of *EHE* is more than 85% at 1000 ppm. The *IE* increases with concentration and decreases with temperature increment. *IE* increases until 6 h, and decreases to maintains a steady-state value after 12 h of immersion. The thermodynamic parameters calculation also supports the weight-loss results. The adsorption of the extract on the mild steel (MS) follows the Langmuir adsorption isotherm, which indicates the monolayer adsorption of inhibitor on MS surface. The values of ΔH^* and E_a indicate that the adsorption process is spontaneous and endothermic. Electrochemical measurement points out as the inhibition behavior of *EHE* is a mixed type by showing negligible shift of OCP.

This result is further supported by only one time constant in EIS. EDX and SEM confirm the suppression of corrosion attack by adsorbed extract on the MS surface.

Acknowledgements

Conflicts of interest

The authors declare no conflicts of interests.

Supplementary material

The corresponding author provides supplementary material upon a reasonable request.

Reference

1. NACE International Institute IMPACT PLUS (n.d.), https://www.nace-impact.org/.
2. D. de la Fuente, I. Díaz, J. Simancas, B. Chico and M. Morcillo, Long-term atmospheric corrosion of mild steel, *Corros. Sci.*, 2011, **53,** no. 2, 604–617. doi: 10.1016/j.corsci.2010.10.007
3. S.B. Ulaeto, U.J. Ekpe, M. Chidiebere and E.E. Oguzie, Corrosion inhibition of mild steel in hydrochloric acid by acid extracts of eichhornia crassipes, *Int. J. Mater. Chem.*, 2012, **2**, 158–164, http://article.sapub.org/10.5923.j.ijmc.20120204.08.html.
4. M.A. Hegazy, A.S. El-Tabei, A.H. Bedair and M.A. Sadeq, Synthesis and inhibitive performance of novel cationic and gemini surfactants on carbon steel corrosion in 0.5 M H_2SO_4 solution, *RSC Adv*., 2015, **5**, 64633–64650. doi: 10.1039/C5RA06473B
5. M. Murmu, S.K. Saha, N.C. Murmu and P. Banerjee, Effect of stereochemical conformation into the corrosion inhibitive behaviour of double azomethine based Schiff bases on mild steel surface in 1 mol L−1 HCl medium: An experimental, density functional theory and molecular dynamics simulation study, *Corros. Sci.*, 2019, **146**, 134–151. doi: 10.1016/j.corsci.2018.10.002
6. E.E. Oguzie, Y. Li and F.H. Wang, Effect of surface nanocrystallization on corrosion and corrosion inhibition of low carbon steel: Synergistic effect of methionine and iodide ion, *Electrochim. Acta*, 2007, **52**, no. 24, 6988–6996. doi: 10.1016/j.electacta.2007.05.023
7. N.I. Kairi and J. Kassim, The Effect of Temperature on the Corrosion Inhibition of Mild Steel in 1 M HCl Solution by Curcuma Longa Extract, *Int. J. Electrochem. Sci.*, 2013, **8**, 18.
8. A. Aytac, U. Ozmen and M. Kabasakaloglu, Investigation of some Schiff bases as acidic corrosion of alloy AA3102, *Mater. Chem. Phys.*, 2005, **89,** no. 1, 176–181. doi: 10.1016/j.matchemphys.2004.09.003

9. M. Scendo, The influence of adenine on corrosion of copper in chloride solutions, *Corros. Sci.*, 2008, **50**, no. 7, 2070–2077. doi: 10.1016/j.corsci.2008.04.007

10. S. Kertit and B. Hammouti, Corrosion inhibition of iron in 1M HCl by 1-phenyl-5-mercapto-1,2,3,4-tetrazole, *Appl. Surf. Sci.*, 1996, **93**, no. 1, 59–66. doi: 10.1016/0169-4332(95)00189-1

11. J.M. Roque, T. Pandiyan, J. Cruz and E. García Ochoa, DFT and electrochemical studies of tris(benzimidazole-2-ylmethyl)amine as an efficient corrosion inhibitor for carbon steel surface, *Corros. Sci.*, 2008, **50**, no. 3, 614–624. doi: 10.1016/j.corsci.2007.11.012

12. E. Machnikova, K.H. Whitmire and N. Hackerman, Corrosion inhibition of carbon steel in hydrochloric acid by furan derivatives, *Electrochim. Acta*, 2008, **53**, no. 20, 6024–6032. doi: 10.1016/j.electacta.2008.03.021

13. A. Ostovari, S.M. Hoseinieh, M. Peikari, S.R. Shadizadeh and S.J. Hashemi, Corrosion inhibition of mild steel in 1 M HCl solution by henna extract: A comparative study of the inhibition by henna and its constituents (Lawsone, Gallic acid, *α-d*-Glucose and Tannic acid), *Corros. Sci.*, 2009, **51**, no. 9, 1935–1949. doi: 10.1016/j.corsci.2009.05.024

14. O.L Riggs, Jr and C.C. Nathan, *Corrosion Inhibitors*, 2nd Edition, Houston, 1973.

15. Y. Li, P. Zhao, Q. Liang and B. Hou, Berberine as a natural source inhibitor for mild steel in 1 M H_2SO_4, *Appl. Surf. Sci.*, 2005, **252**, no. 5, 1245–1253. doi: 10.1016/j.apsusc.2005.02.094

16. H. Ju, Y. Ju and Y. Li, Berberine as an Environmental-Friendly inhibitor for Hot-Dip coated steels in diluted hydrochloric acid, *J. Mater. Sci. Technol.*, 2012, **28**, no. 9, 809–816. doi: 10.1016/S1005-0302(12)60135-2

17. I. Ahamad, R. Prasad and M.A. Quraishi, Adsorption and inhibitive properties of some new Mannich bases of Isatin derivatives on corrosion of mild steel in acidic media, *Corros. Sci.*, 2010, **52**, no. 4, 1472–1481. doi: 10.1016/j.corsci.2010.01.015

18. M.G. Fontana, *Corrosion Engineering*, 3rd edition, McGraw-Hill Book Company, New York, 1985.

19. J. K. Odusote, D. O. Owalude, O. Sunday Joseph and R. A. Yahya, Inhibition efficiency of Moringa Oleifera leaf extract on the corrosion of reinforced steel bar in HCl solution, *West Indian J. Eng.*, 2015, **38**, 64–70.

20. A. Mohammadi, S.M.A. Hosseini, M.J. Bahrami and M. Shahidi, Corrosion inhibition of mild steel in acidic solution by apricot gum as a green inhibitor, *Prog. Color Color. Coat.*, 2016, **9**, 117–134.

21. P.B. Raja and M.G. Sethuraman, Natural products as corrosion inhibitor for metals in corrosive media A review, *Mater. Lett.*, 2008, **62,** no. 1, 113–116. doi: 10.1016/j.matlet.2007.04.079

22. G. Gece, Drugs: A review of promising novel corrosion inhibitors, *Corros. Sci.*, 2011, **53**, no. 12, 3873–3898. doi: 10.1016/j.corsci.2011.08.006

23. T. Hossein, S. Mehdi and K. Nima, Polarization, EIS and EN studies to evaluate the inhibition effect of vanillin as environment-friendly inhibitor on carbon steel in hydrochloric acid solution, *J. Phys. Theor. Chem*., 2014, **10**, 231–246.

24. H. Cang, Z. Fei, J. Shao, W. Shi and Q. Xu, Corrosion inhibition of mild steel by Aloes extract in HCL solution medium, *Int. J. Electrochem. Sci*., 2013, **8**, 720–734.

25. G. Khan, K.M.S. Newaz, W.J. Basirun, H.B.M. Ali, F.L. Faraj and G.M. Khan, Application of natural product extracts as green corrosion inhibitors for metals and alloys in acid pickling processes- A review, *Int. J. Electrochem. Sci*., 2015, **10**, 6120–6134.

26. A. Hamdy and N.S. El-Gendy, Thermodynamic, adsorption and electrochemical studies for corrosion inhibition of carbon steel by henna extract in acid medium, *Egypt. J. Pet*., 2013, **22**, no. 1, 17–25. doi: 10.1016/j.ejpe.2012.06.002

27. S.A. Umoren, I.B. Obot, A.U. Israel, P.O. Asuquo, M.M. Solomon, U.M. Eduok and A.P. Udoh, Inhibition of mild steel corrosion in acidic medium using coconut coir dust extracted from water and methanol as solvents, *J. Ind. Eng. Chem*., 2014, **20**, no. 5, 3612–3622. doi: 10.1016/j.jiec.2013.12.056

28. L. Bammou, M. Belkhaouda, R. Salghi, O. Benali, A. Zarrouk, H. Zarrok and B. Hammouti, Corrosion inhibition of steel in sulfuric acidic solution by the Chenopodium Ambrosioides extracts, *J. Assoc. Arab Univ. Basic Appl. Sci*., 2014, **16**, no. 1, 83–90. doi: 10.1016/j.jaubas.2013.11.001

29. Y. Qiang, S. Zhang, B. Tan and S. Chen, Evaluation of Ginkgo leaf extract as an eco-friendly corrosion inhibitor of X70 steel in HCl solution, *Corros. Sci*., 2018, **133**, 6–16. doi: 10.1016/j.corsci.2018.01.008

30. N.A. Odewunmi, S.A. Umoren and Z.M. Gasem, Watermelon waste products as green corrosion inhibitors for mild steel in HCl solution, *J. Environ. Chem. Eng*., 2015, **3**, no. 1, 286–296. doi: 10.1016/j.jece.2014.10.014

31. A.Y. El-Etre, Inhibition of C-steel corrosion in acidic solution using the aqueous extract of zallouh root, *Mater. Chem. Phys*., 2008, **108**, no. 2–3, 278–282. doi: 10.1016/j.matchemphys.2007.09.037

32 A. Tiwari, Y. Uprety and S.K. Rana, Plant endemism in the Nepal Himalayas and phytoge-ographical implications, *Plant Divers*., 2019, **41**, no. 3, 174–182. doi:10.1016/j.pld.2019.04.004

33 N. Karki, Y. Chaudhary, and A.P. Yadav, Thermodynamic, Adsorption and Corrosion Inhibition Studies of Mild Steel by Artemisia vulgaris Extract from Methanol as Green Corrosion Inhibitor in Acid Medium, *J. Nepal Chem. Soc*., 2018, **39**, 76. doi: 10.3126/jncs.v39i0.27041

34. P.R. Shrestha, H.B. Oli, B. Thapa, Y. Chaudhary, D.K. Gupta, A.K. Das, K.B. Nakarmi, S. Singh, N. Karki and A.P. Yadav, Bark extract of Lantana camara in 1M HCl as green corrosion inhibitor for mild steel, *Eng. J*., 2019, **23**, 205–211. doi: 10.4186/ej.2019.23.4.205

35. B. Thapa, D.K. Gupta and A.P. Yadav, Corrosion inhibition of bark extract of euphobia royleana on mild steel in 1M HCl, *J. Nepal Chem. Soc.*, 2019, **40**, 25–29. doi: 10.3126/jncs.v40i0.27274

36. P.C. Lama, Y. Chaudhary, N. Karki and A.P. Yadav, Study of the corrosion inhibition behavior of pogostemon benghalensis (rudilo) for mild steel in acidic medium by potentiodynamic methodno title, *J. Nepal Chem. Soc.*, 2016, **34**, 120.

37. Y. Chaudhary, N. Karki and A.P. Yadav, Study of the corrosion inhibition behavior of Pogostemo benghalensis (Rudilo) for mild steel in acidic medium by weight loss method, *J. Nepal Chem. Soc.*, 2016, **35**, 139.

38. R. Lama, A.K. Das, B Yadav, Y. Chaudhary, P.C. Lama, S.L. Shrestha, D.K. Gupta, N. Karki and A.P. Yadav, Corrosion inhibition of mild steel in acidic medium using high altitude plant extract, *J. Nepal Chem. Soc.*, 2018, **38**, 48. doi:10.3126/jncs.v38i0.27787

39. N. Karki, S. Neupane, Y. Chaudhary, D.K. Gupta and A.P. Yadav, Berberis aristata: a highly efficient and thermally stable green corrosion inhibitor for mild steel in acidic medium, *Anal. Bioanal. Electrochem.*, 2020, **12**, 970.

40. C.F. dos Santos Alves, P.C. Bonez, M. de Souza Ebling, C. Casagrande, L. Freitas, C. Dolwitsch, F. Pires, M.R. Sagrillo, G.F. de Brum, M.M.A. de Campos and R.C. Vianna Santos, Antimicrobial, cyto and genotoxic activities of equisetum hyemale, *Pharmacogn. J.*, 2019, **11**, no. 6, 1563–1571. doi: 10.5530/pj.2019.11.239

41. M. Jin, C. Zhang, T. Zheng, D. Yao, L. Shen, J. Luo, Z. Jiang, J. Ma, X.J. Jin, J. Cui, J.J. Lee and G. Li, A new phenyl glycoside from the aerial parts of Equisetum hyemale, *Nat. Prod. Res.*, 2014, **28**, 1813–1818. doi: 10.1080/14786419.2014.947491

42. B.J. Park and M. Tomohiko, Feruloyl, caffeoyl, and flavonol glucosides from Equisetum hyemale, *Chem. Nat. Compd.*, 2011, **47**, 363. doi: 10.1007/s10600-011-9934-0

43. G. Pandey and S. Khatoon, Evaluation of phytochemical profile and antioxidant activity of equisetum hyemale l., *World J. Pharm. Res.*, 6–16.

44. C.B. Verma, M.A. Quraishi and A. Singh, 2-Aminobenzene-1,3-dicarbonitriles as green corrosion inhibitor for mild steel in 1 M HCl: Electrochemical, thermodynamic, surface and quantum chemical investigation, *J. Taiwan Inst. Chem. Eng.*, 2015, **49**, 229–239. doi: 10.1016/j.jtice.2014.11.029

45. M. Benabdellah, A. Aouniti, A. Dafali, B. Hammouti, M. Benkaddour, A. Yahyi and A. Ettouhami, Investigation of the inhibitive effect of triphenyltin 2-thiophe-ne carboxylate on corrosion of steel in 2 M H_3PO_4 solutions, *Appl. Surf. Sci.*, 2006, **252**, no. 23, 8341–8347. doi: 10.1016/J.APSUSC.2005.11.037

46. C.M. Fernandes, L.X. Alvarez, N.E. dos Santos, A.C. Maldonado Barrios and E.A. Ponzio, Green synthesis of 1-benzyl-4-phenyl-1H-1,2,3-triazole, its application as corrosion inhibitor for mild steel in acidic medium and new approach of classical electrochemical analyses, *Corros. Sci.*, 2019, **149**, 185–194. doi: 10.1016/j.corsci.2019.01.019

47. K. Jüttner, Electrochemical impedance spectroscopy (EIS) of corrosion processes on inhomogeneous surfaces, *Electrochim. Acta*, 1990, **35**, no. 10, 1501–1508. doi: 10.1016/0013-4686(90)80004-8

48. M. Hosseini, S.F.L. Mertens, M. Ghorbani and M.R. Arshadi, Asymmetrical Schiff bases as inhibitors of mild steel corrosion in sulphuric acid media, *Mater. Chem. Phys.*, 2003, **78**, no. 3, 800–808. doi: 10.1016/S0254-0584(02)00390-5

49. F. Bentiss, M. Traisnel and M. Lagrenee, The substituted 1,3,4-oxadiazoles: a new class of corrosion inhibitors of mild steel in acidic media, *Corros. Sci.*, 2000, **42**, no. 1, 127–146. doi: 10.1016/S0010-938X(99)00049-9

50. S. Shahabi, P. Norouzi and M.R. Ganjali, Theoretical and electrochemical study of carbon steel corrosion inhibition in the presence of two synthesized Schiff base inhibitors: Application of fast Fourier transform continuous cyclic voltammetry to study the adsorption behavior, *Int. J. Electrochem. Sci.*, 2015, **10**, 2646–2662.

51. A.O. Yüce and G. Kardaş, Adsorption and inhibition effect of 2-thiohydantoin on mild steel corrosion in 0.1 MHCl, *Corros. Sci.*, 2012, **58**, 86–94. doi: 10.1016/j.corsci.2012.01.013

52. Q. Ma, S. Qi, X. He, Y. Tang and G. Lu, 1,2,3-Triazole derivatives as corrosion inhibitors for mild steel in acidic medium: Experimental and computational chemistry studies, *Corros. Sci.*, 2017, **129**, 91–101. doi: 10.1016/j.corsci.2017.09.025

53. M.A. Bedair, M.M.B. El-Sabbah, A.S. Fouda and H.M. Elaryian, Synthesis, electrochemical and quantum chemical studies of some prepared surfactants based on azodye and Schiff base as corrosion inhibitors for steel in acid medium, *Corros. Sci.*, 2017, **128**, 54–72. doi: 10.1016/j.corsci.2017.09.016

54. M.A. Veloz and I. González, Electrochemical study of carbon steel corrosion in buffered acetic acid solutions with chlorides and H_2S, *Electrochim. Acta*, 2002, **48**, no. 2, 135–144. doi: 10.1016/S0013-4686(02)00549-2

55. M.A. Hegazy, M. Abdallah, M.K. Awad, M. Rezk, Three novel di-quaternary ammonium salts as corrosion inhibitors for API X65 steel pipeline in acidic solution. Part I: Experimental results, *Corros. Sci.*, 2014, **81**, 54–64. doi: 10.1016/J.CORSCI.2013.12.010

56. B. Xu, W. Yang, Y. Liu, X. Yin, W. Gong and Y. Chen, Experimental and theoretical evaluation of two pyridinecarboxaldehyde thiosemicarbazone compounds as corrosion inhibitors for mild steel in hydrochloric acid solution, *Corros. Sci.*, 2014, **78**, 260–268. doi: 10.1016/J.CORSCI.2013.10.007

57. R. Sadeghi Erami, M. Amirnasr, S. Meghdadi, M. Talebian, H. Farrokhpour, K. Raeissi, Carboxamide derivatives as new corrosion inhibitors for mild steel protection in hydrochloric acid solution, *Corros. Sci.*, 2019, **151**, 190–197. doi: 10.1016/j.corsci.2019.02.019

58. P. Mourya, S. Banerjee and M.M. Singh, Corrosion inhibition of mild steel in acidic solution by Tagetes erecta (Marigold flower) extract as a green inhibitor, *Corros. Sci.*, 2014, **85**, 352–363. doi: 10.1016/j.corsci.2014.04.036

59. F. Bentiss, M. Lagrenee, M. Traisnel and J.C. Hornez, The corrosion inhibition of mild steel in acidic media by a new triazole derivative, *Corros. Sci.*, 1999, **41**, no. 4, 789–803. doi: 10.1016/S0010-938X(98)00153-X

60. M.A. Quraishi and F.A. Ansari, Corrosion inhibition by fatty acid triazoles for mild steel in formic acid, *J. Appl. Electrochem.*, 2003, **33**, 233–238. doi: 10.1023/A:1024106123577

61. F. Bentiss, M. Lebrini, H. Vezin, F. Chai, M. Traisnel and M. Lagrené, Enhanced corrosion resistance of carbon steel in normal sulfuric acid medium by some macrocyclic polyether compounds containing a 1,3,4-thiadiazole moiety: AC impedance and computational studies, *Corros. Sci.*, 2009, **51**, no. 9, 2165–2173. doi: 10.1016/J.CORSCI.2009.05.049

62. J.I. Bhat, D.P. Vijaya, V. Alva, Meclizine hydrochloride as a potential non-toxic corrosion inhibitor for mild steel in hydrochloric acid medium, *Arch. Appl. Sci. Res.*, 2011, **3**, 343.

♦ ♦ ♦

Thermodynamic, Adsorption and Corrosion Inhibition Studies of Mild Steel by *Artemisia vulgaris* Extract from Methanol as Green Corrosion Inhibitor in Acid Medium

Nabin Karki, Yogesh Choudhary and Amar Prasad Yadav[*]

Central Department of Chemistry, Tribhuvan University, Kirtipur, Kathmandu, Nepal
Email: amar2y@yahoo.com

Abstract

Corrosion inhibition of methanol extract of Artemisia vulgaris on the corrosion of mild steel in 1M H_2SO_4 has been investigated using weight loss measurements. The inhibition efficiency increases with increase in concentration and decreases with increase in temperature beyond 308 K. Adsorption of extract on metal follows Langmuir adsorption isotherm. The activation and free energies for the inhibition reactions support the mechanism of physical adsorption. Values of enthalpy and entropy supports that the process is endothermic and spontaneous. Surface and protective film analysis have been carried out by energy dispersive x-ray (EDX) and scanning electron microscopy (SEM).

Keywords: *Artemisia vulgaris, inhibitor, mild steel, thermodynamic*

Introduction

Mild steel has wide spread application in a broad field of industry and machinery due to its availability and low cost. Acid solutions are extensively used in the processes such as acid pickling, cleaning of boilers, descaling and drilling operations in oil and gas industries. Base metal applied in these processes undergoes undesirable dissolution. In order to reduce metal dissolution, various means like surface modification, alloy formation are adopted[1]. However, more accepted practice for the reduction of corrosion is the use of inhibitors which when added in small amount retards rate of corrosion significantly and prevents from economic loss due to metallic corrosion[2]. A substance to be used as corrosion inhibitor must fulfill some requirements. An inorganic compound must be able oxidize the metal, forming a passive layer on its surface. Organic molecules should have feature like a large structure, double bonds, an active centre or groups which gives them to be adsorbed on metal surface by displacing water molecules and cover a large area of a metal surface with a compact barrier film[3]. In chemisorption, electron transfer from inhibitor to metal to form coordinate covalent bond is facilitated by the presence of lone pairs or π electrons in inhibitor molecules[4].

Many organic and synthetic chemical containing oxygen, sulphur, nitrogen are studied as corrosion inhibitor and found effective as well. Unfortunately, most of them are hazardous to human and environment during their synthesis or application. This motivates investigations to develop non toxic,

---

[*] *Corresponding author*

biodegradable, environmentally acceptable, renewable and cheap inhibitor as the demand of recent awareness of green chemistry. These requirements may be achieved in the inhibitor prepared from different parts of plant extracts. Phytochemicals present in plant extracts have similar molecular and electronic structures to the conventional organic inhibitor molecules. Many investigations reveal that plant extracts can be used as effective green inhibitor such as henna[5], coconut coir[6], olive[7], *Cassia auriculata*[8], Aloes[9], *Hunteria umbellata*[10], *Progostemon benghalesis*[11] etc. Plant extracts shows inhibitions efficiency due to presence in their composition of complex organic species such as alkaloids, flavoniods, polyphenol, tannins, nitrogen bases, carbohydrates, protein as well as hydrolysis products.

Like in chemical reactions, rate of corrosion increases with increase in temperature. Acid pickling is done usually at elevated temperature up to 60 °C in HCl and up to 90 °C in H_2SO_4 [12]. Some conclusion regarding mechanism or inhibiting action can be drawn from the temperature dependence of the inhibitor efficiency and the comparison of the obtained thermodynamic data of the corrosion process in both presence and absence of inhibitor. So, the effect of temperature on a corrosion process has practical and theoretical importance.

Experimental Methods

Preparation of specimens

A flat sheet of mild steel available from mild steel supplier of Kathmandu valley was cut into coupons of diameter 4 cm×4 cm×0.15 cm. The coupons were polished with silicon carbide paper of different grades, starting with coarse one (100 grade) and proceeding in steps to finest (1500 grade). Dimension of each coupons were measured with digital vernier calliper, ultrasonicated in ethanol, dried and stored in moisture free desiccators.

Preparation of methanol extract

Aerial parts of *Artemisia vulgaris* were collected from Gundu, Bhaktapur, shade dried and powdered. 200 g of powder was extracted with methanol for 72 hrs followed by filtration to obtain extract as filtrate. Process was repeated until colourless extract was obtained. The extract was initially concentrated using rotary evaporator then dried on water bath to obtain solid residue.

Preparation of solution

1 M H_2SO_4 was prepared by diluting 55.6 mL concentrated H_2SO_4 in 1 litre volumetric flask up to the mark with distilled water. 1 g extract was dissolved in 1000 mL 1 M H_2SO_4 at 318 K temperature. Undissolved extract was removed by filtration. Filtrate was taken as 1000 ppm stock solution of acid in presence of inhibitor. Stock solution was diluted with calculated volume of 1M H_2SO_4 to prepare solution of different concentration of 800, 600, 400 and 200 ppm.

Weight loss measurements

The different parameters used for the study by weight loss measurements were effect of time, concentration of inhibitor solution and temperature. Polished coupons were removed from desiccators and weights were taken in an electronic balance. Weighed coupons were immersed in 100 mL acid (1 M H_2SO_4) without and with 1000 ppm concentration of the inhibitor in different beakers for various time

intervals (3, 6, 9, 12 and 24 hours) at same temperature 298 K to study the effect of time in inhibition efficiency. To study effect of concentration, weighed coupons were immersed in 100 mL acid (1 M H_2SO_4) without and with different concentrations of inhibitor (1000, 800, 600, 400, 200 ppm) in different beakers for 6 hours at same temperature 298 K. Similarly, effect of temperature was studied by immersing polished coupons in 100 mL acid (1 M H_2SO_4) without and with 1000 ppm concentration of the inhibitor in different beakers for 6 hours at various temperatures (298K, 308K, 318K, 328K, 338K). Temperature in experiments was adjusted by using clifton water bath model no. NE2-4D. After the elapsed time, coupons were taken out, washed thoroughly with distilled water, rinsed with acetone, dried, stored in desiccators and reweighed. All experiments were in triplicates and illustrated data are mean values of obtained results.

The corrosion rate (CR), surface coverage (θ) and inhibition efficiency (IE%) were calculated using following equations :

$$CR = \frac{87.6W}{AtD} \qquad \left(\begin{array}{l} Where\, W = Weight\, loss\, in\, solution\, (mg) \\ \quad A = Surface\, area\, of\, coupon\, immersed \\ \quad t = Time\, of\, immersion\, (h) \\ \quad D = Density\, of\, mild\, steel\, (g\,/\,ml) \end{array} \right)$$

$$\theta = \frac{W_1 - W_2}{W_1}$$

$$IE\% = \left(\frac{W_1 - W_2}{W_1} \right) \times 100 \qquad \left(\begin{array}{l} Where\, W_1\, and\, W_2\, are\, the\, weight\, loss\, in\, absence \\ and\ \ presence\, of\, inhibitor\ \ respective\, ly \end{array} \right)$$

Surface analysis

Three polished coupons were immersed in acid solution without and with inhibitor of 400 and 1000 ppm concentrations for 24 hours. Then coupons were washed, dried and stored in desiccators.

SEM analysis

Surface analysis of mild steel coupons were performed using scanning electron microscope at 500x magnification at three different locations to ensure reproducibility. It was performed by using Bio-Logic M470 Ac-SECM scanning electron microscope.

Energy dispersive x-ray (EDX) analysis

Energy dispersive x-ray (EDX) analysis was carried out with Bio-Logic M470 Ac-SECM scanning electron microscope in conjugation with an energy dispersive spectrometer employing beam of accelerating voltage 15 KV to examine surface film formed on the metal specimen.

Results and Discussion

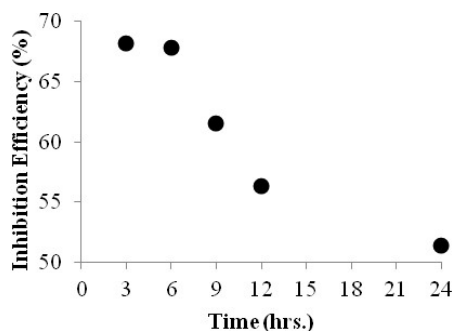### Effect of immersion time

Corrosion rate and inhibition efficiency by methanol extract of *Artemisia vulgaris* in various time are calculated from weight loss data is shown in table 1 and represented in figure 1. Result shows that corrosion rate is inhibited by extract which is due to adsorption of photochemical present in extract.

Inhibition efficiency decreases gradually with increase in time of immersion. It is almost same at 3 and 6 hrs. On the basis of table 1, weight loss for 15 g mild steel coupon with 30 cm^2 surface area is calculated when coupon was immersed in acid with and without inhibitor and plot of weight loss of coupon in different time is shown in figure 2. This data clearly shows that loss of metal by using inhibitor is decreased. This data reveals that adsorbed compounds starts desorption from metal surface after certain time and more metal surface is exposed to acidic media.

Table 1 : *Corrosion rate of mild steel and inhibition efficiency of Artemisia vulgaris for mild steel corrosion at various time*

Time (hours)	Corrosion Rate (mg/cm^{2}h)		Inhibition Efficiency (%)
	For Acid without inhibitor	For acid with inhibitor	
3	55.47	17.66	68.16
6	59.50	19.15	67.81
9	57.65	22.20	61.50
12	54.04	23.62	56.29
24	50.15	24.37	51.42

Figure 1: *Variation of inhibition efficiency with different immersion times of A. vulgaris extract on mild steel surface*
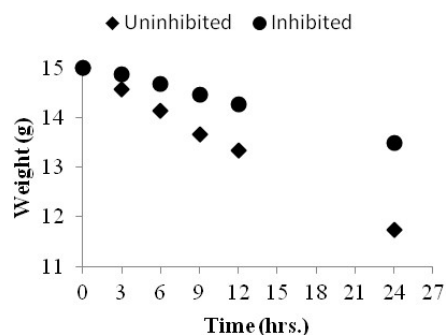

Figure 2: *Variation in weight of mild steel immersed in acid with and without inhibitor*

Effect of Concentration

Corrosion rate and inhibition efficiency by methanol extract of *Artemisia vulgaris* in various concentration at 298 K for 6 hours are calculated from weight loss data is shown in table 2 and represented in figure 3.

Table 2*: Corrosion rate of mild steel and inhibition efficiency of Artemisia vulgaris for mild steel corrosion at various concentration*

| Concentration (ppm)	Corrosion Rate	Inhibition efficiency	Surface Coverage (θ)
Blank (0)	59.50		
200	39.52	33.58	0.336
400	31.30	47.39	0.474
600	26.77	55.00	0.550
800	21.78	63.40	0.634
1000	19.15	67.81	0.678
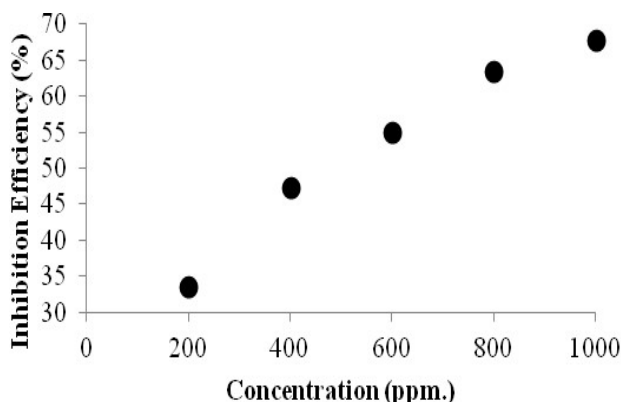
Figure 3: *Variation of inhibition efficiency with different concentration of A. vulgaris extract on mild steel surface*

Results show that inhibition efficiency increases with increase in concentration of inhibition in acid. It is due to the more surface coverage of mild steel with more adsorption of phytochemical compounds on it.

Adsorption isotherm

Adsorption isotherm provides the basic information on the interaction between the inhibitor and mild steel surface since inhibition efficiency is due to adsorption of compounds on metal surface through their polar functions making a barrier for charge and mass transfer between the metal and the environment. Water molecules are adsorbed on metal surface in aqueous solution. So, the adsorption of inhibitor molecules from aqueous solution is a quasi substitution process[13]. The linear relation between θ value and C_{inh} (concentration of inhibitor) should be known to find the adsorption isotherm. To fit θ Value, attempts were made to various isotherms including Langmuir, Tempkin, Freundlich, El-Awady. Both value of linear correlation coefficient (R^2) and slope is almost equal to 1 in Langmuir adsorption isotherm shown

in figure , which indicates that mono-layer of the inhibitor have been adsorbed on metal surface without interaction between the adsorbed molecules .
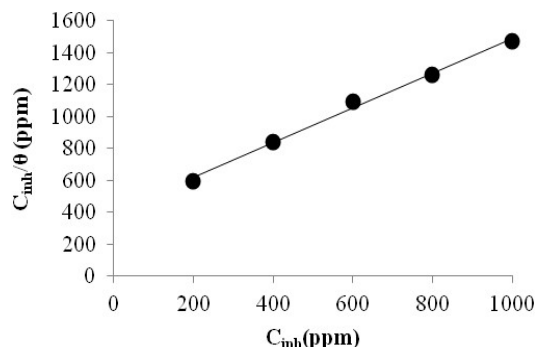

Figure 4 *: Langmuir adsorption isotherm plot for mild steel in 1 M H₂SO₄ with different concentration of A. Vulgaris extract.*

According to Langmuir adsorption isotherm equaltion, $\dfrac{C_{inh}}{\theta} = \dfrac{1}{K_{ads}} + C_{inh}$, value of adsorption constant K_{ads} is calculated from intercept of straight line. This value can be used in the equation, $\Delta G^{o} = -RT \ln(55.5K_{ads})$ to calculate the value of free energy of adsorption (ΔG^{o}), where 55.5 is concentration of water in solution in mol/L and R is universal gas constant (8.314J/mol K). Calculated value of ΔG^{o} according to relation is -12.22 KJ/mol. which is less than the threshold value -40 KJ/mol required for chemisorption. Value of ΔG^{o} less than or around -20 KJ/mol means adsorption is physical adsorption. So, adsorption of *Artemisia vulgaris* extract is physical adsorption.

Effect of temperature

Corrosion rate and inhibition efficiency by 1000 ppm methanol extract of *Artemisia vulgaris* in various temperature for 6 hours are calculated from weight loss data is shown in table 3 and represented in figure 5. IE increases with increase in temperature up to 308 K and beyond this IE decreases. Decrease in IE with increase in temperature might be due to desorption or decomposition inhibitor at higher temperature (14). This data also supports the adsorption is physical adsorption.
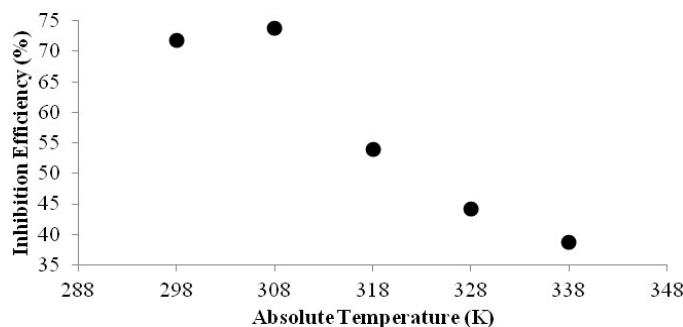
Figure 5: *Variation of inhibition efficiency of A. vulgaris extract on mild steel surface at different temperature.*

Table 3: *Corrosion rate of mild steel and inhibition efficiency of Artemisia vulgaris for mild steel corrosion at various temperature*

Temperature	Corrosion Rate (mg/cm^{2}h)		Inhibition Efficiency (%)
	For Acid without inhibitor	For acid with inhibitor	
298	92.40	26.06	71.80
308	136.86	35.91	73.76
318	206.98	95.20	54.00
328	264.48	147.47	44.24
338	332.83	203.85	38.75

Calculation of activation energy and thermodynamic parameters

The activation energy (E_a) can be calculated from Arrhenius plots for corrosion rate at different temperature according to relation: $\log(C.R.) = \log A - \dfrac{E_a}{2.303\,RT}$

Where, A is the Arrhenius pre-exponential constant, T is absolute temperature.

From the Arrhenius plot shown in figure , Calculated values of E_a for acid without and with inhibitor are 27.09 KJ/mol and 46.38 KJ/mol respectively and value of A for acid without and with inhibitor are 5382697.8 mg/Cm^2 and 3296097122 mg/Cm^2 respectively. Increase in E_a with addition of inhibitor shows the strong adsorption of inhibitor molecules on the metal surface (15). This value is lower than threshold value of 80KJ/mol, required for chemisorption. This indicates that adsorption is physical adsorption.

An alternative form of Arrhenius equation is transition state equation:

$$\log\left(\frac{C.R.}{T}\right) = \left[\log\left(\frac{R}{hN}\right) + \left(\frac{\Delta S^*}{2.303R}\right) - \frac{\Delta H^*}{2.303\,RT}\right]$$

Where h is plank's constant, 6.6261×10^{-34} Js and N is the Avogadro's number, 6.0225×10^{23} mol^{-1}
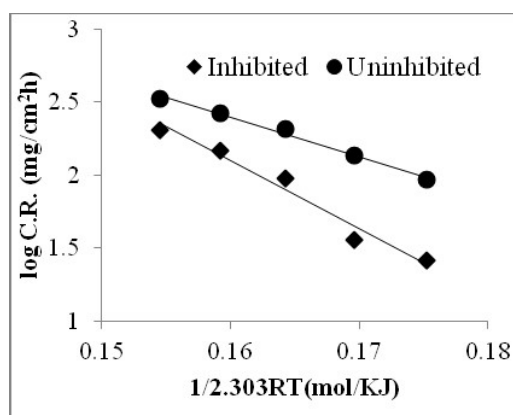
Figure 6 : Arrhenius plot for mild steel in 1 M H$_2$SO$_4$ with and without A. vulgaris extract
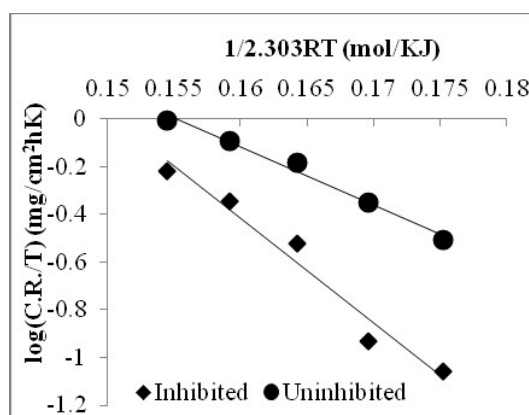
Figure 7 : Transition state plot for mild steel in 1 M H$_2$SO$_4$ with and without A. vulgaris extract

The slope of straight line obtained by plotting log(C.R./T) vs. 1/2.303T shown in figure is enthalpy of activation (ΔH^*) and the entropy of activation (ΔS^*)can be calculated from its intercept. Calculated values of ΔH^* for acid without and with inhibitor are 24.45 KJ/mol and 43.75 KJ/mol respectively. Positive value of ΔH^* indicates the endothermic nature of metal dissolution process. Increase in value of ΔH^* with addition of inhibitor shows the decrease in corrosion rate is controlled by kinetic parameters of activation. (16). Above calculations show that value of E_a is higher than that of ΔH^*, which indicates the involvement of a gaseous reaction, simply the hydrogen evolution reactions, resulting the decrease in the total reaction volume. (17) . The corrosion process is unimolecular in the condition, $E_a – \Delta H^* = RT$. Here difference in value of $E_a – \Delta H^*$ is 2.64 KJ/mol which is nearly equal to RT.

Calculated value of ΔS^* for acid without and with inhibitor are –124.91 J/mol K and –71.50 J/mol K respectively. Large and negative values of ΔS^* indicates that the activated complex in the rate determining step represents an association rather than a dissociation step, meaning that decrease in disordering takes place on going from reactants to the activated complex. In acid, transition state of the rate determining recombination step represents a more orderly arrangement relative to the initial state so a high value for the ΔS^* is obtained. In presence of inhibitor, the surface is covered with adsorbed molecules and rate of discharge of hydrogen ions in rate determining step is decreased resulting the system to pass from random arrangement, hence value of ΔS^* is increased. The increase in value of ΔS^* with addition of inhibitor implies the increase in disorder on going from reactant to activated complex. This behaviour is due to replacement of water molecules during adsorption of extract on metal surface[5].

Surface analysis

Energy dispersive x-ray (EDX) is employed to get the information about the composition of the surface of mild steel sample immersed in acid without and with inhibitor for 24 hours. The results are shown in figure 8. Percentage composition of different elements present in metal surface is listed in table 4. Data shows that there is decrease in iron and increase in N,C and O on surface of mild steel in sample immersed in acid with inhibitor which indicates the formation of protective film due to adsorption of phytochemicals containing N, C and O on surface and inhibit the iron dissolution.

a   b   C
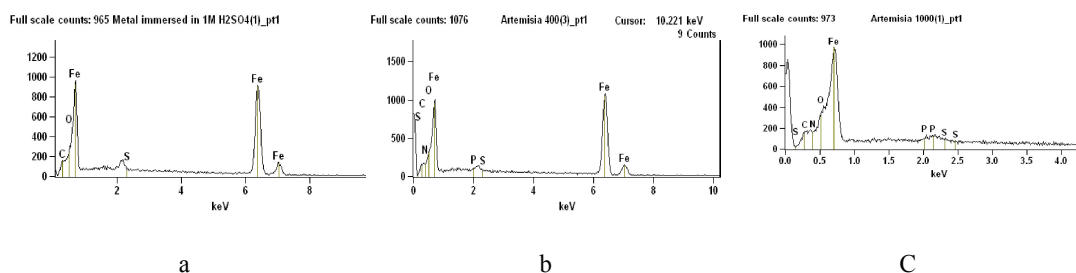
Figure 8 : *EDX spectra of mild steel coupons after 24 hr. immersion in (a) 1 M H₂SO₄ (b) 400 ppm extract solution in 1 M H₂SO₄ (c) 1000 ppm extract solution in 1 M H₂SO₄*

Table 4 *: Percentage of weight of different element on the mild steel surface after immersing in sample in different solution.*

Surface dipped in	Iron	Carbon	Nitrogen	Oxygen	Phosphorus
Polished metal sample	100%				
Acid without inhibitor	97.45%	1.72%		0.83%	
Acid with inhibitor of 400 ppm	94.8%	1.78%	1.31%	2.11%	
Acid with inhibitor of 1000 ppm	92.91%	2.27%	1.58%	3.16%	0.07%

a   b   C
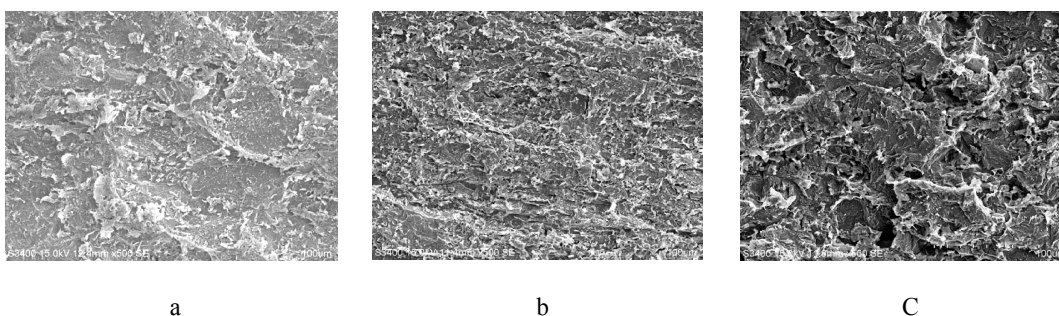
Figure 9 *: SEM micrographs of mild steel coupons after 24 hr. immersion in (a) 1 M H_2SO_4 (b) 400 ppm extract solution in 1 M H_2SO_4 (c) 1000 ppm extract solution in 1 M H_2SO_4*

To study the surface morphology of mild steel, Scanning electron microscope (SEM) images of coupon immersed for 24 hours in acid without and with inhibitor were taken by Bio-Logic M470 Ac-SECM scanning electron microscope. In SEM image of surface of metal sample immersed in acid without inhibitor shown in figure 9, surface was highly porous with deep and large cracks but surface was relatively smooth by the formation of protective film on surface when immersed for same time after addition of inhibitor.

Conclusions

Artemisia vulgaris extract acts as a good inhibitor for corrosion of mild steel in 1 M H_2SO_4 solution. Inhibition efficiency increases with increase in concentration and decreases with increase in temperature beyond 308 K. The adsorption of extract on mild steel follows the Langmuir adsorption isotherm. Values of ΔG^o and Ea indicate the adsorption of molecules on metal surface through physical adsorption. Values of ΔH^* and Ea indicates that the corrosion process is unimolecular and rate is controlled by kinetic parameters of activation. Values of ΔH^*, ΔS^* indicates that adsorption process is spontaneous and endothermic. EDX and SEM confirm the formation of protective film extract on metal surface and inhibit corrosion.

References

1. E. E. Oguzie, Y. Li, F.H. Wang, *Electrochimica Acta*, 2007, **52**, 6988.

2. H. A. Sorkhabi, D. Seifzadeh and M. G. Hosseini, *Corros. Sci.*, 2008, **50**, 3363.

3. S. Muralidharan, K. L. N. Phani, S. Pitchumani, S. Ravichandran, S. V.K. Iyer, *J. Electrochem. Soc.* 1995, **142**, 1478.

4. N. Hackerman, R. M. Hard, *Proc. Int. Congress of Metallic Corrosion*, 1962, 166.

5. A. Hamdy, N. Sh., El-Gendy, *Egyptian Journal of Petrolium*, 2013, **22**, 17.

6. S. A. Umoren, I. B. Obot, A.U. Israel, P. O. Asuquo, M. M. Solomon, U.M. Eduok, A.P. Udoh, *Journal of Industrial and Engineering Chemistry*, 2014, 20, 3612.

7. A.Y. EL-Etre, *Journal of Colloid and Interface Science*, 2007, **314**, 578.

8. J. Rosaline Vimala, A. Leema Rose, S. Raja, *International Journal of ChemTech Research*, 2011, **3**, 1791.

9. H. Cang, Z. Fei, J. Shao, W. Shi, Q. Xu, *Int. J. Electrochem. Sci*, 2013, **8**, 720.

10. A. S. Fouda, A. S. Abousalem, G.Y. El-Ewady, *Int. J. Ind. Chem.*, 2017, **8**, 61.

11. Y. Chaudhary, N. Karki, A. P. Yadav, *J. Nepal Chem. Soc.*, 2016, **35**, 139.

12. E. A. Noor, *Int. J. Electrochem. Sci.* 2007, **2**, 996.

13. L. R. Chauhan, G. Gunasekaran, *Corros. Sci.*, 2007, **49**, 1143.

14. F. Bentiss, M. Lebrini, H. Vezin, F. Chai, M. Traisnel, M. Lagrene, *Corr. Sci.*, 2005, **51**, 2165

15. S. K. Shukla, E.E. Ebenso, *Int. J. Electrochem. Sci.*, 2011, **6**, 3277.

16. J. I. Bhat, D.P. Vijaya, V. Alva, *Arch. Appl. Sci. Res*., 2011, 3, 343.

17. A. H. Ostovari, S. M. Peikari, S. R. Shadizadeh, S. J. Hashemi, *Corros. Sci*., 2009, 51, 1935.

Certificates of awards and participation in national and international conferences.

Oral Presentation :

1. *Study of extract of Mahonia nepalensis as green corrosion inhibitor in acidic media in mild steel of Nepal*, **Nabin Karki**, Yogesh Chaudhary, Amar Prasad Yadav, 18th Asian Pacific Corrosion Control Conference, 5th – 9th, November, 2018, Pattaya, Thailand

2. *Inhibition of acid corrosion of mild steel of Nepal by methanol extract of Berberis aristata stem as green corrosion inhibitor*, **Nabin Karki**, Yogesh Chaudhary, Amar Prasad Yadav, 1st Conference on Corrosion Resistant Steels and the Metallurgic Technology, August 30th to September 1st , 2019, Nanjing, China

3. *Study of extract of Equisetum hyemale (horsetail) as green corrosion inhibitor in acidic media in mild steel of Nepal*, **Nabin Karki**, Yogesh Chaudhary, Amar Prasad Yadav, 23rd International Conference of International Academy of Physical Sciences CONIAPS XXIII on Advances in Physical Sciences, 16th – 18th, November, 2018, Kathmandu, Nepal

4. *Effect of Extract of stem of Mahonia nepalensis on Corrosion Inhibition of Mild Steel of Nepal*, **Nabin Karki**, Yogesh Chaudhary, Amar Prasad Yadav, The Seventh National Conference on Science and Technology, 29th-31st, March, 2016, Kathmandu

5. *Effect of Extract of stem of Berberis aristata on Corrosion Inhibition of Mild Steel of Nepal*, **Nabin Karki**, Yogesh Chaudhary, Amar Prasad Yadav, International Chemical Congress – 2018, 8th-10th, March, 2018, Sauraha, Chitwan, NEPAL

6. *Study of Extract of Berberis aristata as Green Corrosion Inhibitor in Acidic Media in Mild Steel of Nepal*, **Nabin Karki**, Yogesh Chaudhary, Amar Prasad Yadav, International Conference on Advances in Polymer Science & Technology, 1st-3rd, November, 2018 Godavari, NEPAL

7. *Effect of Extract of Artemisia and Equisetum on Corrosion Inhibition of Mild Steel of Nepal*, **Nabin Karki**, Amar Prasad Yadav, International conference on Advance materials and nanotechnology, ICAMN-2014, 4th-6th Nov, 2014, Kathmandu

8. *Effect of Extract of stem of Mahonia nepalensis on Corrosion Inhibition of Mild Steel of Nepal*, **Nabin Karki**, Yogesh Chaudhary, Amar Prasad Yadav,

Regional Chemical Congress, October 14, 2017, Prithivi Narayan Campus, Pokhara

9. *Effect of Extract of Artemisia vulgaris on Corrosion Inhibition of Mild Steel of Nepal*, **Nabin Karki**, Yogesh Chaudhary, Amar Prasad Yadav, National Chemical Congress, August 29, 2017, Amrit Science College, Kathmandu

Poster Presentation :

1. *Effect of Extract of Stem of Mahonia nepalensis Plant on Corrosion Inhibition of Mild Steel of Nepal*, **Nabin Karki** and Amar Prasad Yadav, International Workshop on Science, Environment and Education (IWOSEE)-2015, April 18, 2015, Pokhara, Nepal

2. *Effect of Extract of stem of Mahonia nepalensis (Jamanimandro) plant on Corrosion Inhibition of Mild Steel of Nepal*, **Nabin Karki**, Yogesh Chaudhary and Amar Prasad Yadav, National Chemical Congress, August 29, 2017, Amrit Science College, Kathmandu

APCCC18 Asian Pacific Corrosion Control Conference

5th – 9th November, 2018, Pattaya, Thailand

ASIAN-PACIFIC • CORROSION CONTROL CONFERENCE •

CERTIFICATE OF PRESENTATION

We hereby certify that

Nabin Karki

has presented an oral presentation entitled

Study of Extract of Mahonia nepalensis as Green Corrosion Inhibitor in Acidic Media in Mild Steel of Nepal

Gobboon Lothongkum

Assoc. Prof. Dr.-Ing. Gobboon Lothongkum
APCCC18 Chairman
President of Thai Corrosion of Metals and Materials Association
Head of Metallurgical Engineering Department,
Faculty of Engineering, Chulalongkorn University
Thailand

Dr. Julathep Kajornchaiyakul
APCCC18 Chairman
Executive Director
National Metal and Materials Technology Center
Thailand

OG-156

The 1ˢᵗ International Conference on Corrosion-resistant Steels and the Metallurgic Technology

Chinese Society for Corrosion and Protection (CSCP)

Certificate

This is to certify that Nabin Karki , Associate Professor in Chemistry, Bhaktapur Multiple Campus, Tribhuvan University, Bhaktapur, Nepal, has participated and delivered an invited talk entitled " Inhibition of Acid Corrosion of Mild Steel of Nepal by Methanol Extract of Berberis aristata Stem as Green Corrosion Inhibitor " in The 1st International Conference on Corrosion-resistant Steels and the Metallurgic Technology during Aug. 30 to Sept. 1, 2019 in Nanjing, China.

Xiaogang li

Prof. Xiaogang li
Chair of the Conference
Executive Vice President of CSCP

ICC-2018

International Chemical Congress

- Chemistry for Sustainable Development -

Organized by

Nepal Chemical Society

In co-operation with

Department of Chemistry

Birendra M. Campus, Bharatpur, Tribhuvan University
Chitwan, Nepal

Young Scientist Award

This is to certify that

Nabin Karki

was awarded as Best Oral Presenter in the

International Chemical Congress Chemistry for Sustainable Development

March 8-10, 2018, Sauraha, Chitwan, Nepal

Dr. Surya Kant Kalauni
General Secretary
Nepal Chemical Society

Govind Sapkota
Co-patron ICC-2018
Campus Chief, Birendra M. Campus

Chief Guest

Prof. Dr. Amar Prasad Yadav
Convener ICC-2018
President Nepal Chemical Society

Nepal Academy of Science and Technology

CERTIFICATE

Awarded to

NABIN KARKI

for active participation/paper presentation/poster presentation

in

THE 7th NATIONAL CONFERENCE ON SCIENCE AND TECHNOLOGY

SCIENCE, TECHNOLOGY AND INNOVATION FOR NEPAL'S GRADUATION TO DEVELOPING COUNTRY STATUS

March 29-31, 2016
Kathmandu, Nepal

Mrs. Ramila Shrestha Raut
Chief, Promotion Division

Dr. Buddhi Ratna Khadge
Secretary

Prof. Dr. Jiba Raj Pokharel
Vice-Chancellor

23RD INTERNATIONAL CONFERENCE OF INTERNATIONAL ACADEMY OF PHYSICAL SCIENCES

(CONIAPS XXIII)

On

Advances in Physical Sciences to Achieve Sustainable Development Goals

November 18, 2018

Organized by

NEPAL ACADEMY OF SCIENCE AND TECHNOLOGY, KATHMANDU, NEPAL

Certificate

This is to certify that Prof. /Dr./ Mr./Ms. .....Nabin Karki........................... has participated in the Department of ...chemistry.., T.U, Nepal............... 23rd International Conference of International Academy of Physical Sciences on **Advances in Physical Sciences to Achieve Sustainable Development Goals** held at **Nepal Academy of Science and Technology** during November 16-18, 2018 and delivered Invited Lecture/Chaired a Session/ Presented a paper /Presented a paper in Young Scientist Award Category.
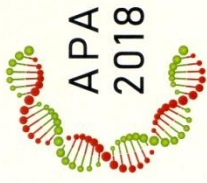
Title of the Invited Lecture/Paper ......Study of extract of Equisetem as green corrosion inhibitor in acidic Media in mild steel, Nepal......................

Prof. P. N. Pandey
General Secretary
IAPS

Dr. Buddhi Ratna Khadge
Convenor
CONIAPS XXIII

Ms. Ramila Raut
Organizing Secretary
CONIAPS XXIII

International Conference on
Advances in Polymer Science & Technology

November 1-3, 2018 | Kathmandu, Nepal

CERTIFICATE OF PARTICIPATION

This is to certify that

Nabin Karki

Participated as a Delegate & Presented Oral Talk

Titled

Study of Extract of Berberis Aristata as Green
Corrosion Inhibitor in Acidic Media in Mild Steel of Nepal

Amar Yadav
Chairman (Nepal)

Bhuvanesh Gupta
Chairman (India)

APA
2018

Organised by

Asian Polymer Association   Nepal Chemical Society

In association with

Tribhuvan University
Kathmandu, Nepal

Society for Biomaterials &
Artificial Organs India (Delhi)

stermi

IIF
Indo Italian Forum on
Biomaterials & Tissue Engineering

Society For Tissue Engineering &
Regenerative Medicine India, Delhi

International Conference on

Advanced Materials and Nanotechnology

for Sustainable Development

Regd. No.: 8/042/043

Organized by

Nepal Chemical Society

In co-operation with

Central Department of Chemistry, Tribhuvan University

Kirtipur, Kathmandu, Nepal

Certificate of Participation

This is to certify that

Nabin Karki

participated as Keynote/Invited/Oral Lecture/Poster/Delegate in the

International Conference on Advanced Materials and Nanotechnology for Sustainable Development

November 4-6, 2014 Kathmandu, Nepal

Prof. Dr. Megh Raj Pokhrel
Organizing Chair
Head of Central Department of Chemistry

Honorable Minister Chitralekha Yadav
Chief Guest
Minister for Education

Dr. Amar Prasad Yadav
General Secretary
Nepal Chemical Society

Dr. Deba Bahadur Khadka
Convener of ICAMN-2014 &
President of Nepal Chemical Society

National Chemical Congress

Organized by

Nepal Chemical Society

In co-operation with

Amrit Campus

Lainchaur, Kathmandu, Nepal

Best Poster Award

This is to certify that

Mr. *Nabin Karki*

is awared Best Poster in the National Chemical Congress

held on August 29, 2017, Amrit Campus, Lainchaur, Kathmandu, Nepal

Institute of Science & Technology
Amrit Campus

Dr. Surya Kant Kalauni
General Secretary
Nepal Chemical Society

Prof. Dr. Jiba Raj Pokharel
Vice Chancellor
Nepal Academy of Science & Technology
Chief Guest

Prof. Dr. Amar Prasad Yadav
President
Nepal Chemical Society

International Workshop on Science, Environment, and Education (IWOSEE)-2015

Organized by

Action Research Consultancy-Nepal

(Reg. No. 1786 (DAO-Kaski) / Affiliation No. 22461 SWC-Kathmandu)

CERTIFICATE

This is to certify that Prof./Dr./Mr./Ms. **Nabin Karki** ....

participated in and presented a paper/ poster titled... **Effect of Extract of Stem of Mehonia**

Nepalansis Plant on Corrosion Inhibition of Mild Steel of Nepal
....

at the International Workshop on Science, Environment, and Education (IWOSEE)-2015

held in Pokhara, Nepal on April 18, 2015.

Prof. Dr. Ramawatar Yadav
Organizing Chair
President, ARC-Nepal
Former Vice Chancellor, Purbanchal University

Prof. Dr. Ishwar Chandra Dutta
Chief Guest
Chairman, Tribhuvan University Service Commission

Prof. em. Dr. Jörn H. Kruhl
Chief Advisor
Technische Universität München, Germany